



HAL
open science

Degradable Polymer Prodrugs by Nitroxide-Mediated Radical Ring-Opening Polymerization

Elise Guegain

► **To cite this version:**

Elise Guegain. Degradable Polymer Prodrugs by Nitroxide-Mediated Radical Ring-Opening Polymerization. Polymers. Université Paris Saclay (COMUE), 2017. English. NNT : 2017SACLS569 . tel-03029790

HAL Id: tel-03029790

<https://theses.hal.science/tel-03029790v1>

Submitted on 29 Nov 2020

HAL is a multi-disciplinary open access archive for the deposit and dissemination of scientific research documents, whether they are published or not. The documents may come from teaching and research institutions in France or abroad, or from public or private research centers.

L'archive ouverte pluridisciplinaire **HAL**, est destinée au dépôt et à la diffusion de documents scientifiques de niveau recherche, publiés ou non, émanant des établissements d'enseignement et de recherche français ou étrangers, des laboratoires publics ou privés.

Prodrogues Polymères Dégradables par Polymérisation Radicalaire par Ouverture de Cycle Contrôlée par les Nitroxydes

Thèse de doctorat de l'Université Paris-Saclay
préparée à l'Université Paris-Sud
Institut Galien Paris Sud (UMR CNRS 8612)

École doctorale n°569 Innovation Thérapeutique :
du fondamental à l'appliqué
Spécialité de doctorat : Pharmacotechnie et Physico-chimie Pharmaceutique

Thèse présentée et soutenue à Chatenay-Malabry, le 28 novembre 2017, par

Elise Guégain

Composition du Jury :

Sophie Guillaume Directrice de Recherche CNRS, Université Rennes 1 (ISCR)	Rapporteur
Sagrario Pascual Maître de Conférences, Le Mans Université (IMMM)	Rapporteur
Patrick Couvreur Professeur, Université Paris Saclay (IGPS)	Président du jury
Elias Fattal Professeur, Université Paris Saclay (IGPS)	Examineur
Philippe Guégain Professeur, Université Pierre et Marie Curie (IPCM)	Examineur
Yohann Guillaneuf Chargé de Recherche CNRS, Aix-Marseille Université (ICR)	Examineur
Sébastien Lecommandoux Professeur, Université Bordeaux (LCPO)	Examineur
Julien Nicolas Directeur de Recherche CNRS, Université Paris Saclay (IGPS)	Directeur de thèse

À mon Père,

Remerciements

Tout d'abord, j'aimerais remercier le Pr. Elias Fattal, directeur de l'Institut Galien Paris Sud qui m'a accueilli pendant ces trois années au sein d'un laboratoire à l'atmosphère conviviale et dynamique. Je souhaite également remercier chaleureusement le Pr. Patrick Couvreur qui m'a intégré dans son équipe et a toujours fait preuve de bienveillance.

Je tiens à exprimer ma reconnaissance aux Dr. Sophie Guillaume et Sagrario Pascual, qui m'ont fait l'honneur d'accepter d'évaluer mon travail en tant que rapporteurs ainsi qu'aux Pr./Dr. Patrick Couvreur, Elias Fattal, Philippe Guégan, Yohann Guillaneuf et Sébastien Lecommandoux qui ont accepté de juger mon travail en tant qu'examineurs.

Un remerciement tout particulier au Dr. Julien Nicolas, mon directeur de thèse. Merci de m'avoir fait confiance pendant ces trois ans, de m'avoir offert la possibilité de travailler sur un sujet de thèse passionnant et de m'avoir prêté le marteau qui m'a permis de rentrer chez moi lorsque ma porte était cassée. Les nombreuses discussions que nous avons eues m'ont permis d'évoluer aussi bien professionnellement que personnellement. Tu m'as montré le chemin à suivre. *Conseil aux futurs thésards/post-docs : un gâteau au chocolat (ou tout autre douceur chocolatée) peut faire des miracles.*

Tout ce travail n'aurait pas été possible sans tous les membres de l'Institut Galien, et plus particulièrement : merci au Dr. Simona Mura pour son aide et pour les nombreux TPs « comprimés » partagés ; merci au Dr. Didier Desmaële pour les conseils en chimie organique ; merci au Dr. Jean-Philippe Michel, pour tout le travail effectué en AFM et pour son expertise. Sans oublier les services communs : merci à Stéphanie Denis qui m'a formé à la culture cellulaire ; à Camille Dejean du service de RMN et à Remi Pires pour la MEB.

Aux stagiaires qui ont travaillé avec moi, Johanna Tran, Quentin Deguettes et Erika Giovanardi ; merci pour le travail considérable que vous avez accompli et pour la bonne humeur que vous avez apportée au labo. Vous êtes grands maintenant, à vous de jouer ! 😊

Ces trois années n'auraient pas été aussi agréables sans l'équipe de doctorants et post-docs : mes co-bureaux, Johanna Tran et Daniele Vinciguerra ; la team 7 : Marie Rouquette,

Gianpiero Lazarri, Julie Mougin, Arnaud Peramo, Flavio Dormont et Yinyin Bao ; et les copains des autres équipes : Mathilde Lorschneider, Sophie Houvenagel, Claire Albert, Marion Quaillet, Quentin Deguettes, Alexandre Bordat, Tanguy Boissenot. Merci pour tous ces moments passés ensemble : les traditionnelles soirées raclettes ; les soirées déguisées du mardi gras, avec une dédicace spéciale pour les crêpes de Clairalbert ; les 'Friday Beer' ; la plage de Juan les Pins ; le covoiturage parfois drôle, parfois calme et parfois engagé ; et enfin les énigmes et devinettes du déjeuner. Un clin d'œil tout particulier au Dr. Vianney Delplace, qui m'a appris beaucoup et a enchanté mes oreilles avec ses reprises mythiques pendant mon stage de M2. Sans oublier le restaurant universitaire, qui m'a accueilli tous les midis pendant trois ans et son cuisinier, expert en nutrition.

Et enfin, merci à ma famille (ma mère, mes sœurs) et à mes amis, toujours présents. Je remercie tout particulièrement ma mère pour son soutien et son amour inébranlable et mon père, si aimant et courageux. Comme je le dis souvent, la qualité prime sur la quantité. Et ces 25 ans ont été d'une qualité rarement égalée. Je tiens également à remercier Guido, mon chat, pour son enthousiasme (surtout au moment de la pâté) et son accueil tous les soirs. Pour finir, un grand merci à ma moitié, Pablo, pour son soutien de tous les instants. Partons maintenant pour de nouvelles aventures !

Sommaire

Remerciements	1
Sommaire.....	4
Abréviations	10
Introduction Générale.....	14
Chapter 0 Context & Previous Works	18
I. Introduction.....	18
II. Polymer prodrug approach and drug-initiated strategy in cancer therapy.	19
III. Degradable vinyl polymers	27
Chapter 1 NMP of Methacrylic Esters: Insights and Solutions to a Long- Standing Problem.....	37
I. Introduction.....	39
II. NMP of MMA: why does it fail?	40
III. Use of additives.....	50
IV. The copolymerization approach.....	51
V. Development of dedicated nitroxides.....	57
VI. New processes.....	63
VII. Materials with uncontrolled polymethacrylate segments.....	68
VIII. Conclusion.....	69
Chapter 2 On the Structure-Control Relationship of Amide- Functionalized SG1-Based Alkoxyamines for Nitroxide-Mediated Polymerization and Conjugation.....	76
I. Introduction.....	78
II. Experimental part.....	81
a. Materials	81

b.	Analytical Techniques	81
c.	Methods	82
III.	Results and Discussion.....	86
a.	Synthesis and dissociation behavior of amide-functionalized SG1-based alkoxyamines.....	86
b.	NMP of vinyl monomers initiated by different SG1-based alkoxyamine	92
IV.	General discussion	97
V.	Conclusion.....	98
Chapter 3 Efficient synthesis of 2-methylene-4-phenyl-1,3-dioxolane, a cyclic ketene acetal for controlling the NMP of methyl methacrylate and conferring tunable degradability.....		116
I.	Introduction.....	118
II.	Experimental Part.....	120
a.	Materials	120
b.	Analytical Techniques	121
c.	Synthetic pathways to 2-methylene-4-phenyl-1,3-dioxolane (MPDL)	121
d.	Polymerization reactions	124
e.	Hydrolytic degradation	125
III.	Results and Discussion.....	125
a.	Synthesis of MPDL	125
b.	Nitroxide-mediated copolymerization with methyl methacrylate	127
c.	Structural characterization.....	128
d.	Hydrolytic degradation	130
e.	Thermal characterization	133
IV.	Conclusion.....	134

Chapter 4 A Ring to Rule Them All: A Cyclic Ketene Acetal Comonomer Controls the Nitroxide-Mediated Polymerization of Methacrylates and Confers Tunable Degradability 143

I.	Introduction.....	145
II.	Experimental Part.....	146
a.	Materials	146
b.	Analytical methods	146
c.	Methods	147
d.	Cytotoxicity study.....	149
III.	Results and Discussion.....	150
IV.	Conclusion.....	155

Chapter 5 Degradation of Copolymers Prepared by Nitroxide-Mediated Radical Ring-Opening Polymerization and Point-by-Point Comparison with Traditional Polyesters 166

I.	Introduction.....	168
II.	Experimental part.....	171
a.	Materials	171
b.	Analytical methods	172
c.	Polymer synthesis	173
d.	Degradation experiments	175
	Enzymatic degradation.....	176
e.	Intravenous injections and preliminary toxicity to mice	176
III.	Results and Discussion.....	176
a.	Synthesis and characterization of degradable copolymers	176
b.	Long-term hydrolytic degradation in PBS.....	178
c.	Hydrolytic degradation of polymer films	182
d.	Enzymatic degradation	188

e. Preliminary in vivo toxicity	189
IV. Conclusion.....	190
Chapter 6 Degradable Polymer Prodrugs with Adjustable Activity from Drug-Initiated Radical Ring-Opening Copolymerization.....	202
I. Introduction.....	204
II. Experimental section.....	206
a. Material.....	206
b. Analytical method.....	207
c. Synthetic procedures.....	208
d. Deprotection of the copolymers.....	213
e. Hydrolytic degradation	214
f. Nanoparticle preparation	214
g. Nanoprecipitation yield	214
h. Biological Evaluation	215
III. Results and Discussions	216
a. Synthetic strategy	216
b. Synthesis of Gem-based alkoxyamine initiators	218
c. Copolymerization kinetics.....	219
d. Synthesis of low molar mass polymer prodrugs for biological evaluations.....	222
e. Hydrolytic degradation of the prodrugs.....	223
f. Physicochemical properties	224
g. Drug release in human serum	226
h. In vitro anticancer activity	227
IV. Conclusion.....	230
Chapter 7 General Discussions.....	242
I. Structure-Control Relationship of Amide-Functionalized SG1-Based Alkoxyamines	243

a.	Pre-functionalization of secondary alkoxyamine with primary amine: toward a slower dissociation rate constant?	243
b.	Determination of the best polymerization conditions for the NMP of methyl methacrylate from secondary alkoxyamines	245
II.	New Degradable Copolymers Based on Nitroxide-Mediated Radical Ring-Opening Copolymerization of 2-Methylene-4-Phenyl-1,3-Dioxolane (MPDL) and Methacrylic Esters	247
a.	Synthesis of MPDL: a new reliable and robust method	247
b.	MPDL: the first degradable, controlling comonomer for the NMP of methacrylates	248
c.	Degradation of methacrylic ester-based copolymers under various conditions	251
d.	Biocompatibility of PEG-based degradable copolymers.....	255
III.	Degradable Polymer Prodrugs with Adjustable Activity from Drug-Initiated Radical Ring-Opening Copolymerization	256
a.	Drug-initiated synthesis of degradable polymer prodrugs	257
b.	Hydrolytic degradation of the prodrugs under accelerated conditions.....	259
c.	Physico-chemical characterization	259
d.	Biological evaluation.....	260
IV.	Limitations, remaining questions and perspectives	262
a.	Disenchantment of MMA-based prodrug nanoparticles.....	262
b.	Promising OEGMA-based prodrugs	263
c.	Design of new CKAs	264
V.	Experimental part (grey boxes).....	265
a.	Degradation experiments	265
b.	Polymer synthesis	265
c.	Nanoparticle preparation	266
	Conclusion Générale	273

Abréviations

AcGalEMA	glucose-functionalized methacryloyl galactose
AFM	atomic force microscopy
AN	acrylonitrile
ATRP	atom-transfer radical polymerization
<i>n</i> BMA	<i>n</i> -butyl methacrylate
BlocBuilder	2-methyl-2-[<i>N</i> - <i>tert</i> -butyl- <i>N</i> -(1-diethoxyphosphoryl-2,2-dimethylpropyl) aminoxy]propionic acid alkoxyamine
BMDO	5,6-benzo-2-methylene-1,3-dioxepane
BzMA	benzyl-methacrylate
CdA	cladribine
CDCl ₃	deuterated chloroform
CHCl ₃	chloroform
CKA	cyclic ketene acetal
CryoTEM	cryo-transmission electron microscopy
\mathcal{D}	dispersity (M_w/M_n)
DLS	dynamic light scattering
DMA	<i>N,N</i> -dimethylacrylamide
DMAEMA	(dimethylamino)ethyl methacrylate
DMSO	dimethyl sulfoxide
DP _n	number-average degree of polymerization
D_z	nanoparticle average diameter (in intensity)
E_a	activation energy
EPR	enhanced permeability and retention
ESR	spin resonance spectroscopy
f	alkoxyamine efficacy
FDA	food and drug administration
F_{MPDL}	molar fraction of MPDL in the copolymer
$f_{\text{MPDL}, 0}$	initial molar fraction of MPDL in the comonomer feed
Gem	gemcitabine
HCl	hydrogen chloride
HPLC	high-performance liquid chromatography
I	isoprene
IC ₅₀	half maximal inhibitory concentration

IHB	intramolecular hydrogen-bonding
K	activation-deactivation equilibrium constant
k_d	dissociation rate constant
KOH	potassium hydroxide
LD ₅₀	median lethal dose
MDO	2-methylene-1,3-dioxepane
MeOH	methanol
MMA	methyl methacrylate
M_n	number-average molar mass
M_p	peak-average molar mass
M_w	weight-average molar mass
MPDL	2-methylene-4-phenyl-1,3-dioxolane
MS	microsphere
MTT	3-(4,5-dimethylthiazol-2-yl)-2,5-diphenyltetrazolium bromide
Napht	naphtalimide
<i>n</i> BA	<i>n</i> -butyl acrylate
NCA	<i>N</i> -carboxyanhydride
NHS	<i>N</i> -hydrosuccinimide
NMP	nitroxide-mediated polymerization
NMR	nuclear magnetic resonance
NMrROP	nitroxide-mediated radical ring-opening polymerization
NP	nanoparticle
OEGMA	oligo(ethylene glycol) methyl ether methacrylate
PACA	poly(alkyl cyanoacrylate)
PBS	phosphate buffer saline
PCL	polycaprolactone
PEG	poly(ethylene glycol)
PFS	pentafluorostyrene
PI	polyisoprene
PLA	poly(lactic acid)
PLGA	poly(lactic- <i>co</i> -glycolic acid)
PMMA	poly(methyl methacrylate)
PMPDL	poly(2-methylene-4-phenyl-1,3-dioxolane)
<i>Pn</i> BA	poly(<i>n</i> -butyl acrylate)
POEGMA	poly[oligo(ethylene glycol) methyl ether methacrylate]

PS	polystyrene
PSD	particle size distribution
PyBOP	(benzotriazol-1-yloxy)tris(pyrrolidino)phosphonium hexafluorophosphate
RAFT	reversible addition-fragmentation chain transfer polymerization
RDRP	reversible deactivation radical polymerization
ROP	ring-opening polymerization
rROP	radical ring-opening polymerization
S	styrene
SEC	size exclusion chromatography
SEM	scanning-electron microscopy
SG1	<i>N-tert</i> -butyl- <i>N</i> -[1-diethylphosphono-(2,2-dimethylpropyl)]
SS	4-styrene sulfonate
THF	tetrahydrofuran
VBK	9-(4-vinylbenzyl)-9H-carbazole
2VP	2-vinyl pyridine

Introduction Générale

Depuis l'introduction de la notion de macromolécule par Hermann Staudinger (récompensé par un prix Nobel en 1953) et ses premiers travaux sur la polymérisation de monomères vinyliques dans les années 1920, les méthodes de polymérisation se sont rapidement développées, notamment avec l'essor des techniques de polymérisations radicalaires contrôlées, et permettent maintenant de synthétiser de manière aisée des polymères ayant des architectures complexes et offrant une grande flexibilité en termes de composition et de fonctionnalisation. De nombreuses études académiques tendent à les utiliser dans le domaine biomédical, notamment avec le développement de nanoparticules pour la délivrance de principe actif pour la thérapie du cancer en allant vers des matériaux innovants, capables de cibler spécifiquement les cellules tumorales, de libérer un principe actif après un stimulus ou de combiner thérapie et diagnostique (la théranostique). Par rapport aux polymères biocompatibles et dégradables de références (tels que les polyesters aliphatiques), les polymères vinyliques permettent d'atteindre un degré de sophistication élevé, ce qui en fait des candidats idéals pour des applications biologiques.

Cependant, du fait de leur squelette carboné, les polymères vinyliques traditionnels résistent à la dégradation et l'accumulation de matériaux transporteurs dans l'organisme peut s'avérer néfaste et induire de la toxicité. Rendre ces polymères (bio)dégradables représente donc un défi majeur dans le panorama actuel de la recherche académique et industrielle. Une stratégie prometteuse consiste à copolymériser des monomères vinyliques traditionnels avec des acétals de cétène cycliques, qui sont des précurseurs de fonction ester, afin d'insérer des groupements dégradables dans le squelette polymère.

Le sujet principal de la thèse porte sur le développement de polymères vinyliques dégradables et sur leur application à la délivrance de principes actifs. Les nanoparticules polymères traditionnelles sont généralement obtenues par encapsulation physique (i.e., piégeage) d'un principe actif lors de la formulation de la nanoparticule. Cependant, des verrous technologiques persistent limitant ainsi leur efficacité et leur transposition clinique : (i) le relargage rapide et non contrôlé d'une fraction de principe actif simplement adsorbé à la surface de la nanoparticule (« burst release ») ; (ii) des taux de chargement en principe actif faibles, de l'ordre de quelques pourcents et (iii) des incompatibilités entre le principe actif et la matrice polymère, donnant lieu notamment à des instabilités colloïdales et nécessitant l'utilisation de co-solvant organiques. La stratégie « prodrogue », pour laquelle le principe

actif est lié de manière covalente au polymère, permet d'amoinrir, voire de contourner certaines de ces limitations. Par exemple, non seulement le phénomène de « burst release » est absent car le principe actif doit être clivé du polymère pour être actif, mais les taux de charge en principe actif sont généralement plus élevés. La conception de tels objets reste néanmoins délicate avec de nombreuses étapes de synthèse et de faibles rendements. Dans un tel contexte, une nouvelle méthode pour la synthèse de nanoparticules de prodrogues polymères, appelée '*principe actif amorceur*', a été récemment développée au sein du laboratoire à partir de monomères vinyliques. L'idée est de faire croître une courte chaîne de polymère à partir d'un principe actif fonctionnalisé avec un amorceur/agent de transfert de polymérisation radicalaire contrôlée. Les conjugués ainsi obtenus peuvent alors donner lieu, par nanopréciipitation, à des nanoparticules auto-stabilisées en suspension aqueuse induisant de fortes activités anticancéreuses in vitro et in vivo. Néanmoins, la limitation majeure de ces systèmes réside dans leur caractère non-dégradable, ce qui pourrait entraîner des effets indésirables in vivo.

Dans ce contexte, l'objectif principal de la thèse est de préparer **des prodrogues polymères dégradables**, en copolymérisant des **esters méthacryliques** avec des **acétals de cétène cycliques (CKA)**, en utilisant la stratégie du '*principe actif amorceur*'. Ce manuscrit commencera par une partie introductive s'attachant à présenter le contexte scientifique et les travaux qui ont précédé nos recherches (**Chapitre 0**). Elle sera suivie d'une étude bibliographique (**Chapitre 1**) des différentes stratégies permettant de contrôler la polymérisation radicalaire contrôlée par les nitroxydes (NMP) des esters méthacryliques, qui représente toujours un défi important en ingénierie macromoléculaire. Le travail de recherche débutera avec le **Chapitre 2** permettant d'établir des relations entre la structure d'alkoxyamines fonctionnelles basées sur le nitroxyde SG1 et leur capacité à contrôler la NMP de monomères vinyliques traditionnels. Cette étude permettra notamment de déterminer les conditions expérimentales adaptées à la synthèse de prodrogues à partir d'alkoxyamines fonctionnalisées avec une molécule anticancéreuse, la gemcitabine. Avant cela, nous avons développé, au cours des deux chapitres suivants, deux familles de copolymères vinyliques dégradables. Le **Chapitre 3** porte sur la mise au point d'une nouvelle voie de synthèse du 2-méthylène-4-phényl-1,3-dioxolane (MPDL), le CKA que nous utiliserons durant toute la thèse, qui est plus efficace et reproductible, puis nous nous sommes intéressés à la préparation de copolymères hydrophobes dégradables via sa copolymérisation avec le méthacrylate de méthyl (MMA). Le **Chapitre 4** décrit quant à lui une synthèse similaire mais adaptée à la

préparation de copolymères dégradables hydrosolubles portant des chaînes de PEG pendantes. Il s'agira de démontrer lors de ces deux chapitres : (i) la capacité du MPDL à agir comme un comonomère de contrôle lors la NMP des esters méthacryliques ; (ii) son insertion dans le squelette polymère et (iii) la dégradabilité de ces deux familles de copolymères. Le **Chapitre 5** sera quant à lui consacré à l'étude de la dégradation en conditions physiologiques de ces deux familles de copolymères. Les copolymères seront dégradés sous différentes formes (solution, films) et dans différentes conditions (pH 7.4 ou 5.5, incubation avec des enzymes). Une étude comparative avec les polyesters de référence (PLGA, PLA et PCL) sera également menée. Enfin, le **Chapitre 6** décrira la synthèse et l'évaluation biologique de prodrogues polymères dégradables obtenues à partir des deux familles de copolymères précédemment développées. Cette fois-ci, la polymérisation sera amorcée par une alcoxyamine fonctionnalisée avec la gemcitabine. Plus particulièrement, nous soulignerons l'influence : (i) de la nature de la liaison entre le copolymère et la gemcitabine ; (ii) de l'hydrophilie/hydrophobie de l'ester méthacrylique utilisé et (iii) du taux de MPDL incorporé dans le copolymère, sur le relargage du principe actif et sur la cytotoxicité in vitro. Pour finir, une **Discussion générale (Chapitre 7)** mettant en perspectives tous les travaux clôturera ce manuscrit.

Chapter 0

Context & Previous Works

I. Introduction

The design of advanced polymers intended for biomedical applications, such as drug delivery or tissue engineering, is still the focus of intensive research in both academia and industry. They should usually meet the following criteria: (i) biodegradability (mainly for administered materials) and biocompatibility (to avoid toxic side-effects); (ii) uniformity in polymer chain length and composition to ensure a reproducible behavior and biological response and, in some instances (iii) functionalizability with biologically active (macro)molecules (e.g., drugs, targeting ligands)^{1,2} and imaging probes³ for therapeutic and diagnostic/tracing purposes, respectively, together with (iv) stimuli-responsiveness to confer spatiotemporal drug release.⁴

Several key biocompatible and (bio)degradable copolymers such as aliphatic polyesters are extensively used, already commercially available and approved by the Food and Drug Administration (FDA) for use in Humans.^{5,6} It includes polylactide (PLA), poly(lactide-*co*-glycolide) (PLGA) and polycaprolactone (PCL) that are synthesized by ring-opening polymerization (ROP).⁷ Other (bio)degradable polymers also emerged as key players such as synthetic polypeptides,⁸⁻¹⁰ polyanhydrides,¹¹ poly(alkyl cyanoacrylates),¹² natural polysaccharides (e.g. chitosan, dextran),¹³ poly(ortho esters),^{14,15} polyamides, etc.⁶

However, in light of the literature, the most promising (bio)degradable polymers, such as aliphatic polyesters, poly(alkyl cyanoacrylate)s and synthetic polypeptides are generally obtained under stringent reaction conditions, exhibit rather limited diversity in terms of nature and composition, and are still difficult to functionalize,^{12,16-19} as multistep procedures with low yields are often witnessed. As for natural polysaccharides, post-modification is perhaps the only strategy that can be used to tune the materials structure and properties, which is somewhat limited and generally excludes the design of well-defined materials.

Conversely, vinyl polymers obtained by reversible deactivation radical polymerization (RDRP) techniques offers numerous advantages, including high degree of control (e.g., tunable molar mass, low dispersity, high chain-end fidelity, etc.) and functionalization to be reached, while maintaining the advantages of a free-radical mechanism (e.g., mild reaction

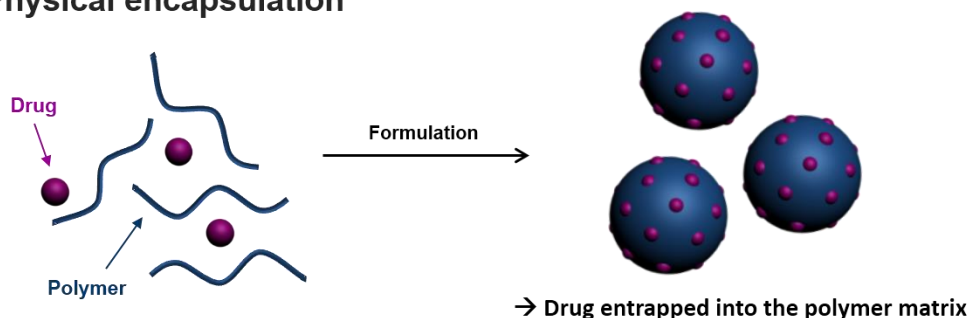
conditions, ease of use, applicability to a broad range of monomers, tolerance to numerous processes and water, etc.). The past few years have been marked by a surge in the design of innovative and more sophisticated vinyl materials especially intended for biomedical applications. However, despite significant advances from synthetic and conceptual points of view, the persistence and non-degradability of most of these materials may cause undesired toxicity and/or immune responses which still represents a major obstacle. Therefore, a great amount of work still need to be done to challenge key (bio)degradable polymers.

II. Polymer prodrug approach and drug-initiated strategy in cancer therapy

Cancer is a major public health problem worldwide and is the second leading cause of death worldwide, with approximately 10 millions new cases in 2012.²⁰ Current cancer treatments include surgical intervention, radiation and chemotherapeutic drugs, which also often kill healthy cells and cause toxicity to the patient. To deliver therapeutic agents to tumor cells in vivo, one must overcome the following problems: (i) drug resistance at the tumor level due to physiological barriers (non-cellular based mechanisms), (ii) drug resistance at the cellular level (cellular mechanisms), and (iii) distribution, biotransformation and clearance of anticancer drugs in the body. To circumvent these issues, drugs are physically encapsulated into nanoparticulate systems such as liposomes or polymer nanoparticles (NPs).^{21,22} These drug delivery nanocarriers are generally obtained from the encapsulation of a drug during the formulation of the nanocarrier, and offer the following advantages (Figure 1): (i) they protect healthy tissues from the drug's toxicity and protect the drug from early metabolization, thus increasing their circulation time; (ii) cancer cells can be more efficiently targeted, either by passive targeting by means of the so-called enhanced permeation and retention (EPR) effect,^{23,24} or through active targeting by surface functionalization with ligands whose receptors are overexpressed at the surface of cancer cells;² (iii) spatiotemporal drug release can be implemented by means of either exogenous (e.g., temperature, magnetic field, light) or endogenous (e.g., pH, enzymes, redox) stimuli⁴ and (iv) combining therapeutic and imaging agents within a single drug delivery system gives access to the so-called theranostic approach.³ However, important limitations still remain that could restrict their broad clinical translation, in particular: the “burst release” (a fast and uncontrolled release of a fraction of the drug post-administration) that can induce toxicity and the poor drug loadings (usually a

few percent), which necessitates the administration of a large amount of nanocarrier to expect a therapeutic effect.

(a) Physical encapsulation



(b) Chemical encapsulation: the prodrug approach

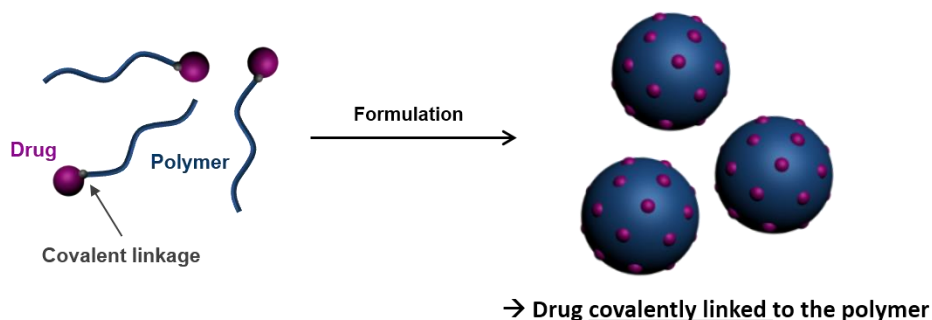


Figure 1. Design of polymer nanoparticles by the (a) physical encapsulation during the formulation and (b) chemical encapsulation (the prodrugs approach).

The prodrug approach, that relies on the covalent linkage between the drug and a polymer scaffold, represents a clever way to circumvent, or at least alleviate, these limitations (Figure 1b).^{1,25,26} For instance, given the drug must be cleaved off from the polymer to be active, the burst released is avoided.

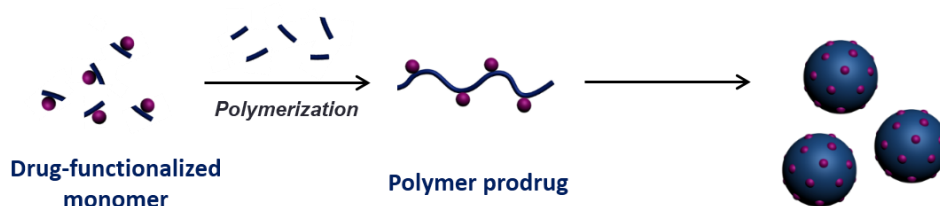
The most common strategies to synthesize polymer prodrugs is undoubtedly the “grafting to” approach (in analogy with macromolecular engineering). It consists in linking the drug to a preformed polymer (Figure 2a).^{16,27} Despite a few polymer–drug conjugates in clinical trials as anticancer agents,²⁸⁻³⁷ numerous protection/deprotection and purification steps to remove unreacted drug molecules and coupling agents are required and the high steric hindrance provided by the polymer chain and the proximity of the different functionalizable moieties prevents high coupling efficiency.^{25,26,36,38} Another interesting pathway, termed “grafting through”, relies on the synthesis of drug-bearing monomers, prior their

polymerization (Figure 2b).³⁹⁻⁴² Due to lower steric hindrance, this strategy usually leads to higher drug-loadings than the “grafting to” approach. Additionally, purification is facilitated as only unreacted drug-functionalized monomer needs be removed.

(a) “Grafting to” method



(b) “Grafting through” method



(c) “Grafting from” method (drug-initiated)

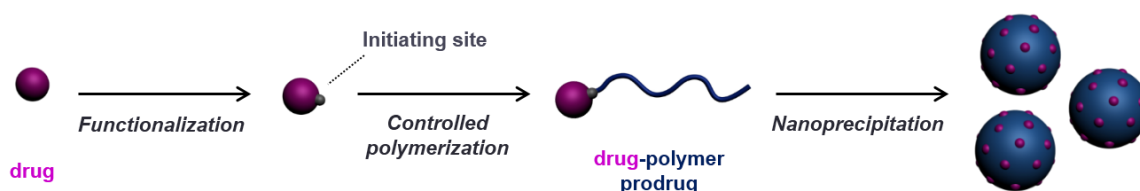


Figure 2. Design of polymer prodrugs by the (a) “grafting to” and (b) “grafting through” and (c) “drug-initiated” methods.

More recently, a new strategy, called “drug-initiated” (or “grafting from”), was developed and offered a new way to overcome the previously-mentioned limitations (Figure 2c).⁴³ This method relies on the controlled growth of short polymer chains from the drug. Consequently, the structure of the prodrug is well defined, with one drug molecule positioned at the extremity of each polymer chain. Thereby, purification is easy as only unreacted monomer has to be removed. Importantly, high drug-loadings can be obtained by targeting short polymer chains. Drug-initiated synthesis of polymer prodrugs can be achieved using native moieties of drugs, such as hydroxyl groups for ring-opening polymerization (ROP)^{44,45} or via drug functionalization with RDRP moieties, such as alkoxyamine for nitroxide-mediated polymerization (NMP)⁴⁶⁻⁴⁸ or chain transfer agent for reversible addition-fragmentation transfer (RAFT) polymerization.^{46,49,50} RDRP techniques offer the possibility to confer

attractive features to the resulting prodrugs such as: (i) a large variety of polymers in terms of nature and composition can be grown; (ii) depending on the nature of the polymer, either water-soluble prodrugs or self-assembled nanocarriers can be obtained without post-stabilization with additional surfactant; (iii) mild reaction conditions can be used because a radical mechanism is involved and (iv) *in vitro* and *in vivo* anticancer activity has already been reported.

INSERT 1: REVERSIBLE DEACTIVATION RADICAL POLYMERIZATION (RDRP) AND NITROXIDE-MEDIATED POLYMERIZATION (NMP)

Among various polymerization techniques, conventional free-radical polymerization is a simple polymerization technique, compatible with a broad range of vinyl monomers.⁵¹ However, the high reactivity and concentration of radical species induces rapid irreversible termination reactions leading to broad molar mass distributions and ill-defined polymers.

To obtain polymers with predictable molecular weight, well-defined architectures and low dispersity, RDRP techniques were developed since the 90's.⁵²⁻⁵⁴ To reduce the instantaneous radical concentration and thus the occurrence of irreversible termination reaction, RDRP mechanisms are governed by an activation-deactivation equilibrium based on the reversible inactivation of propagating (macro)radical into dormant specie (i.e., which cannot propagate). Ideal RDRP system should meet the following criteria:

- a linear evolution of $\ln[1/(1-\text{conversion})]$ with time, accounting for a constant concentration of propagating radicals;
- a linear increase of the number-average molar mass, M_n , with monomer conversion;
- low dispersity, M_w/M_n (\mathcal{D}), with M_w the weight-average molar mass;
- a quantitative α - and ω -functionalization;
- livingness; that is the possibility for polymer chains to grow again when additional monomer is introduced, allowing the synthesis of block copolymers.

Among the different RDRP techniques (Figure 3), nitroxide-mediated polymerization (NMP)⁵⁵ is perhaps the simplest one: its mechanism is governed by temperature and based on the reversible termination reaction between a propagating (macro)radical and a nitroxide (NO^\bullet radicals) acting as control agent, resulting in the formation of a dormant (macro)alkoxyamine. Given the activation-deactivation equilibrium is simply governed by a thermal process, which does not require the addition of catalyst, NMP is particularly

suitable for biomedical purposes.

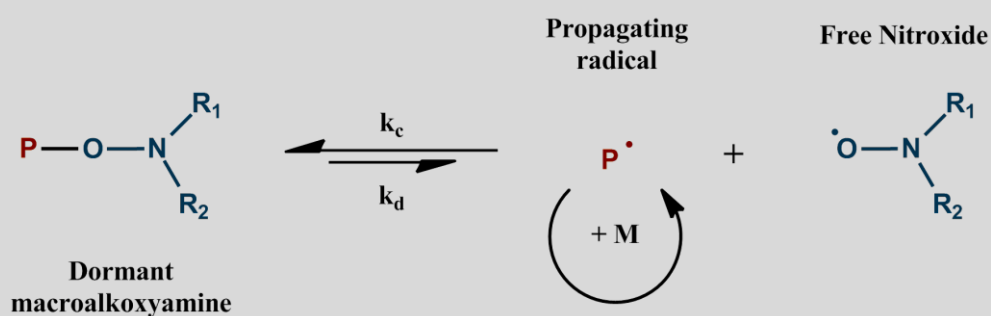


Figure 3. Activation-deactivation mechanism in nitroxide-mediated polymerization.

Initially, NMP was carried out using bicomponent initiating systems, composed of a conventional thermal initiator such as 2,2'-azobis(2-methylpropionitrile) (AIBN) and a stable free nitroxide such as 2,6,6-tetramethyl-1-piperidinyloxy (TEMPO, Figure 4a). Later, unimolecular initiation systems, called alkoxyamine, were developed as two-in-one molecules that thermally decompose into an initiating radical and the nitroxide. Experimentally, the control over molecular weight and dispersities was better than with bimolecular initiating systems. *N*-(2-methylpropyl)-*N*-(1-diethylphosphono-2,2-dimethylpropyl)-*O*-(2-carboxylprop-2-yl) hydroxylamine (BlocBuilder, Figure 4c), based on *N*-*tert*-butyl-*N*-[1-diethylphosphono-(2,2-dimethylpropyl)] (SG1, Figure 4b) nitroxide and developed by Arkema, represents one of the most potent alkoxyamine able to control the NMP of various vinyl monomer (styrenics, acrylates, dienes, *etc.*).

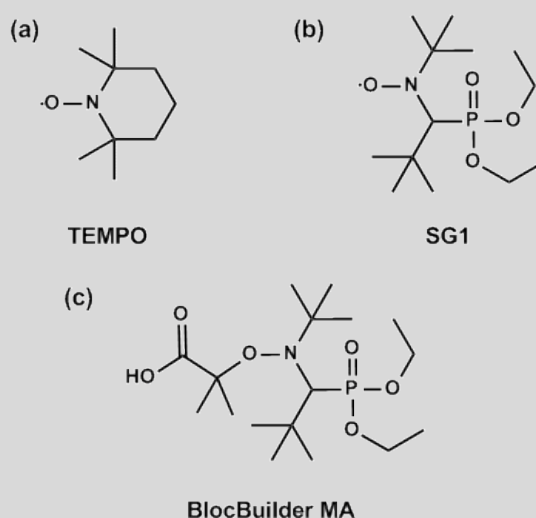


Figure 4. Representative nitroxides (a) TEMPO and (b) SG1, and alkoxyamine (c) BlocBuilder for NMP.

Nicolas and coworkers reported a new and versatile strategy for the synthesis of polymer prodrugs from the “drug-initiated” approach, relying on derivatization of anticancer drugs with SG1-based alkoxyamine to initiate the NMP of isoprene (I) leading to well-defined PI chains (Figure 5). PI was selected because isoprene is the basic structural motif of many naturally occurring and biocompatible polyisoprenoids (e.g., squalene, retinol, vitamin E, etc.). So short and well-defined PI was thought to be a good polymer candidate for biomedical applications. The first prodrugs synthesized were based on gemcitabine (Gem), an anticancer nucleoside analogue.⁴⁶ Supposedly due to the amphiphilic nature of the Gem-PI bioconjugates, they self-assembled in aqueous solution by nanoprecipitation to form very stable NPs of ~140 nm in diameter with high drug loadings, up to 30 %. Their anticancer activity was successfully demonstrated both in vitro on different cancer cells and in vivo in tumor-bearing mice.

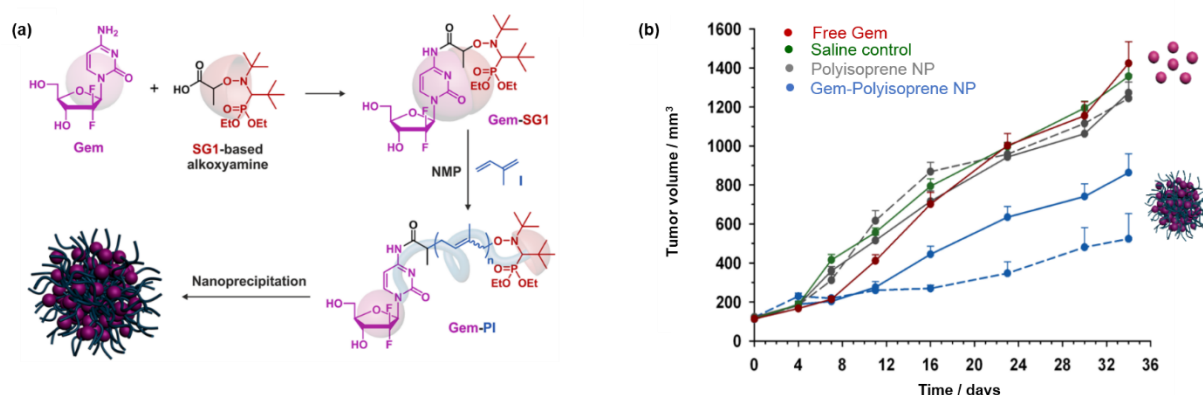


Figure 5. (a) Drug-initiated synthesis of polymer prodrug nanoparticles based on Gem and (b) in vivo anticancer activity.

More recently, this approach was extended to Cladribine (CdA), another chemotherapeutic (Figure 6).⁵⁶ In a similar way, short PI chains were grown from CdA-based alkoxyamines to yield two small libraries of well-defined CdA-PI conjugates, only differing in the nature of the linker between CdA and PI (either an ester bond or the diglycolate linker, Figure 6a). They both formed stable nanoparticles but exhibited significant differences in terms of drug release and anticancer activity. Because the diglycolate linker is more labile than a simple ester bond, the prodrugs containing the diglycolate linker gave greater CdA release kinetics (Figure 6b) and exhibited enhanced cytotoxicity in vitro (Figure 6c and 6d).

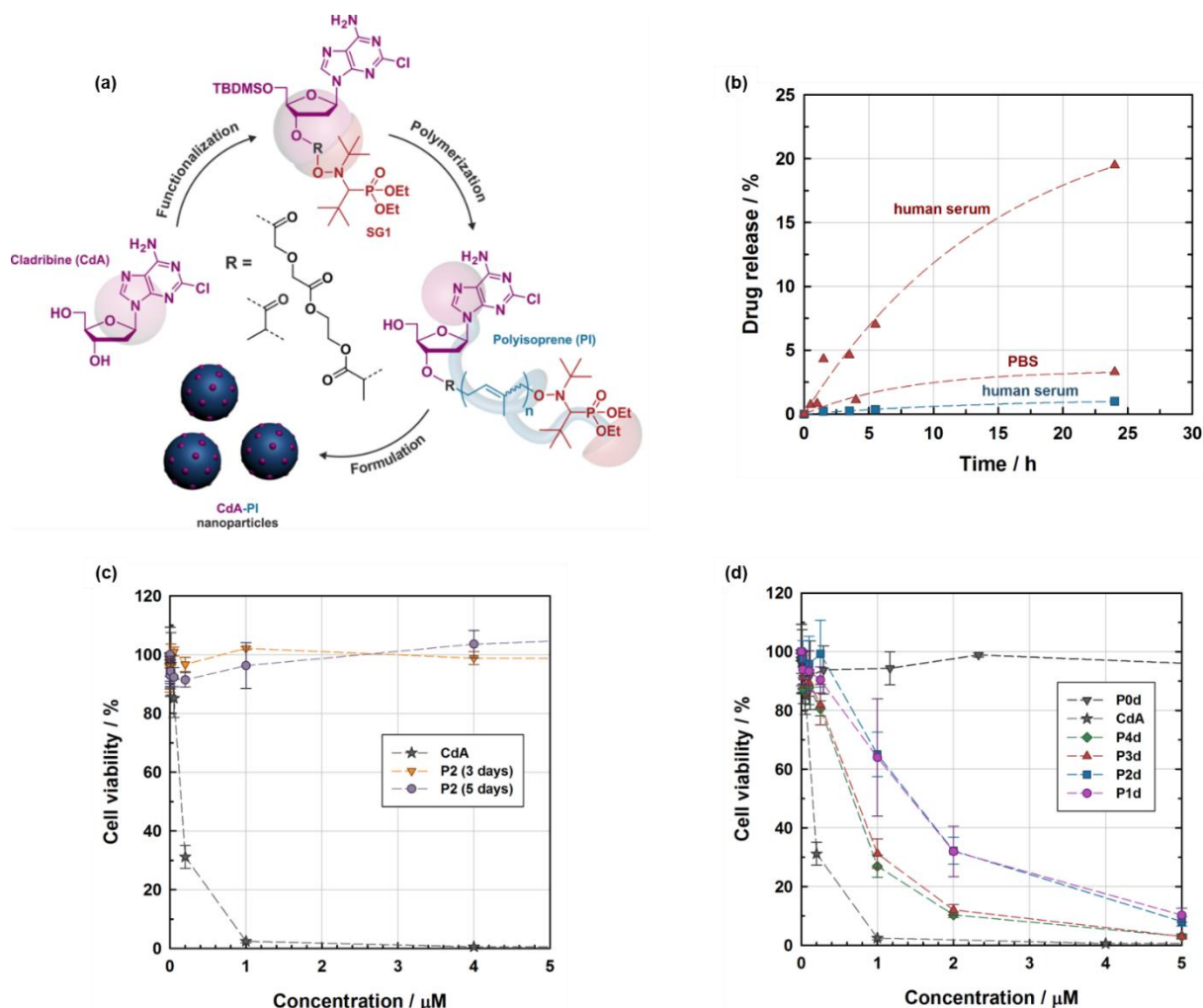


Figure 6. (a) Drug-initiated synthesis of polymer prodrug nanoparticles based on CdA with different CdA/polymer linkers, (b) CdA release profiles at 37 °C from CdA-PI nanoparticles (■) and from CdA-digly-PI nanoparticles (▲), (c) and (d) Viability assay (MTT test) on L1210 cells with increasing concentrations of (c) CdA-PI nanoparticles or (d) CdA-digly-PI nanoparticles.

The great versatility of the “*drug-initiated*” approach was further illustrated by the synthesis of fluorescent polymer nanoparticles for imaging purposes.⁴⁸ Short and well-defined PI chains were grown from an aggregation-induced emission (AIE) dye, Naphtalimide (Napht), whose feature is to be fluorescent under the aggregated state only (Figure 7a and 7b). This specificity could be useful to report additional information about the nanoparticle intracellular trafficking and integrity after cellular internalization. Mixed nanoparticles were even obtained by co-nanoprecipitation of Napht-PI with CdA-digly-PI, leading to sharp fluorescence signal allowing intracellular imaging (Figure 7c) together with in vitro cytotoxicity.

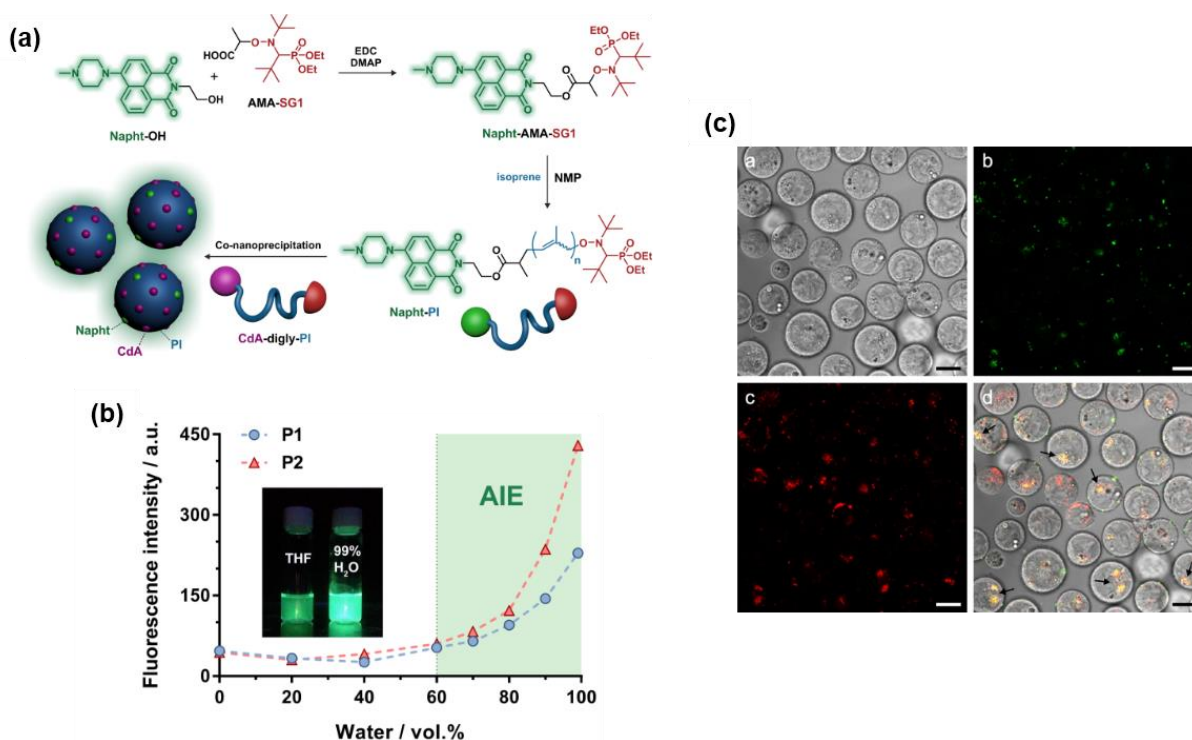


Figure 7. (a) Synthesis of Naphth-PI conjugate by NMP and its co-nanoprecipitation with cladribine-diglycolate-polyisoprene (CdA-digly-PI), (b) Evolution of the fluorescence intensity ($\lambda_{\text{ex}} = 420 \text{ nm}$) with the volume fraction of water in THF, (c) a) L1210 cells Normarski image b) and c) confocal microscopy images [green (Naphth, b), red (LysoTracker Red, c)] and d) merge of red and green fluorescence images with Nomarski image after a 24 h incubation of L1210 cells with AIE-active polymer prodrug nanoparticles. Scale bars = 20 μm . Arrows indicate colocalization.

In conclusion, this newly-developed “*drug-initiated*” method applied to vinyl polymers offers a robust, versatile and flexible tool for the synthesis of advanced polymer prodrug nanocarriers. Not only the synthesis of well-defined polymer prodrug nanoparticles with high drug loading is possible, but also the synthesis of fluorescent-labeled polymer-dye conjugates and their co-self-assembly with drug-polymer prodrugs to yield mixed nanocarriers for theranostic applications. Note that this technique was also extended to RAFT polymerization, with the synthesis of Gem-poly(squalenyl methacrylate) prodrugs.^{50,57}

However, despite these recent achievements, and as previously mentioned earlier in this section, the carbon-carbon backbone of vinyl polymers, such as PI, resists degradation. Therefore, even though the targeted M_n are usually rather short, employing these polymers (or others) as biomaterials, in particular when excretion of the foreign materials is desirable (such as for drug delivery systems), may cause prohibitive toxicity especially when repeated administration is envisioned (like in cancer therapy). Therefore, one of the aims of this PhD was to develop a new class of degradable prodrugs that fulfill the criteria required for

biomedical purposes while retaining the flexibility offered by vinyl polymerization. Therefore, the next section is intended to briefly cover the various techniques allowing to confer degradability to vinyl materials.

III. Degradable vinyl polymers

Conferring degradability to vinyl polymer requires introduction of labile group into their carbon-carbon polymer backbone. Numerous strategies have been elaborated, however, the level of degradation varies significantly from one technique to another.⁵⁸

For instance, the use of difunctional RDRP initiators containing a cleavable function enables insertion of a single degradable bond in the middle of the polymer chain, leading to an average decrease of M_n by half (Figure 8).⁵⁹ Among various difunctional, cleavable RDRP initiators, the most relevant ones for biological applications are those containing a disulfide bond (redox-cleavage by glutathione)⁶⁰ and an hemiacetal ester group (acid hydrolysis).⁶¹

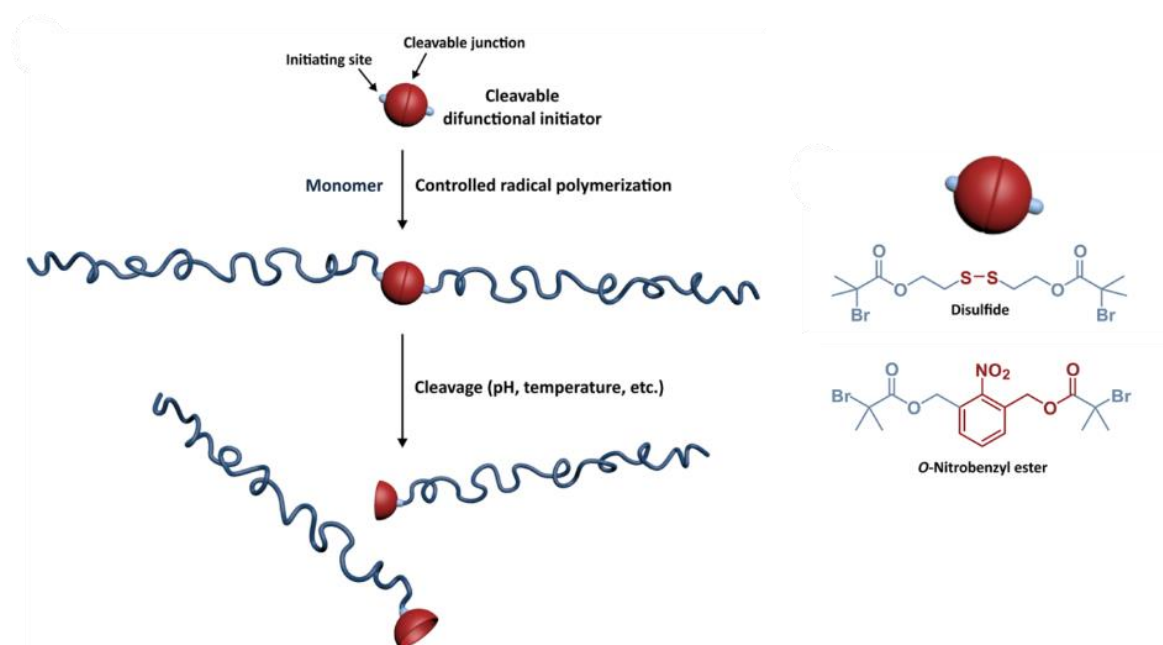


Figure 8. Cleavable difunctional initiators to prepare mid-chain degradable polymers.

To achieve extensive degradation, which could be more desirable for biomedical applications to facilitate excretion of degraded materials, multiple cleavable bonds can be introduced into the polymer backbone. One strategy is based on the coupling of short polymer chains via difunctional, cleavable linkers to yield multisegmented degradable polymers.⁶² For instance, α,ω -telechelic poly(*N*-(2-hydroxypropyl) methacrylamide) (PHPMA) chains prepared by

RAFT polymerization were further connected to each other by a difunctional and biodegradable peptide sequence (GFLG) via click chemistry and resulted in enzymatically degradable multisegmented PHPMA (Figure 9).^{63,64}

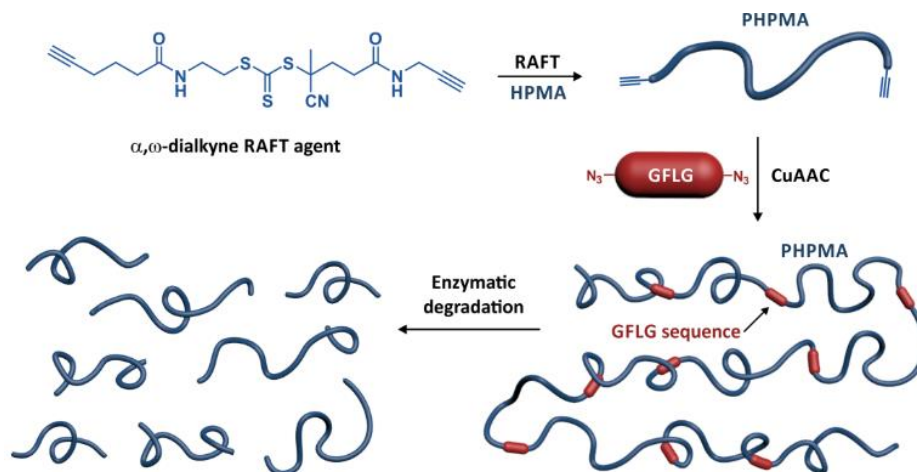


Figure 9. Multisegmented polymer comprising biodegradable sequences in the main chain.

However, the technique of choice, in terms of versatility and robustness, is undoubtedly the radical ring-opening polymerization (rROP) of cyclic monomers.⁶⁵ Cyclic monomers bearing vinyl or exomethylene group (for instance spiro ortho carbonates, cyclic acrylate, cyclic ketene acetals, etc.) are susceptible to polymerize by a radical pathway through a ring-opening mechanism.

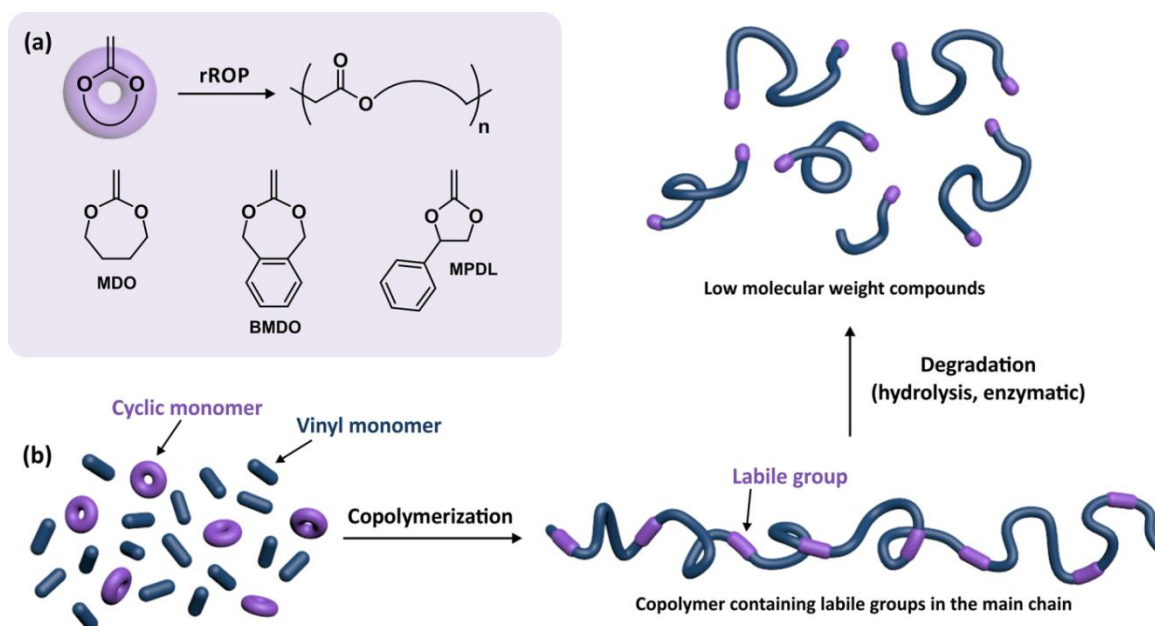


Figure 10. (a) Radical ring-opening polymerization (rROP) of cyclic ketene acetals⁶⁶ and structures of three representative CKAs (MDO, BMDO and MPDL). (b) Synthesis of

(bio)degradable polymers by radical copolymerization between a vinyl monomer and a cyclic monomer polymerizing by ring opening polymerization (rROP).

Among them, cyclic ketene acetals⁶⁶ are ester bond precursors reported by Bailey in the 80's. They have been extensively studied as suitable monomers for rROP.⁶⁷⁻⁶⁹ The most studied CKAs are 7-membered 2-methylene-1,3-dioxepane (MDO)⁶⁷ and 5,6-benzo-2-methylene-1,3-dioxepane (BMDO)⁶⁸ and, to a lesser extent, 5-membered 2-methylene-4-phenyl-1,3-dioxolane (MPDL)⁶⁹ (Figure 10a). The rROP of CKA proceeds in two steps: first, the radical addition onto the alkene moiety followed by the β -scission producing a cleavable ester function and an alkyl radical for subsequent radical polymerization (Figure 11).⁷⁰ However, radical addition can be followed by vinyl propagation, leading to ring retaining and an aliphatic carbon-based backbone. In that case, the resulting polymer is not degradable.

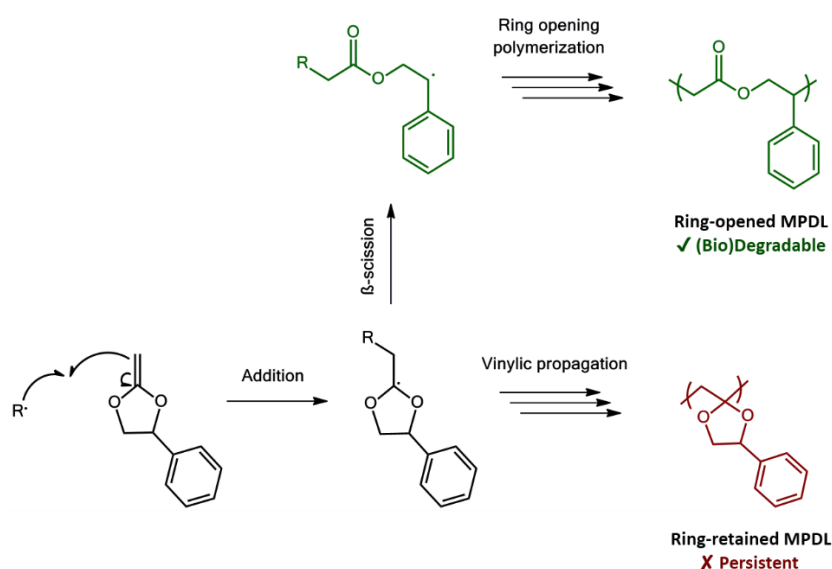


Figure 11. Mechanism of radical ring-opening polymerization (rROP) of cyclic ketene acetals (CKAs), applied to 2-methylene-4-phenyl-1,3-dioxolane (MPDL).

Since a few decades, copolymerization of CKA with traditional vinyl monomers is the focus of increasing attention for the design of degradable vinyl copolymers containing multiple ester functions in the main chain (Figure 10b). This technique combines the advantages of ROP, that is the introduction of heteroatom or functional group in the polymer main chain and of free-radical polymerization in terms of ease-of-use, flexibility and robustness. Mainly RAFT⁷¹⁻⁷³ and ATRP⁷⁴⁻⁷⁹ techniques were employed while only a few studies were devoted to NMP.

INSERT 2: NMP OF METHACRYLIC ESTER: A LONG-STANDING PROBLEM

NMP of methacrylic esters still represents an important challenge in macromolecular engineering. The activation-deactivation equilibrium of methacrylic esters is indeed strongly shifted toward the formation of propagating radicals, favoring the occurrence of irreversible reactions. Consequently, polymerization stops at low conversion and highly dispersed polymers with low molecular mass and poor living fractions are obtained.

A simple method to improve NMP of methacrylic esters consists in the addition of a small amount (typically < 10 mol.%) of a suitable controlling comonomer possessing favorable kinetic parameters (i.e., low activation-deactivation equilibrium constant, together with low cross-propagation rate constant). Nicolas and coworkers demonstrated that the SG1-mediated polymerization of methyl methacrylate (MMA) is well controlled when a small amount of styrene (S)⁸⁰⁻⁸² or acrylonitrile (AN)⁸³ (typically 2-9 mol.%) is introduced in the comonomer feed, enabling high conversion to be reached and narrowly dispersed polymers to be synthesized. In addition, chain end investigation by ³¹P NMR (using the phosphorous atom held by the SG1 nitroxide) revealed that the copolymer chains were predominantly terminated by a controlling comonomer unit, favoring the reversible deactivation of the propagating radical and therefore reducing the extent of irreversible reactions.⁸¹

A review (Guégain et al. *Macromol. Rapid. Commun.* 2015, 36, 1227) aiming at discussing the most successful strategies directed toward the control of methacrylic ester's NMP is presented in Chapter 1.

Recently, Delplace et al. reported on the preparation of degradable and comb-like PEG-based polymethacrylates by nitroxide-mediated radical ring-opening polymerization (NMrROP).⁸⁴ Copolymerizations of OEGMA with three different CKAs (MDO, BMDO or MPDL) and a small amount of AN (acting as “controlling comonomer” for NMP of methacrylic esters) were initiated by the BlocBuilder at 90 °C in toluene (Figure 12a). The addition of MDO and BMDO resulted in very slow and poorly controlled polymerization (almost inhibited as soon as one MDO/BMDO unit was inserted in the polymer likely because of the too strong MDO-/BMDO-SG1 bond). Conversely, the use of MPDL resulted in high monomer conversions and

copolymers with well-defined architecture and adjustable amount of ester groups in the main chain (7–29 %) (Figure 12b). Encouraging results suggesting appropriateness of these copolymers for biomedical applications were obtained: (i) they were completely degraded by hydrolysis under accelerated conditions (aqueous KOH 5%) (Figure 10c) and (ii) neither the copolymers nor their degradation products were cytotoxic against different cell lines (Figure 12d). The nature of the chain-end was also investigated by ^{31}P NMR and it was shown that copolymers were mainly terminated by a MPDL unit rather than AN unit, suggesting that MPDL could compete with AN for being the last monomer unit (Figure 13).⁸⁵ This raised a crucial question: is MPDL able to act as a controlling comonomer for the NMP of methacrylic esters?

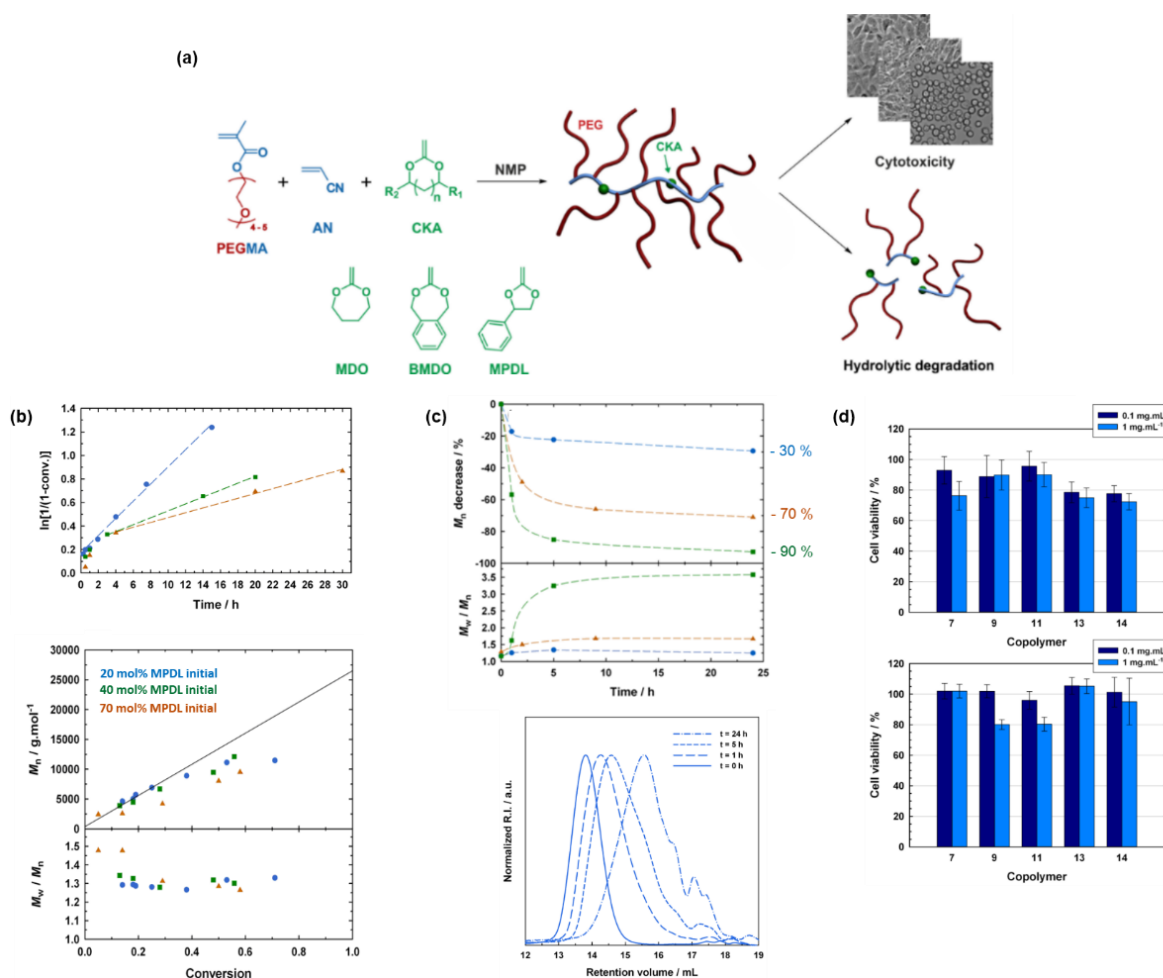


Figure 12. (a) PEG-based copolymers from NMrROP of OEGMA, AN and, (b) NMP of OEGMA, AN and MPDL, initiated by the BlocBuilder alkoxyamine, as a function of the MPDL initial amount in the feed ($f_{\text{MPDL},0}$): $\ln[1/(1 - \text{conv.})]$ vs. time (conv. = OEGMA conversion), and number-average molar mass, M_n and dispersity, M_w/M_n , vs conv.. The full line represents the theoretical M_n and the dashed ones represent the best fit of the linear domains. (c) Evolution of the number-average molar mass, M_n , and the dispersity, M_w/M_n , of

(P(OEGMA-*co*-AN-*co*-MPDL)) during degradation. And evolution of the SEC chromatograms at different time for $F_{\text{MPDL}} = 29\%$. (d) Representative cell viability (MTT assay) after incubation of J774.A1 cells and HUVEC cells with different CKA-containing copolymers. Results were expressed as percentages of absorption of treated cells (\pm SD) in comparison to that of untreated ones as a control.

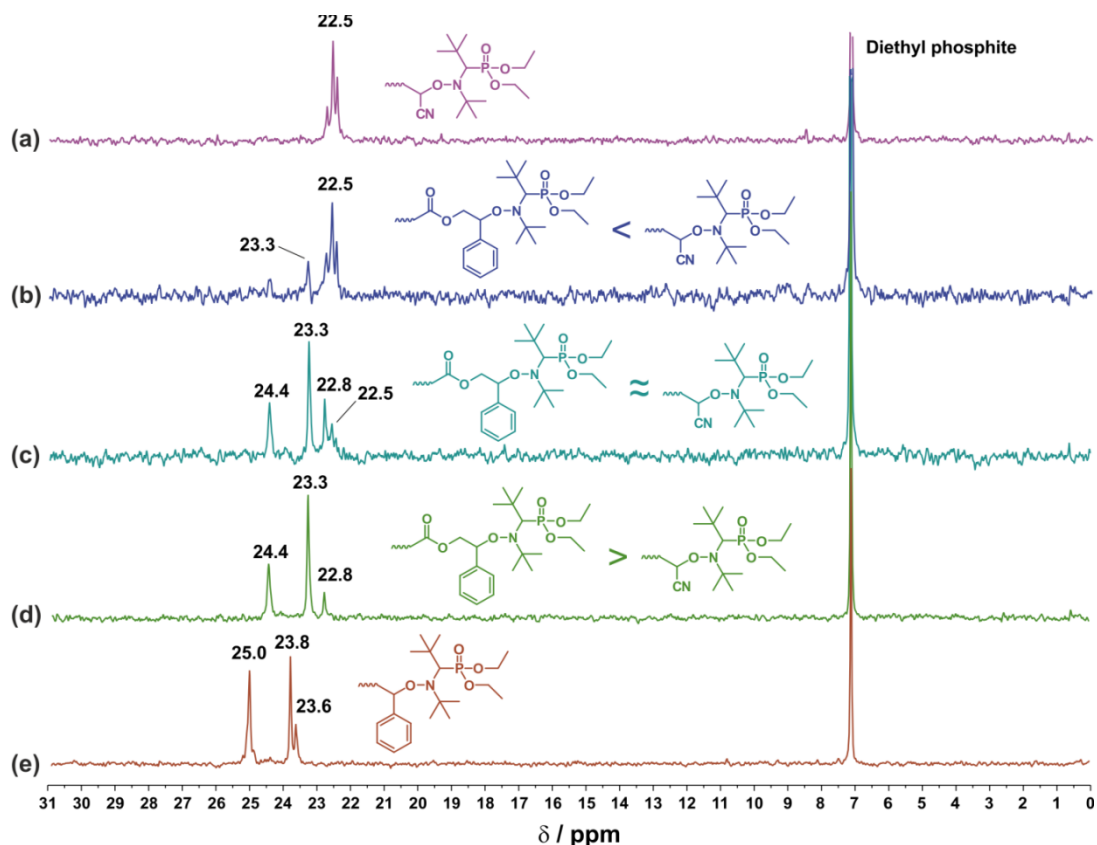


Figure 13. ^{31}P NMR spectra in CDCl_3 of: (a) P(OEGMA-*co*-AN)-SG1; (b) P(OEGMA-*co*-AN-*co*-MPDL)-SG1 ($f_{\text{MPDL},0} = 0.2$); (c) P(OEGMA-*co*-AN-*co*-MPDL)-SG1 ($f_{\text{MPDL},0} = 0.4$); (d) P(OEGMA-*co*-AN-*co*-MPDL)-SG1 ($f_{\text{MPDL},0} = 0.7$) and (e) PS-SG1.

The main aim of this thesis was to combine the best of two worlds for the design of degradable drug-initiated polymer prodrugs. In other words, the idea was to apply the drug-initiated method to rROP to grow a degradable vinyl polymer chain from a drug-bearing RDRP moiety. We will first investigate a new copolymerization system involving MPDL as the sole “controlling comonomer” during the NMrROP of different methacrylic esters (Chapter 3 & 4). Hydrolytic degradation of the resulting copolymers will then be thoroughly investigated under physiological conditions (Chapter 3) before the synthesis and biological evaluation of various polymer prodrugs synthesized by the “drug-initiated” method (Chapter 4).

References

- (1) Delplace, V.; Couvreur, P.; Nicolas, J. *Polym. Chem.* **2014**, *5*, 1529.
- (2) Nicolas, J.; Mura, S.; Brambilla, D.; Mackiewicz, N.; Couvreur, P. *Chem. Soc. Rev.* **2013**, *42*, 1147.
- (3) Mura, S.; Couvreur, P. *Adv. Drug Delivery Rev.* **2012**, *64*, 1394.
- (4) Mura, S.; Nicolas, J.; Couvreur, P. *Nat. Mater.* **2013**, *12*, 991.
- (5) Nair, L. S.; Laurencin, C. T. *Prog. Polym. Sci.* **2007**, *32*, 762.
- (6) Ulery, B. D.; Nair, L. S.; Laurencin, C. T. *J. Polym. Sci. Pol. Phys.* **2011**, *49*, 832.
- (7) Anderson, J. M.; Shive, M. S. *Adv. Drug Delivery Rev.* **2012**, *64*, 72.
- (8) Deming, T. J. *Chem. Rev.* **2015**, *116*, 786.
- (9) Deming, T. J. *Prog. Polym. Sci.* **2007**, *32*, 858.
- (10) Bae, Y.; Kataoka, K. *Adv. Drug Delivery Rev.* **2009**, *61*, 768.
- (11) Tamada, J.; Langer, R. *J. Biomater. Sci., Polym. Ed.* **1992**, *3*, 315.
- (12) Nicolas, J.; Couvreur, P. *Wiley Interdisciplinary Reviews: Nanomedicine and Nanobiotechnology* **2009**, *1*, 111.
- (13) Rinaudo, M. *Polym. Int.* **2008**, *57*, 397.
- (14) Sparer, R. V.; Chung, S.; Ringeisen, C. D.; Himmelstein, K. J. *J. Control. Rel.* **1984**, *1*, 23.
- (15) Solheim, E.; Sudmann, B.; Bang, G.; Sudmann, E. *J. Biomed. Mater. Res.* **2000**, *49*, 257.
- (16) Bae, Y.; Fukushima, S.; Harada, A.; Kataoka, K. *Angew. Chem., Int. Ed.* **2003**, *42*, 4640.
- (17) Zou, J.; Yu, Y.; Yu, L.; Li, Y.; Chen, C. K.; Cheng, C. *J. Polym. Sci. Pol. Chem.* **2012**, *50*, 142.
- (18) Yu, Y.; Zou, J.; Yu, L.; Ji, W.; Li, Y.; Law, W.-C.; Cheng, C. *Macromolecules* **2011**, *44*, 4793.
- (19) Nicolas, J.; Bensaid, F.; Desmaële, D.; Grogna, M.; Detrembleur, C.; Andrieux, K.; Couvreur, P. *Macromolecules* **2008**, *41*, 8418.
- (20) Ferlay, J.; Shin, H.; Bray, F.; Forman, D.; Mathers, C.; Parkin, D. 2012.
- (21) Elsabahy, M.; Wooley, K. L. *Chem. Soc. Rev.* **2012**, *41*, 2545.
- (22) Couvreur, P.; Vauthier, C. *Pharm. Res.* **2006**, *23*, 1417.
- (23) Torchilin, V. *Adv. Drug Delivery Rev.* **2011**, *63*, 131.
- (24) Fang, J.; Nakamura, H.; Maeda, H. *Adv. Drug Delivery Rev.* **2011**, *63*, 136.
- (25) Duncan, R. *Curr. Opin. Biotechnol.* **2011**, *22*, 492.
- (26) Duncan, R.; Vicent, M. J. *Adv. Drug Delivery Rev.* **2013**, *65*, 60.
- (27) Du, J.-Z.; Du, X.-J.; Mao, C.-Q.; Wang, J. *J. Am. Chem. Soc.* **2011**, *133*, 17560.
- (28) Duncan, R. *Adv. Drug Delivery Rev.* **2009**, *61*, 1131.
- (29) Pasut, G.; Veronese, F. M. *Adv. Drug Delivery Rev.* **2009**, *61*, 1177.
- (30) Langer, C. J.; O'Byrne, K. J.; Socinski, M. A.; Mikhailov, S. M.; Leśniewski-Kmak, K.; Smakal, M.; Ciuleanu, T. E.; Orlov, S. V.; Dediu, M.; Heigener, D. *Journal of Thoracic Oncology* **2008**, *3*, 623.
- (31) O'Brien, M. E.; Socinski, M. A.; Popovich, A. Y.; Bondarenko, I. N.; Tomova, A.; Bilynsky, B. T.; Hotko, Y. S.; Ganul, V. L.; Kostinsky, I. Y.; Eisenfeld, A. J. *Journal of Thoracic Oncology* **2008**, *3*, 728.
- (32) Homsí, J.; Simon, G. R.; Garrett, C. R.; Springett, G.; De Conti, R.; Chiappori, A. A.; Munster, P. N.; Burton, M. K.; Stromatt, S.; Allievi, C. *Clin. Cancer Res.* **2007**, *13*, 5855.
- (33) Vicent, M. J.; Duncan, R. *Trends Biotechnol.* **2006**, *24*, 39.

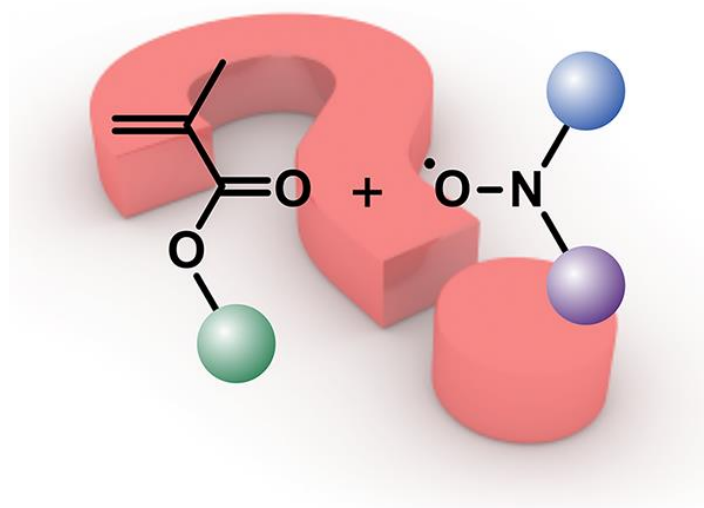
- (34) Springett, G.; Takimoto, C.; McNamara, M.; Doroshow, J.; Syed, S.; Eastham, E.; Spriggs, D.; Pezzulli, S.; Michelson, G.; Dupont, J. *J. Clin. Oncol.* **2004**, *22*, 3127.
- (35) Daud, A.; Garrett, C.; Simon, G.; Munster, P.; Sullivan, D.; Stromatt, S.; Allevi, C.; Bernareggi, B. *J. Clin. Oncol.* **2006**, *24*, 2015.
- (36) Seymour, L. W.; Ferry, D. R.; Kerr, D. J.; Rea, D.; Whitlock, M.; Poyner, R.; Boivin, C.; Hesslewood, S.; Twelves, C.; Blackie, R. *Int. J. Oncol.* **2009**, *34*, 1629.
- (37) Rademaker-Lakhai, J. M.; Terret, C.; Howell, S. B.; Baud, C. M.; de Boer, R. F.; Pluim, D.; Beijnen, J. H.; Schellens, J. H.; Droz, J.-P. *Clin. Cancer Res.* **2004**, *10*, 3386.
- (38) Duncan, R. *Nat. Rev. Cancer* **2006**, *6*.
- (39) Hu, X.; Hu, J.; Tian, J.; Ge, Z.; Zhang, G.; Luo, K.; Liu, S. *J. Am. Chem. Soc.* **2013**, *135*, 17617.
- (40) Hasegawa, U.; Van Der Vlies, A. J.; Wandrey, C.; Hubbell, J. A. *Biomacromolecules* **2013**, *14*, 3314.
- (41) Khan, A. R.; Magnusson, J. P.; Watson, S.; Grabowska, A. M.; Wilkinson, R. W.; Alexander, C.; Pritchard, D. *Polym. Chem.* **2014**, *5*, 5320.
- (42) Liu, J.; Liu, W.; Weitzhandler, I.; Bhattacharyya, J.; Li, X.; Wang, J.; Qi, Y.; Bhattacharjee, S.; Chilkoti, A. *Angew. Chem., Int. Ed.* **2015**, *54*, 1002.
- (43) Nicolas, J. *Chem. Mater.* **2016**, *28*, 1591.
- (44) Tong, R.; Cheng, J. *J. Am. Chem. Soc.* **2009**, *131*, 4744.
- (45) Tong, R.; Cheng, J. *Macromolecules* **2012**, *45*, 2225.
- (46) Harrisson, S.; Nicolas, J.; Maksimenko, A.; Bui, D. T.; Mougin, J.; Couvreur, P. *Angew. Chem., Int. Ed.* **2013**, *52*, 1678.
- (47) Bao, Y.; Boissenot, T.; Guégain, E.; Desmaële, D.; Mura, S.; Couvreur, P.; Nicolas, J. *Chem. Mater.* **2016**, *28*, 6266.
- (48) Bao, Y.; Guégain, E.; Nicolas, V.; Nicolas, J. *Chem. Commun.* **2017**.
- (49) Williams, C. C.; Thang, S. H.; Hantke, T.; Vogel, U.; Seeberger, P. H.; Tsanaktsidis, J.; Lepenies, B. *ChemMedChem* **2012**, *7*, 281.
- (50) Maksimenko, A.; Bui, D. T.; Desmaële, D.; Couvreur, P.; Nicolas, J. *Chem. Mater.* **2014**, *26*, 3606.
- (51) Matyjaszewski, K.; Davis, T. P. *Handbook of radical polymerization*; John Wiley & Sons, 2003.
- (52) Braunecker, W. A.; Matyjaszewski, K. *Prog. Polym. Sci.* **2007**, *32*, 93.
- (53) Jenkins, A. D.; Jones, R. G.; Moad, G. *Pure Appl. Chem.* **2009**, *82*, 483.
- (54) Matyjaszewski, K. *Prog. Polym. Sci.* **2005**, *30*, 858.
- (55) Nicolas, J.; Guillaneuf, Y.; Lefay, C.; Bertin, D.; Gimes, D.; Charleux, B. *Prog. Polym. Sci.* **2013**, *38*, 63.
- (56) Bao, Y.; Boissenot, T.; Guégain, E.; Desmaële, D.; Mura, S.; Couvreur, P.; Nicolas, J. *Chem. Mater.* **2016**.
- (57) Trung Bui, D.; Maksimenko, A.; Desmaële, D.; Harrisson, S.; Vauthier, C.; Couvreur, P.; Nicolas, J. *Biomacromolecules* **2013**, *14*, 2837.
- (58) Delplace, V.; Nicolas, J. *Nature Chem.* **2015**, *7*, 771.
- (59) Rikkou, M. D.; Patrickios, C. S. *Prog. Polym. Sci.* **2011**, *36*, 1079.
- (60) Tsarevsky, N. V.; Matyjaszewski, K. *Macromolecules* **2002**, *35*, 9009.
- (61) Rikkou-Kalourkoti, M.; Loizou, E.; Porcar, L.; Matyjaszewski, K.; Patrickios, C. S. *Polym. Chem.* **2012**, *3*, 105.
- (62) Zhang, L.-J.; Dong, B.-T.; Du, F.-S.; Li, Z.-C. *Macromolecules* **2012**, *45*, 8580.
- (63) Luo, K.; Yang, J.; Kopečková, P.; Kopeček, J. *Macromolecules* **2011**, *44*, 2481.
- (64) Pan, H.; Sima, M.; Miller, S. C.; Kopečková, P.; Yang, J.; Kopeček, J. *Biomaterials* **2013**, *34*, 6528.

- (65) Tardy, A.; Nicolas, J.; Gigmes, D.; Lefay, C.; Guillaneuf, Y. *Chem. Rev.* **2017**, *117*, 1319.
- (66) Kopčanský, P.; Tomašovičová, N.; Koneracka, M.; Timko, M.; Závašová, V.; Tomčo, L. *Acta Electrotechnica et Informatica* **2010**, *10*, 10.
- (67) Bailey, W. J.; Ni, Z.; Wu, S. R. *J. Polym. Sci. Pol. Chem.* **1982**, *20*, 3021.
- (68) Bailey, W. J.; Ni, Z.; Wu, S. R. *Macromolecules* **1982**, *15*, 711.
- (69) Bailey, W. J.; Wu, S. R.; Ni, Z. *Macromol. Chem. Phys.* **1982**, *183*, 1913.
- (70) Agarwal, S. *Polym. Chem.* **2010**, *1*, 953.
- (71) Hedir, G. G.; Bell, C. A.; Jeong, N. S.; Chapman, E.; Collins, I. R.; O'Reilly, R. K.; Dove, A. P. *Macromolecules* **2014**, *47*, 2847.
- (72) Kobben, S.; Ethirajan, A.; Junkers, T. *Journal of Polymer Science Part A: Polymer Chemistry* **2014**, *52*, 1633.
- (73) Ganda, S.; Jiang, Y.; Thomas, D. S.; Eliezar, J.; Stenzel, M. H. *Macromolecules* **2016**, *49*, 4136.
- (74) Huang, J.; Gil, R.; Matyjaszewski, K. *Polymer* **2005**, *46*, 11698.
- (75) Lutz, J.-F.; Andrieu, J.; Üzgün, S.; Rudolph, C.; Agarwal, S. *Macromolecules* **2007**, *40*, 8540.
- (76) Riachi, C.; Schüwer, N.; Klok, H.-A. *Macromolecules* **2009**, *42*, 8076.
- (77) Wickel, H.; Agarwal, S. *Macromolecules* **2003**, *36*, 6152.
- (78) Chung, I. S.; Matyjaszewski, K. *Macromolecules* **2003**, *36*, 2995.
- (79) Smith, Q.; Huang, J.; Matyjaszewski, K.; Loo, Y.-L. *Macromolecules* **2005**, *38*, 5581.
- (80) Charleux, B.; Nicolas, J.; Guerret, O. *Macromolecules* **2005**, *38*, 5485.
- (81) Nicolas, J.; Dire, C.; Mueller, L.; Belleney, J.; Charleux, B.; Marque, S. R.; Bertin, D.; Magnet, S.; Couvreur, L. *Macromolecules* **2006**, *39*, 8274.
- (82) Nicolas, J.; Mueller, L.; Dire, C.; Matyjaszewski, K.; Charleux, B. *Macromolecules* **2009**, *42*, 4470.
- (83) Nicolas, J.; Brusseau, S.; Charleux, B. *J. Polym. Sci. Pol. Chem.* **2010**, *48*, 34.
- (84) Delplace, V.; Tardy, A.; Harriison, S.; Mura, S.; Gigmes, D.; Guillaneuf, Y.; Nicolas, J. *Biomacromolecules* **2013**, *14*, 3769.
- (85) Delplace, V.; Harriison, S.; Tardy, A.; Gigmes, D.; Guillaneuf, Y.; Nicolas, J. *Macromol. Rapid Commun.* **2014**, *35*, 484.

Chapter 1

NMP of Methacrylic Esters: Insights and Solutions to a Long-Standing Problem

*Elise Guégain, Yohann Guillaneuf, Julien Nicolas**



Macromolecular rapid communications **2015**, 36 (13), 1227-1247

ABSTRACT

Nitroxide-mediated polymerization (NMP) is one of the most powerful reversible deactivation radical polymerization techniques and has incredibly gained in maturity and robustness over the last decades. However, among the different aspects of NMP that would benefit from some improvements certainly is the control of methacrylic esters. This family of monomers always represented an important challenge for NMP, despite the many different nitroxide structures that have been designed over the course of time. This review aims at presenting and discussing the most successful strategies directed toward the control by the NMP technique of methacrylic esters, and especially methyl methacrylate. NMP-derived materials comprising uncontrolled methacrylate segments will also be covered.

I. Introduction

Reversible deactivation radical polymerization (RDRP) techniques are widely-recognized as powerful and simple methods to prepare well-defined polymer architectures with high complexity and degree of functionalization.¹ Among RDRP methods developed so far, nitroxide-mediated polymerization (NMP),² atom-transfer radical polymerization (ATRP)^{3,4} and its derivatives,⁵⁻⁷ and reversible addition-fragmentation chain transfer polymerization (RAFT)^{8,9} are by far the most representative ones, although cobalt- and tellurium-mediated polymerizations have recently gained in popularity.¹⁰ Over the past few decades, a great deal of effort has been constantly devoted to their optimization and the discovery of new fields of application by pushing forward their boundaries.^{2,8,11,12} Each technique exhibits its own pros and cons; none of them being ideal and perfect.

In the case of NMP, early drawbacks mainly concerned the requirement for high temperatures (typically >120°C) and the applicability to a limited number of monomers; namely styrene and its derivatives.^{13,14} This was due to the inability of TEMPO (2,2,6,6-tetramethylpiperidiny-1-oxyl), the first and main nitroxide at that time, to perform at lower temperature and to control a broader range of monomers. Extensive structural variation of various cyclic nitroxides including TEMPO was then undertaken in order to modulate their controlling abilities.² However, the major breakthrough was witnessed with the development of acyclic and more active (the so-called second generation) nitroxides in particular based on 2,2,5-trimethyl-4-phenyl-3-azahexane-3-oxyl (TIPNO)¹⁵ and *N-tert-butyl-N*-[1-diethylphosphono-(2,2-dimethylpropyl)] nitroxide (SG1).¹⁶ Not only they extended the range of monomers to be successfully controlled to acrylates, acrylamides and dienes, but they also drastically reduced the polymerization temperature; typically down to 90°C.² The latter point was crucial as it enabled NMP to take place below 100°C and therefore to perform in aqueous dispersed media (e.g., emulsion, microemulsion, miniemulsion) under atmospheric pressure.¹⁷⁻¹⁹

Due to the great deal of work devoted to NMP in the past few years, this technique has incredibly gained in efficiency and robustness. This was illustrated by the various fields of application where NMP-derived materials have been successfully employed. This includes for instance additives,²⁰ nanoporous materials,²¹ bioconjugates,²² micro/optoelectronic devices²³ and electrolytes for lithium-metal batteries.²⁴ Yet, among the different aspects of NMP that would benefit from some improvements certainly is the control of methacrylic esters. This family of monomers, from which methyl methacrylate (MMA) was the most investigated,

always represented an important challenge for NMP. Briefly, the disproportionation reaction between TEMPO and the growing radical, which yields an alkene chain-end along with a hydroxylamine, dominates over the reversible combination with the nitroxide. Therefore, it prevents the polymerization to reach large conversions and to produce nitroxide-terminated polymers. With TIPNO and SG1, the activation-deactivation equilibrium strongly favors the production of propagating radicals, resulting in a high level of irreversible termination reactions by homotermination between propagating radicals but also, in the case of SG1, by β -hydrogen transfer from the propagating radical to the nitroxide.²⁵ Therefore, the polymerization rapidly stops and the formation of polymers with high dispersities and low molar masses is observed.

The NMP of methacrylic esters was therefore the focus of intensive research from both academia and industry. This review aims at presenting the different strategies directed toward the control by the NMP technique of MMA and other methacrylic esters. Some examples of NMP-derived materials comprising uncontrolled methacrylate segments will also be given, showing that a high quality of control is not systematically mandatory and mainly depends on the envisioned application.

II. NMP of MMA: why does it fail?

Early attempts concerning to perform NMP of methacrylic esters were reported by the CSIRO group in 1998.²⁶ The bulk polymerization of MMA was performed at 90 °C and mediated by several nitroxides (Figure 1). For all of them, the reaction stopped after about 1 h and the purified polymers exhibited an alkene chain-end. From low to moderate conversions were obtained (~10-40 %) with experimental M_n s close to the theoretical values, indicating an efficient initiation with no side-reaction creating new polymer chains. Although a higher activation-deactivation equilibrium constant, K , than that of S was determined from numerical simulations, the loss of control was assigned to the occurrence of disproportionation reactions, leading to methylene chain-ends.

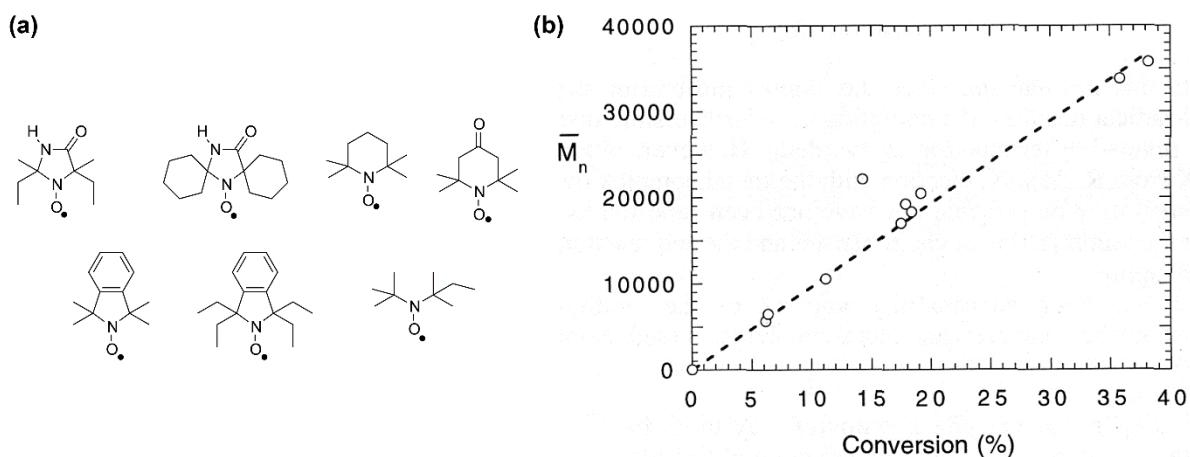


Figure 1. Structures of the different nitroxides used for the bulk polymerization of MMA at 90 °C initiated with azobis(2,4-dimethyl-2-pentanitrile) (a). Evolution of M_n vs MMA conversion plot for the different polymerizations (b). The dashed line indicates the theoretical M_n (the initiator efficiency is considered to be 90%). Reproduced with permission.²⁶ Copyright 1996, American Chemical Society.

With a n-butyl methacrylate (nBMA)/TEMPO system, it was later shown by Charleux and co-workers, by a combination of $^1\text{H-NMR}$ and MALDI-TOF, that the resulting PnBMA was quantitatively terminated by a methylene insaturation.²⁷ More importantly, this was not the result of conventional disproportionation reaction between two propagating radicals but essentially caused by β -hydrogen transfer from a propagating radical to TEMPO (also called disproportionation reaction), which represented the main chain-breaking event.

Two distinct disproportionation mechanisms can cause the formation of unsaturated macromonomer and hydroxylamine (Figure 2): (i) a regular radical disproportionation reaction (disproportionation reaction rate constant, k_{cD}) which competes with the cross-coupling (termination reaction rate constant, k_c), and (ii) a non-radical alkene elimination (disproportionation reaction rate constant by non-radical elimination, k_{dD}) that parallels the cleavage (dissociation rate constant, k_d).

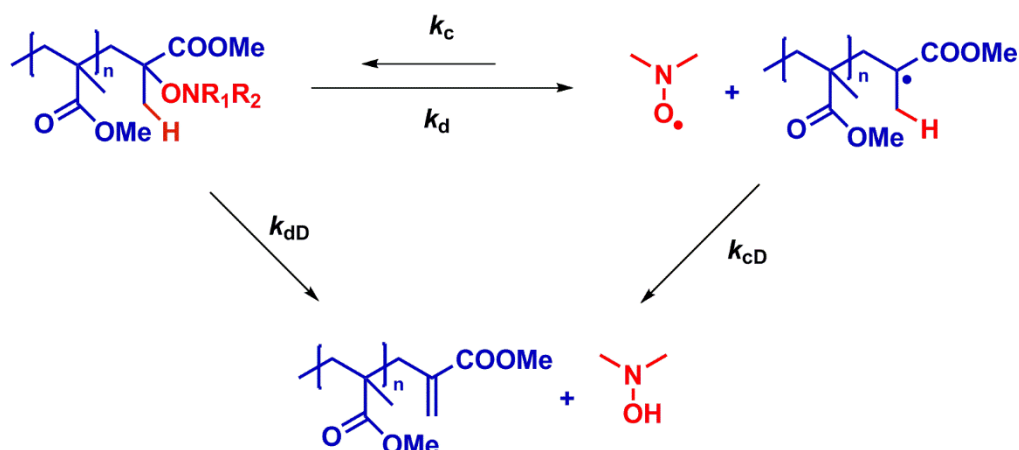


Figure 2. The two mechanisms of the disproportionation reaction for the NMP of methyl methacrylate.

However, the overall influence of the two modes of disproportionation has been predicted to be nearly macroscopically undistinguishable (Figure 3a).²⁸ In the absence of other sources of initiation, since the concentration of alkoxyamine functionality decreases with the occurrence of this side reaction, the monomer conversion ceases in both cases at a time corresponding to $2(k_d f_D)^{-1}$, where f_D is the fraction of disproportionation. The latter could be defined either by $f_D = k_{cD} / (k_{cD} + k_c)$ or by $f_D = k_{dD} / k_d$.

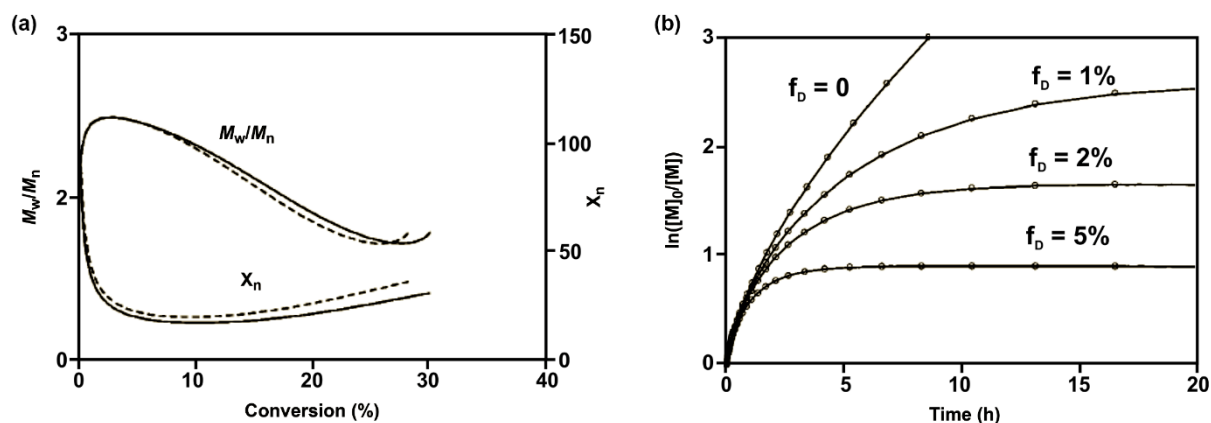


Figure 3. Evolution of the number-average degree of polymerization and the dispersity vs monomer conversion, computed including 20% of hydroxylamine and macromonomer formation during the cross-termination (solid line) or during alkoxyamine decomposition (broken line) (a). Evolution of $\ln([M]_0/[M])$ vs time for different fractions of disproportionation (b). Parameters for both figures: $k_d = 4.5 \times 10^{-3} \text{ s}^{-1}$, $k_t = 108 \text{ M}^{-1} \text{ s}^{-1}$, $k_c = 2.2 \times 10^7 \text{ M}^{-1} \text{ s}^{-1}$, $k_p = 5000 \text{ M}^{-1} \text{ s}^{-1}$, $[I]_0 = 10^{-1} \text{ M}$, and $[M]_0 = 10 \text{ M}$. Reproduced with permission.²⁸ Copyright 2001, American Chemical Society.

Note that even for relatively small values of f_D , the moment when the polymerization stops may occur long time before complete monomer conversion (eq. 1), with a concomitant increase of the dispersity.²⁸

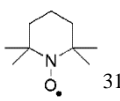
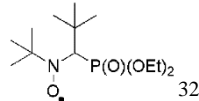
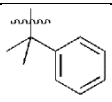
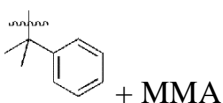
$$C_{max} = 1 - \exp\left(-\frac{3}{2}k_p\left(\frac{[R-Y]_0}{3f_D^2k_d(k_c+k_{cD})k_t}\right)^{1/3} \times F_\infty\right) \quad (1)$$

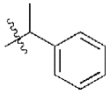
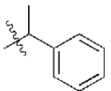
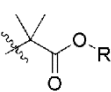
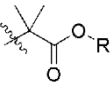
with $F_\infty = 2^{2/3}(\Gamma(2/3))/2/3\Gamma(1/3) \approx 1.08$

For example, using usual values of k_p , k_t , k_d and k_c , the maximum monomer conversion for $f_D = 1\%$, 2% and 5% is 93% , 81% and 59% , respectively (Figure 3b).

The disproportionation reaction during the homolysis of alkoxyamines has been studied experimentally on model systems. Priddy²⁹ and Fukuda³⁰ first investigated the decomposition of styryl-TEMPO as a model alkoxyamine and showed that disproportionation occurred to a very low extent with a probability factor of about 0.4% . In particular, they estimated the activation energy of the probability factor to be $29 \text{ kJ}\cdot\text{mol}^{-1}$. This study was further extended to others TEMPO-based alkoxyamines (e.g., cumyl, styryl, 1-*tert*-butoxy carbonyl-1methyl-ethyl, 1-*tert*-butoxy carbonyl-ethyl).³¹ It was demonstrated that alkene chain ends and TEMP-OH were formed by intermolecular disproportionation between the carbon-centered radicals and free TEMPO. Only the alkoxyamine with the 1-*tert*-butoxy carbonyl-ethyl moiety also gave substantial disproportionation via a non-radical elimination reaction. The fractions of disproportionation were also estimated by ^1H NMR analysis of the alkoxyamine decomposition in the presence or absence of S/MMA to produce *in situ* different macroradicals (Table 1).

Table 1. Fraction Of Disproportionation f_D Determined By ^1H NMR For Various TEMPO- And SG1-Based Alkoxyamines.

Alkyl fragment (a)	 31	 32
	0.6%	-
	20%	-

	0.8%	0%
 + MMA	20%	-
	2.2%	0%
 + MMA	20%	0%

^(a) MMA was added at 10-50 equiv. with respect to the alkoxyamine.

Styryl and cumyl alkyl fragments led to similar fractions of disproportionation (0.6%), whereas it reached 2.2% for the 1-*tert*-butoxy carbonyl-1-methyl-ethyl moiety, mimicking the methacrylate functionality. In the presence of MMA (leading to PMMA macroradicals), the occurrence of disproportionation reaction increased up to at least 20 %. This showed that steric substituent factors have a significant role and that disproportionation is favored if the reversible coupling leads to a sterically strained bond. A similar investigation was conducted with SG1-based alkoxyamines and showed that, conversely to TEMPO, there is little or no disproportionation of SG1 with both 1-ethoxy carbonyl-ethyl and styryl alkyl moieties.³² An upper limit of $f_D = 0.2\%$ for the SG1 nitroxide was estimated. Also, the occurrence of disproportionation reaction was not significantly affected by the presence of MMA (Table 1). A recent study based on the ^1H NMR analysis of the thermal decomposition of alkoxyamine in the presence and absence of thiophenol as a radical scavenger enabled to discriminate the two modes of disproportionation for various structures (Figure 4a).³³ The experiment performed with TEMPO-based alkoxyamines demonstrated that the disproportionation is an intermolecular process (Figure 4b and 4c) with $f_D = 3.5\%$, that is a k_{cD} value of $2.0 \times 10^7 \text{ M}^{-1} \text{ s}^{-1}$.

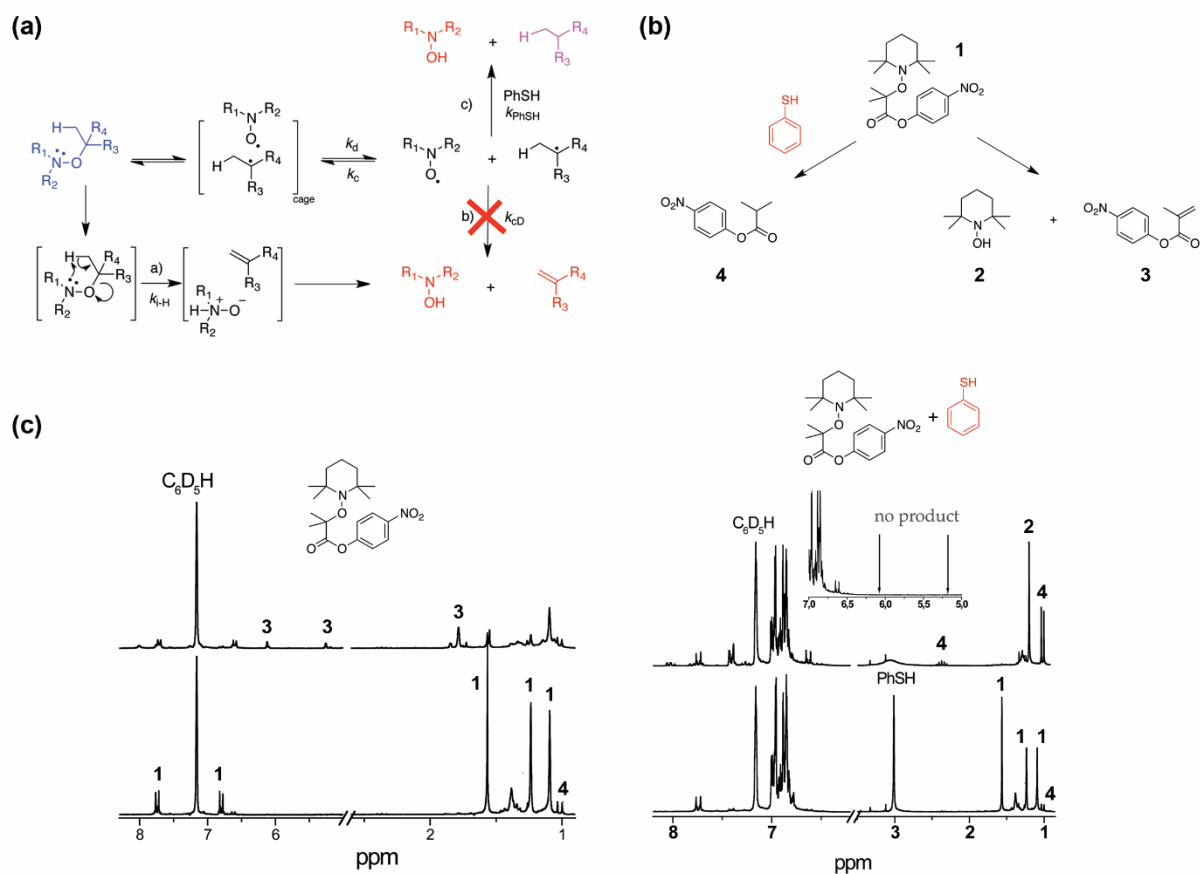


Figure 4. Intra-/inter-hydrogen transfer reaction during the thermal decomposition of alkoxyamines in the presence of thiophenol as scavenger (a). Decomposition pathway of 4-nitrophenyl 2-(2,2,6,6-tetramethylpiperidine-1-yloxy)-2-methylpropionate alkoxyamine (b). Comparison of ^1H NMR spectra before (lower spectra) and after (upper spectra) thermolysis of a 0.02 M solution of alkoxyamine 1 in benzene- d_6 in the presence of 0.24 M radical scavenger PhSH (right) and in its absence (left) at 351 K (c). Reproduced with permission.³³ Copyright 2008, Wiley.

The H-atom transfer reaction was also studied for a series of imidazoline-, imidazolidine-, and pyrrolidine-based alkoxyamines bearing the isobutyrate-2-yl moiety (Figure 5a).³⁴ Alkoxyamines based on cyclic nitroxides have recently been shown to be good model compounds for studying the influence of various substituents on the nitroxide. Depending of the nitroxide structure, both intra and inter, or inter only H-transfer reactions were observed.³⁴ However, they all gave a fraction of disproportionation higher than that of TEMPO, making them unable to control the polymerization of methacrylate derivatives.

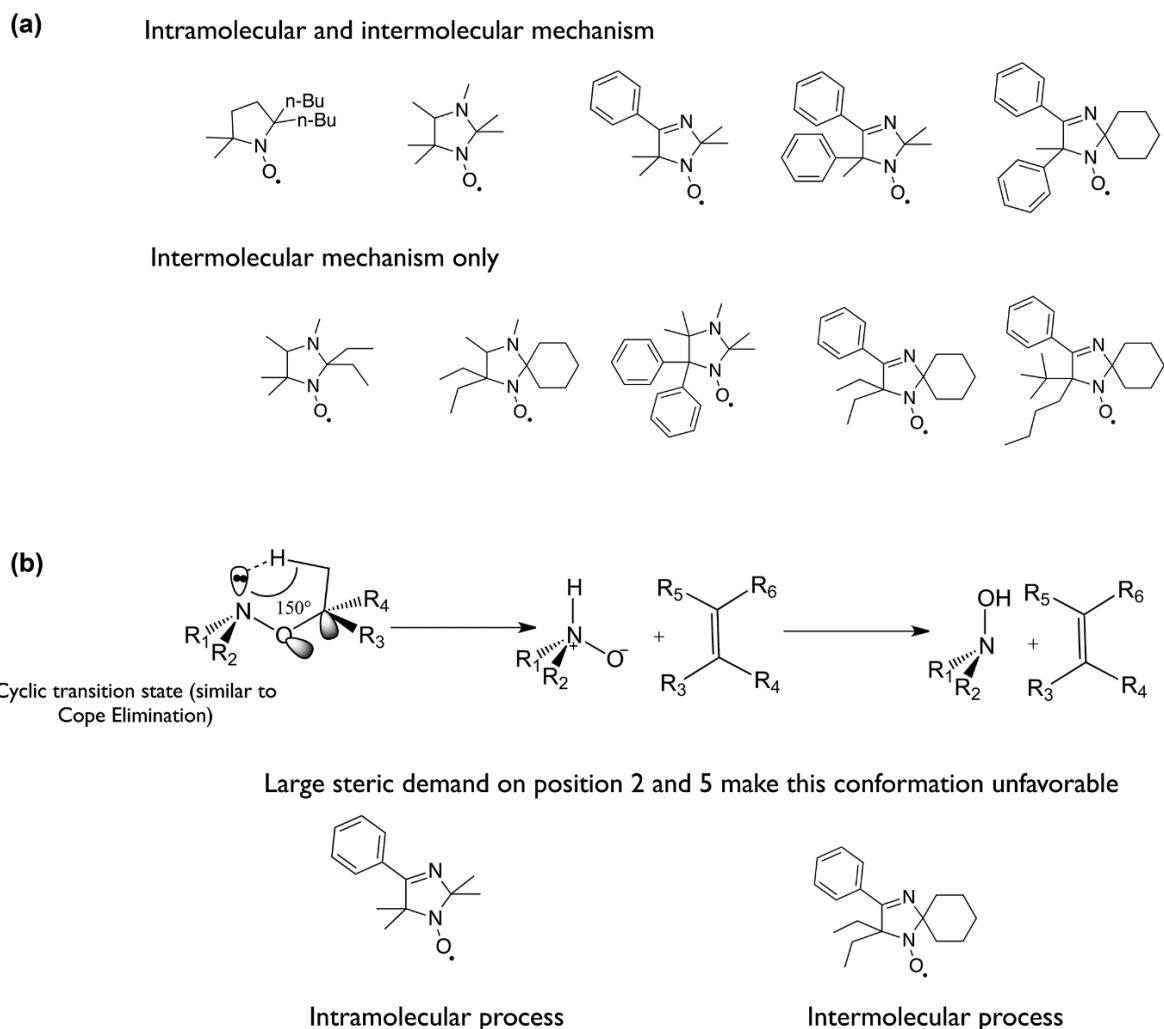


Figure 5. Structure of imizadoline-, imizadolidine- and pyrrolidine-based nitroxides whose disproportionation ratio were determined (a). Conformation of the transition state for the intramolecular H-transfer (b).

The intramolecular mechanism requires a cyclic transition state with a good overlapping of the nitrogen orbital n_{σ} and the antibonding orbital σ^* of the C-H bond (Figure 5b). This explains why the steric demand of the substituents at positions 2 and 5 of the nitroxide is the main parameter influencing the occurrence of this reaction. For instance, the less sterically hindered compound (with 4 methyl groups in position 2 and 5) led to intramolecular H-transfer as opposed to the highly sterically hindered one (with a cyclohexyl and two ethyl groups) (Figure 5b). Temperature dependence study of this reaction showed Arrhenius type behavior for k_{dD} with a frequency factor A close to 10^{15} s^{-1} and a high activation energy ($E_a \sim 140 \text{ kJ}\cdot\text{mol}^{-1}$). The latter value denotes a strong dependence on the temperature and a late transition state; thus indicating a non-favored reaction.

The occurrence of intramolecular H-atom transfer reaction in alkoxyamines is known to be governed by the activation energy of the homolytic dissociation but not by the nature of the nitroxide neither the geometry of the transition state.³⁵ Quantitatively speaking, such a reaction is highly probable for C–ON bond homolysis with $E_a > 125 \text{ kJ.mol}^{-1}$ and weakly probable for $E_a < 115 \text{ kJ.mol}^{-1}$.

As opposed to the intramolecular mechanism, the intermolecular H-atom transfer reaction requires a linear transition state between the aminoxyl group and the hydrogen. The reaction thus occurs with a very low activation barrier ($< 15 \text{ kJ.mol}^{-1}$) and rather high k_{cD} values. Similarly to k_c , k_{cD} decreased from 10^8 to $8 \times 10^6 \text{ M}^{-1} \text{ s}^{-1}$ with the increase of the bulkiness of the groups at positions 2 and 5 of the nitroxide. A thorough analysis of k_{cD} values also showed ring conformation effects (e.g., imidazolidine, imidazoline) balancing the steric effect of the groups flanking the aminoxyl moiety.³⁴

Early attempt to control the polymerization of MMA at $120 \text{ }^\circ\text{C}$ by the SG1 nitroxide under AIBN initiation was unsuccessful,³⁶ despite the absence of disproportionation from SG1 later reported by Fischer.³² Some improvements were however witnessed at $45 \text{ }^\circ\text{C}$ ³⁷ by using the highly labile BlocBuilder alkoxyamine,^{38,39} giving partial livingness at low monomer conversion ($< 15 \%$) and no disproportionation side products. Kinetic modeling using the PREDICI software showed good agreements with the kinetic and the molar mass evolutions with estimated k_d and k_c values of 10^{-2} s^{-1} and $1.4 \times 10^4 \text{ L mol}^{-1} \text{ s}^{-1}$, respectively. This gave an activation-deactivation equilibrium constant, K , of $7 \times 10^{-7} \text{ M}$ at $45 \text{ }^\circ\text{C}$. This is two order of magnitude higher than the one expected by Fischer⁴⁰ and is also higher than the upper limit K_{Max} ($K_{\text{Max}} = (k_p \times [I]_0) / (2 \times \ln(10) \times k_t) = 1.0 \times 10^{-7} \text{ M}$) that allowed for both a controlled and a living polymerization.⁴⁰ It thus prevents the nitroxide to recombine efficiently with the macroradicals and to avoid irreversible bimolecular terminations. In addition, a high concentration of SG1 in the medium is obtained, which slows down the decomposition of the BlocBuilder alkoxyamine without exerting any effect on the control and the livingness of the polymerization. Although k_d and k_c values were significantly different from the literature data, k_c was later found in good agreement with the value determined experimentally ($2.0 \times 10^4 \text{ L mol}^{-1} \text{ s}^{-1}$ at $35 \text{ }^\circ\text{C}$) using the RNR-PLP-SEC method.^{37,41}

The k_d value was estimated by modeling to be 35 fold higher than the model methyl 1-carbonyl-1-methyl-ethyl moiety.⁴² The penultimate effect, which is usually neglected, becomes very important when a bulky substituent (such as a tertiary alkyl group as employed here) is present and can drastically change the k_d value. Decomposition of alkoxyamines can be well-described by structure-reactivity relationships linking k_d to polar, stabilization and

steric parameters.⁴³ In the case of MMA and PMMA macroradicals, an increase of the steric constant resulted in a 35-fold increase in the value of k_d at 120 °C, in good agreement with the modeling study. Interestingly, the same trend was observed by Matyjaszewski for ATRP but to a lesser extent.⁴⁴ The effect of a bulky substituent (i.e., a tertiary alkyl group) in penultimate position of SG1-based alkoxyamines was later demonstrated on alkoxyamines that are 1,2 adducts of the BlocBuilder onto activated olefins.⁴⁵ The increase of the measured k_d values (~18 times increase between the styryl-SG1 and the corresponding 1,2 adduct) were in good agreement with the 35 times increase expected for a PMMA alkyl moiety (Figure 6).

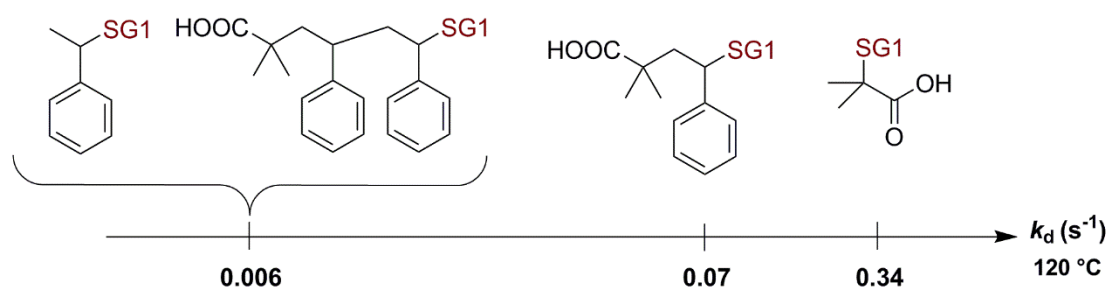


Figure 6. Influence of the penultimate unit on the k_d value of SG1-based alkoxyamines.

Considering the particular values of k_d and k_c , the SG1-mediated homopolymerization of MMA is expected to be unsuccessful. Further studies investigated the influence of excess SG1 or the alkoxyamine concentration on the control and the livingness.^{37,46} In particular, it was shown that intermolecular H-transfer from PMMA propagating radicals to the nitroxide played an important role at 110 °C as well as at 45 °C using a bicomponent system in the presence of a large excess of free SG1 (from 38 % to 315 %).⁴⁶ The use of a bicomponent initiating system may however not entirely reflect a polymerization that would have been initiated by an alkoxyamine insofar as the latter releases the nitroxide and the alkyl radical at the same rate. By a combination of ¹H NMR and MALDI-TOF, the rate constant of β -hydrogen transfer, $k_{\beta\text{Htr}}$, was estimated to be $1.69 \times 10^3 \text{ L mol}^{-1} \text{ s}^{-1}$ at 70 °C for the NMP of MMA initiated by the BlocBuilder alkoxyamine in the presence of excess SG1.²⁵ This corresponds to a fraction of disproportionation of 7.8 % with a $k_{\beta\text{Htr}}$ value three orders of magnitude lower than the one found for the *n*-butyl methacrylate/TEMPO system at 130 °C,²⁷ thus confirming a lower propensity of the SG1 nitroxide for hydrogen abstraction in comparison to TEMPO.

The thermal decomposition of SG1-based alkoxyamines bearing a tertiary alkyl moiety (i.e., alkyl carbonyl-1-methyl-ethyl derivatives) was also evaluated by ¹H NMR in the

presence or absence of radical scavenger.⁴⁷ In the absence of scavenger and in a “highly degassed solution” (e.g., 10^{-5} – 10^{-6} mbar), alkoxyamine decomposition proceeded with intramolecular H-transfer with $k_{cD} = 1.7 \times 10^3 \text{ L mol}^{-1} \text{ s}^{-1}$ at 75 °C, which is in good agreement with the value previously reported for PMMA macroradicals and SG1.²⁵ The fraction of disproportionation for the model alkoxyamine is thus close to 0.1 % since its k_c value is two orders of magnitude higher than the macroradical/SG1 pair. The role of residual oxygen was also examined by studying the decomposition of the same alkoxyamines in less-degassed solutions (i.e., 10^{-3} mbar), that would correspond to degassing performed by conventional oil pumps or by inert gas bubbling. It was found that the presence of residual oxygen affected the amount of alkene detected in the reaction products (25% with low vacuum vs 90% under high vacuum, see Figure 7b). Also, the starting alkoxyamine completely decomposed and the formation of a new phosphorus species were identified such as an ester derivative of the SG1 hydroxylamine (Figure 7a).

In summary, it can be concluded that the penultimate effect, which increases the decomposition rate constant and decreases the recombination rate constant, leads to an uncontrolled polymerization since K_{max} is not reached. It also leads to an increase f_D from 0.1 % to 7.8 %, above the $f_{D\text{max}}$ value of 3 %, also preventing the polymerization to be controlled.

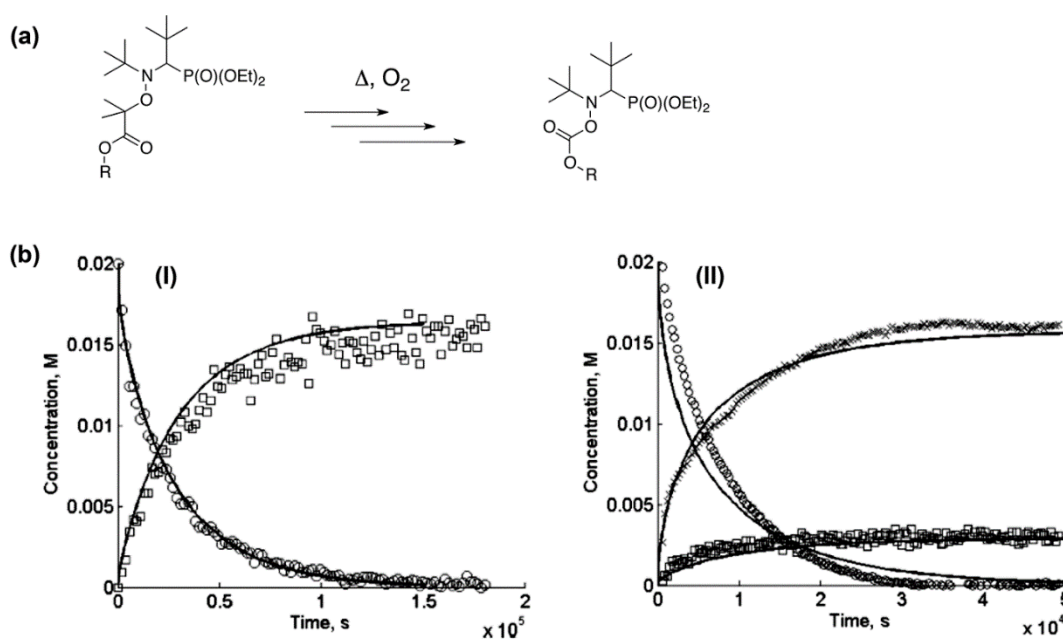


Figure 7. Mechanism of decomposition occurring during the thermolysis of alkyl carbonyl-1-methyl-ethyl SG1-based alkoxyamines with low vacuum degassing (a). Experimental (symbols) and calculated (full line) kinetics for decomposition of the methyl carbonyl-1-methyl-ethyl-SG1 alkoxyamine in the absence of scavenger for solution degassed under high

vacuum (I) and for poorly degassed solution ³⁰: (o) alkoxyamine, (□) alkene, (+) oxygen product (b). Reproduced with permission.⁴⁷ Copyright 2013, Wiley.

III. Use of additives

Some research was focused on the use of additives to decrease the occurrence of β -hydrogen transfer for the TEMPO-mediated polymerization of MMA. In this context, acid-catalyzed conditions have been investigated.⁴⁸⁻⁵⁰ Broadly speaking, the polymerization rate is increased and the activation-deactivation equilibrium rate constant is significantly shifted towards the formation of propagating radicals, via protonation of TEMPO into the corresponding hydroxylamine. It therefore prevents the extensive occurrence of β -hydrogen transfer and helps reaching higher molar masses. From the mechanistic point of view (Figure 8), a nitroxide is protonated to form a radical cation, which further reacts with another nitroxide to form the corresponding hydroxylamine and an oxoammonium derivative (the latter is then reduced by traces of water from the medium into another hydroxylamine molecule).

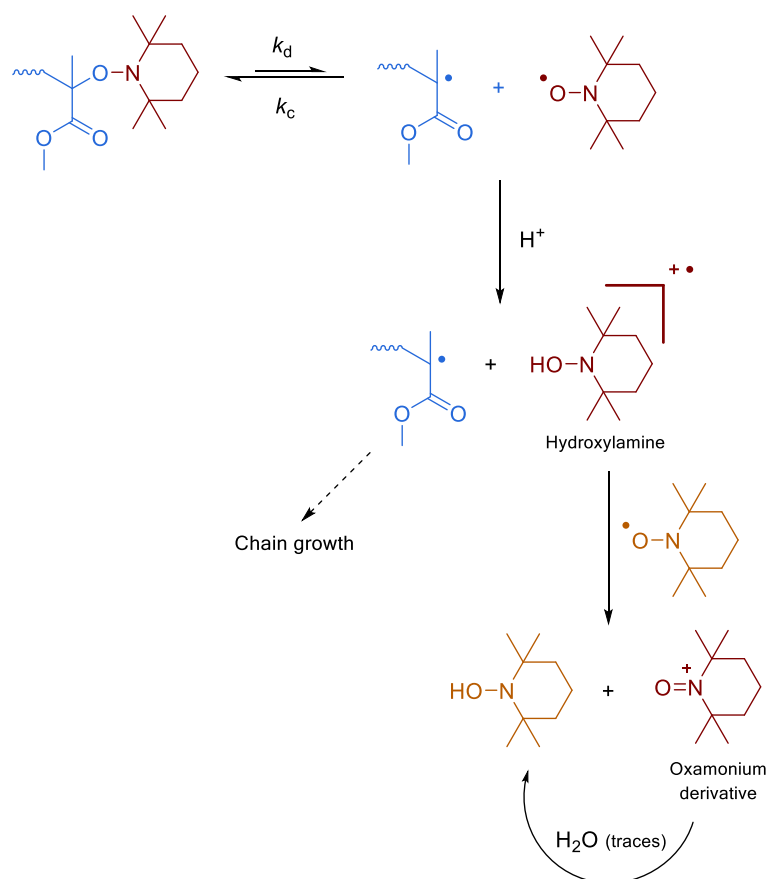


Figure 8. Mechanism of the acid effect and β -hydrogen transfer for the TEMPO-mediated polymerization of methyl methacrylate.

The efficiency of this approach mainly depends on the protonic acidity of the additive. Nitroxides are weakly basic and are therefore easily protonated by strong acids such as camphorsulfonic acid (CSA)⁴⁸ or sulfuric acid (H₂SO₄).^{49,50} When CSA was added equimolarly to TEMPO, the polymerization was indeed accelerated (40% monomer conversion after 2 h) and led to high molar mass (44 000 g.mol⁻¹), but a high dispersity ($\mathcal{D} = 2.5$) was obtained.⁴⁸ With a smaller amount of CSA, the polymerizations did not start or proceeded in an even more uncontrolled fashion. H₂SO₄ is a stronger acid than CSA due to its two available protons. The protonation of TEMPO was therefore more efficient and the polymerizations were better controlled. For instance, using a bicomponent system (AIBN/TEMPO) at 70 °C and 5.8 mol.% of H₂SO₄, > 90% monomer conversion were obtained after 16 h with low dispersities (~1.1–1.3). The livingness of the polymer was confirmed by conducting the polymerization of S from a PMMA macroinitiator.⁵¹ Other catalysts such as Lewis acids (ZnCl₂) or ferrous ammonium sulfate were also investigated to promote the polymerization of methacrylate derivatives but the polymerization remained uncontrolled.⁵¹

Interestingly, a similar beneficial effect of the acidity on the occurrence of β -hydrogen transfer reaction was also observed directly by using the BlocBuilder alkoxyamine whose structure comprises a carboxylic acid.⁴⁷

IV. The copolymerization approach

A straightforward approach to control the NMP of methacrylic esters is to copolymerize them with easy-to-control comonomers (e.g., S). Hawker and co-workers investigated the copolymerization of MMA in the presence of variable initial molar fractions (f_{S0}) of S (i.e., from 30 to 90 mol.%) using a styryl-TEMPO-based alkoxyamine.⁵² The quality of control was greatly influenced by the initial amount of S. As expected, the higher f_{S0} , the better the control, with a minimum of 50 mol.% of S to obtain a dispersity of about 1.5. For lower f_{S0} , predominance of terminations by H transfer led to broader molar mass distributions (e.g., \mathcal{D} was 1.67 for $f_{S0} = 30$ mol.%). A similar copolymerization approach was also conducted from a styryl-TIPNO alkoxyamine.¹⁵ For a given f_{S0} , it resulted in a substantially better control than the one obtained from styryl-TEMPO, especially for f_{S0} values lower than 60 mol.%.

This was only 6 years later that the benefits provided by the copolymerization approach by NMP between MMA and S was fully rationalized from a kinetics point of view and drastically improved. Charleux and co-workers established the theoretical expression of

the average activation-deactivation equilibrium constant, $\langle K \rangle$, and its product with the average propagation rate constant, $\langle k_p \rangle \langle K \rangle$, that is a direct function of the slope of $\ln[1/(1-\text{conv})]$.⁵³ Both the terminal model (TM) and the implicit penultimate unit effect model (IPUE) have been considered for the propagation reaction $\langle k_p \rangle$, whereas the activation–deactivation equilibrium constant was supposed to depend only on the terminal monomer unit. Using the TM, $\langle K \rangle$ can be described by eq. 2 and the product $\langle K \rangle \langle k_p \rangle$ by eq. 3.

$$\langle K \rangle = -\frac{(r_A f_A / k_{p,A}) + (r_B f_B / k_{p,B})}{(r_A f_A / k_{p,A} K_A) + (r_B f_B / k_{p,B} K_B)} \quad (2)$$

$$\langle k_p \rangle \langle K \rangle = \frac{r_A f_A^2 + 2f_A f_B + r_B f_B^2}{(r_A f_A / k_{p,A} K_A) + (r_B f_B / k_{p,B} K_B)} \quad (3)$$

In these equations, r_A and r_B are the reactivity ratios defined by $r_A = k_{p,A}/k_{AB}$ and $r_B = k_{p,B}/k_{BA}$, where $k_{p,A}$ and $k_{p,B}$ are the homopropagation rate constants, k_{AB} and k_{BA} are the cross-propagation rate constants and f_A and f_B are the molar fraction of A and B in the initial comonomer mixture.

Using the IPUE model, eqs. 2 and 3 are still valid, by replacing $k_{p,A}$ and $k_{p,B}$ by eqs. 4 and 5.

$$\overline{k_{p,A}} = k_{p,A} \frac{r_A f_A + f_B}{r_A f_A + (f_B/s_A)} \quad (4)$$

$$\overline{k_{p,B}} = k_{p,B} \frac{r_B f_B + f_A}{r_B f_B + (f_A/s_B)} \quad (5)$$

In eqs. 4 and 5, s_A and s_B are the radical reactivity ratios given by $s_A = k_{BAA}/k_{AAA}$ and $s_B = k_{ABB}/k_{BBB}$ where $k_{AAA} = k_{p,A}$ and $k_{BBB} = k_{p,B}$ are the homopropagation rate constants and the other rate constants, k_{BAA} and k_{ABB} , correspond to the propagation reactions.

Eq. 2 presents interesting features. Not only $\langle K \rangle$ depends on the individual activation-deactivation equilibrium constants (K_A and K_B) but also on the cross-propagation rate constants expressed by the ratio of the homopropagation rate constant over the corresponding monomer reactivity ratio. Additionally, it is a function of the comonomer mixture composition (f_A and f_B). Since f_A and f_B continuously change during the copolymerization, so does $\langle K \rangle$. This is important as a slow cross-propagation of the comonomer-based macroradical will ensure a longer lifetime, which will favor its efficient deactivation by the

nitroxide. As a consequence, in the context of MMA copolymerization, a small amount of a comonomer with a much smaller K than the one of MMA, together with a low k_p induces a dramatic decrease of $\langle K \rangle$. In turns, this has the consequence of reducing the instantaneous concentration of propagating radicals and hence decreasing the contribution of the irreversible termination. By using appropriate kinetic parameters, it was predicted that S, which satisfies the above-mentioned criteria, would be a suitable comonomer for the NMP of MMA (Figure 9). Above 3–4 mol%, the value of $\langle K \rangle$ is closed to that for S homopolymerization. Then, at best, the system should provide the same quality of control than for the SG1-mediated homopolymerization of S.

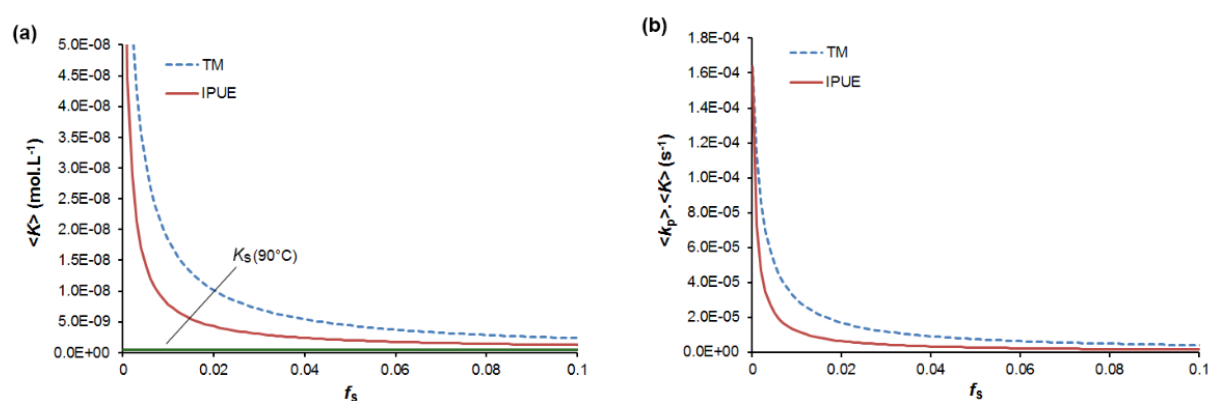


Figure 9. Predicted values of the average activation-deactivation equilibrium constant $\langle K \rangle$ (a) and of $\langle k_p \rangle \langle K \rangle$ (b) as function of the molar fraction of styrene in the copolymerization mixture (f_s), for the copolymerization of methyl methacrylate and styrene at 90°C, using either the terminal model (TM) or the implicit penultimate unit effect model (IPUE). Reproduced with permission.⁵³ Copyright 2005, American Chemical Society.

This has been experimentally demonstrated by performing the NMP of MMA at 90°C in the presence of very small amounts of S as a comonomer; typically $f_{S0} = 2.2$ –8.8% (Figure 10).^{53,54} To ensure fast and quantitative initiation, the BlocBuilder SG1-based alkoxyamine was used and 10 mol.% of free SG1 were added to reduce initial irreversible termination reactions. Whereas when no S is added in the monomer feed the polymerization rapidly stops in agreement with expectations, already 2.2 mol.% of S had a dramatic impact on the copolymerization reaction. It led to a progressive increase of monomer conversion with time and a linear evolution of M_n with monomer conversion and lower \mathcal{D} of about 1.4 at best (typically 40–50% monomer conversion). With 4.4 mol.% of S, the copolymerizations were

nearly ideal with first order kinetics, linear evolution of M_n with conversion and decreasing dispersities reaching low values of about 1.3.

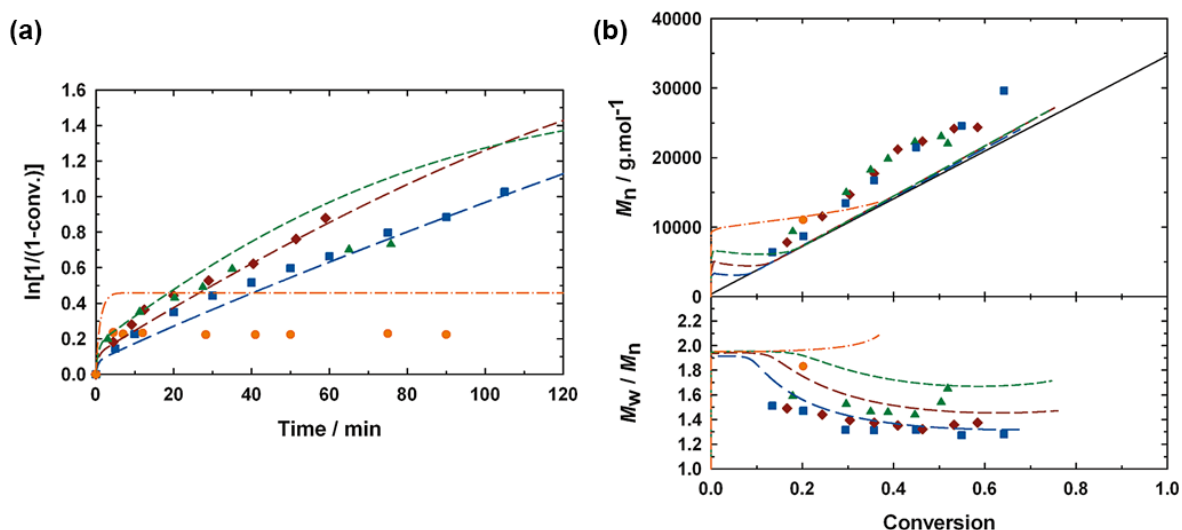


Figure 10. SG1-mediated bulk polymerization of methyl methacrylate initiated by the BlocBuilder alkoxyamine at 90 °C with 10 mol % of free SG1 as a function of the initial amount of styrene: ■, $f_{S0} = 0.088$; ◆, $f_{S0} = 0.044$; ▲, $f_{S0} = 0.022$; ●, $f_{S0} = 0$. (a) $\ln[1/(1 - \text{conv.})]$ vs time; (b) number average molar mass, M_n , and dispersity, M_w/M_n , vs conversion; the dotted-lines correspond to the modeling studies and the full line represents the theoretical M_n . Reproduced with permission.⁵⁴ Copyright 2009, American Chemical Society.

By a combination of electron spin resonance (ESR) and ^{31}P NMR, it was shown that the resulting P(MMA-*co*-S) copolymers ($f_{S0} = 0.088$) exhibited high living chain fractions (~90%) and that a vast majority of the chain-end structures exhibited a MMA-S-SG1 sequence.⁵⁵ Well-defined diblock copolymers were also reported using P(MMA-*co*-S)-SG1 macroinitiators. As S promoted the reversible deactivation of the propagating radicals by the SG1 nitroxide, side reactions were decreased. Moreover, incorporation of S as an isolated terminal unit in conjunction with the steric effect of the penultimate MMA unit resulted in MMA-S-SG1 macroalkoxyamine able to dissociate at a much lower temperature than that of a PS-SG1 counterpart. As a consequence, the polymerization can be efficiently performed below 90 °C (typically in the 80–90 °C temperature range).

A comprehensive kinetic study of this copolymerization system was performed using the PREDICI software based on the penultimate unit effect model using kinetic parameters from the literature.⁵⁴ Not only the benefit of adding a small amount of S was confirmed and validated previously obtained experimental results (see Figure 10), but it also gave a better insight into the complex mechanism of nitroxide-mediated radical copolymerization. Notably,

it showed that an increase in S concentration caused an increase in the S-S-SG1 macroalkoxyamine concentration, which only slowly reinitiated under the polymerization conditions. Therefore, it is important to find an appropriate balance for the S concentration to obtain the best polymerization conditions.

This copolymerization approach with a small amount of comonomer has been well-received by the polymer community as, beyond various studies performed by various research groups with MMA,^{22,53-61} it was also successfully applied to numerous methacrylates such as methacrylic acid (MAA)^{62,63}, *n*-butyl methacrylate (nBMA)⁶⁴, benzyl-methacrylate (BzMA),⁶⁵ (dimethylamino)ethyl methacrylate (DMAEMA),⁶⁶⁻⁶⁸ poly(ethylene glycol) methyl ether methacrylate (MePEGMA)^{22,57,63,69,70} and glucose-functionalized methacryloyl galactose (AcGalEMA).⁷¹ This copolymerization approach was also applied to a sterically hindered alkoxyamine initiator based on a cyclic nitroxide,⁷² thus showing a certain universality of the method.

Not only S can act as a suitable comonomer but also styrenic derivatives including 4-styrene sulfonate (SS)⁶² and pentafluorostyrene (PFS);⁶⁸ the latter being easily modified with thiols by click reaction. Maric and co-workers used 9-(4-vinylbenzyl)-9H-carbazole (VBK) as a controlling comonomer.^{59,60,66,69} VBK is a styrenic-based monomer with a carbazole unit that provides hole transport properties and fluorescence to the final copolymer. For the copolymerization of MMA with VBK, using the BlocBuilder alkoxyamine, an initial feed of 1 mol.% VBK was enough to obtain a controlled/living system. The higher reactivity ratio for VBK compared to S resulted in both a faster addition of VBK to the propagating macroradical and a lowered average activation-deactivation equilibrium rate constant ($\langle K \rangle_{\text{MMA/VBK}} < \langle K \rangle_{\text{MMA/S}}$).⁵⁹ MeOEGMA⁶⁹ and DMAEMA⁶⁶ were also copolymerized with VBK in order to obtain materials exhibiting a temperature and/or pH-dependent fluorescence.

However, S and its derivatives presents serious drawbacks: (i) they are highly hydrophobic (except SS) thus making it impossible to perform aqueous polymerizations; (ii) the use of S may alter the well-known optical properties of PMMA and (iii) it may induce toxicity in the context of biomedical applications. Therefore, alternative structures have been investigated. 2-vinyl pyridine (2VP)⁶⁷ was employed as a comonomer for the NMP of DMAEMA but led to moderate control ($\bar{D} = 1.56$ for $f_{2VP} = 0.2$). Nevertheless, the resulting copolymers were successfully employed as building blocks to prepare pH- and temperature-sensitive materials. Whereas isoprene⁷³ had beneficial effects at 20 mol.% for the NMP of MMA, no effect on the control has been shown with *n*BA and isobornyl acrylate except at very high concentrations (> 30 mol.%),^{74,75} which makes all these results out of the scope of

the copolymerization approach with a small amount of a comonomer. In fact, in addition to S and VBK, two other comonomers turned out to be very efficient for the control of methacrylic esters by NMP: *N,N*-dimethylacrylamide^{58,76} and acrylonitrile (AN).^{22,56,57} 10% DMA were shown to control the NMP of MMA leading to dispersities of about 1.4, yielding a spontaneous gradient copolymer.⁵⁸ AN was employed from 2.2 to 8.8 mol.% during the polymerization of MMA and all the features of a controlled/living system were obtained (Figure 11).⁵⁶

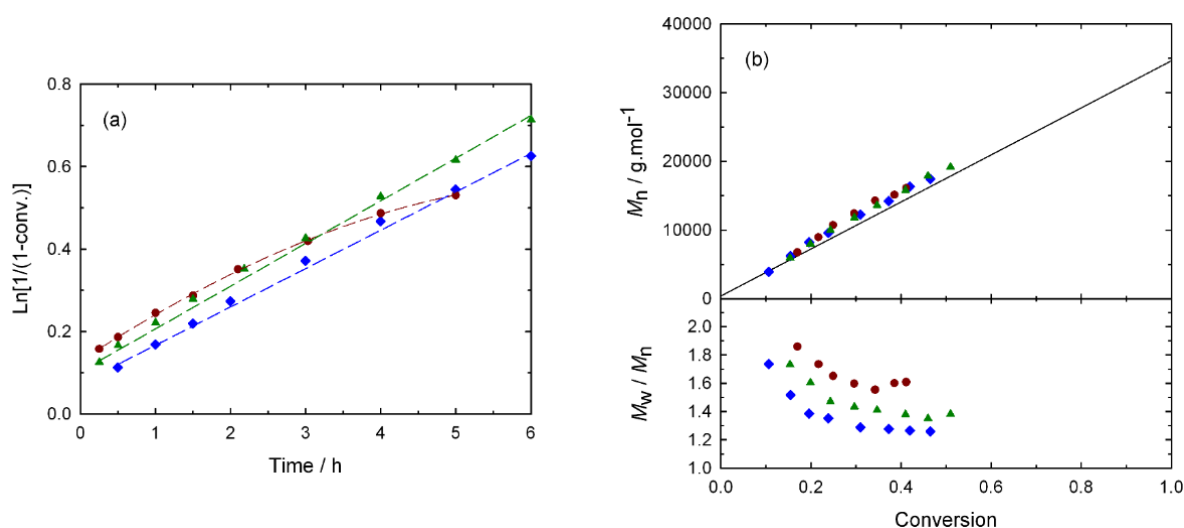


Figure 11. SG1-mediated controlled free-radical bulk copolymerization of MMA at 90 °C initiated by the BlocBuilder alkoxyamine as a function of the initial molar fraction of AN ($f_{\text{AN}0}$): \blacklozenge ($f_{\text{AN}0} = 0.088$); \blacktriangle , ($f_{\text{AN}0} = 0.044$); \bullet , ($f_{\text{AN}0} = 0.022$). $\text{Ln}[1/(1 - \text{conv.})]$ vs. time (conv. = MMA conversion) (a); number-average molar mass, M_n , and dispersity, M_w/M_n , vs. conversion (b); the full line represents the theoretical M_n . Dashed lines represent the best fit of the data. Reproduced with permission.⁵⁶ Copyright 2010, Wiley.

Nicolas and co-workers also copolymerized OEGMA with AN and the high water-solubility of AN enables both to perform copolymerizations in water-rich hydroalcoholic solutions (up to 75% water) and to reduce the polymerization temperature down to 71°C due to the accelerating effect of water.⁵⁷ It is worth mentioning that a successful NMP (i.e., good control and acceptable polymerization rate), whatever the experimental conditions (e.g., solvent, monomer, nitroxide), has never been performed at such a low temperature. The resulting PEG-based polymethacrylates had no obvious cytotoxicity on various cell lines up to high concentrations (e.g., 10 mg.mL⁻¹). By using NHS-functional, SG1-based alkoxyamines (NHS-BlocBuidler, **A1** and NHS-AMA-SG1, **A2**), α -functional PEG-based copolymers were prepared and successfully conjugated to amine-containing compounds such as a

neuroprotective tripeptide and lysozyme as a model protein (Figure 12).²² This represents the first example of protein PEGylation by NMP.

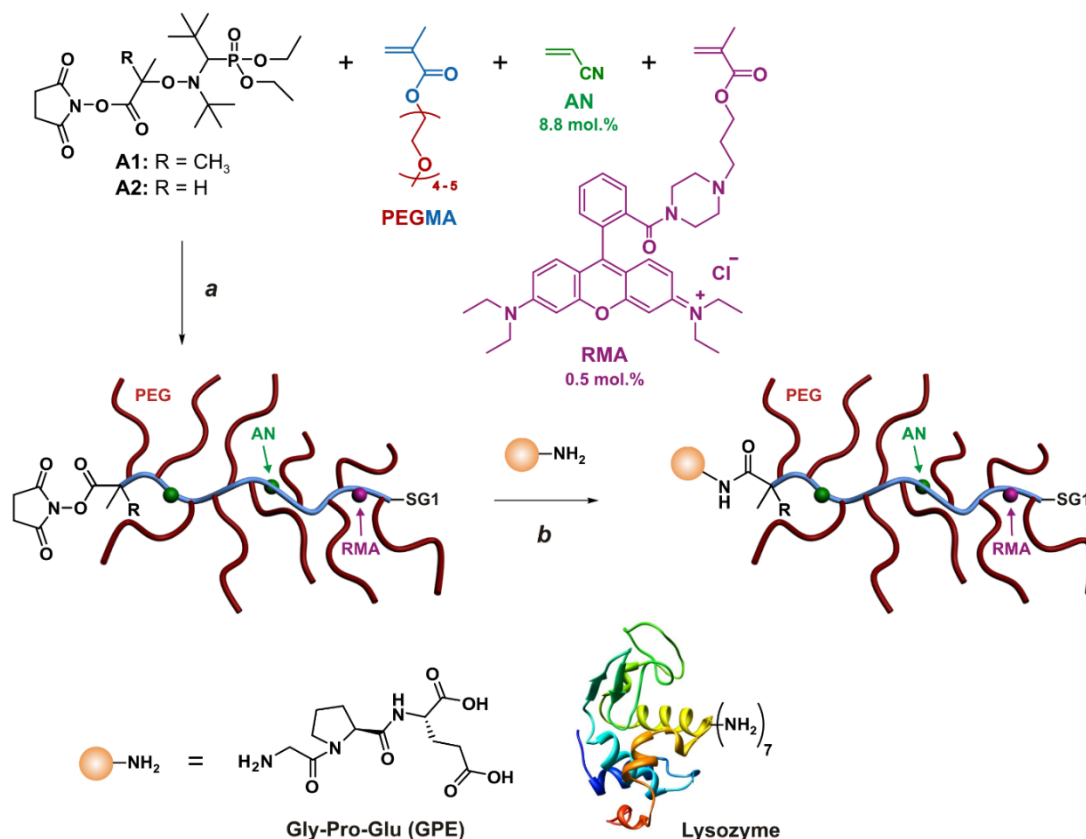


Figure 12. Strategy to design α -functional, fluorescent comb-shaped polymethacrylates with PEG side chains for bioconjugation purposes. Adapted with permission.²² Copyright 2011, Royal Society of Chemistry.

Recently, different cyclic ketene acetals (CKAs), which polymerize by radical ring-opening polymerization (rROP) and enable the insertion of degradable ester functions in the polymer backbone, were added to the OEGMA/AN copolymerization system to prepare degradable, PEG-based copolymers.⁷⁷ Among the different CKAs tested, 2-methylene-4-phenyl-1,3-dioxolane (MPDL) gave the best results as it enabled the synthesis of well-defined P(OEGMA-*co*-AN-*co*-MPDL) copolymer with tunable MPDL insertion leading to extensive degradability, no cytotoxicity and MPDL-SG1 as the main terminal sequence.^{77,78}

V. Development of dedicated nitroxides

A great deal of work has been recently focused on the development of dedicated nitroxides to control the homopolymerization of methacrylate derivatives. Not only suitable nitroxides should not be prone to disproportionation reactions but, according to kinetic simulations,⁷⁹ they should also conduct to both a slower homolysis than in the case of SG1 (e.g., by a factor

close to 50) and a faster recombination with macroradicals (by a factor close to 100). In this context, the 2,2-diphenyl-3-phenylimino-2,3-dihydroindol-1-yloxy nitroxide (DPAIO, Figure 13) met with some success.⁷⁹ This nitroxide, previously synthesized by Greci,⁸⁰ exhibits radical delocalization on the phenyl ring, which should avoid disproportionation reaction. Optimal polymerization temperature was determined from the measurement of k_d and k_c values ($k_c = 1.4 \times 10^6 \text{ L mol}^{-1} \text{ s}^{-1}$ and $E_a = 125.6 \text{ kJ mol}^{-1}$ for the dissociation), and from the Fischer phase diagram.⁸¹ Guillauneuf and co-workers reported the bulk polymerizations of MMA initiated by DPAIO-based alkoxyamines at 100 °C and showed a rather good control for targeted $M_n = 40\,000 \text{ g mol}^{-1}$ (Figure 13) and also for high targeted M_n (e.g., $80\,000 \text{ g mol}^{-1}$), thus showing the absence of disproportionation reaction.⁷⁹ This was later supported by ^1H NMR analysis of model DPAIO-based alkoxyamines.^{33,82}

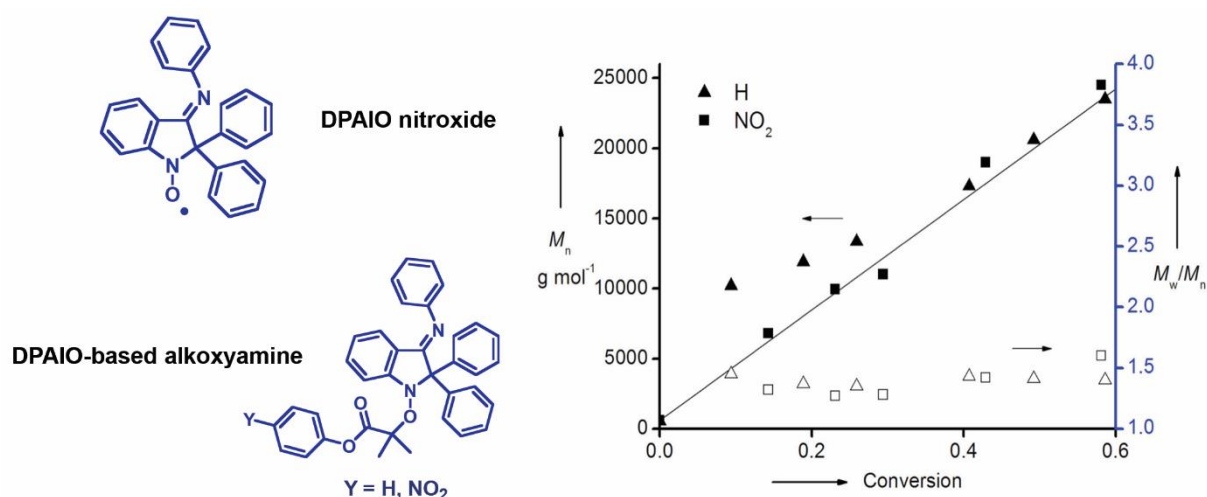


Figure 13. Evolution of number-average molar mass (M_n , full symbols) and dispersity (M_w/M_n , empty symbols) vs conversion for the bulk MMA polymerization at 100 °C initiated by DPAIO-based alkoxyamines for a targeted $M_n = 40\,000 \text{ g mol}^{-1}$ ($[\text{alkoxyamine}]_0 = 2.5 \times 10^{-2} \text{ mol L}^{-1}$). The solid line corresponds to the theoretical M_n . Reproduced with permission.⁷⁹ Copyright 2007, Royal Society of Chemistry.

As a consequence of the penultimate effect occurring during MMA polymerization, the choice of the initiating alkoxyamine is crucial. If it decomposes too slowly with respect to the macroalkoxyamine or to the polymerization time, no linear evolution of the M_n vs conversion is observed.^{38,83} Consequently, a very high dissociation rate constant alkoxyamine has to be used with an initiating $k_{d,0}$ at least as high as that of the corresponding MMA-nitroxide model alkoxyamine. By analogy with alkoxyamines based on SG1 analogues,^{84,85} an increase of the dissociation rate constant can be achieved using an initiating fragment with a long range polar

effect. With the phenylcarbonyl-1-methyl-ethyl moiety ($Y = H$, Figure 13), the evolution of the molar masses vs conversion showed a regular increase of M_n proving the controlled nature of the polymerization. Nevertheless, for early monomer conversions ($< 30\%$), the experimental values were slightly higher than the theoretical ones, accounting for a slow initiation due to a too slow decomposition of the alkoxyamine. This also caused relatively high dispersity (~ 1.4 for a targeted M_n of $40\,000\text{ g mol}^{-1}$ at 60% MMA conversion). However, by introducing a nitro group in *para* position of the phenyl ring, k_{d1} was increased (long-range polar effect) and this improved the control of the polymerization, even at low monomer conversion (Figure 13). The presence of DPAIO at the polymer chain-end was also investigated by ESR and concluded to partial livingness.

By further examining by ESR the decomposition of various DPAIO-based alkoxyamines (Figure 14), it was showed that when a primary alkyl radical is used, only N-OC bond dissociation occurred.⁸⁶ In the case of a stabilized secondary radical (e.g., *n*-butyl acrylate radical), both the N-OC and the NO-C bond dissociations occurred. For a stabilized tertiary radical (e.g., MMA radical), the desired N-OC bond is the major breaking event, which enabled the polymerization of MMA derivatives to be well controlled. These observations were also confirmed by ^1H NMR spectroscopy.³³

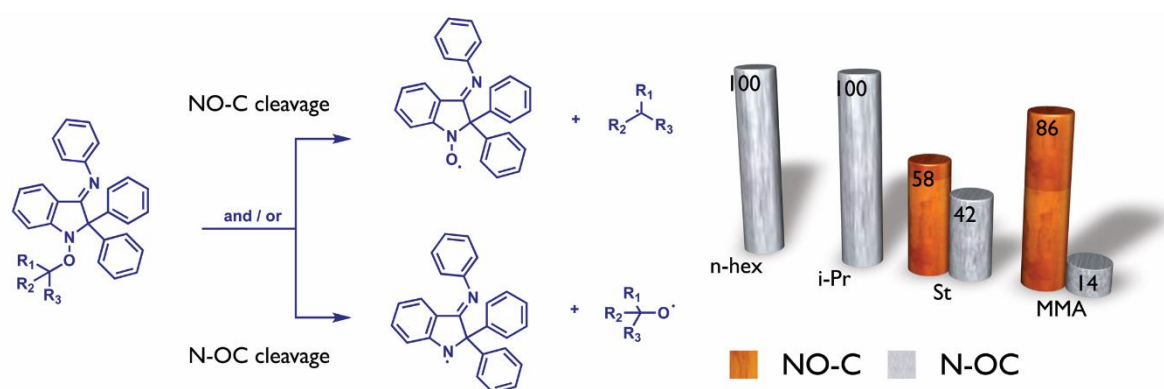


Figure 14. The two modes of decomposition for alkoxyamines based on the 2,2-diphenyl-3-phenylimino-2,3-dihydroindol-1-yloxyl (DPAIO) nitroxide.

The significant improvements offered by the DPAIO nitroxide has however a strong limitation as it prevents the control of the polymerization of other monomers than methacrylic esters. For instance, in the presence of either S or acrylates, which give less hindered and stabilized propagating radicals than methacrylates, the required temperature to dissociate the corresponding DPAIO macroalkoxyamine is too high ($> 150\text{ }^\circ\text{C}$) to perform a controlled polymerization. In addition, when the steric hindrance and the stabilization of the released

alkyl moiety decreased, DPAIO alkoxyamines could suffer from undesired CO–N homolytic dissociation. The influence of the indolinic nitroxide structure on both the C–ON bond dissociation energy and the selectivity of the homolytic dissociation (C–ON and/or CO–N) was recently investigated.⁸⁷ The ideal candidate should exhibit a lower C–ON bond dissociation energy compared to DPAIO-based alkoxyamines and undergo 100% of C–ON bond dissociation for both methacrylate- and styrene-based alkoxyamines. To this end, a small library of different alkoxyamines was prepared by changing one of the phenyl rings attached to the carbon at the alpha position to the aminoxyl function by several alkyl fragments (Figure 15a).

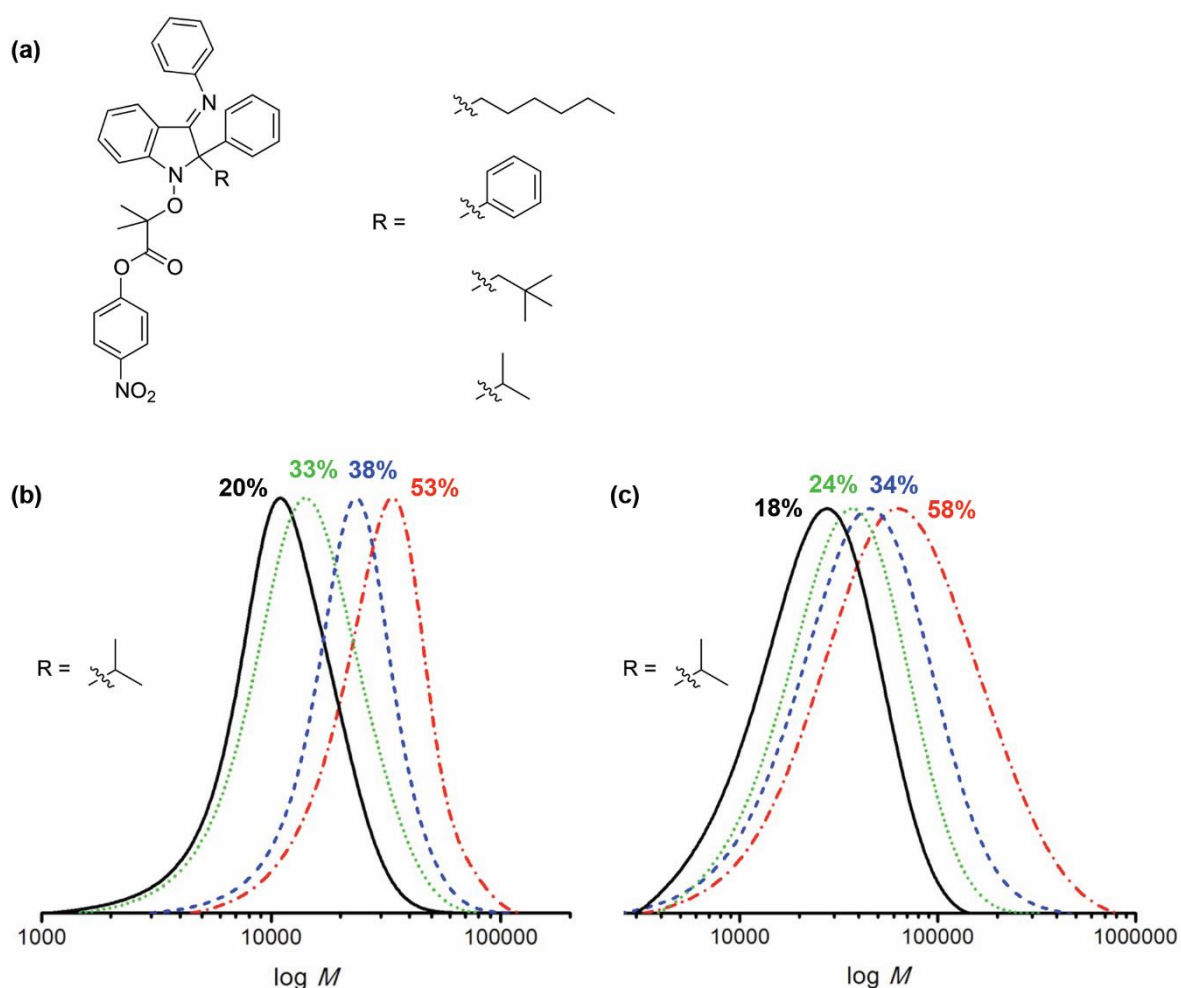


Figure 15. Structure of the different alkoxyamines prepared by changing one of the phenyl rings attached to the carbon at the alpha position to the aminoxyl function by several alkyl fragments (a). Molar mass distribution obtained from the bulk polymerization of MMA at 85 °C (b) or S at 120 °C (c) initiated with 2-phenyl-2-isopropyl-3-phenylimino-indoline-1-yloxy-*O*-(*p*-nitrophenyl)-methylpropanoate alkoxyamine (percentages indicate monomer conversions). Reproduced with permission.⁸⁷ Copyright 2013, Royal Society of Chemistry.

The steric hindrance introduced by either the isopropyl group or the neopentyl group led to a quasi-exclusive C–ON bond dissociation for the methacrylate derivatives and about 80% of C–ON bond dissociation for S. With a lower steric hindrance, the homolysis was less selective. In fact, increasing the steric hindrance also resulted in an increase of the rate of dissociation, which allowed the polymerization to be performed at lower temperature. At 85°C, the MMA polymerization was initiated by the isopropyl-based DPAIO derivative and indeed gave low dispersity (~ 1.2 at 50 % MMA conversion) and nice shifts of SEC traces towards high molar masses (Figure 15b). Interestingly, the improved selectivity during the homolysis of styryl-based alkoxyamines enabled the polymerization of S to be drastically improved, conversely to the same polymerization initiated by a DPAIO-based alkoxyamine.⁸⁷ Even if dispersities are a bit high and the experimental M_n s are above the predicted values, these promising results opened the door to controlled polymerizations of both methacrylic esters and styrene derivatives from the same nitroxide.

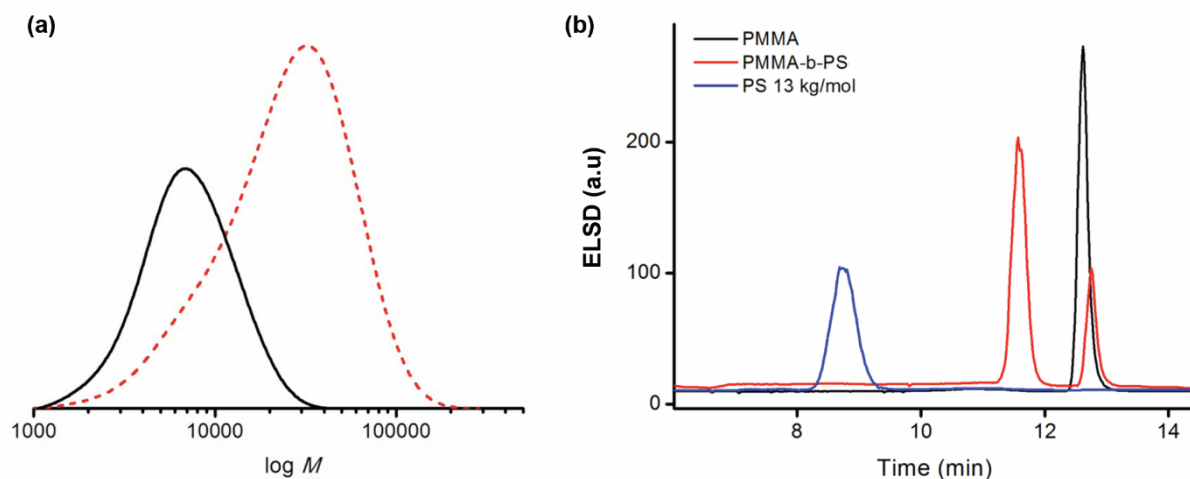


Figure 16. Molar mass distributions obtained for the bulk polymerization of S initiated with a PMMA-DPAIOiPr macroinitiator ($M_n = 5900 \text{ g mol}^{-1}$, $\bar{D} = 1.4$), black solid line: macroinitiator, red dotted line: PMMA-*b*-PS copolymer ($M_n = 16\,400 \text{ g mol}^{-1}$, $\bar{D} = 1.9$) (a). LC-LCD chromatograms of the PMMA-*b*-PS-DPAIOiPr, the precursor PMMA-DPAIOiPr and a PS standard ($13 \text{ kg}\cdot\text{mol}^{-1}$) (b). Reproduced with permission.⁸⁷ Copyright 2013, Royal Society of Chemistry.

This was illustrated by the design of PMMA-*b*-PS diblock copolymer from the isopropyl-based DPAIO derivative (Figure 16a). Although the shift of the molar mass distribution showed a good reinitiation of the polymerization, a tailing in the low molar masses range was observed. This was explained by the presence of a significant amount of “dead” PMMA chains, as determined by liquid chromatography at limiting condition of desorption (LC-

LCD), that have been created either during the synthesis of the first block or during the establishment of the persistent radical effect. Interestingly, no residual PS in the copolymer sample was formed, thus indicating the absence of undesired CO–N cleavage of the macroinitiator (Figure 16b).

Although a great deal of work remains to be done, all these results showed that the design of a “universal” nitroxide that could control the polymerization of a wide range of monomers is still possible. Ongoing research is notably focused on the tuning of the reactivity of indolinic nitroxides to improve the polymerization of mono-substituted monomers.

As an alternative to DPAIO nitroxide and derivatives, *N*-phenyl alkoxyamines have been reported using a methodology based on the addition of C-centered radicals obtained from alkyl halides precursors onto nitroso compounds (Figure 17).^{88,89} These alkoxyamine are advantageously prepared in a “one pot” reaction from commercially available compounds. Nevertheless, whatever the alkyl halide precursors, only moderate control at low monomer conversions is obtained. Further ¹H NMR analyses of the polymers showed the presence of vinylic protons resulting from disproportionation reaction that rapidly stopped the polymerization. Among the three alkoxyamines that have been reported, the *para*-nitro derivative led to the best results due to the increased rate of dissociation of the initiating alkoxyamine, as previously mentioned.⁷⁹

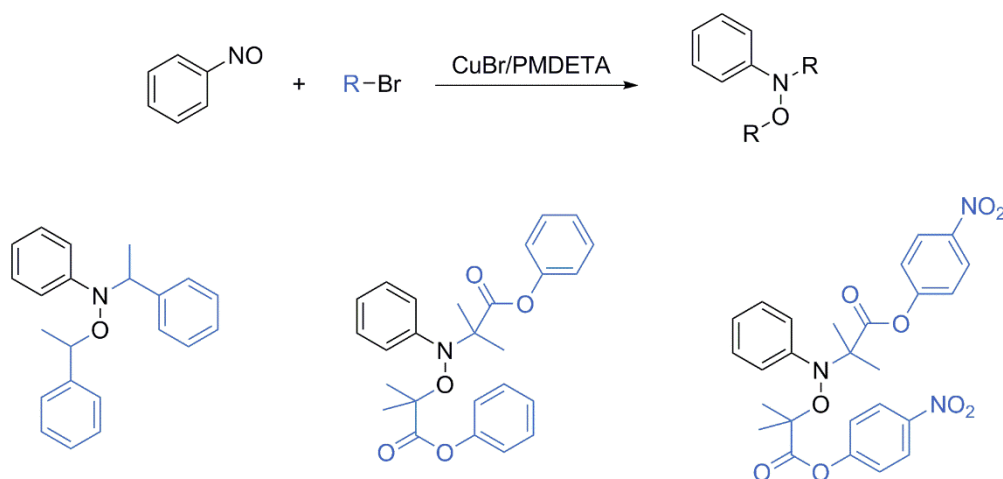


Figure 17. Synthetic pathway for the preparation of *N*-phenyl alkoxyamines and some of the different reported structures.

In order to influence the rate of the intermolecular H-transfer by playing with the steric hindrance, a highly crowded nitroxide, 1-*tert*-butyl-3,3,5,5-tetraethyl-2-piperazinon-4-oxyl nitroxide, has been tested for the polymerization of MMA using a microflow reactor.⁹⁰

Unfortunately, at 55 or 90 °C, the disproportionation reaction stopped the polymerization at low or moderate monomer conversion, thus preventing successful NMP of methacrylate derivatives. Building on previous results showing that a sterically hindered imidazoline nitroxide has a low k_{cD} value but also a low stability,⁹¹ several imidazoline nitroxides and their corresponding alkoxyamines bearing a spiro cyclic moiety were prepared via 1,3-dipolar cycloaddition reaction, enabling the facile synthesis of a library of compounds (Figure 18a).⁹² The fraction of disproportionation was found to be low (1.3–3%), making them potential initiators for the NMP of methacrylic esters. Bulk polymerization of MMA performed at 80 °C only gave a linear increase of M_n up to 30% MMA conversion, followed by a plateauing (Figure 18b). Dispersity also slightly increased and reached 1.4. Although a rather high livingness was obtained by ESR (~80 %), reinitiation experiments performed with MMA and S, together with the synthesis of a PMMA-*b*-PS diblock copolymer were poorly convincing.

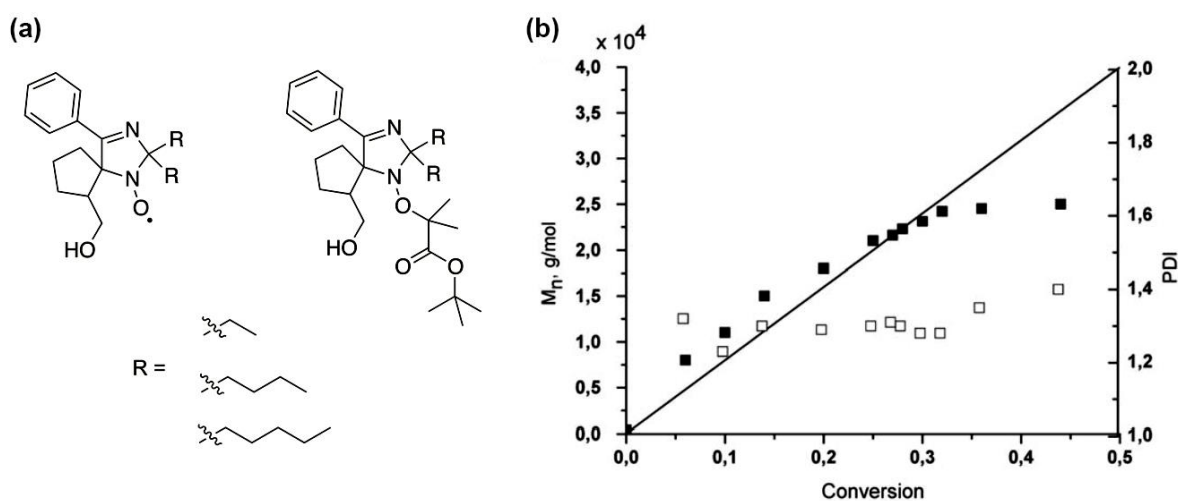


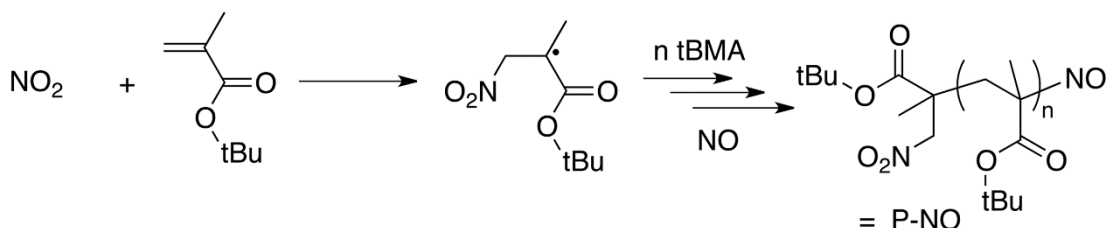
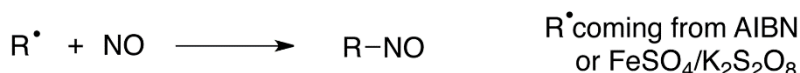
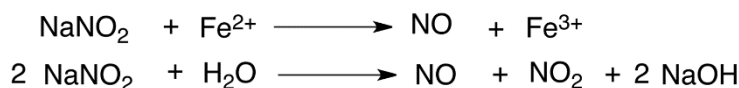
Figure 18. Structure of imidazoline-based nitroxides and related alkoxyamines (a). Evolution of M_n and \mathcal{D} with monomer conversion for the NMP of MMA initiated with the ethyl-based alkoxyamine at 80 °C with a monomer-to-initiator ratio of 800:1 (b). Reproduced with permission.⁹² Copyright 2014, Wiley.

VI. New processes

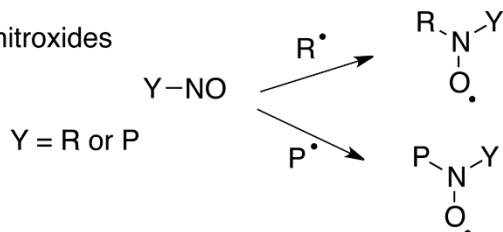
An alternative strategy to traditional NMP consists in preparing nitroxides and alkoxyamines in situ in the polymerization medium from readily and/or commercially available and inexpensive precursors. In this case, both the initiating radicals and the controlling agent are produced in a one-pot technique, usually termed in situ nitroxide-mediated polymerization (in situ NMP). This topic has been recently thoroughly discussed in the following review

reference.⁹³ Nitroso compounds represent an important family of alkyl radical scavengers and therefore have been widely applied in in situ NMP. Matyjaszewski investigated the polymerization of MMA at 80 °C using the AIBN/2-methyl-2-nitrosopropane (MNP) or 2,4,6-tri(*tert*-butyl)nitrosobenzene (TBNB) pairs, and observed that the polymerization rate was governed by the concentration of nitroso compound for constant nitroso compound/initiator molar ratios.⁹⁴ The controlled and living characters of the polymerization were however not investigated. A precursor of nitroso compounds, sodium nitrite (NaNO_2), was used to control the polymerization at 80 °C of *tert*-butyl methacrylate (*t*BMA) in water.⁹⁵ Reduction of NaNO_2 by an acidic solution of FeSO_4 is known to release NO, which is able to trap free radicals generated from conventional initiator (AIBN or potassium persulfate), resulting in the formation of nitroso, then nitroxides and after all parent alkoxyamines (Figure 19). The simultaneous formation of NO and NO_2 that occurred during the reduction in the presence of *t*BMA, produced in parallel α -nitro- ω -nitroso PtBMA.

Synthesis of nitroso compounds



Formation of the various nitroxides



Reversible equilibrium

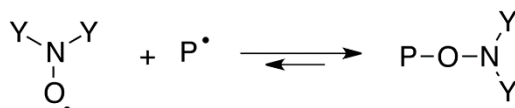


Figure 19. Mechanism of the in situ NMP of *t*BMA in the presence of NaNO_2 and FeSO_4 . Reproduced with permission.⁹⁵ Copyright 2002, American Chemical Society.

The molar mass was shown to be governed by the monomer/ NaNO_2 molar ratio rather than by the amount of FeSO_4 . Nevertheless, the deviation of $\ln([M]_0/[M])$ vs time from linearity, and the increase in dispersity when the monomer conversion is increased showed that side reactions occurred during the polymerization. The nitrite system is complex because several species are formed *in situ* because of the addition of both the initiating and the propagating radicals onto different scavengers. Therefore, several nitroso compounds and thus nitroxides and alkoxyamines coexist in the polymerization medium. This was subsequently improved by performing the polymerization of MMA or tBMA in organic medium at 25 °C with a mixture of NO/ NO_2 to produce *in situ* the nitroso compounds.⁹⁶ The polymerization of MMA, tBMA and a mixture of HEMA/MMA (1:10) was then successfully carried out at 60 °C using AIBN as radical initiator.

Recently, Detrembleur and coworkers simplified the system by preparing and isolating the methyl 2-methyl-3-nitro-2-nitrosopropionate (NMMA) before the polymerization, so that only one nitroso compound is present in the reaction medium.⁹⁷ The nitroso compound is then reacted with various methacrylate derivatives in combination with V70 as a low temperature azo initiator. The bulk polymerizations of methyl methacrylate (MMA), bezyl methacrylate (BzMA), trifluoroethyl methacrylate (TFMA) were successfully performed at moderate temperature (~40–50 °C) with good control and high livingness (Figure 20). Reinitiation experiments from low molar masses PMMA macroinitiators led to very high M_n (280,000 and 82,000 $\text{g}\cdot\text{mol}^{-1}$) diblock copolymers with still low dispersities ($\mathcal{D} = 1.46$ and 1.38, respectively).

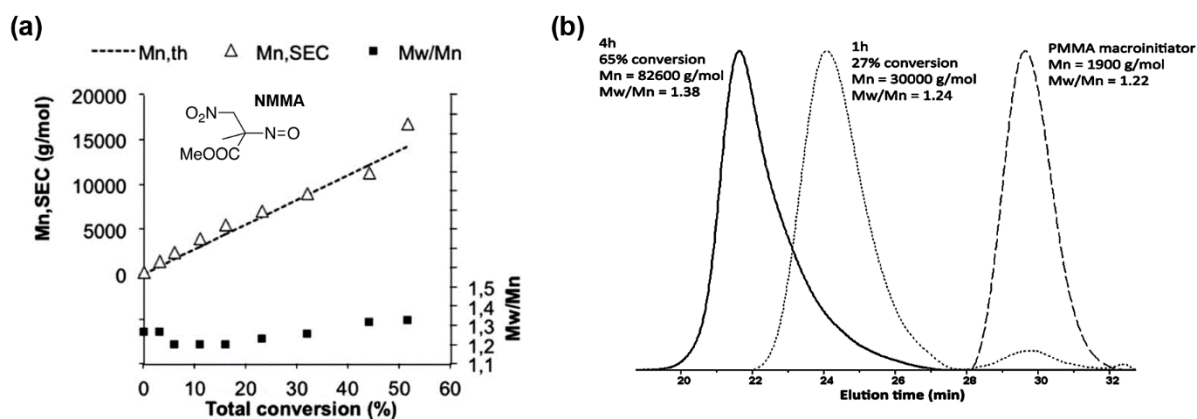


Figure 20. Molar mass and dispersity evolution with monomer conversion for the bulk polymerization of MMA initiated by V70 in the presence of NMMA at 50 °C ($[\text{MMA}]/[\text{V70}]/[\text{NMMA}] = 275/1/1$) (a). Insert: structure of the methyl 2-methyl-3-nitro-2-

nitrosopropionate (NMMA). Bulk polymerization of MMA at 50 °C initiated from a PMMA macroinitiator ($M_n = 1900 \text{ g}\cdot\text{mol}^{-1}$; PDI = 1.22) with ($[\text{MMA}]_0/[\text{PMMA}]_0 = 1776$) (b). Reproduced with permission.⁹⁷ Copyright 2014, Royal Society of Chemistry.

In addition to in-situ NMP, Junkers and Barner-Kowollik⁹⁸⁻¹⁰⁰ developed a system named enhanced spin capturing polymerization (ESCP) to control the polymerization of vinylic monomers based on the use of nitrones as radical scavenger. The mechanism is governed by the ability of nitrones to limit the lifetime of a propagating radical and to induce termination by coupling between propagating macroradicals via two consecutive spin capturing reactions (Figure 21a). As the reactions are performed below the bond dissociation temperature of the generated alkoxyamine, the system enables the prediction of the number-average molar mass, similarly to any controlled polymerization techniques, but does not feature living characteristics since no reversible cleavage of the macroalkoxyamine is possible. The reader interested by this technique should refer to the following review.¹⁰¹ ESCP has been employed for controlling the polymerization of S, *n*BA, ethylene and NIPAAm in either organic or aqueous solutions, and via thermally or photo-chemically initiated systems.^{98,100,102,103}

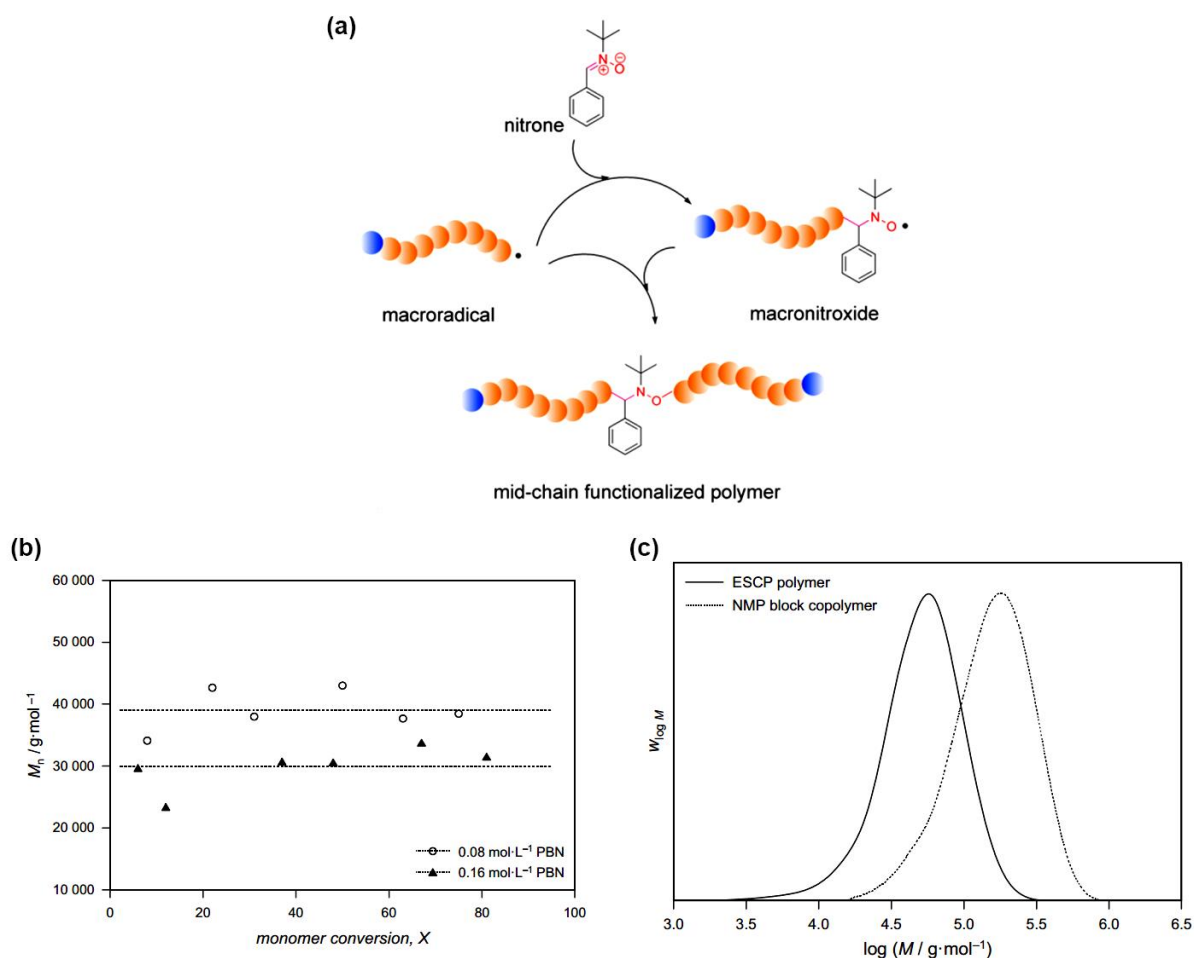


Figure 21. Mechanism of the ESCP process (a). Monomer-to-polymer conversion dependence of the M_n in the bulk ESCP of MMA with 5 vol.% S content at 60 °C, mediated with PBN and initiated by 0.04 mol L⁻¹ AIBN (b). Molecular weight distribution of polymer made via ESCP of MMA with 5 vol.% S as comonomer and the distribution of the polymer after reactivation of the alkoxyamine bonds at 110 °C and chain extension with pure S via NMP (c). Reproduced with permission.¹⁰⁴ Copyright 2010, Elsevier.

Contrary to other monomers, the polymerization of MMA in the presence of nitrone (α -phenyl-*N-tert*-butylnitron, PBN) occurred without any control over molecular weight, which was ascribed to the low rate of addition to PMMA macroradicals onto the nitron functionality.¹⁰⁴ This was however circumvented¹⁰⁴ by using the copolymerization approach that was originally proposed by Charleux and coworkers.⁵³ With 5–10 mol% of S added into the monomer mixture, a good control was achieved. The average molecular weight of the samples varied between 57 000 g mol⁻¹ for the uncontrolled reaction (absence of nitron) and close to 7000 g mol⁻¹ for a PBN concentration of 0.4 mol L⁻¹, Figure 21b). The presence of the alkoxyamine functionality at the middle of the polymer chains was assessed by reinitiation from S at 110 °C (Figure 21c). A good increase of the M_n was observed and the preparation of

PMMA-*b*-PS-*b*-PMMA triblock copolymer was achieved even if a significant tailing was present for low molar masses, which indicates a significant proportion of inactivated chains.

VII. Materials with uncontrolled polymethacrylate segments

Although homopolymerization of MMA fails to be controlled by TEMPO, SG1 or TIPNO nitroxides, this does not prevent the synthesis of advanced PMMA-containing architectures and materials by NMP. The most representative example is perhaps the synthesis of diblock copolymers comprising a PMMA block and triblock copolymers comprising PMMA outer blocks, yielding nanostructured materials. Early work about block copolymer self-assembly derived from anionic polymerization, leading to model block copolymer systems with very narrow molecular weight distributions of all blocks.¹⁰⁵ Preparation of block copolymers with relatively broad molecular weight distributions in one or more block has however become increasingly common, and dispersity has been shown to influence nearly every aspect of diblock copolymer self-assembly.¹⁰⁶ Whereas the behavior during impact tests was shown to be linked to the processing conditions (injection molding or solvent-casting), the nanoscale order, which is characterized here by the lamellar period size and obtained by solvent casting, strongly influenced the impact resistance.¹⁰⁷

High molar mass *Pn*BA/PMMA diblock and triblock copolymers prepared by bulk NMP were recently shown to self-assemble despite an uncontrolled radical polymerization process for synthesis of the PMMA blocks.¹⁰⁸ Various nanostructures were obtained (e.g., lamellar and poorly ordered bicontinuous, cylindrical, or spherical morphologies) without any occurrence of macrophase separation. More importantly, morphology boundaries were strongly shifted compared to those commonly accepted for model monodisperse block copolymers. Hence, symmetric copolymers adopted morphologies with highly curved interfaces while lamellae were displaced to PMMA-rich compositions. These results suggested that unbalanced dispersity between the two blocks can induce interfacial curvature toward to broadest molecular weight distribution, thereby releasing stretching energy of the whole chain.

From an application standpoint, block copolymers directly obtained under a stable latex form should produce useful nanostructured films, compatibilizers or even nanostructuring agents to be blended with homopolymers. The self-assembling capability of block copolymers and resulting regular nanostructures are indeed highly appreciated to develop materials with unique combinations of properties. The possibility to obtain these

nanostructures directly inside latex particles is an extra advantage not offered by conventional block copolymer synthesis methods. The ability of similar block copolymers to self-assemble and spontaneously produce nanostructured latex particles was also investigated.¹⁰⁹ AFM and TEM images of latex films obtained from 27 % solids suspensions of PnBA-*b*-PS or PMMA-*b*-PnBA-*b*-PMMA block copolymers synthesized by the multistep emulsion polymerization process (the PMMA outer blocks of the latter being obtained in an uncontrolled fashion), revealed the occurrence of “onion-like” lamellar microphases inside the latex particles, providing the purity of the second/outer block(s) and the copolymer molar mass were high enough (Figure 22). It was also shown that this particular organization was not affected by the molar mass distribution and evolved toward more classical block copolymer lamellar morphologies upon re-dissolution and/or annealing of the latex films.

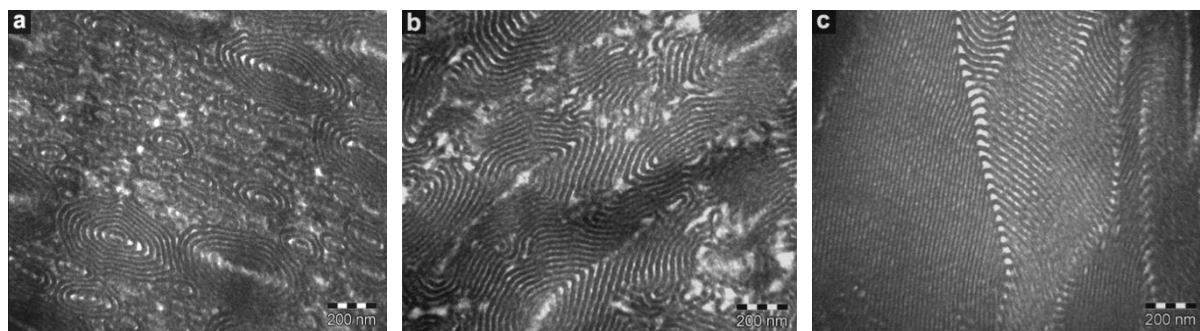


Figure 22. Transmission electron micrographs of latex films obtained from a 27 wt% solids PnBA-*b*-PS diblock copolymer suspension following different thermal treatments. Drying of the latex at room temperature for 4 days (a); annealing of the latex film at 150 °C under vacuum for 48 h (b) and re-dissolution of the latex film in dichloromethane and annealing under vacuum at 150 °C for 48 h (c). Reproduced with permission.¹⁷ Copyright 2007, Elsevier.

VIII. Conclusion

In this review, the different strategies to control the polymerization by the NMP technique of methacrylic esters, and especially of methyl methacrylate, have been covered and discussed. In light of this literature survey, it appears that despite the great deal of work currently being done on the topic, some limitations still exist even though significant improvements have been witnessed in the past few years. Two distinct strategies, each with pros and cons, have indeed emerged and hold great promise: (i) the copolymerization approach that uses only a very small amount of a suitable comonomer is appealing for its simplicity, its robustness and by the fact that commercially available nitroxides and alkoxyamine initiators, also suitable for other monomer families, can be used, even though contamination of the resulting

polymethacrylates by isolated comonomer units cannot be prevented; (ii) the use of dedicated nitroxides and associated alkoxyamines is interesting for its ability to yield true homopolymers of methacrylic esters, even though controlling the polymerization of other monomer families is not yet totally efficient. Note that, even though in the fringe of traditional NMP, in situ NMP has recently shown great ability to control the polymerization of MMA at rather low temperature and is therefore believed to be a credible alternative.

Consequently, the search for a universal nitroxide able to control the polymerization of all families of vinyl monomers is still an ongoing quest and no doubt that forthcoming achievements will be witnessed in that direction in the near future.

References

- (1) Braunecker, W. A.; Matyjaszewski, K. *Prog. Polym. Sci.* **2007**, *32*, 93.
- (2) Nicolas, J.; Guillaneuf, Y.; Lefay, C.; Bertin, D.; Gigmes, D.; Charleux, B. *Prog. Polym. Sci.* **2013**, *38*, 63.
- (3) Matyjaszewski, K.; Xia, J. *Chem. Rev.* **2001**, *101*, 2921.
- (4) Kamigaito, M.; Ando, T.; Sawamoto, M. *Chem. Rev.* **2001**, *101*, 3689.
- (5) Jakubowski, W.; Matyjaszewski, K. *Angew. Chem., Int. Ed.* **2006**, *45*, 4482.
- (6) Rosen, B. M.; Percec, V. *Chem. Rev.* **2009**, *109*, 5069.
- (7) Konkolewicz, D.; Wang, Y.; Kryszewski, P.; Zhong, M.; Isse, A. A.; Gennaro, A.; Matyjaszewski, K. *Polym. Chem.* **2014**, *5*, 4396.
- (8) Moad, G.; Rizzardo, E.; Thang, S. H. *Aust. J. Chem.* **2009**, *62*, 1402.
- (9) Perrier, S.; Takolpuckdee, P. *J. Polym. Sci., Part A: Polym. Chem.* **2005**, *43*, 5347.
- (10) Debuigne, A.; Poli, R.; Jérôme, C.; Jérôme, R.; Detrembleur, C. *Prog. Polym. Sci.* **2009**, *34*, 211.
- (11) Tsarevsky, N. V.; Matyjaszewski, K. *Chem. Rev.* **2007**, *107*, 2270.
- (12) Destarac, M. *Macromol. React. Eng.* **2010**, *4*, 165.
- (13) Georges, M. K.; Veregin, R. P. N.; Kazmaier, P. M.; Hamer, G. K. *Macromolecules* **1993**, *26*, 2987.
- (14) Georges, M. K.; Veregin, R. P. N.; Kazmaier, P. M.; Hamer, G. K.; Saban, M. *Macromolecules* **1994**, *27*, 7228.
- (15) Benoit, D.; Chaplinski, V.; Braslau, R.; Hawker, C. J. *J. Am. Chem. Soc.* **1999**, *121*, 3904.
- (16) Benoit, D.; Grimaldi, S.; Robin, S.; Finet, J.-P.; Tordo, P.; Gnanou, Y. *J. Am. Chem. Soc.* **2000**, *122*, 5929.
- (17) Charleux, B.; Nicolas, J. *Polymer* **2007**, *48*, 5813.
- (18) Cunningham, M. F. *Prog. Polym. Sci.* **2008**, *33*, 365.
- (19) Zetterlund, P. B.; Kagawa, Y.; Okubo, M. *Chem. Rev.* **2008**, *108*, 3747.
- (20) Lefay, C.; Charleux, B.; Save, M.; Chassenieux, C.; Guerret, O.; Magnet, S. *Polymer* **2006**, *47*, 1935.
- (21) Bloch, E.; Llewellyn, P. L.; Phan, T.; Bertin, D.; Hornebecq, V. *Chem. Mater.* **2009**, *21*, 48.
- (22) Chenal, M.; Boursier, C.; Guillaneuf, Y.; Taverna, M.; Couvreur, P.; Nicolas, J. *Polym. Chem.* **2011**, *2*, 1523.
- (23) Deng, L.; Furuta, P. T.; Garon, S.; Li, J.; Kavulak, D.; Thompson, M. E.; Fréchet, J. M. J. *Chem. Mater.* **2006**, *18*, 386.
- (24) Bouchet, R.; Maria, S.; Meziane, R.; Aboulaich, A.; Lienafa, L.; Bonnet, J.-P.; Phan, T. N. T.; Bertin, D.; Gigmes, D.; Devaux, D.; Denoyel, R.; Armand, M. *Nat. Mater.* **2013**, *12*, 452.
- (25) Dire, C.; Belleney, J.; Nicolas, J.; Bertin, D.; Magnet, S.; Charleux, B. *J. Polym. Sci., Part A: Polym. Chem.* **2008**, *46*, 6333.
- (26) Moad, G.; Anderson, A. G.; Ercole, F.; Johnson, H. J.; Krstina, J.; Moad, C. L.; Rizzardo, E.; Spurling, T. H.; Thang, S. H. *ACS Symp. Ser.* **1998**, *685*, 332.
- (27) Burguiere, C.; Dourges, M. A.; Charleux, B.; Vairon, J. P. *Macromolecules* **1999**, *32*, 3883.
- (28) Souaille, M.; Fischer, H. *Macromolecules* **2001**, *34*, 2830.
- (29) Li, I.; Howell, B. A.; Matyjaszewski, K.; Shigemoto, T.; Smith, P. B.; Priddy, D. B. *Macromolecules* **1995**, *28*, 6692.
- (30) Ohno, A.; Tsujii, Y.; Fukuda, T. *Macromolecules* **1997**, *30*, 2503.
- (31) Ananchenko, G. S.; Fischer, H. *J. Polym. Sci., Part A: Polym. Chem.* **2001**, *39*, 3604.

- (32) Ananchenko, G. S.; Souaille, M.; Fischer, H.; Le Mercier, C.; Tordo, P. *J. Polym. Sci., Part A: Polym. Chem.* **2002**, *40*, 3264.
- (33) Edeleva, M.; Marque, S. R. A.; Bertin, D.; Gignes, D.; Guillaneuf, Y.; Morozov, S. V.; Bagryanskaya, E. G. *J. Polym. Sci., Part A: Polym. Chem.* **2008**, *46*, 6828.
- (34) Edeleva, M. V.; Kirilyuk, I. A.; Zubenko, D. P.; Zhurko, I. F.; Marque, S. R. A.; Gignes, D.; Guillaneuf, Y.; Bagryanskaya, E. G. *J. Polym. Sci., Part A: Polym. Chem.* **2009**, *47*, 6579.
- (35) Parkhomenko, D.; Bagryanskaya, E. G.; Marque, S. R. A.; Siri, D. *Phys. Chem. Chem. Phys.* **2013**, *15*, 13862.
- (36) Benoit, D., PhD dissertation, Université de Bordeaux I, France, 1997.
- (37) Guillaneuf, Y.; Gignes, D.; Marque, S. R. A.; Tordo, P.; Bertin, D. *Macromol. Chem. Phys.* **2006**, *207*, 1278.
- (38) Chauvin, F.; Dufils, P.-E.; Gignes, D.; Guillaneuf, Y.; Marque, S. R. A.; Tordo, P.; Bertin, D. *Macromolecules* **2006**, *39*, 5238.
- (39) Gignes, D.; Vinas, J.; Chagneux, N.; Lefay, C.; Phan, T. N. T.; Trimaille, T.; Dufils, P.-E.; Guillaneuf, Y.; Carrot, G.; Boue, F.; Bertin, D. *ACS Symp. Ser.* **2009**, *1024*, 245.
- (40) Fischer, H. *ACS Symp. Ser.* **2003**, *854*, 10.
- (41) Guillaneuf, Y.; Bertin, D.; Castignolles, P.; Charleux, B. *Macromolecules* **2005**, *38*, 4638.
- (42) Beaudoin, E.; Bertin, D.; Gignes, D.; Marque, S. R. A.; Siri, D.; Tordo, P. *Eur. J. Org. Chem.* **2006**, 1755.
- (43) Bertin, D.; Gignes, D.; Marque, S. R. A.; Tordo, P. *Chem. Soc. Rev.* **2011**, *40*, 2189.
- (44) Nanda, A. K.; Matyjaszewski, K. *Macromolecules* **2003**, *36*, 8222.
- (45) Bertin, D.; Dufils, P.-E.; Durand, I.; Gignes, D.; Giovanetti, B.; Guillaneuf, Y.; Marque, S. R. A.; Phan, T.; Tordo, P. *Macromol. Chem. Phys.* **2008**, *209*, 220.
- (46) McHale, R.; Aldabbagh, F.; Zetterlund, P. B. *J. Polym. Sci., Part A: Polym. Chem.* **2007**, *45*, 2194.
- (47) Edeleva, M.; Marque, S. R. A.; Kabytaev, K.; Guillaneuf, Y.; Gignes, D.; Bagryanskaya, E. *J. Polym. Sci., Part A: Polym. Chem.* **2013**, *51*, 1323.
- (48) Steenbock, M.; Klapper, M.; Müllen, K.; Pinhal, N.; Hubrich, M. *Acta Polym.* **1996**, *47*, 276.
- (49) Ansong, O. E.; Jansen, S.; Wei, Y.; Pomrink, G.; Li, S.; Patel, A. *Polym. Int.* **2008**, *57*, 863.
- (50) Ansong, O. E.; Jansen, S.; Wei, Y.; Pomrink, G.; Lu, H.; Patel, A.; Li, S. X. *Polymer International* **2009**, *58*, 54.
- (51) Ansong, O. E.; Jansen, S.; Wei, Y.; Pomrink, G.; Lu, H.; Patel, A.; Li, S. *Polym. Int.* **2009**, *58*, 54.
- (52) Hawker, C. J.; Elce, E.; Dao, J. L.; Volksen, W.; Russell, T. P.; Barclay, G. G. *Macromolecules* **1996**, *29*, 2686.
- (53) Charleux, B.; Nicolas, J.; Guerret, O. *Macromolecules* **2005**, *38*, 5485.
- (54) Nicolas, J.; Mueller, L.; Dire, C.; Matyjaszewski, K.; Charleux, B. *Macromolecules* **2009**, *42*, 4470.
- (55) Nicolas, J.; Dire, C.; Mueller, L.; Belleney, J.; Charleux, B.; Marque, S. R. A.; Bertin, D.; Magnet, S.; Couvreur, L. *Macromolecules* **2006**, *39*, 8274.
- (56) Nicolas, J.; Brusseau, S.; Charleux, B. *J. Polym. Sci., Part A: Polym. Chem.* **2010**, *48*, 34.
- (57) Chenal, M.; Mura, S.; Marchal, C.; Gignes, D.; Charleux, B.; Fattal, E.; Couvreur, P.; Nicolas, J. *Macromolecules* **2010**, *43*, 9291.

- (58) Phan, T. N. T.; Maiez-Tribut, S.; Pascault, J.-P.; Bonnet, A.; Gerard, P.; Guerret, O.; Bertin, D. *Macromolecules* **2007**, *40*, 4516.
- (59) Lessard, B. H.; Guillaneuf, Y.; Mathew, M.; Liang, K.; Clement, J.-L.; Gigmes, D.; Hutchinson, R. A.; Marić, M. *Macromolecules* **2013**, *46*, 805.
- (60) Lessard, B.; Ling, E. J. Y.; Morin, M. S. T.; Marić, M. *J. Polym. Sci., Part A: Polym. Chem.* **2011**, *49*, 1033.
- (61) Miura, Y.; Nakamura, N.; Taniguchi, I.; Ichikawa, A. *Polymer* **2003**, *44*, 3461.
- (62) Brusseau, S.; Bellenev, J.; Magnet, S.; Couvreur, L.; Charleux, B. *Polym. Chem.* **2010**, *1*, 720.
- (63) Dire, C.; Nicolas, J.; Brusseau, S.; Charleux, B.; Magnet, S.; Couvreur, L. *ACS Symp. Ser.* **2009**, *1024*, 303.
- (64) Qiao, X.; Lansalot, M.; Bourgeat-Lami, E.; Charleux, B. *Macromolecules* **2013**, *46*, 4285.
- (65) Zhang, C.; Lessard, B.; Maric, M. *Macromol. React. Eng.* **2010**, *4*, 415.
- (66) Lessard, B.; Marić, M. *J. Polym. Sci., Part A: Polym. Chem.* **2011**, *49*, 5270.
- (67) Zhang, C.; Maric, M. *J. Polym. Sci., Part A: Polym. Chem.* **2012**, *50*, 4341.
- (68) Becer, C. R.; Kokado, K.; Weber, C.; Can, A.; Chujo, Y.; Schubert, U. S. *J. Polym. Sci., Part A: Polym. Chem.* **2010**, *48*, 1278.
- (69) Lessard, B. H.; Ling, E. J. Y.; Marić, M. *Macromolecules* **2012**, *45*, 1879.
- (70) Nicolas, J.; Couvreur, P.; Charleux, B. *Macromolecules* **2008**, *41*, 3758.
- (71) Ting, S. R. S.; Min, E.-H.; Escala, P.; Save, M.; Billon, L.; Stenzel, M. H. *Macromolecules* **2009**, *42*, 9422.
- (72) Wienhofer, I. C.; Luftmann, H.; Studer, A. *Macromolecules* **2011**, *44*, 2510.
- (73) Benoit, D.; Harth, E.; Fox, P.; Waymouth, R. M.; Hawker, C. J. *Macromolecules* **2000**, *33*, 363.
- (74) Dufils, P.-E., PhD dissertation, Université de Provence, France, 2005.
- (75) Nicolas, J., PhD dissertation, Université Pierre et Marie Curie, France, 2005.
- (76) Solheim, E.; Sudmann, B.; Bang, G.; Sudmann, E. *Journal of biomedical materials research* **2000**, *49*, 257.
- (77) Delplace, V.; Tardy, A.; Harrisson, S.; Mura, S.; Gigmes, D.; Guillaneuf, Y.; Nicolas, J. *Biomacromolecules* **2013**, *14*, 2837.
- (78) Delplace, V.; Harrisson, S.; Tardy, A.; Gigmes, D.; Guillaneuf, Y.; Nicolas, J. *Macromol. Rapid Commun.* **2014**, *35*, 484.
- (79) Guillaneuf, Y.; Gigmes, D.; Marque, S. R. A.; Astolfi, P.; Greci, L.; Tordo, P.; Bertin, D. *Macromolecules* **2007**, *40*, 3108.
- (80) Berti, C.; Colonna, M.; Greci, L.; Marchetti, L. *Tetrahedron* **1975**, *31*, 1745.
- (81) Fischer, H.; Souaille, M. *Chimia* **2001**, *55*, 109.
- (82) Edeleva, M.; Marque, S. R. A.; Bertin, D.; Gigmes, D.; Guillaneuf, Y.; Bagryanskaya, E. *Polymers* **2010**, *2*, 364.
- (83) Gigmes, D.; Bertin, D.; Lefay, C.; Guillaneuf, Y. *Macromol. Theory Simul.* **2009**, *18*, 402.
- (84) Bertin, D.; Gigmes, D.; Marque, S.; Milardo, S.; Peri, J.; Tordo, P. *Coll. Czec. Chem. Commun.* **2004**, *69*, 2223.
- (85) Bertin, D.; Gigmes, D.; Marque, S.; Maurin, R.; Tordo, P. *J. Polym. Sci., Part A: Polym. Chem.* **2004**, *42*, 3504.
- (86) Gigmes, D.; Gaudel-Siri, A.; Marque, S. R. A.; Bertin, D.; Tordo, P.; Astolfi, P.; Greci, L.; Rizzoli, C. *Helv. Chim. Acta* **2006**, *89*, 2312.
- (87) Astolfi, P.; Greci, L.; Stipa, P.; Rizzoli, C.; Ysacco, C.; Rollet, M.; Autissier, L.; Tardy, A.; Guillaneuf, Y.; Gigmes, D. *Polym. Chem.* **2013**, *4*, 3694.
- (88) Greene, A. C.; Grubbs, R. B. *Macromolecules* **2009**, *42*, 4388.

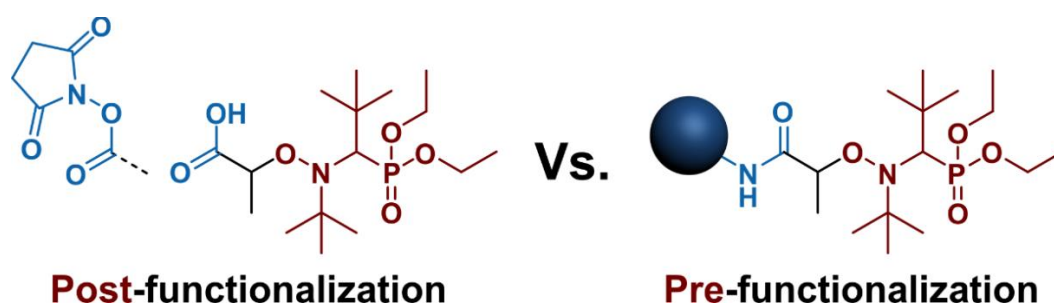
- (89) Greene, A. C.; Grubbs, R. B. *Macromolecules* **2010**, *43*, 10320.
- (90) Fukuyama, T.; Kajihara, Y.; Ryu, I.; Studer, A. *Synthesis-Stuttgart* **2012**, *44*, 2555.
- (91) Edeleva, M. V.; Kirilyuk, I. A.; Zubenko, D. P.; Zhurko, I. F.; Marque, S. R. A.; Gimes, D.; Guillaneuf, Y.; Bagryanskaya, E. G. *Journal of Polymer Science Part A-Polymer Chemistry* **2009**, *47*, 6579.
- (92) Edeleva, M. V.; Parkhomenko, D. A.; Morozov, D. A.; Dobrynin, S. A.; Trofimov, D. G.; Kanagatov, B.; Kirilyuk, I. A.; Bagryanskaya, E. G. *J. Polym. Sci., Part A: Polym. Chem.* **2014**, *52*, 929.
- (93) Sciannamea, V.; Jerome, R.; Detrembleur, C. *Chem. Rev.* **2008**, *108*, 1104.
- (94) Matyjaszewski, K.; Gaynor, S.; Greszta, D.; Mardare, D.; Shigemoto, T. *Macromol. Symp.* **1995**, *98*, 73.
- (95) Detrembleur, C.; Teyssie, P.; Jérôme, R. *Macromolecules* **2002**, *35*, 1611.
- (96) Detrembleur, C.; Claes, M.; Jerome, R. In *Advances in Controlled/Living Radical Polymerization*; Matyjaszewski, K., Ed. 2003; Vol. 854, p 496.
- (97) Detrembleur, C.; Jerome, C.; De Winter, J.; Gerbaux, P.; Clement, J. L.; Guillaneuf, Y.; Gimes, D. *Polym. Chem.* **2014**, *5*, 335.
- (98) Junkers, T.; Wong, E. H. H.; Stenzel, M. H.; Barner-Kowollik, C. *Macromolecules* **2009**, *42*, 5027.
- (99) Wong, E. H. H.; Stenzel, M. H.; Junkers, T.; Barner-Kowollik, C. *J. Polym. Sci., Part A: Polym. Chem.* **2009**, *47*, 1098.
- (100) Wong, E. H. H.; Junkers, T.; Barner-Kowollik, C. *J. Polym. Sci., Part A: Polym. Chem.* **2008**, *46*, 7273.
- (101) Wong, E. H. H.; Junkers, T.; Barner-Kowollik, C. *Polym. Chem.* **2011**, *2*, 1008.
- (102) Dommanget, C.; Boisson, C.; Charleux, B.; D'Agosto, F.; Monteil, V.; Boisson, F.; Junkers, T.; Barner-Kowollik, C.; Guillaneuf, Y.; Gimes, D. *Macromolecules* **2013**, *46*, 29.
- (103) Junkers, T.; Zang, L.; Wong, E. H. H.; Dingenouts, N.; Barner-Kowollik, C. *J. Polym. Sci., Part A: Polym. Chem.* **2011**, *49*, 4841.
- (104) Zang, L.; Wong, E. H. H.; Barner-Kowollik, C.; Junkers, T. *Polymer* **2010**, *51*, 3821.
- (105) Ruzette, A.-V.; Leibler, L. *Nat. Mater.* **2005**, *4*, 19.
- (106) Lynd, N. A.; Meuler, A. J.; Hillmyer, M. A. *Prog. Polym. Sci.* **2008**, *33*, 875.
- (107) Tran, T. A.; Leonardi, F.; Bourrigaud, S.; Gerard, P.; Derail, C. *Polym. Test.* **2008**, *27*, 945.
- (108) Ruzette, A.-V.; Tence-Girault, S.; Leibler, L.; Chauvin, F.; Bertin, D.; Guerret, O.; Gerard, P. *Macromolecules* **2006**, *39*, 5804.
- (109) Nicolas, J.; Ruzette, A.-V.; Farcet, C.; Gerard, P.; Magnet, S.; Charleux, B. *Polymer* **2007**, *48*, 7029.

Chapter 2

On the Structure-Control Relationship of Amide-Functionalized SG1-Based Alkoxyamines for Nitroxide-Mediated Polymerization and Conjugation

Elise Guégain, Vianney Delplace, Thomas Trimaille, Didier Gigmes, Didier

*Siri, Sylvain R. A. Marque, Yohann Guillaneuf, Julien Nicolas**



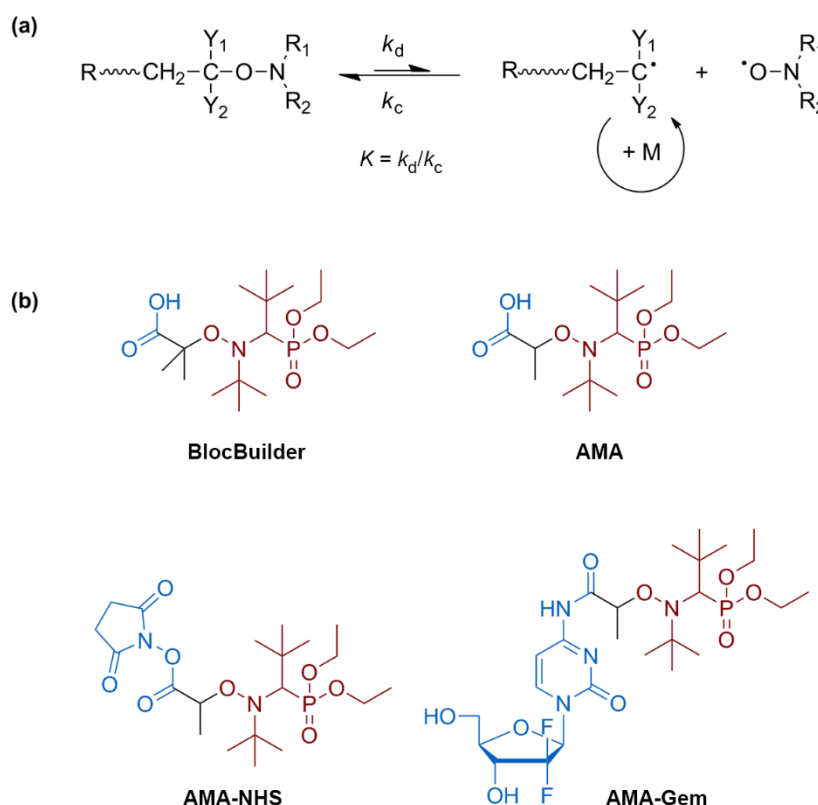
Polymer Chemistry **2015**, 6 (31), 5693-5704

ABSTRACT

The functionalization of alkoxyamines prior to nitroxide-mediated polymerization (NMP) induces important structural variations compared to the parent molecules. This may have important consequences in the design of functionalized materials by pre-functionalization. In this context, a wide range of amide-functionalized alkoxyamines (a functionality often obtained after conjugation from COOH- and *N*-succinimidyl-containing alkoxyamines) based on the nitroxide SG1 (*N-tert*-butyl-*N*-(1-diethyl phosphono-2,2-dimethylpropyl) nitroxide) have been synthesized and their dissociation rate constants ¹ have been determined. To rationalize their reactivity, a multi-parameter procedure was applied and enabled to discriminate disubstituted amide-functionalized alkoxyamines from monosubstituted ones. Monosubstituted alkoxyamines exhibited lower k_d than their disubstituted counterparts (E_a increase of $\sim 7\text{--}10\text{ kJ}\cdot\text{mol}^{-1}$) because of the occurrence of intramolecular hydrogen bonding (IHB) between the alkyl and the nitroxide fragments. NMP of styrene, *n*-butyl acrylate and methyl methacrylate with a small amount of acrylonitrile was then successfully performed from two representative secondary SG1-based alkoxyamines employed for conjugation; namely AMA (COOH-containing) and AMA-NHS (*N*-succinimidyl derivative), and compared to polymerizations initiated with AMA-Gem, an AMA-based alkoxyamine pre-functionalized with the anticancer drug Gemcitabine (Gem) and subjected to IHB. Although AMA-NHS showed the best results due to its lower E_a , the strong polarity of the Gem moiety that counter-balanced the detrimental effect of IHB over its k_d still allowed for a reasonable control.

I. Introduction

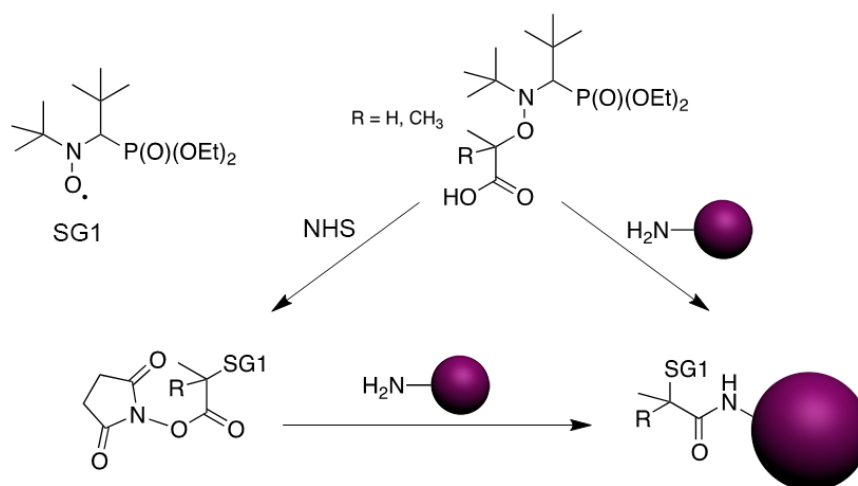
Nitroxide-mediated polymerization (NMP),^{2,3} atom-transfer radical polymerization (ATRP)^{4,5} and reversible addition-fragmentation chain transfer (RAFT)^{1,6} polymerization –to mention only the most popular– are very efficient reversible deactivation radical polymerization (RDRP) techniques. Since a few decades, the field of macromolecular synthesis is been revolutionized as the design of well-defined, complex and functional architectures is now possible with great ease. The use of a preformed alkoxyamine,² a 2-in-1 molecule which undergoes reversible thermal homolysis to produce an initiating radical and a persistent nitroxide, is definitely the most efficient procedure to perform NMP. The NMP mechanism is governed by a reversible activation-deactivation equilibrium where the nitroxide reversibly deactivates the growing radicals into dormant alkoxyamine functionalities (Scheme 1a).^{2,7}



Scheme 1. General scheme of the NMP mechanism with k_c = combination rate constant, k_d = dissociation rate constant and K = activation-deactivation equilibrium constant (a). Structures of the BlocBuilder, AMA, AMA-NHS and AMA-Gem SG1-based alkoxyamines (b).

Among the features of NMP that benefited from recent developments is the ease of access to functionalized alkoxyamines for (bio)conjugation purposes.² For instance, carboxylic acid-containing SG1-based alkoxyamines, such as the BlocBuilder alkoxyamine (2-methyl-2-(*N*-

tert-butyl-*N*-(1-diethoxyphosphoryl-2,2-dimethylpropyl)aminoxy) propionic acid) or its secondary counterpart, the AMA-SG1 (2-(*N*-*tert*-butyl-*N*-(1-diethoxyphosphoryl-2,2-dimethylpropyl)aminoxy) propionic acid) alkoxyamine (Scheme 1b), enabled coupling with primary amines. This is achieved either after their conversion into the corresponding *N*-succinimidyl (NHS) ester derivative⁸⁻¹⁰ or through their direct use in combination with benzotriazol-1-yloxytripyrrolidinophosphonium hexafluorophosphate (PyBOP) as a coupling agent (Scheme 2).^{11,12}



Scheme 2. Functionalization of SG1-based alkoxyamines via an amide linkage.

In particular, these NHS-based alkoxyamines were employed for the linkage of preformed NHS-functional PEG-based polymers to a protein⁹ whereas PyBOP was used for the direct coupling of the alkoxyamine to the terminal amine group of a peptide through solid-phase peptide synthesis¹¹ or to an anticancer drug,¹² prior to performing NMP. This last strategy, which can be assimilated to a “*grafting from*” approach in case of bulky substrates, exhibits two main benefits compared to the reverse strategy involving the coupling of preformed α -functional polymers (generally termed “*grafting to*”): (i) the efficiency of the conjugation is generally higher, especially for bulky substrates, due to a lower steric hindrance and (ii) the purification of the resulting conjugates is facilitated as only the unreacted monomer has to be removed. However, pre-functionalizing alkoxyamines induces important structural changes compared to the parent molecules. In particular, all pre-functionalized SG1-based alkoxyamines employed for (bio)conjugation so far have amide functionalities whereas the parent BlocBuilder and AMA alkoxyamines have a carboxylic acid group (see Scheme 2). Since the dissociation rate constant¹ of the alkoxyamine is governed by the structure of the alkyl moiety, with a combination of polar, steric and stabilization effects,¹³ such structural

modifications are likely to impact their dissociation. This is of high importance since for a given monomer and nitroxide, the k_d value determines the degree of control over the polymerization.¹⁴ Therefore, pre-functionalization of alkoxyamines could alter their control ability compared to that of non-functionalized counterparts.

This context prompted us to first investigate the reactivity of a series of functionalized amide-containing alkoxyamines based on the SG1 nitroxide and deriving from the BlocBuilder or the AMA alkoxyamines to see whether their radical reactivity was influenced by the functionalization. In a second step, NMP of representative monomers (i.e., styrene, *n*-butyl acrylate and methyl methacrylate with a small amount of acrylonitrile) was achieved from a selection of alkoxyamines to illustrate our findings. We selected three secondary SG1-based alkoxyamines (they usually give higher coupling yields due to their less hindered structures compared to tertiary analogs),^{9,15} that can find application in the “grafting from” strategy (Scheme 2): (i) the AMA alkoxyamine, bearing a carboxylic group; (ii) its NHS derivative (AMA-NHS) and (iii) an amide-functionalized alkoxyamine bearing the anticancer drug Gemcitabine (AMA-Gem, Scheme 1), synthesized by the direct coupling between AMA and Gemcitabine. The main idea was to perform point-by-point comparisons between these three alkoxyamines to highlight potential influence of the functionalization over the polymerization. Comparing AMA, AMA-NHS and AMA-Gem gave indications about structure-control relationships for each class of monomer and helped to predict their behavior for the design of functional materials depending on the grafting strategy (i.e., “grafting from” vs. “grafting to”). Note that AMA-Gem is of high interest as we recently showed that the controlled growth of short polyisoprene chains from this alkoxyamine enabled the resulting amphiphilic species to self-assemble into stable, narrowly dispersed nanoparticles of 130–160 nm in diameter with significant *in vivo* anticancer activity on human pancreatic carcinoma-bearing mice.¹² Considering the great potential of this strategy, in-depth investigation on the behavior and the control ability of AMA-Gem towards different monomer families is of high importance to design well-defined functionalized materials for anticancer applications.

II. Experimental part

a. Materials

2-Methoxyethylamine (99%), *tert*-butylamine (98%), *N*-isopropylacrylamide (>99%), CuBr (98%), copper powder (< 10 microns, 99%), 2-bromo propionic acid (99%), *N,N,N',N'',N'''*-pentamethyldiethylenetriamine (PMDETA, 99%), *N,N'*-dicyclohexylcarbodiimide (DCC, 99%), *N,N*-diisopropylethylamine (DIPEA, 99%) and (benzotriazol-1-yl)oxy)tripyrrolidinophosphonium hexafluorophosphate (PyBOP, 98%) were purchased from Aldrich. *N*-hydroxysuccinimide (NHS, 98%) was supplied by Acros and Gemcitabine hydrochloride (Gem HCl) from Sequoia Research Products Limited. Styrene (S, 99%), *n*-butyl acrylate (*n*BA, 99%), methyl methacrylate (MMA, 99%), acrylonitrile (AN, 99+) were purchased from Aldrich and used as received (except for MMA which was distilled). Deuterated chloroform (CDCl₃) was obtained from Euristop. Dry dimethylformamide (DMF) and dry toluene were obtained from Aldrich and all other solvents were purchased from Carlo Erba. *N-tert*-butyl-*N*-(1-diethyl phosphono-2,2-dimethylpropyl) nitroxide (SG1, 86%) and BlocBuilder **1** were kindly supplied by Arkema. The *O*-acetylated-glucosamine was synthesized as described in reference ¹⁶. 2-bromo-*N,N*-dimethylpropanamide and 2-bromo-*N*-isopropylpropanamide were prepared as described in reference ¹⁷. 2-Bromo-2-methyl-*N,N*-dimethylpropanamide was prepared as described in reference ¹⁸. Alkoxyamine **2** was prepared as described in reference ¹⁹. Alkoxyamine **3b** was prepared as described in reference ²⁰. Alkoxyamine **4** was prepared as described in reference ¹¹. Alkoxyamine **13–15** were prepared as described in reference ²¹. 2-[*N-tert*-butyl-*N*-(1-diethoxyphosphoryl-2,2-dimethylpropyl)aminoxy]-propionic acid (AMA, **8**),²² 2-[*N-tert*-butyl-*N*-(1-diethoxyphosphoryl-2,2-dimethylpropyl)aminoxy]-*N*-propionyloxysuccinimide (AMA-NHS, **11**)⁹ and AMA-Gem **12**¹² were synthesized according to previously reported methods. Note that for AMA, enhancement of crystallization is performed by dissolving the colorless oil in 1 mL of ethyl acetate followed by coevaporation of both ethyl acetate and residual dichloromethane (DCM) under vacuum. For AMA-NHS alkoxyamine, only the major diastereoisomer was obtained.

b. Analytical Techniques

^1H NMR spectroscopy was performed in 5 mm diameter tubes in CDCl_3 on a Bruker Avance-300 (300 MHz) spectrometer. The chemical shift scale was calibrated on the basis of the solvent peak ($\delta = 7.26$ ppm). ^{13}C NMR spectroscopy was performed in 5 mm diameter tubes in CDCl_3 on a Bruker Avance-300 (75 MHz) spectrometer. The chemical shift scale was then calibrated on the basis of the solvent peak ($\delta = 77.0$ ppm). Size exclusion chromatography (SEC) was performed at 30 °C with two columns from Polymer Laboratories (PL-gel MIXED-D; 300×7.5 mm; bead diameter, 5 μm ; linear part, $400\text{--}4 \times 10^5$ $\text{g}\cdot\text{mol}^{-1}$) and a differential refractive index detector (Spectrasystem RI-150 from Thermo Electron Corp.), using chloroform (CHCl_3) as eluent, a Waters 515 pump at a flow rate of 1 $\text{mL}\cdot\text{min}^{-1}$, and toluene as a flow-rate marker. The conventional calibration curve was based on poly(methyl methacrylate) (PMMA) standards (peak molar masses, $M_p = 625\text{--}625\ 500$ $\text{g}\cdot\text{mol}^{-1}$) or polystyrene²³ standards²⁴ (peak molar masses, $M_p = 162\text{--}523\ 000$ $\text{g}\ \text{mol}^{-1}$) from Polymer Laboratories. This technique allowed M_n (number-average molar mass), M_w (weight-average molar mass), and M_w/M_n (dispersity, D) to be determined.

c. Methods

Synthesis of SG1-based alkoxyamines. *Alkoxyamine 3a.* 2-Methoxyethylamine (0.75 mL, 8.6 mmol) was added through a syringe to a solution of BlocBuilder-NHS alkoxyamine (2 g, 4.2 mmol) in DCM (100 mL) at 0°C under inert atmosphere. After 1 h under stirring, the reaction mixture was concentrated under reduced pressure until a white gum was obtained. The latter was washed with distilled water, dissolved in DCM and poured in cold pentane. After filtration of insoluble part (several milligrams), the filtrate was placed at -20°C overnight. The white gum formed in the bottom of the flask was separated from pentane by removing the latter with a pipette. The product was briefly washed with cold pentane, and dried under vacuum. Yield: 55% (1.01 g). ^1H NMR (CDCl_3 , δ , ppm): 1.12 (s, 9H), 1.19 (s, 9H), 1.34 (m, 6H), 1.60 (s, 3H), 1.66 (s, 3H), 3.31 (d, $J(\text{H,P})$: 27 Hz, 1H), 3.32 (s, 3H), 3.48 (m, 2H), 3.60 (m, 2H), 4.00-4.30 (m, 4H), 7.88 (bs, 1H). ^{31}P NMR (CDCl_3 , δ , ppm): 28.07. ESI-MS: $[\text{M}+\text{H}]^+ = 439$, $[\text{M}+\text{Na}]^+ = 461$. Anal. Calcd for $\text{C}_{20}\text{H}_{43}\text{N}_2\text{O}_6\text{P}$: C, 54.78%; H, 9.88%; N, 6.39%. Found: C, 54.55%; H, 10.19%; N, 6.38%.

Alkoxyamine 5. BlocBuilder (1.0 g, 2.6 mmol), *tert*-butylamine (0.29 g, 4 mmol, 1.5 equiv), benzotriazol-1-yl-oxytripyrrrolidinophosphonium hexafluorophosphate (PyBOP, 2.1 g, 4 mmol, 1.5 equiv), and DCM (10 mL) were introduced in a round-bottomed flask, and the

dispersion was deoxygenated for 20 min by argon bubbling. *N,N*-diisopropylethylamine (DIPEA, 1.35 mL, 7.8 mmol, 3 equiv) was then added with a syringe through a septum. The mixture was stirred at room temperature for 70 minutes. The DCM was removed under reduced pressure, and the residue dissolved in ethyl acetate. After filtration over silica gel, ethyl acetate was distilled off and the obtained final product further dried under vacuum. Yield: 49% (0.57 g). ¹H NMR (CDCl₃, δ, ppm): 1.16 (s, 9H), 1.18 (s, 9H), 1.33 (m, 6H), 1.37 (s, 9H), 1.55 (s, 3H), 1.63 (s, 3H), 3.33 (d, J(H,P): 27 Hz, 1H), 4.00-4.30 (m, 4H), 6.96 (bs, 1H). ³¹P NMR (CDCl₃, δ, ppm): 26.02. ESI-HRMS: calcd for C₂₁H₄₅N₂O₅P [M+H]⁺ 437.3139, found 437.3140.

Alkoxyamine 6. BlocBuilder (0.5 g, 1.3 mmol), acetylated glucosamine hydrochloride (0.754 g, 2.17 mmol, 1.5 equiv), PyBOP (1.0 g, 1.92 mmol, 1.5 equiv), and chloroform (5 mL) were introduced in a round-bottomed flask, and the dispersion was deoxygenated for 20 min by argon bubbling. DIPEA (0.68 mL, 7.42 mmol, 5.5 equiv) was then added with a syringe through a septum. The mixture was stirred at room temperature for 3.0 h. The mixture was then washed with successively a 5 wt.% HCl solution, NaCl-saturated aqueous solution, NaHCO₃-saturated solution, NaCl-saturated solution, and finally HCl 5 wt.% solution, then dried on magnesium sulfate, and filtrated. After evaporation of chloroform, the product was obtained in 50 % yield. ¹H NMR (CDCl₃, δ, ppm): 7.68-7.17 (dd, 1H), 6.13-6.08 (dd, 1H), 5.38 (m, 1H), 5.12 (m, 1H), 4.58(m, 1H), 4.28-3.95 (m, 7H), 3.29-3.22 (dd, 1H), 2.31–1.96 (m, 12H), 1.68–1.46 (m, 6H), 1.43–1.21 (m, 6H), 1.12-1.08 (m, 18 H). ³¹P NMR (CDCl₃, δ, ppm): 25.82, 25.60. ESI-HRMS: calcd for C₃₁H₅₅N₂O₁₄P [M+H]⁺ 711.3464, found 711.3463.

Alkoxyamine 7. Under inert atmosphere, a solution of SG1 (8.33 mmol, 2.88 g) and 2-bromo-2-methyl-*N,N*-dimethylpropanamide (12.5 mmol, 2.425 g) in THF (30 mL) was added to a deoxygenated mixture of CuBr (12.5 mmol, 1.793 g), PMDETA (25.0 mmol, 4.332 g), and Cu(0) (12.5 mmol, 794 mg) in THF (20 mL). After 24 h stirring at room temperature, the mixture was evaporated, diluted with diethyl oxide and filtered off on Celite. The mixture was then washed with successively a 5 wt.% hydrochloric acid (HCl) solution, NaCl-saturated aqueous solution, NaHCO₃-saturated solution, NaCl-saturated solution, and finally HCl 5 wt.% solution, then dried on magnesium sulfate, and filtrated. After evaporation of diethyl ether, the mixture was precipitated in cold pentane to obtain the alkoxyamine as a white powder. Yield: 63%. ¹H NMR (CDCl₃, δ, ppm): 0.95 (s, 9H), 1.02 (s, 9H), 1.16 (m, 6H), 1.38 (s, 3H), 1.55 (s, 3H), 2.74 (bs, 3H), 3.07 (d, J(H,P): 27 Hz, 1H), 3.31 (bs, 3H), 3.88-4.05 (m,

4H). ^{31}P NMR (CDCl_3 , δ , ppm): 25.83. ESI-HRMS: calcd for $\text{C}_{19}\text{H}_{41}\text{N}_2\text{O}_5\text{P}$ $[\text{M}+\text{H}]^+$ 409.2826, found 409.2827.

Alkoxyamine 9. Under inert atmosphere, a solution of SG1 (8.33 mmol, 2.88 g) and 2-bromo-*N,N*-dimethylpropanamide (12.5 mmol, 2.25 g) in THF (30 mL) was added to a deoxygenated mixture of CuBr (12.5 mmol, 1.793 g), PMDETA (25.0 mmol, 4.332 g), and Cu(0) (12.5 mmol, 794 mg) in THF (20 mL). After 24 h stirring at room temperature, the mixture was evaporated, diluted with diethyl oxide and filtered off on Celite. The mixture was then washed with successively a 5 wt.% HCl solution, NaCl-saturated aqueous solution, NaHCO_3 -saturated solution, NaCl-saturated solution, and finally HCl 5 wt.% solution, then dried on magnesium sulfate, and filtrated. After evaporation of diethyl ether, the mixture was precipitated in cold pentane to obtain the alkoxyamine as a white powder. Yield: 63%. ^1H NMR (CDCl_3 , δ , ppm): 1.0-1.15 (m, 18H), 1.15-1.25 (m, 6H), 1.28-1.45 (m, 3H), 2.78-2.93 (m, 3H), 2.93-3.10 (m, 3H), 3.14-3.37 (m, 1H), 3.82-4.33 (m, 4H), 4.77-5.10 (m, 1H). ^{31}P NMR (CDCl_3 , δ , ppm): 24.70, 24.22. ESI-HRMS: calcd for $\text{C}_{18}\text{H}_{39}\text{N}_2\text{O}_5\text{P}$ $[\text{M}+\text{H}]^+$ 395.2669, found 395.2670.

Alkoxyamine 10. Under inert atmosphere, a solution of SG1 (10.3 mmol, 3.165 g) and 2-bromo-*N*-isopropylpropanamide (15.5 mmol, 3.0 g) in THF (30 mL) was added to a deoxygenated mixture of CuBr (15.5 mmol, 2.218 g), PMDETA (31.0 mmol, 5.359 g), and Cu(0) (15.5 mmol, 982 mg) in THF (20 mL). After 24h stirring at room temperature, the mixture was evaporated, diluted with diethyl oxide and filtered off on Celite. The mixture was then washed with successively a 5 wt.% HCl solution, NaCl-saturated aqueous solution, NaHCO_3 -saturated solution, NaCl-saturated solution, and finally HCl 5 wt.% solution, then dried on magnesium sulfate, and filtrated. After evaporation of diethyl ether, the mixture was precipitated in cold pentane to obtain the alkoxyamine as a white powder. Yield: 65%. ^1H NMR (CDCl_3 , δ , ppm): 0.98-1.20 (m, 24H), 1.20-1.31 (m, 6H), 1.33-1.56 (m, 3H), 3.15-3.44 (m, 1H), 3.71-4.51 (m, 6H), 8.0-7.24 (d, 1H). ^{31}P NMR (CDCl_3 , δ , ppm): 25.91, 25.83. ESI-HRMS: calcd for $\text{C}_{19}\text{H}_{41}\text{N}_2\text{O}_5\text{P}$ $[\text{M}+\text{H}]^+$ 409.2826, found 409.2829.

Alkoxyamine 16. A solution of BlocBuilder (4.04 g, 10.6 mmol) and *N*-isopropyl acrylamide (1.0 g, 8.84 mmol) in THF was introduced in a Schlenk tube, deoxygenated by nitrogen bubbling and heated at 100 °C for 1 h under stirring. The reaction mixture was then concentrated under reduced pressure. The yellowish oil was dissolved in DCM and washed with water. After drying on magnesium sulfate, filtration and evaporation of DCM, the mixture was precipitated in cold pentane to obtain the alkoxyamine as a white powder. Yield:

57%. ^1H NMR (CDCl_3 , δ , ppm): 1.05-1.40 (m, 36H), 2.07-2.15 (dd, 1H), 2.63-2.67 (dd, 1H), 3.28-3.32 (dd, 1H), 3.96-4.48 (m, 6H), 6.79-6.82 (d, 1H). ^{31}P NMR (CDCl_3 , δ , ppm): 24.73, 25.03. ESI-HRMS: calcd for $\text{C}_{23}\text{H}_{47}\text{N}_2\text{O}_7\text{P}$ $[\text{M}+\text{H}]^+$ 495.3194, found 495.3187.

Determination of the dissociation rate constants¹. *Determination by ESR.* The time evolution of the doubly integrated ESR signal of the nitroxide radicals was followed by ESR spectroscopy. The appearance of the nitroxides was followed in *tert*-butylbenzene (0.6 mL) containing initially typically 10^{-4} M solution of alkoxyamines. O_2 was used as radical scavenger. Samples with known concentrations of nitroxide served as calibration standards.

Determination by ^{31}P NMR. Values of the homolysis rate constant k_d were determined by monitoring the concentration of alkoxyamine by ^{31}P NMR in the presence of nitroxyl radical TEMPO as alkyl radicals scavenger during the heating of the corresponding alkoxyamines. A stock solution of alkoxyamine (0.02 M) in *tert*-butylbenzene with 2 equiv. of TEMPO was prepared and sampled in 15 NMR probes (0.5 mL in each probe). They were immersed in a pre-heated oil bath, withdrawn at various time intervals and quenched in ice-water bath. Then, 0.1 mL of C_6D_6 with $(\text{EtO})_3\text{PO}$ (0.002 M) as internal standard ($\delta = 0$ ppm) were added to each sample. ^{31}P NMR signal was recorded with conventional conditions on 400 MHz machine.

Polymerization reactions

In all cases, the targeted M_n at 100% monomer conversion was $20\,000\text{ g}\cdot\text{mol}^{-1}$.

Polymerization of styrene (S). S (2.5 g, 2.40×10^{-2} mol) and the alkoxyamine (AMA-SG1 (expt. 1): 46.8 mg; AMA-NHS (expt. 2): 59.5 mg; AMA-Gem (expt. 3): 78.5 mg, 1.28×10^{-4} mol) were introduced in a 5 mL vial, fitted with a rubber septum and a magnetic bar. The mixture was deoxygenated under stirring by nitrogen bubbling for 15 min at room temperature. The mixture was then immersed in a preheated oil bath at $120\text{ }^\circ\text{C}$, corresponding to the time zero of the reaction (according to the small volume of solution and its quasi-instantaneous heating). Samples were periodically taken to follow S conversion by ^1H NMR spectroscopy, and molar mass and dispersity evolutions by SEC. Identical experiments (expts. 4–6, respectively) were performed with the addition of 10 mol.% free SG1 (3.8 mg, 1.29×10^{-5} mol).

Polymerization of *n*-butyl acrylate²⁵. A typical polymerization procedure is as follows. *n*BA (1.0 g, 7.81×10^{-3} mol), alkoxyamine (AMA-SG1 (expt. 7): 18.5 mg; AMA-NHS (expt. 8): 23.5 mg; AMA-Gem (expt. 9): 30.9 mg, 5.05×10^{-5} mol), free SG1 (1.5 mg, 5.10×10^{-6}

mol) and anhydrous toluene (1.0 g, 1.15 mL) were introduced in a 5 mL vial, fitted with a rubber septum and a magnetic bar. The mixture was deoxygenated under stirring by nitrogen bubbling for 15 min at room temperature. The mixture was then immersed in a preheated oil bath at 120 °C, corresponding to the time zero of the reaction (according to the small volume of solution and its quasi-instantaneous heating). Samples were periodically taken to follow *n*BA conversion by ¹H NMR spectroscopy, and molar mass and dispersity evolutions by SEC.

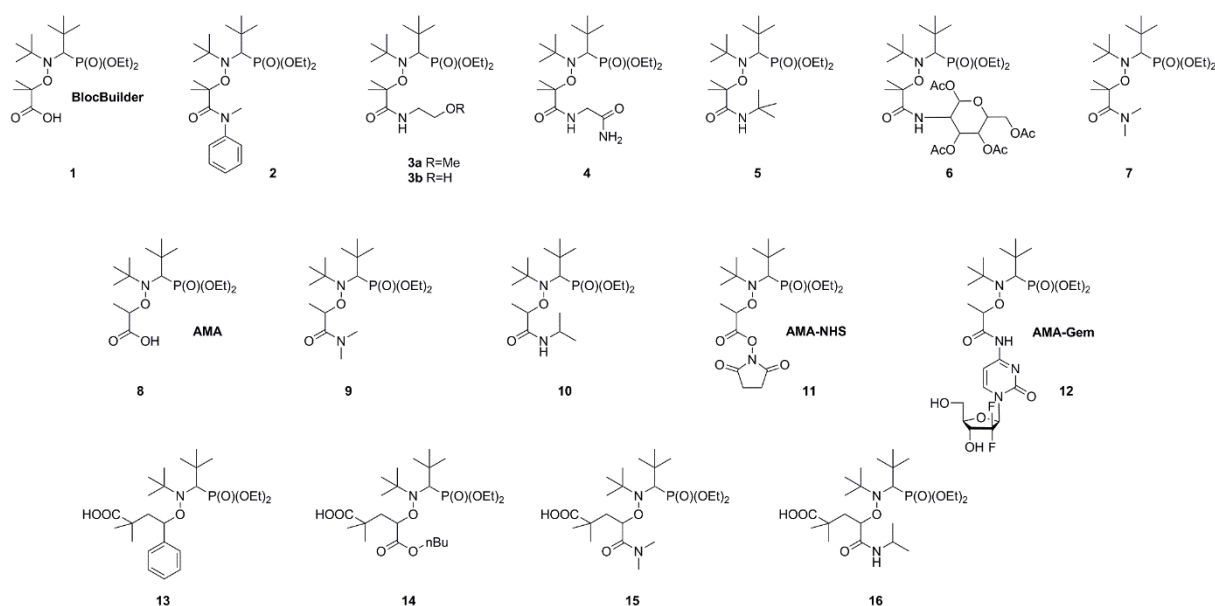
Copolymerization of methyl methacrylate (MMA) with a small amount of acrylonitrile (AN). Distilled MMA (1.0 g, 1.00×10^{-2} mol), acrylonitrile (AN, 52.5 mg, 9.91×10^{-4} mol), alkoxyamine (AMA-SG1 (expt. **10**): 20.5 mg; AMA-NHS (expt. **11**): 25.9 mg; AMA-Gem (expt. **12**): 34.2 mg, 5.59×10^{-5} mol), free SG1 (1.6 mg, 5.59×10^{-6} mol) and anhydrous toluene (1.0 g, 1.15 mL) were introduced in a 5 mL vial, fitted with a rubber septum and a magnetic bar. The mixture was deoxygenated under stirring by nitrogen bubbling for 15 min at room temperature. The mixture was then immersed in a preheated oil bath at 100 °C, corresponding to the time zero of the reaction (according to the small volume of solution and its quasi-instantaneous heating). Samples were periodically taken to follow MMA conversion by ¹H NMR spectroscopy, and molar mass and dispersity evolutions by SEC. Identical experiments (expts. **13–15**) were performed with 15 mol.% of AN (93.5 mg, 1.76×10^{-3} mol).

III. Results and Discussion

a. Synthesis and dissociation behavior of amide-functionalized SG1-based alkoxyamines

A broad library of different SG1-based alkoxyamines was prepared by varying the structure of the amide group and the stabilization of the alkyl moiety (i.e., tertiary or secondary alkyl moiety) (**1–16**, Scheme 3). Alkoxyamine **8** (AMA) was prepared by copper metal-mediated synthesis²² whereas its *N*-succinimidyl derivative **11** (AMA-NHS) was obtained from AMA by DCC-assisted coupling reaction with *N*-hydroxysuccinimide.⁹ Alkoxyamines **3a** and **3b** were prepared by the reaction of the corresponding *N*-succinimidyl derivatives of the BlocBuilder alkoxyamine **1**.⁸ For hindered alkoxyamines **4–6** and **12**, a direct coupling between the parent molecule and the corresponding amine was performed by using PyBOP as a coupling agent.¹¹ The reaction proceeded through the formation of an activated benzotriazole ester of the BlocBuilder under basic conditions, followed by the nucleophilic attack of the amino compound, leading to the desired alkoxyamine in nearly quantitative

yields after only 20–30 min (or 24 h for alkoxyamine **12**). Tertiary alkoxyamines **2** and **7** with disubstituted amine moieties were prepared by atom transfer radical addition (ATRA) from the corresponding alkyl bromides.^{26,27} Alkoxyamines **13–16** were prepared by 1,2 intermolecular radical addition onto the corresponding olefins.²⁸ This synthetic route was shown to be very efficient for the preparation of secondary functionalized SG1-based alkoxyamines that can also act as precursors for macromolecular engineering. The penultimate unit effect (PUE) is known to drastically increase the dissociation rate constant of alkoxyamines **13–16** due to the presence of the hindered 1-carboxy-1-methyl-ethyl fragment.²⁹ Therefore, the corresponding secondary SG1-based alkoxyamines **9** and **10** were also prepared with a simple methyl group in place of the 1-carboxy-1-methyl-ethyl fragment from the alkyl halide derivatives by ATRA.²⁷



Scheme 3. Structure of the different amide-functionalized SG1-based alkoxyamines synthesized and evaluated in this study.

The dissociation rate constant ¹ measurements were performed either by monitoring the alkoxyamine concentration decay by means of ³¹P NMR in the presence of an excess of thiophenol as alkyl radical and nitroxide scavenger or by monitoring the increasing of nitroxide concentration using ESR with oxygen as alkyl radical scavenger. It was already shown that *k_d* values were not significantly different whatever the techniques used.³⁰ All experiments were carried out twice and activation energies *E_a* were estimated using the averaged frequency factor $A = 2.4 \times 10^{14} \text{ s}^{-1}$.³¹ The results are summarized in Table 1.

Table 1. Experimental Activation Energy of the C-ON Bond Dissociation for Various Alkoxyamines

Alkoxyamine	E_a (kJ.mol ⁻¹)	Reference
1 (BlocBuilder)	112	13
2	105.5 ^a	this work
3a	122 ^b	this work
3b	125	20
4	117.9 ^a	this work
5	123.5 ^b	this work
6	121.6 ^b	this work
7	112.3 ^b	this work
8 (AMA)	130.7/132.8	30
9	124.5 ^b	this work
10	135 ^b	this work
11 (AMA-NHS)	127.2 ^b	this work
12 (AMA-Gem)	131 ^b	this work
13	115/116	29
14	124.5	29
15	122.5/123.4	29
16	130 ^b	this work

^aMeasured by ³¹P NMR. ^bMeasured by ESR.

To rationalize the reactivity observed with molecules **1–16**, a multi-parameter procedure was applied. This approach was shown to be very robust to describe and emphasize the various effects involved during the C–ON bond homolysis of alkoxyamines. Considering that parameters given in the literature cannot fully describe many alkyl moieties, they were estimated to characterize steric, polar and stabilization effects (see ESI for details). Experimental k_d values were then plotted against the steric Charton constant ν , the electrical Hammett constants σ_I , and the radical stabilization constants σ_{RS} , representing the steric, polar and stabilization effects, respectively (Figure 1).

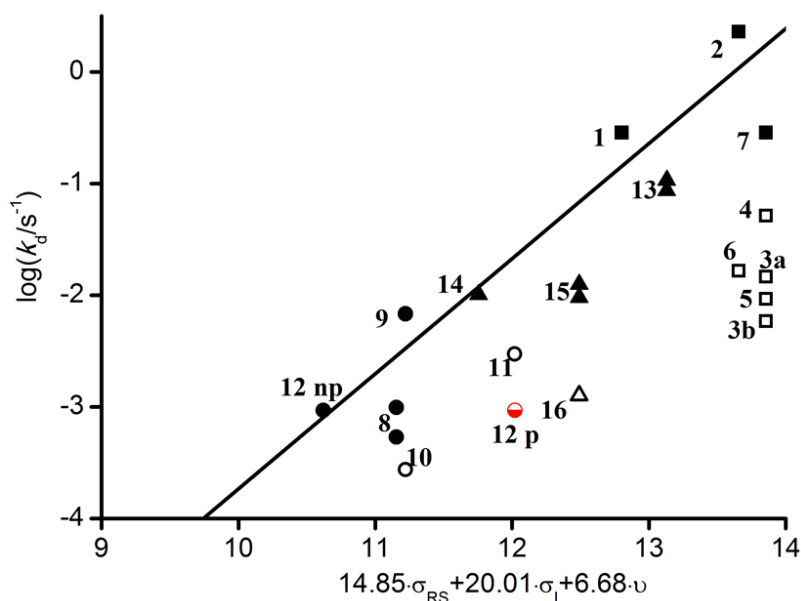


Figure 1. Plot of $\log(k_d/s^{-1})$ vs the steric Charton constant ν , the electrical Hammett constants σ_I , and the radical stabilization constants σ_{RS} parameters. (■ and □) tertiary alkoxyamines, (○ and ●) alkoxyamine exhibiting penultimate unit effect (PUE), (▲ and △) secondary alkoxyamines. Empty symbols denote outliers. For alkoxyamine 12, 2 data are presented; one with a low polar parameter (12 np) and one with a high polar parameter (12 p); see text and ESI for details.

Each experimental $\log k_d$ at 120 °C of all alkoxyamines has then been correlated to the steric Charton constant ν , the electrical Hammett constants σ_I , and the radical stabilization constants σ_{RS} parameters to give the best linear relationship. The obtained parameters leading to a linear relationship did not significantly differ from those already reported³¹ showing that alkoxyamines **2**, **7**, **9** and **15** behave as expected for SG1-based alkoxyamines. In contrast, alkoxyamines **3–6**, **10** and **16** exhibited a higher E_a than expected (ca. 7–10 kJ.mol⁻¹). The main difference between these two groups of alkoxyamines comes from the nature of the nitrogen in the amide function (i.e., disubstituted for the former and monosubstituted for the latter). It is known that long-range steric or polar effects arise for SG1-based alkoxyamines bearing different ester chains. Nevertheless, in the case of amide bonds, similar unusual behaviours reported for alkoxyamines **3–6** denote that the type of alkyl groups has a marginal influence on E_a , as opposed to ester-functionalized analogues. This reactivity could be ascribed to the predominance of the *Z* diastereoisomer configuration which is favoured due to the relief of steric strain (Figure 2).

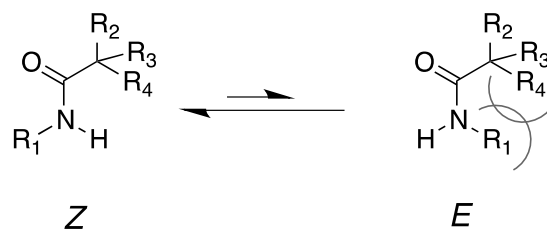
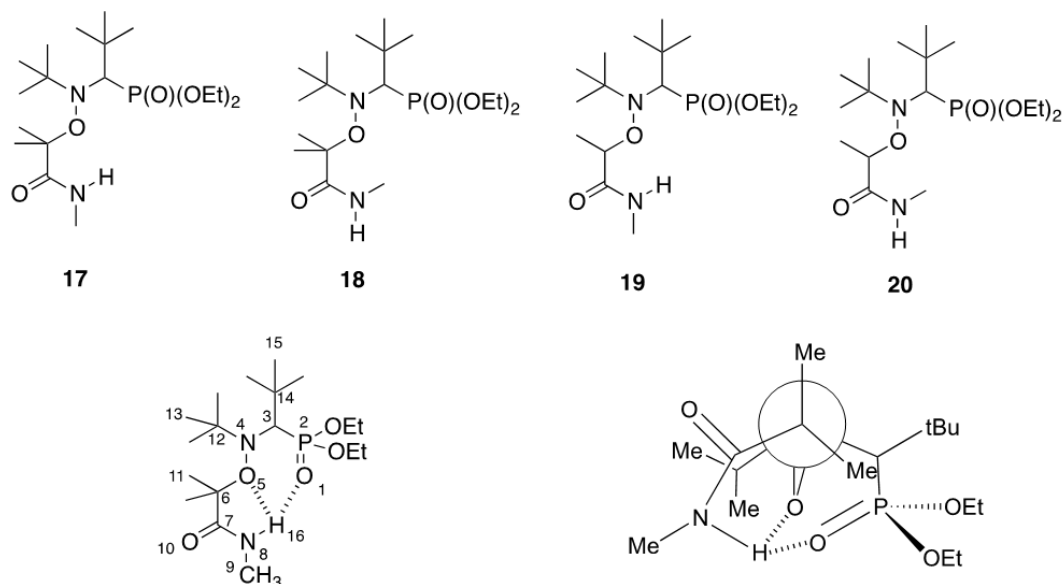


Figure 2. Structure of the *Z* and *E* diastereoisomer configurations for amide-functionalized SG1-based alkoxyamines. The *E* diastereoisomer is discarded due to the relief of the steric strain.

The *Z* configuration with the hydrogen atom pointing towards the nitroxide moiety could also explain the decreased lability of alkoxyamines bearing a monosubstituted nitrogen on the amide function. It might indeed induce some intramolecular hydrogen-bonding (IHB) between the alkyl and the nitroxide fragments, which generates a new bond to cleave hence increasing the activation energy. The predominance of the *Z* isomer configuration was assessed by X-ray analysis of alkoxyamine **3b** (see ESI). As for alkoxyamines **3–6**, only one signal was observed by ^{31}P NMR in the crude materials. Based on **3b**, it was assumed that all these alkoxyamines exhibited the *Z* configuration. The IHB interaction was then studied by DFT calculations on a selection of representative model alkoxyamines **17** and **19** (IHB capable), and **18** and **20** (no IHB capable) (Scheme 4). DFT optimized structures of **3b** and **1** (BlocBuilder) were very close to their corresponding X-ray structures (see ESI for details) demonstrating that the level of theory applied was suitable. The calculated bond distances are summarized in ESI and showed that, whatever the alkyl moieties, all nitroxides fragments exhibited close conformations. Multi IHB between the hydrogen on the amide group and the oxygens of the nitroxide was highlighted by the bond distances in alkoxyamine **17**, giving $d_{\text{H16}\dots\text{O5}} = 2.101 \text{ \AA}$ and $d_{\text{H16}\dots\text{O1}} = 2.586 \text{ \AA}$. In both cases, these values were smaller than the sum of the van der Waals radii of H atom and oxygen atoms ($r_{\text{H}} = 1.34 \text{ \AA}$, $r_{\text{O}} = 1.68 \text{ \AA}$, and $\Sigma_{\text{vdW}} = 3.02 \text{ \AA}$). The value for the valence angle $\langle \text{N}_8\text{H}_{16}\text{O}_1 \rangle$ (larger than 170°) highlighted a strong IHB whereas the value of 106° for $\langle \text{N}_8\text{H}_{16}\text{O}_5 \rangle$ gave a weak to moderate IHB (Scheme 4). Note that a weak to moderate IHB has already been reported for BlocBuilder alkoxyamine^{32,33} as well as for a SG1-based alkoxyamine carrying hydroxyl group on the alkyl moiety.^{34,35}



Scheme 4. Structures of the calculated amide-functionalized alkoxyamines and representation of the multiple intramolecular hydrogen-bonding interactions.

In conclusion, the establishment of IHB increasing the dissociation energy by ca. 7–10 $\text{kJ}\cdot\text{mol}^{-1}$ for a series of monosubstituted amide-functionalized SG1-based alkoxyamines has been evidenced. The situation for AMA-Gem **12** is however more complex since the estimation of its polar parameter cannot be performed (the value for the cytosine group is not reported). We used the polarity value of the model phenyl ring in first approximation and the predicted dissociation behavior fulfilled the linear relationship already reported for SG1-based alkoxyamines (**12np** in Figure 1). Nevertheless, as the cytosine moiety should be prone to IHB, a higher activation was expected. A better estimation was then performed by using an oxypyrimidinyl group (**12p** in Figure 1). As expected for such alkoxyamine, the activation energy was increased of ca. 10 $\text{kJ}\cdot\text{mol}^{-1}$, due to the occurrence of IHB.

The experimental activation energy of **12** ($E_a = 131 \text{ kJ}\cdot\text{mol}^{-1}$) was similar to that of the acid-functionalized analogue ($E_a = 130/132 \text{ kJ}\cdot\text{mol}^{-1}$ for the diastereoisomers). This value was lower than that of alkoxyamine **10** ($E_a = 135 \text{ kJ}\cdot\text{mol}^{-1}$), a model of amide-functionalized SG1-based alkoxyamine, and similar to the reference MONAMS alkoxyamine.³⁶ In the case of AMA-Gem **12**, the influence of IHB over the dissociation was entirely counter-balanced by the presence of the polar cytosine ring on the amide function that promoted the dissociation.

The aim of the next section was therefore to estimate its performance in NMP in comparison with two precursors of amide-functionalized alkoxyamines; namely the acid-functionalized AMA alkoxyamine and its NHS derivative (AMA-NHS).

b. NMP of vinyl monomers initiated by different SG1-based alkoxyamine

NMP of styrene (S). The bulk polymerization of S at 120°C was investigated, as it is one of the most widely-used monomers in radical polymerization. Experiments were first performed without any addition of free SG1 (expts. 1–3). First-order kinetics were obtained up to 50–80% monomer conversion for the three alkoxyamines tested (Figure 3a), accounting for a constant concentration of propagating radicals during the polymerizations. Although molar masses increased linearly in all cases, some differences were highlighted. AMA-NHS led to the higher polymerization rate (Figure 3a), whereas a low apparent initiation efficiency (calculated according to $f = \text{theoretical } M_n / \text{experimental } M_n$) of ~60% was obtained with AMA compared to ~80% for AMA-NHS and AMA-Gem (Figure 3b). Also, AMA-NHS led to low dispersities ($\bar{D} \sim 1.2$) compared to AMA and AMA-Gem, for which dispersities approached 1.5 at the end of the polymerization. This latter observation was likely attributed to the higher dissociation rate constant of AMA-NHS (Table 1), which is known to be a key parameter to achieve a good control of the NMP process.¹⁴

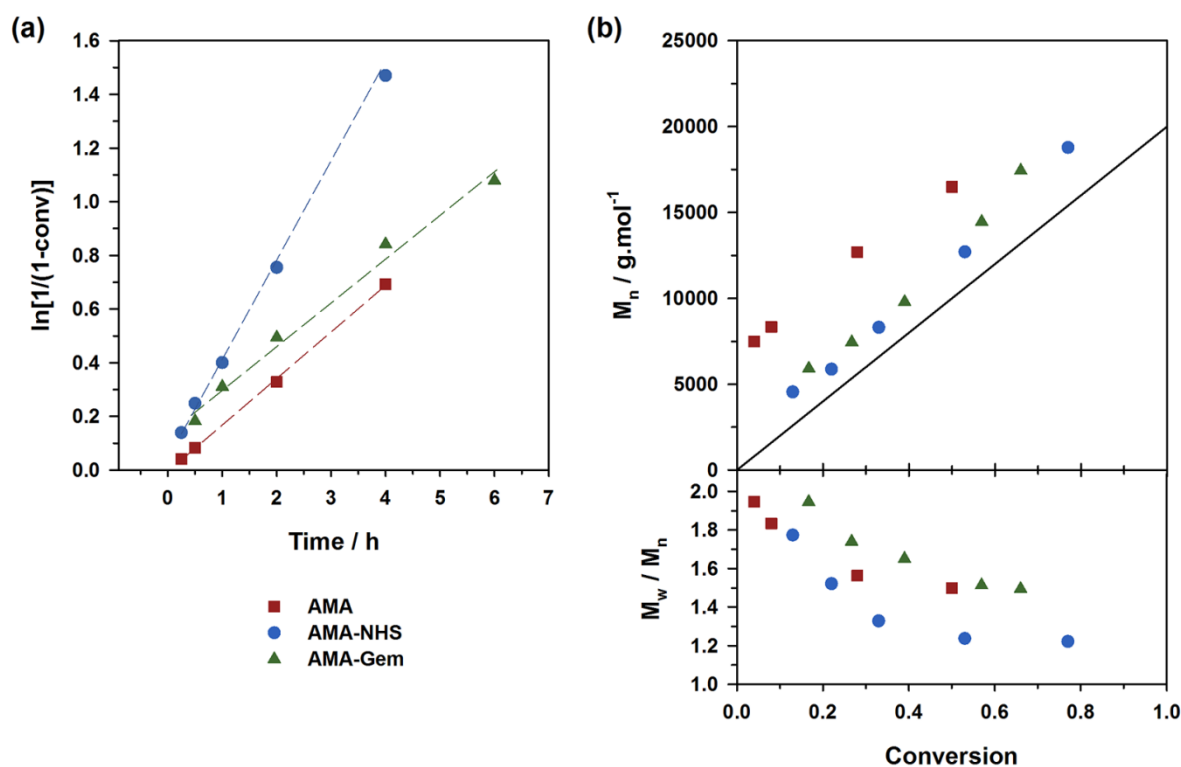


Figure 3. Bulk NMP of S at 120 °C initiated by different SG1-based alkoxyamines: ■, expt. 1 (AMA); ●, expt. 2 (AMA-NHS); ▲, expt. 3 (AMA-Gem). (a) Evolution of $\ln[1/(1-\text{conv})]$ with time (t); (b) evolution of the number-average molar mass³⁷ and dispersity (\bar{D}) with conv.

The full lines represent the theoretical M_n and lines connecting data points are guides for the eye only.

The situation was however less marked by adding 10 mol.% of free SG1 at the onset of the polymerizations (expts. 4–6, Figure 4). This drastically reduced the differences of behavior between the three alkoxyamines as: (i) kinetics rather exhibited the same slope (Figure 4a); (ii) the initiation efficiency was greatly improved for AMA (expt. 4, Figure 4b) with M_n values almost overlaying with those obtained from AMA-Gem and AMA-NHS and (iii) dispersities reached lower values for AMA and AMA-Gem ($\mathcal{D} \sim 1.4$), and so was for AMA-NHS ($\mathcal{D} \sim 1.15$). The presence of 10 mol.% of free SG1 at the very beginning of the polymerization helped in reducing the occurrence of irreversible terminations and therefore reduced the differences between the dissociation abilities of these three alkoxyamines.

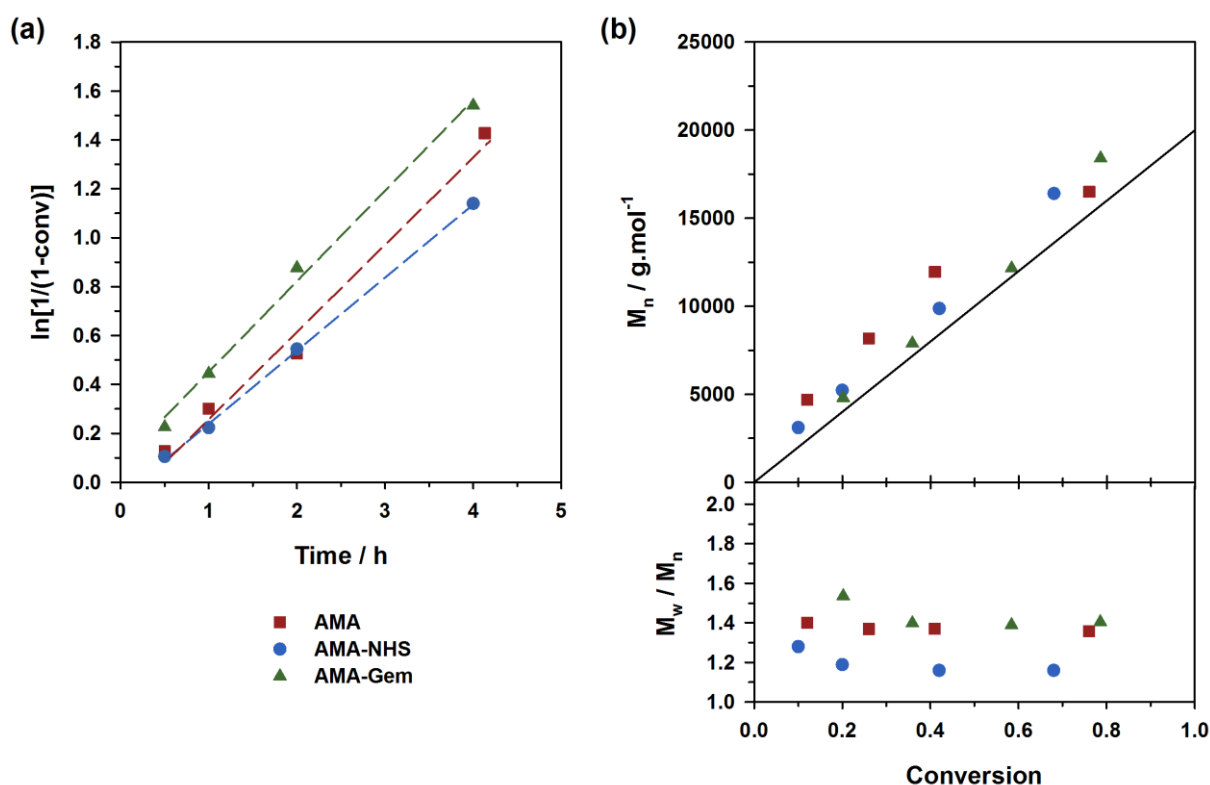


Figure 4. Bulk NMP of S at 120 °C initiated by different SG1-based alkoxyamines in the presence of 10 mol.% free SG1: ■, expt. 4 (AMA); ●, expt. 5 (AMA-NHS); ▲, expt. 6 (AMA-Gem). (a) Evolution of $\ln[1/(1-\text{conv.})]$ with time (t); (b) evolution of the number-average molar mass³⁷ and dispersity (\mathcal{D}) with conv. The full lines represent the theoretical M_n and lines connecting data points are guides for the eye only.

NMP of *n*-butyl acrylate²⁵. SG1 is an efficient controlling agent for the polymerization of a broad variety of different acrylic esters.² A representative acrylic ester that is often polymerized by NMP is *n*BA. Many studies have reported the SG1-mediated polymerization

of *n*BA in many different conditions.³⁸⁻⁴¹ NMP was performed at 120 °C in the presence of 10 mol.% of free SG1 (expts. 7–9, Figure 5). A small amount of free SG1 is indeed mandatory to efficiently control the polymerization of *n*BA, especially initiated by secondary SG1-based alkoxyamines.³⁹ For the three alkoxyamines, not so much difference was observed. As expected, AMA-NHS gave the highest polymerization rate (Figure 5a) but the quality of control was identical whatever the nature of the alkoxyamine (Figure 5b). M_n values linearly increased during the polymerization with high initiating efficiencies and decreasing dispersities ($\bar{D} \sim 1.35$) up to 70 % *n*BA conversion. As expected, dispersities increased above 80% *n*BA conversion due to side reactions such as chain transfer to polymer.^{42,43}

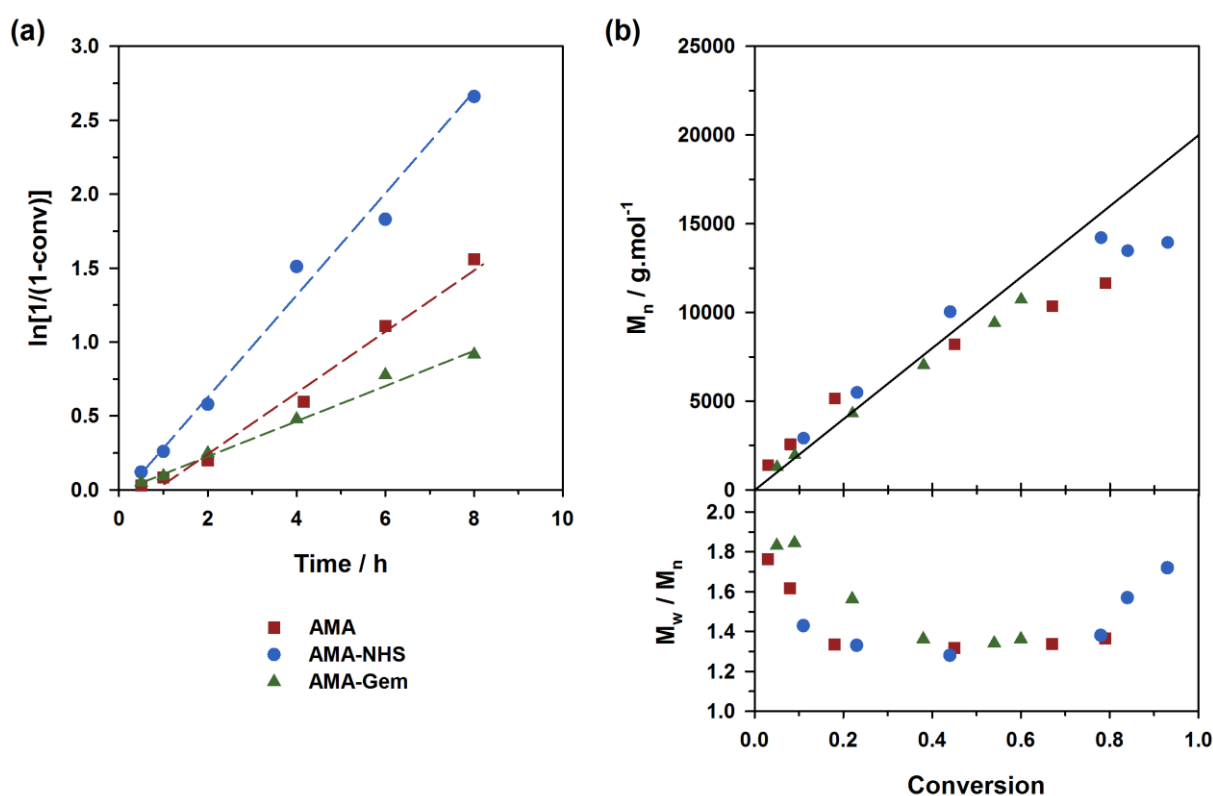


Figure 5. Solution NMP of *n*BA at 120 °C initiated by different SG1-based alkoxyamines: ■, expt. 7 (AMA); ●, expt. 8 (AMA-NHS); ▲, expt. 9 (AMA-Gem). (a) Evolution of $\ln[1/(1-\text{conv})]$ with time (*t*); (b) evolution of the number-average molar mass³⁷ and dispersity (\bar{D}) with conv. The full lines represent the theoretical M_n and lines connecting data points are guides for the eye only.

NMP of methyl methacrylate (MMA). NMP of MMA and methacrylates in general has always been challenging.⁴⁴ Using SG1 as a controlling agent results in a high activation-deactivation equilibrium rate constant that favors the production of propagating radicals.^{45,46} This leads to a high level of irreversible termination reactions (both homotermination between

propagating radicals and β -hydrogen transfer from the propagating radical to the nitroxide).⁴⁶⁻
⁴⁹ The polymerization is therefore rapidly stopped and polymers with high dispersities and low molar masses are obtained. However, the addition of a small amount of S during the SG1-mediated polymerization of MMA initiated with a high dissociation rate constant alkoxyamine such as BlocBuilder, enabled well-defined and living polymers to be readily synthesized due to the drastic decrease of the average activation-deactivation equilibrium rate constant, $\langle K \rangle$.^{48,50} This was attributed to favorable kinetic parameters of S (*i.e.*, low K and low cross-propagation rate constant).^{48,51} This strategy is versatile as it can be extended to other methacrylic esters⁵²⁻⁵⁷ and other ‘controlling’ comonomers such as acrylonitrile (AN)⁵⁸ and 9-(4-vinylbenzyl)-9H-carbazole (VBK).⁵⁹

Controlling the NMP of MMA with secondary alkoxyamines is therefore not straightforward due to their slower decomposition rates compared to their tertiary analogues. Polymerizations were performed at 100°C (and not at 90°C to alleviate the detrimental effect of their relatively high E_a) in the presence of 9 mol.% of AN (expts. **10–12**, Figure 6). Results showed a substantially better control with AMA-NHS compared to AMA and AMA-Gem. With AMA-NHS, M_n values were closer to the predicted ones (indicating a higher initiation efficiency, although quite modest as $f = 60\%$) and dispersities progressively decreased to ~ 1.4 . In contrast, although M_n values were still increasing linearly with MMA conversion for AMA and AMA-Gem up to ca. 30% conversion, significantly higher dispersities ($D \sim 1.6–1.7$) were obtained during the polymerization. This particular case, for which a fast-dissociating alkoxyamine is necessary, highlighted the pivotal role of the k_d value on the control of the NMP process and exalted the difference between the behaviors of the three alkoxyamines.

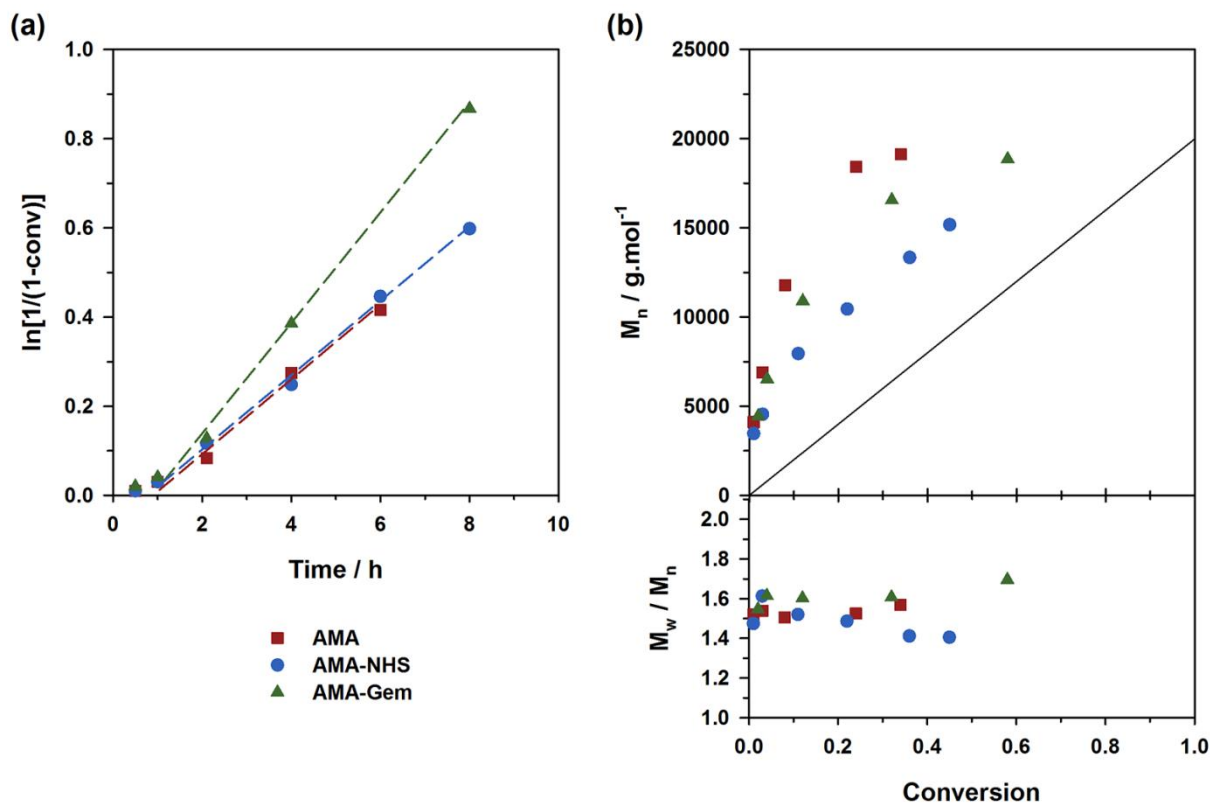


Figure 6. Solution NMP of methyl methacrylate (MMA) with a small amount of acrylonitrile (AN, $f_{\text{AN}0} = 9$ mol.%) at 100°C initiated by different SG1-based alkoxyamines: ■, expt. 10 (AMA); ●, expt. 11 (AMA-NHS); ▲, expt. 12 (AMA-Gem). (a) Evolution of $\ln[1/(1-\text{conv.})]$ with time (t); (b) evolution of the number-average molar mass³⁷ and dispersity (\mathcal{D}) with conv. The full lines represent the theoretical M_n and lines connecting data points are guides for the eye only.

A strategy to improve the control is to slightly increase the initial amount of the ‘controlling’ comonomer, but while still targeting low values to avoid decreasing too much the amount of methacrylic units in the resulting copolymer. By using $f_{\text{AN}0} = 15$ mol.%, significant improvement was indeed witnessed (expts. 13–15, Figure 7). Whereas similar first-order kinetics were observed in all cases, AMA-NHS and AMA-Gem led to higher initiation efficiencies ($f = 89\%$ and 75% , respectively) whereas that of AMA was rather unchanged and still poor. Also, dispersities for AMA and AMA-Gem were slightly improved and reached lower values at the end of the polymerization ($\mathcal{D} \sim 1.5$) compared to similar experiments with 9 mol.% AN (see Figure 6b). However, no beneficial effect on the dispersity was observed with AMA-NHS (expt. 14).

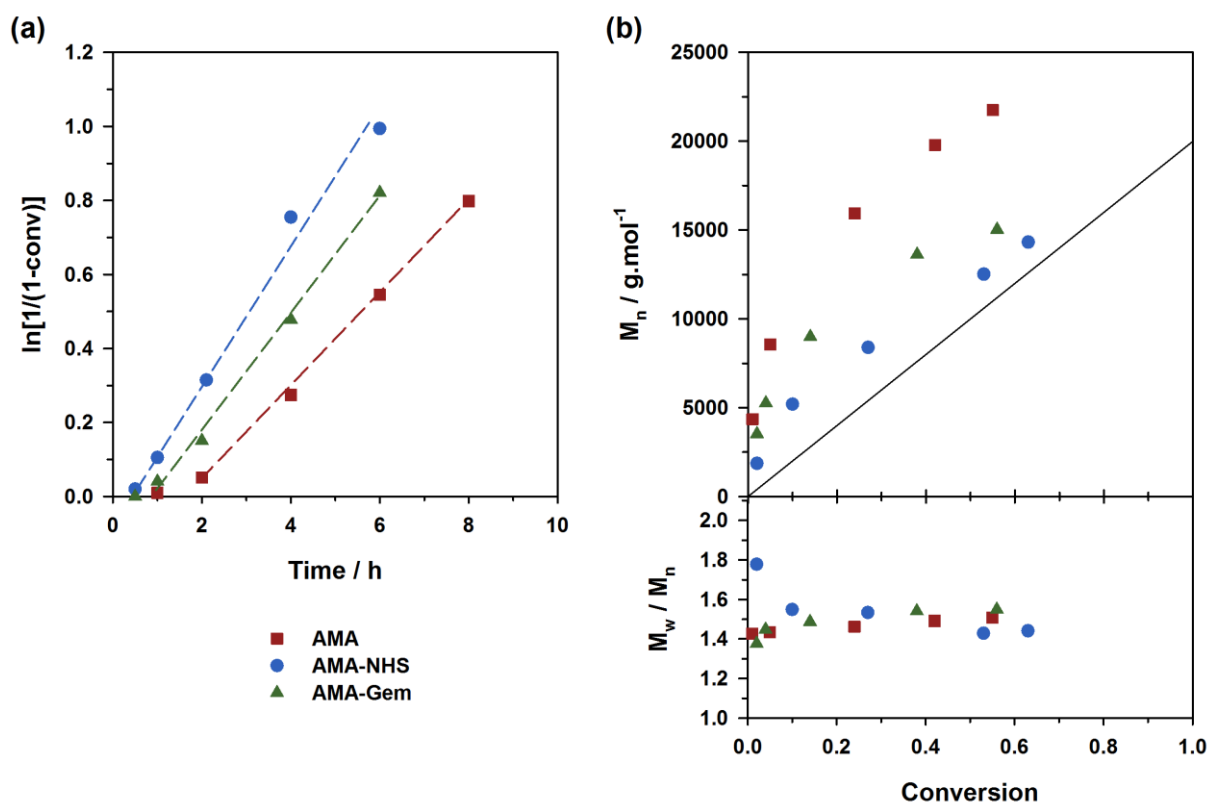


Figure 7. Solution NMP of methyl methacrylate (MMA) with a small amount of acrylonitrile (AN, $f_{\text{AN}0} = 15$ mol.%) at 100°C initiated by different SG1-based alkoxyamines in the presence of 10 mol.% free SG1: ■, expt. 13 (AMA); ●, expt. 14 (AMA-NHS); ▲, expt. 15 (AMA-Gem). (a) Evolution of $\ln[1/(1-\text{conv})]$ with time (t); (b) evolution of the number-average molar mass³⁷ and dispersity (\mathcal{D}) with conv. The full lines represent the theoretical M_n and lines connecting data points are guides for the eye only.

IV. General discussion

What resulted from this series of polymerizations with different monomers is an overall good agreement between the controlling ability of each alkoxyamine tested (i.e., AMA, AMA-NHS and AMA-Gem) and the value of their activation energy (and implicitly of their dissociation rate constant). AMA-NHS, which exhibits the lowest E_a by ca. $4\text{--}5 \text{ kJ}\cdot\text{mol}^{-1}$, indeed led to a better control than AMA and AMA-Gem in terms of initiation efficiency and dispersity, although differences were quite moderate. The addition of a small amount of free SG1 (10 mol.%) had the beneficial effect of reducing these differences and improving the control. A similar effect was observed on the MMA polymerization by increasing the amount of controlling comonomer ($f_{\text{AN}0} = 15$ mol.% vs. 9 mol.%).

Despite the establishment of IHB for AMA-Gem, the presence of the polar cytosine ring on the amide function, which favors the dissociation, enabled a fair control of different monomer families. In fact, the initiation efficiency of AMA-Gem was slightly better than the

AMA alkoxyamine, although they exhibited very close E_a . This result could be explained by a higher rate of decomposition during the polymerization process. The occurrence of IHB is indeed likely prone to variation with the polarity of the solvent (without IHB, the dissociation of AMA-Gem would be dramatically increased with a theoretical $E_a = 121 \text{ kJ.mol}^{-1}$, see ESI for details), as recently observed for the NMP of isoprene.³³ Note that the nature of the solvent can also impact the alkoxyamine reactivity.^{60,61}

Importantly, it appears that when the ‘*grafting from*’ strategy is envisioned from NHS- or COOH-containing AMA-based alkoxyamines, the coupling with a polar amine moiety may still allow the synthesis of well-defined polymers (i.e., IHB will be counter-balanced). In contrast, when a non-polar amine group is envisioned, IHB might reach its maximum value and lead to a significantly higher E_a , thus impacting the quality of control. In this case, the coupling of a preformed polymer could be the preferable pathway toward well-defined functionalized materials. Further investigations are therefore necessary to assess this hypothesis by probing the influence of the polarity of the amine group on the quality of the control.

V. Conclusion

In this article, a series of different amide-functionalized alkoxyamines (which is a functionality often obtained after conjugation from COOH- or NHS-containing alkoxyamines) based on the nitroxide SG1 have been synthesized and their k_d have been determined. A multi-parameter procedure was applied to rationalize their reactivity. It enabled to discriminate disubstituted alkoxyamines from monosubstituted ones. Whereas disubstituted alkoxyamines displayed expected dissociation abilities for SG1-based alkoxyamines, monosubstituted counterparts exhibited lower k_d (E_a increase of $\sim 7\text{--}10 \text{ kJ.mol}^{-1}$) because of the occurrence of IHB between the alkyl and the nitroxide fragments. To probe potential consequences on the synthesis of functionalized materials, S, *n*BA and MMA with a small amount of AN were successfully polymerized by NMP from AMA and AMA-NHS, that are two representative secondary SG1-based alkoxyamines employed for conjugation, displaying a carboxylic acid and a NHS group, respectively. Their performances were compared to that of AMA-Gem, a pre-functionalized alkoxyamine subjected to IHB bearing an anticancer drug as functional moiety via an amide bond. It resulted that the strong polarity of the Gem moiety still enabled a fair control despite the detrimental effect of IHB over its k_d . Overall, this work

may have important consequences toward the design of polymer conjugates from functional alkoxyamines and help in determining the most suitable approach for their design.

References

- (1) Perrier, S.; Takolpuckdee, P. *Journal of Polymer Science, Part A: Polymer Chemistry* **2005**, *43*, 5347.
- (2) Nicolas, J.; Guillaneuf, Y.; Lefay, C.; Bertin, D.; Gigmes, D.; Charleux, B. *Prog. Polym. Sci.* **2013**, *38*, 63.
- (3) Grubbs, R. B. *Polymer Reviews* **2011**, *51*, 104.
- (4) Matyjaszewski, K.; Xia, J. *Chem. Rev.* **2001**, *101*, 2921.
- (5) Kamigaito, M.; Ando, T.; Sawamoto, M. *Chem. Rev.* **2001**, *101*, 3689.
- (6) Moad, G.; Rizzardo, E.; Thang, S. H. *Aust. J. Chem.* **2009**, *62*, 1402.
- (7) Goto, A.; Fukuda, T. *Prog. Polym. Sci.* **2004**, *29*, 329.
- (8) Vinas, J.; Chagneux, N.; Gigmes, D.; Trimaille, T.; Favier, A.; Bertin, D. *Polymer* **2008**, *49*, 3639.
- (9) Chenal, M.; Boursier, C.; Guillaneuf, Y.; Taverna, M.; Couvreur, P.; Nicolas, J. *Polym. Chem.* **2011**, *2*, 1523.
- (10) Parvole, J.; Ahrens, L.; Blas, H.; Vinas, J.; Boissiere, C.; Sanchez, C.; Save, M.; Charleux, B. *J. Polym. Sci., Part A: Polym. Chem.* **2010**, *48*, 173.
- (11) Trimaille, T.; Mabrouk, K.; Monnier, V.; Charles, L.; Bertin, D.; Gigmes, D. *Macromolecules* **2010**, *43*, 4864.
- (12) Harrisson, S.; Nicolas, J.; Maksimenko, A.; Bui, D. T.; Mougin, J.; Couvreur, P. *Angew. Chem., Int. Ed.* **2013**, *52*, 1678.
- (13) Bertin, D.; Gigmes, D.; Marque, S. R. A.; Tordo, P. *Macromolecules* **2005**, *38*, 2638.
- (14) Chauvin, F.; Dufils, P.-E.; Gigmes, D.; Guillaneuf, Y.; Marque, S. R. A.; Tordo, P.; Bertin, D. *Macromolecules* **2006**, *39*, 5238.
- (15) Gigmes, D.; Vinas, J.; Chagneux, N.; Lefay, C.; Phan, T. N. T.; Trimaille, T.; Dufils, P.-E.; Guillaneuf, Y.; Carrot, G.; Boue, F.; Bertin, D. *ACS Symp. Ser.* **2009**, *1024*, 245.
- (16) Klein, J.; Herzog, D. *Die Makromolekulare Chemie* **1987**, *188*, 1217.
- (17) Weaver, W. E.; Whaley, W. M. *J. Am. Chem. Soc.* **1947**, *69*, 1144.
- (18) Hama, T.; Culkun, D. A.; Hartwig, J. F. *J. Am. Chem. Soc.* **2006**, *128*, 4976.
- (19) Leroi, C.; Bertin, D.; Dufils, P.-E.; Gigmes, D.; Marque, S.; Tordo, P.; Couturier, J.-L.; Guerret, O.; Ciufolini, M. A. *Org. Lett.* **2003**, *5*, 4943.
- (20) Chagneux, N.; Trimaille, T.; Rollet, M.; Beaudoin, E.; Gerard, P.; Bertin, D.; Gigmes, D. *Macromolecules* **2009**, *42*, 9435.
- (21) Dufils, P.-E.; Chagneux, N.; Gigmes, D.; Trimaille, T.; Marque, S. R. A.; Bertin, D.; Tordo, P. *Polymer* **2007**, *48*, 5219.
- (22) Harrisson, S.; Couvreur, P.; Nicolas, J. *Polym. Chem.* **2011**, *2*, 1859.
- (23) Deng, L.; Furuta, P. T.; Garon, S.; Li, J.; Kavulak, D.; Thompson, M. E.; Fréchet, J. M. J. *Chemistry of Materials* **2006**, *18*, 386.
- (24) The PS calibration is appropriate for PnBA samples as shown by the Mark-Houwink-Sakurada parameters: actually, it leads to an error of about 3-5%, which is within the accepted range for SEC analysis. Indeed, the MHS parameters in THF at 30 °C are the following: KPS = 11.4 10⁻⁵ dL g⁻¹ and PS = 0.716 for PS [see: Hutchinson, R. A.; Paquet, D. A., Jr.; McMinn, J. H.; Beuermann, S.; Fuller, R. E.; Jackson, C. *Dechema Monographs* 1995, *131*, 467]; KPnBA = 12.2 10⁻⁵ dL g⁻¹ and PnBA = 0.700 for PnBA [see: Beuermann, S.; Paquet, D. A., Jr.; McMinn, J. H.; Hutchinson, R. A. *Macromolecules* 1997, *29*, 1918].

- (25) Breitenbach, A.; Pistel, K.; Kissel, T. *Polymer* **2000**, *41*, 4781.
- (26) Matyjaszewski, K.; Woodworth, B. E.; Zhang, X.; Gaynor, S. G.; Metzner, Z. *Macromolecules* **1998**, *31*, 5955.
- (27) Bertin, D.; Gimes, D.; Le Mercier, C.; Marque, S. R. A.; Tordo, P. *J. Org. Chem.* **2004**, *69*, 4925.
- (28) Gimes, D.; Dufils, P.-E.; Gle, D.; Bertin, D.; Lefay, C.; Guillaneuf, Y. *Polym. Chem.* **2011**, *2*, 1624.
- (29) Bertin, D.; Dufils, P.-E.; Durand, I.; Gimes, D.; Giovanetti, B.; Guillaneuf, Y.; Marque, S. R. A.; Phan, T.; Tordo, P. *Macromol. Chem. Phys.* **2008**, *209*, 220.
- (30) Bertin, D.; Gimes, D.; Marque, S.; Tordo, P. *e-Polymers* **2003**, *002*, 1.
- (31) Bertin, D.; Gimes, D.; Marque, S. R. A.; Tordo, P. *Chem. Soc. Rev.* **2011**, *40*, 2189.
- (32) Harrisson, S.; Couvreur, P.; Nicolas, J. *Macromolecules* **2011**, *44*, 9230.
- (33) Harrisson, S.; Couvreur, P.; Nicolas, J. *Macromol. Rapid Commun.* **2012**, *33*, 805.
- (34) Bagryanskaya, E. G.; Brémond, P.; Butscher, T.; Marque, S. R. A.; Parkhomenko, D.; Roubaud, V.; Siri, D.; Viel, S. *Macromol. Chem. Phys.* **2014**, n/a.
- (35) Brémond, P.; Butscher, T.; Roubaud, V.; Siri, D.; Viel, S. *The Journal of Organic Chemistry* **2013**, *78*, 10524.
- (36) Marque, S.; Le Mercier, C.; Tordo, P.; Fischer, H. *Macromolecules* **2000**, *33*, 4403.
- (37) Liu, J.; Liu, W.; Weitzhandler, I.; Bhattacharyya, J.; Li, X.; Wang, J.; Qi, Y.; Bhattacharjee, S.; Chilkoti, A. *Angewandte Chemie International Edition* **2015**, *54*, 1002.
- (38) Farcet, C.; Nicolas, J.; Charleux, B. *J. Polym. Sci., Part A: Polym. Chem.* **2002**, *40*, 4410.
- (39) Lacroix-Desmazes, P.; Lutz, J.-F.; Chauvin, F.; Severac, R.; Boutevin, B. *Macromolecules* **2001**, *34*, 8866.
- (40) Nicolas, J.; Charleux, B.; Guerret, O.; Magnet, S. *Angew. Chem., Int. Ed.* **2004**, *43*, 6186.
- (41) Nicolas, J.; Charleux, B.; Magnet, S. *J. Polym. Sci., Part A: Polym. Chem.* **2006**, *44*, 4142.
- (42) Farcet, C.; Belleney, J.; Charleux, B.; Pirri, R. *Macromolecules* **2002**, *35*, 4912.
- (43) Guillaneuf, Y.; Gimes, D.; Junkers, T. *Macromolecules* **2012**, *45*, 5371.
- (44) Guégain, E.; Guillaneuf, Y.; Nicolas, J. *Macromol. Rapid Commun.* **2015**, submitted.
- (45) Ananchenko, G. S.; Souaille, M.; Fischer, H.; Le Mercier, C.; Tordo, P. *J. Polym. Sci., Part A: Polym. Chem.* **2002**, *40*, 3264.
- (46) Guillaneuf, Y.; Gimes, D.; Marque, S. R. A.; Tordo, P.; Bertin, D. *Macromol. Chem. Phys.* **2006**, *207*, 1278.
- (47) Dire, C.; Belleney, J.; Nicolas, J.; Bertin, D.; Magnet, S.; Charleux, B. *J. Polym. Sci., Part A: Polym. Chem.* **2008**, *46*, 6333.
- (48) Charleux, B.; Nicolas, J.; Guerret, O. *Macromolecules* **2005**, *38*, 5485.
- (49) McHale, R.; Aldabbagh, F.; Zetterlund, P. B. *J. Polym. Sci., Part A: Polym. Chem.* **2007**, *45*, 2194.
- (50) Nicolas, J.; Dire, C.; Mueller, L.; Belleney, J.; Charleux, B.; Marque, S. R. A.; Bertin, D.; Magnet, S.; Couvreur, L. *Macromolecules* **2006**, *39*, 8274.
- (51) Nicolas, J.; Mueller, L.; Dire, C.; Matyjaszewski, K.; Charleux, B. *Macromolecules* **2009**, *42*, 4470.
- (52) Nicolas, J.; Couvreur, P.; Charleux, B. *Macromolecules* **2008**, *41*, 3758.
- (53) Lessard, B.; Maric, M. *J. Polym. Sci., Part A: Polym. Chem.* **2009**, *47*, 2574.
- (54) Lessard, B.; Marić, M. *J. Polym. Sci., Part A: Polym. Chem.* **2011**, *49*, 5270.
- (55) Lessard, B.; Tervo, C.; De Wahl, S.; Clerveaux, F. J.; Tang, K. K.; Yasmine, S.; Andjelic, S.; D'Alessandro, A.; Maric, M. *Macromolecules* **2010**, *43*, 868.

- (56) Lessard, B. H.; Ling, E. J. Y.; Marić, M. *Macromolecules* **2012**, *45*, 1879.
- (57) Ting, S. R. S.; Min, E.-H.; Escale, P.; Save, M.; Billon, L.; Stenzel, M. H. *Macromolecules* **2009**, *42*, 9422.
- (58) Nicolas, J.; Brusseau, S.; Charleux, B. *J. Polym. Sci., Part A: Polym. Chem.* **2010**, *48*, 34.
- (59) Lessard, B.; Ling, E. J. Y.; Morin, M. S. T.; Marić, M. *J. Polym. Sci., Part A: Polym. Chem.* **2011**, *49*, 1033.
- (60) Audran, G.; Bremond, P.; Marque, S. R. A.; Obame, G. *Polym. Chem.* **2012**, *3*, 2901.
- (61) Audran, G.; Brémond, P.; Marque, S. R. A.; Obame, G. *The Journal of Organic Chemistry* **2012**, *77*, 9634.

Supporting Information

1. DFT Calculations

All calculations were performed with the Gaussian 03 molecular orbital package.¹ The geometry optimizations were carried out without constraints at the UB3LYP/6-31++G(d,p) level of theory. Vibrational frequencies were calculated at the UB3LYP/6-31++G(d,p) level to determine the nature of the located stationary points. Frequency calculations were performed to confirm that the geometry was a minimum (zero imaginary frequency). The single-point energies were then calculated at the UB3LYP/6-311++G(3df,3pd) level of theory.

2. Estimation of Charton constant ν , the electrical Hammett constants σ_I , and the radical stabilization constants σ_{RS}

The values reported in Table S1 were determined as reported in the literature. However, many of the alkyl moieties cannot be described by parameters given in the literature. For example, the effect of polar groups attached to the nitrogen atom of amide on the electrical Hammett constants σ_I is not reported. For the sake of simplicity, $\sigma_I = 0.07$, *i.e.* no influence of the long-range polar group, was chosen to **3**, **4**, and **6** to plot Figure 1.

In a similar manner, the steric Charton ν for CONMe_2 is not reported. However, based on the similitude approach, as $\nu_{\text{CONH}_2} = \nu_{\text{COOH}}$, it was assumed $\nu_{\text{CONMe}_2} = \nu_{\text{COOMe}} = 0.90$. For the steric Charton ν of monosubstituted *N*-alkyl amide moieties, it must be mentioned that amide group exhibit two diastereoisomers *Z* (H *s-trans* to the C=O) and *E* (H *s-cis* to the C=O), the isomer *Z* being favored due to relief of steric strain. Hence, since the steric hindrance is assumed to be only due to the group pointing to the nitroxide, the bulkiness of the amide group should be well-described by the value of CONH_2 , that is: $\nu_{\text{CONHR}} = \nu_{\text{CONH}_2} = 0.5$.

Alkoxyamine	E_a (kJ.mol ⁻¹)	σ_{RS}	σ_I	ν
BlocBuilder (1)	112	0.21	0.07	1.24
2	105.5	0.20	0.06	1.42
3a	122.0	0.20	0.07	1.25
3b	125.0	0.20	0.07	1.25
4	117.9	0.20	0.07	1.25
5	123.5	0.20	0.07	1.25
6	121.6	0.20	0.06	1.25
7	112.3	0.20	0.07	1.42
AMA (8)	130.7/132.8	0.18	0.09	0.83
9	124.5	0.18	0.09	1.01
10	135	0.18	0.09	1.01
AMA-NHS (11)	127.2	0.18	0.19	0.83
AMA-Gem (12)	131	0.18	0.06/0.13	1.01
13	115/116	0.34	0.05	1.06
14	124.5	0.18	0.11	1.03
15	123.4	0.18	0.09	1.2
16	130	0.18	0.09	1.03

The 7 kJ.mol⁻¹ lower E_a for **2** compared to **7** is due to the presence of the phenyl group, which significantly increases the polarity. Interestingly, alkoxyamine **3–6** exhibit 5–12 kJ.mol⁻¹ higher E_a than **7**. This difference is due to the occurrence of hydrogen-bonding between the hydrogen-atom of the secondary amide and the P=O moiety. The influence of this intramolecular hydrogen bonding (IHB) is slightly modified by the occurrence of a second weak hydrogen-bonding, between the hydrogen-atom of the secondary amide and the O-N moiety, the polarity (**4** and **6**) and the bulkiness (**5** and **6**) of the alkyl substituent. The same trend is observed for **9**, **10**, **12**, **15** and **16**.

It was not possible to estimate σ_I for alkoxyamine **12**. To have a first approximation, we used the σ_I that was used for alkoxyamine **2**, that is the polarity of an aromatic ring linked to the amide functionality. This value could be seen as a lower limit of σ_I . To estimate the polarity of the cytosine moiety, we used the polar parameter of the oxo-pyrimidinyl group² ($\sigma_{I,R1} = 0.41$). With this value the polar parameter σ_I increases from 0.06 to 0.13.

Equation for Figure 1 is the following:

$$y\text{-intercept} = -13.90 \text{ (40)}$$

$$RS = 14.85 \text{ (77)}$$

I = 20.01 (145)

u = 6.68 (29)

N = 40

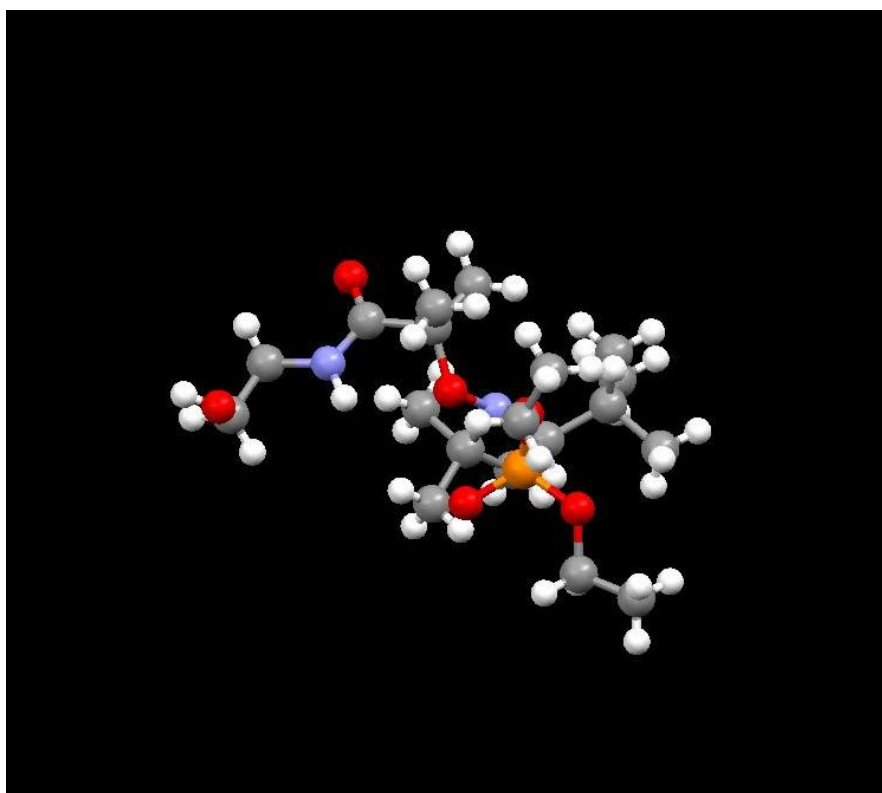
R² = 0.96

SD = 0.39

F = 287

∇t > 99.99%

3. RX data for alkoxyamine 3b

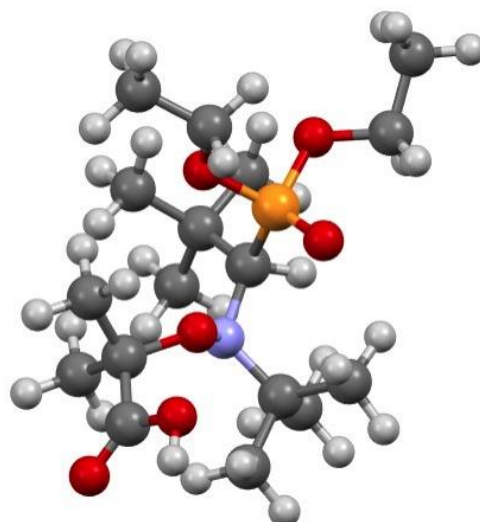


4. DFT Calculations

Cartesian coordinates for alkoxyamines **1**, **17**, **18**, **19** and **20**.

4.1 BlocBuilder 1

Chapter 2 – On the Structure-Control Relationship of Amide-Functionalized SG1-Based Alkoxyamines
for Nitroxide-Mediated Polymerization and Conjugation

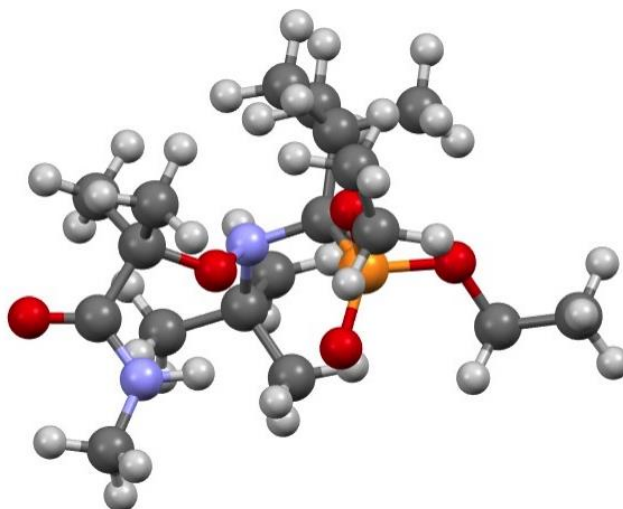


C	-5.22900	-0.35900	-1.28200
C	-3.76400	-0.75000	-1.38000
O	-3.02700	0.00200	-0.39100
P	-1.43700	0.34000	-0.61300
C	-0.54500	-0.98900	0.38800
C	-0.96100	-1.15500	1.92000
C	-0.01600	-2.17300	2.59500
O	-1.09800	0.43600	-2.05700
O	-1.33000	1.70800	0.24100
C	-1.85200	2.91700	-0.37000
C	-1.82400	4.02200	0.66900
N	0.92500	-1.02000	0.13700
C	1.39000	-2.03700	-0.89500
C	2.91000	-1.89000	-1.08100
O	1.31600	0.30800	-0.28300
C	2.37600	0.97400	0.46700
C	3.60800	1.12500	-0.45200
C	-2.38700	-1.74700	2.01000
C	-0.93600	0.14900	2.74300
C	1.13500	-3.44500	-0.32300
C	0.73000	-1.90800	-2.28000
C	1.85400	2.40000	0.72300
O	4.76100	0.99200	-0.10200
H	-3.63400	-1.82100	-1.17400
H	-3.35500	-0.53500	-2.37200
H	-1.23500	3.16000	-1.24100
H	-2.87600	2.72900	-0.71300
H	-0.95300	-1.88500	-0.09700
H	-5.62100	-0.55800	-0.28000
H	-5.81900	-0.93400	-2.00500
H	-5.35900	0.70600	-1.49900
H	-2.44800	3.76400	1.53000
H	-2.20800	4.95100	0.23100
H	-0.80500	4.20400	1.02100
H	-2.61700	-1.97900	3.05600
H	-2.46700	-2.68400	1.44400
H	-3.14700	-1.05800	1.63900
H	-1.69900	0.85500	2.41100
H	0.02900	0.65700	2.68700
H	-1.12600	-0.08800	3.79600

Chapter 2 – On the Structure-Control Relationship of Amide-Functionalized SG1-Based Alkoxyamines
for Nitroxide-Mediated Polymerization and Conjugation

H	1.02800	-1.86400	2.54200
H	-0.09900	-3.16500	2.13900
H	-0.29700	-2.27500	3.65000
H	1.65300	-3.59100	0.62900
H	1.51500	-4.18600	-1.03600
H	0.07300	-3.66400	-0.17400
H	-0.33800	-2.14500	-2.26200
H	1.21000	-2.61200	-2.97000
H	0.83300	-0.89600	-2.67100
H	3.15400	-0.98700	-1.63900
H	3.28000	-2.74100	-1.66200
H	3.44300	-1.88600	-0.12600
H	1.51100	2.84500	-0.21500
H	1.01600	2.36600	1.42100
C	2.80400	0.30400	1.76900
H	1.97500	0.27100	2.47600
H	3.16700	-0.71100	1.61200
H	3.61700	0.88900	2.20500
H	2.64800	3.02800	1.14300
O	3.27300	1.50800	-1.70600
H	4.11700	1.61800	-2.18300

4.2 Alkoxyamine 17



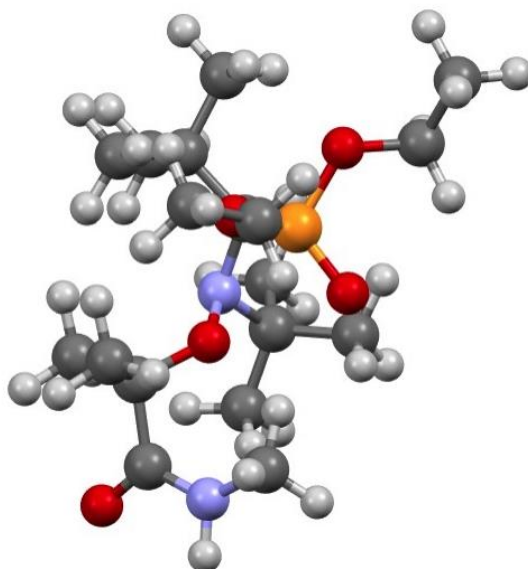
C	4.83100	-0.33000	-2.32500
C	3.37200	0.06400	-2.17900
O	2.94800	-0.26300	-0.83600
P	1.36900	-0.53800	-0.49900
C	0.83400	1.07200	0.34100
C	1.42500	1.35700	1.78500
C	1.11600	2.82700	2.14200
O	0.63900	-1.02000	-1.70700
O	1.50200	-1.60500	0.70900
C	1.91700	-2.95900	0.39100
C	1.91200	-3.76600	1.67600
N	-0.63400	1.31900	0.23600
C	-1.03900	2.20000	-0.94400
C	-2.57100	2.29500	-1.00800
O	-1.21900	0.00300	0.08400
C	-2.33800	-0.44900	0.91300

Chapter 2 – On the Structure-Control Relationship of Amide-Functionalized SG1-Based Alkoxyamines
for Nitroxide-Mediated Polymerization and Conjugation

C	-3.40500	-0.99800	-0.07800
N	-2.91100	-1.39400	-1.28200
C	-3.73700	-2.03500	-2.28800
C	2.96000	1.19300	1.79000
C	0.82800	0.47800	2.89600
C	-0.51500	3.62400	-0.67100
C	-0.52700	1.72800	-2.31900
C	-1.84500	-1.67100	1.71300
C	-2.96100	0.58300	1.84700
O	-4.57600	-1.13000	0.26700
H	3.24400	1.14400	-2.33300
H	2.73600	-0.46300	-2.89600
H	1.22500	-3.37300	-0.34900
H	2.91900	-2.92200	-0.05200
H	1.33300	1.80500	-0.30200
H	-3.81700	-1.41900	-3.19200
H	-4.73200	-2.17300	-1.86200
H	5.45200	0.18600	-1.58700
H	5.19100	-0.06600	-3.32600
H	4.95500	-1.40900	-2.18700
H	2.60300	-3.33700	2.40800
H	2.22400	-4.79600	1.46800
H	0.91100	-3.79100	2.11600
H	3.35100	1.54200	2.75300
H	3.43700	1.78800	1.00300
H	3.27000	0.15500	1.65900
H	1.02200	-0.58200	2.72900
H	-0.25000	0.63100	2.98300
H	1.27600	0.75900	3.85700
H	0.03900	3.01500	2.15300
H	1.58500	3.52600	1.44000
H	1.51000	3.05000	3.14100
H	-0.87200	4.00200	0.29100
H	-0.88700	4.29000	-1.45800
H	0.57700	3.69300	-0.68400
H	0.56500	1.75600	-2.39400
H	-0.91700	2.39800	-3.09300
H	-0.84500	0.71000	-2.54300
H	-3.03700	1.32400	-1.18000
H	-2.84900	2.94500	-1.84500
H	-2.98100	2.73800	-0.09700
H	-1.32400	-2.37000	1.05300
H	-2.70500	-2.18400	2.15600
H	-1.16300	-1.37000	2.50900
H	-2.21400	1.00200	2.52300
H	-3.73200	0.07800	2.43300
H	-3.44400	1.39700	1.30900
H	-1.92700	-1.22800	-1.46400
H	-3.32300	-3.01100	-2.56700

4.3 Alkoxyamine 18

Chapter 2 – On the Structure-Control Relationship of Amide-Functionalized SG1-Based Alkoxyamines
for Nitroxide-Mediated Polymerization and Conjugation

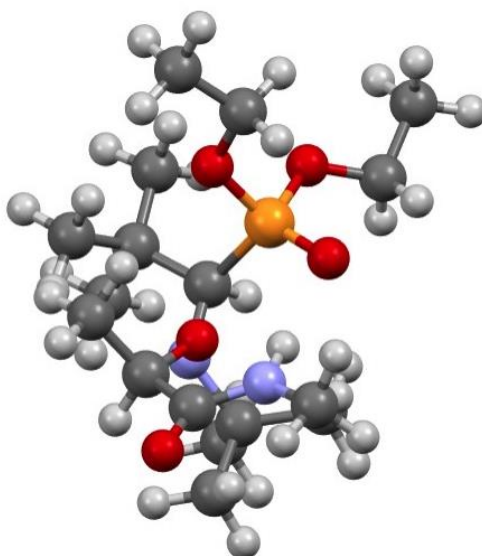


C	-5.11600	-0.09300	-1.78000
C	-3.64800	-0.48000	-1.74400
O	-3.05500	0.10000	-0.56000
P	-1.45400	0.43700	-0.50500
C	-0.70100	-1.05500	0.37700
C	-1.17000	-1.33000	1.87500
C	-0.46800	-2.61000	2.37700
O	-0.93000	0.78900	-1.85400
O	-1.45400	1.63500	0.58000
C	-1.96700	2.93000	0.17100
C	-1.90300	3.86100	1.36700
N	0.76600	-1.18100	0.14800
C	1.16700	-2.10500	-0.99700
C	2.68300	-1.99600	-1.22700
O	1.26900	0.15200	-0.09200
C	2.37600	0.64600	0.73500
C	3.60800	0.93100	-0.17900
N	3.43800	1.54500	-1.39100
C	-2.69100	-1.60500	1.90300
C	-0.87500	-0.20200	2.88300
C	0.86800	-3.55000	-0.55100
C	0.46700	-1.83600	-2.34400
C	1.90700	1.99400	1.31400
C	2.81400	-0.28800	1.86100
O	4.73900	0.64700	0.20500
H	-3.53600	-1.57100	-1.69100
H	-3.11400	-0.11800	-2.62700
H	-1.36100	3.29900	-0.66200
H	-2.99800	2.80500	-0.17900
H	-1.16800	-1.86900	-0.19100
H	-5.63400	-0.44000	-0.88000
H	-5.60100	-0.54400	-2.65300
H	-5.22800	0.99400	-1.84600
H	-2.51300	3.48000	2.19200
H	-2.28300	4.85000	1.08600
H	-0.87300	3.97400	1.71900
H	-2.97400	-1.95000	2.90400
H	-2.97200	-2.39400	1.19300

**Chapter 2 – On the Structure-Control Relationship of Amide-Functionalized SG1-Based Alkoxyamines
for Nitroxide-Mediated Polymerization and Conjugation**

H	-3.28400	-0.71900	1.67000
H	-1.41000	0.71600	2.64200
H	0.19000	0.03000	2.93900
H	-1.18900	-0.52900	3.88200
H	0.61900	-2.51100	2.34600
H	-0.74900	-3.48700	1.78600
H	-0.76900	-2.80300	3.41300
H	1.38300	-3.79400	0.38300
H	1.22100	-4.23900	-1.32700
H	-0.20100	-3.74200	-0.41600
H	-0.61200	-2.02100	-2.30400
H	0.87900	-2.51600	-3.09800
H	0.61300	-0.80800	-2.67600
H	2.95800	-1.02600	-1.64200
H	2.98200	-2.76300	-1.95000
H	3.25400	-2.16600	-0.31200
H	1.55300	2.66300	0.52500
H	2.73700	2.48400	1.83600
H	1.08700	1.84000	2.01700
H	1.99800	-0.46800	2.55900
H	3.64200	0.18500	2.39200
H	3.16900	-1.24800	1.48900
C	2.27300	2.14000	-2.03700
H	2.38600	2.03500	-3.12100
H	1.35700	1.63000	-1.74600
H	2.18500	3.21200	-1.81000
H	4.33800	1.73300	-1.81800

4.4 Alkoxyamine 19



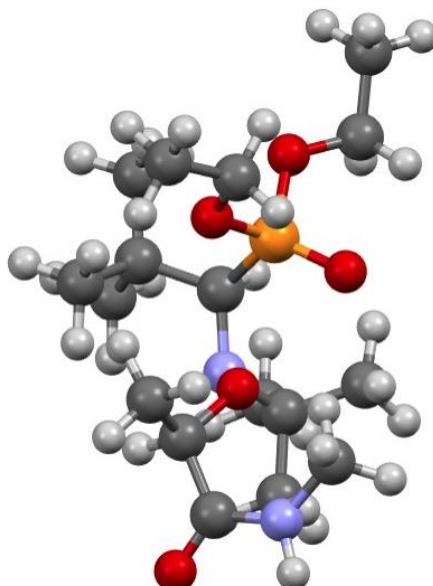
C	4.56900	-0.61200	-2.49600
C	3.14400	-0.13600	-2.27600
O	2.77700	-0.42800	-0.90800
P	1.20500	-0.58400	-0.48300
C	0.81500	1.09100	0.30500
C	1.50300	1.40700	1.69600
C	1.38600	2.92400	1.95500
O	0.38400	-1.05400	-1.63800

**Chapter 2 – On the Structure-Control Relationship of Amide-Functionalized SG1-Based Alkoxyamines
for Nitroxide-Mediated Polymerization and Conjugation**

O	1.32300	-1.60900	0.76000
C	1.61400	-3.00300	0.48200
C	1.58300	-3.75900	1.79700
N	-0.64600	1.38500	0.31900
C	-1.15500	2.23800	-0.83300
C	-2.68000	2.39600	-0.69300
O	-1.25000	0.06200	0.27700
C	-2.44900	-0.17200	1.03700
C	-3.46700	-0.86800	0.10900
N	-2.94200	-1.39700	-1.02700
C	-3.74400	-2.15500	-1.96900
C	3.00600	1.05800	1.68100
C	0.82100	0.68600	2.86900
C	-0.54800	3.64700	-0.67900
C	-0.84000	1.69900	-2.24000
C	-2.19900	-1.08300	2.24200
O	-4.64300	-0.96500	0.45100
H	3.06900	0.94900	-2.43400
H	2.44100	-0.63100	-2.95100
H	0.86600	-3.38300	-0.22000
H	2.60000	-3.06600	0.01000
H	1.28900	1.76800	-0.41500
H	-3.78800	-1.65800	-2.94600
H	-4.75300	-2.23200	-1.56200
H	5.25700	-0.12500	-1.79700
H	4.88900	-0.37700	-3.51800
H	4.64100	-1.69500	-2.35200
H	2.32900	-3.36300	2.49300
H	1.80000	-4.81900	1.62100
H	0.59700	-3.68300	2.26600
H	3.46200	1.41600	2.61200
H	3.53000	1.53900	0.84700
H	3.18400	-0.01700	1.61400
H	0.84300	-0.39900	2.75100
H	-0.21700	1.01300	2.96400
H	1.33700	0.94100	3.80300
H	0.34100	3.24100	1.99600
H	1.90000	3.51300	1.18500
H	1.84900	3.16700	2.91800
H	-0.80900	4.09000	0.28600
H	-0.95500	4.28800	-1.46800
H	0.54000	3.66200	-0.78300
H	0.23500	1.67100	-2.44500
H	-1.29500	2.36100	-2.98600
H	-1.22900	0.69200	-2.38300
H	-3.21600	1.46800	-0.90300
H	-3.02800	3.14100	-1.41600
H	-2.95200	2.74900	0.30700
H	-1.66400	-1.98500	1.92600
H	-3.16400	-1.37600	2.66600
H	-1.61100	-0.58100	3.01100
H	-1.95200	-1.25500	-1.20700
H	-3.33300	-3.16200	-2.11000
H	-2.87800	0.77600	1.36200

4.5 Alkoxyamine 20

Chapter 2 – On the Structure-Control Relationship of Amide-Functionalized SG1-Based Alkoxyamines
for Nitroxide-Mediated Polymerization and Conjugation

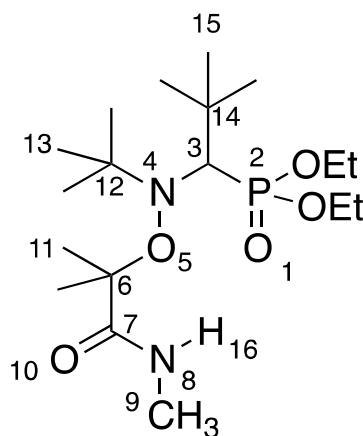


C	0.00000	0.00000	0.00000
C	0.00000	0.00000	1.51900
O	1.37300	0.00000	1.96900
P	1.75300	-0.53200	3.47100
C	1.93600	1.05800	4.46500
C	3.15500	2.00600	4.09700
C	2.92000	3.37400	4.77200
O	0.78400	-1.55800	3.94400
O	3.26900	-1.04000	3.22500
C	3.46700	-2.27200	2.48300
C	4.96000	-2.49600	2.33200
N	1.79500	0.85200	5.93100
C	0.42200	1.11000	6.52000
C	0.48900	0.80700	8.02700
O	2.17600	-0.52300	6.20000
C	3.24200	-0.67000	7.16100
C	2.79500	-1.32000	8.48500
N	1.97900	-2.41700	8.45900
C	3.23500	2.25000	2.57600
C	4.51300	1.47900	4.59000
C	0.10300	2.61100	6.37200
C	-0.71300	0.28100	5.89200
C	4.37100	-1.51500	6.55900
O	3.22600	-0.87500	9.54500
H	-0.49800	0.90000	1.90600
H	-0.51300	-0.87700	1.92400
H	2.98800	-3.09000	3.03000
H	2.98100	-2.17500	1.50600
H	1.04600	1.60300	4.12500
H	0.53400	0.87200	-0.39100
H	-1.03000	0.02800	-0.37400
H	0.48400	-0.90300	-0.38600
H	5.42500	-1.66700	1.78900
H	5.14200	-3.42100	1.77500
H	5.44300	-2.58300	3.31100
H	3.99800	3.01300	2.37800
H	2.28500	2.61900	2.17100
H	3.50800	1.35100	2.02100

**Chapter 2 – On the Structure-Control Relationship of Amide-Functionalized SG1-Based Alkoxyamines
for Nitroxide-Mediated Polymerization and Conjugation**

H	4.77800	0.53400	4.11400
H	4.51600	1.34900	5.67500
H	5.29300	2.21100	4.34600
H	2.86800	3.27600	5.85900
H	1.99900	3.85300	4.42000
H	3.75200	4.04600	4.53200
H	0.84800	3.23200	6.87500
H	-0.87000	2.80400	6.83700
H	0.02800	2.93600	5.33000
H	-0.91100	0.56400	4.85300
H	-1.63800	0.45100	6.45600
H	-0.48100	-0.78400	5.90300
H	0.52000	-0.26600	8.22100
H	-0.40900	1.20300	8.51300
H	1.36100	1.27500	8.49300
H	4.01100	-2.51000	6.27800
H	5.16900	-1.63600	7.30000
H	4.78000	-1.03600	5.66900
C	1.49400	-3.20900	7.33500
H	0.47600	-3.55000	7.55000
H	1.46000	-2.61000	6.42600
H	2.12100	-4.09600	7.16200
H	1.83400	-2.79600	9.38800
H	3.60300	0.32300	7.43300

**5. Bond length, distance between atoms and valence angle determined for alkoxyamines
1, 3b, 17, 18, 19 and 20**



	17	18	1	19	20	3b (X-ray)
<i>l</i> (Å)						
N4—O5	1.448	1.445	1.447	1.455	1.452	1.460
C3—P2	1.893	1.890	1.888	1.892	1.884	1.842
P2—O1	1.491	1.489	1.486	1.493	1.488	1.460
O5—C6	1.464	1.467	1.459	1.439	1.443	1.471

Chapter 2 – On the Structure-Control Relationship of Amide-Functionalized SG1-Based Alkoxyamines
for Nitroxide-Mediated Polymerization and Conjugation

N8—H16	1.014	1.014	-	1.016	1.014	0.977
d (Å)						
N4 ^{•••} C6	2.547	2.505	2.488	2.488	2.434	2.503
O1 ^{•••} C7	4.360	4.839	5.020	4.233	4.972	4.992
O1 ^{•••} H16	2.586	5.352	-	2.384	5.681	2.373
O5 ^{•••} H16	2.101	3.860	-	2.105	3.930	2.373
α (°)						
<N4O5C6>	122.0	118.7	117.8	118.6	114.4	117.3
<C11,HC6C7>	107.7	108.5	109.1	108.2	105.4	109.2
<C7C6O5>	105.8	109.9	108.5	107.8	113.6	109.0
<C11,HC6O5>	116.8	115.2	116.2	110.1	108.5	114.9
<C6C7N8>	114.7	120.2	-	115.1	119.7	117.3
<C7N8H16>	117.6	110.2	-	118.0	111.6	118.0
<O5H16N8>	106.7	-	-	106.7	-	102.9
<O1H16N8>	173.0	-	-	176.8	-	154.5
<C3N4O5>	104.7	106.9	107.1	103.1	109.1	106.5
θ (°)						
<O10C7C6 σ^*_{O5-C6} > <O5C6C7O10> + 180° $n_{p,O10} \rightarrow \sigma^*_{O5-C6}$	18.9	39.2	38.6	12.6	41.2	55.5
<O5C6C7O10>	-161.1	-140.8	-141.4	-167.4	-138.8	-145.5
< $\pi_{C7}C7C6O5$ > <O5C6C7O10> + 90° $\pi_{C7} \rightarrow \sigma^*_{O5-C6}$	-71.1	-50.8	-51.4	-77.4	-48.8	-55.5
<N4O5C6H,Me>	6.3	-4.7	-10.2	13.8	-4.6	-11.2
<C6O5N4 $n_{\sigma,N4}$ >	12.9	11.3	10.7	26.8	10.1	10.3
<C7C6O5N4>	129.6	117.6	113.5	131.6	112.3	111.7
<C7C6O5 $n_{p,O5}$ > <C7C6O5N4> - 90° $n_{p,O5} \rightarrow \sigma^*_{C6-C7}$	39.6	27.6	23.5	41.6	22.3	21.7
<O10C7N8H16>	179.5	171.5	-	179.9	171.3	177.2
<C15C14C3N4>	-175.4	-162.5	-154.1	-178.3	-177.5	-155.1

<C13C12N4O5>	174.4	168.3	172.2	176.5	173.5	179.1
<HC3N4O5>	135.2	136.5	134.2	134.7	135.7	134.0
<O1P2C3N4>	32.2	37.3	46.6	35.7	35.4	46.1

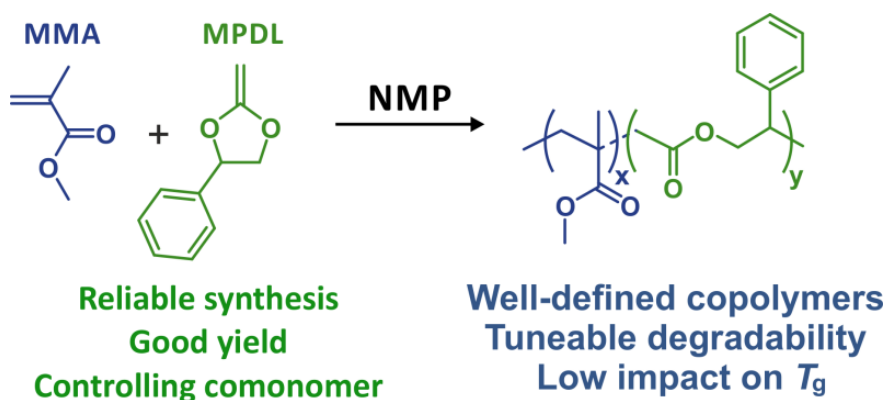
References

- (1) Frisch, M. J.; Trucks, G. W.; Schlegel, H. B.; Scuseria, G. E.; Robb, M. A.; Cheeseman, J. R.; Scalmani, G.; Barone, V.; Mennucci, B.; Petersson, G. A.; Nakatsuji, H.; Caricato, M.; Li, X.; Hratchian, H. P.; Izmaylov, A. F.; Bloino, J.; Zheng, G.; Sonnenberg, J. L.; Hada, M.; Ehara, M.; Toyota, K.; Fukuda, R.; Hasegawa, J.; Ishida, M.; Nakajima, T.; Honda, Y.; Kitao, O.; Nakai, H.; Vreven, T.; Montgomery Jr., J. A.; Peralta, J. E.; Ogliaro, F.; Bearpark, M. J.; Heyd, J.; Brothers, E. N.; Kudin, K. N.; Staroverov, V. N.; Kobayashi, R.; Normand, J.; Raghavachari, K.; Rendell, A. P.; Burant, J. C.; Iyengar, S. S.; Tomasi, J.; Cossi, M.; Rega, N.; Millam, N. J.; Klene, M.; Knox, J. E.; Cross, J. B.; Bakken, V.; Adamo, C.; Jaramillo, J.; Gomperts, R.; Stratmann, R. E.; Yazyev, O.; Austin, A. J.; Cammi, R.; Pomelli, C.; Ochterski, J. W.; Martin, R. L.; Morokuma, K.; Zakrzewski, V. G.; Voth, G. A.; Salvador, P.; Dannenberg, J. J.; Dapprich, S.; Daniels, A. D.; Farkas, Ö.; Foresman, J. B.; Ortiz, J. V.; Cioslowski, J.; Fox, D. J.; Gaussian, Inc.: Wallingford, CT, USA, 2009.
- (2) Hansch, C.; Leo, A.; Taft, R. W. *Chemical Reviews* **1991**, *91*, 165.

Chapter 3

Efficient synthesis of 2-methylene-4-phenyl-1,3-dioxolane, a cyclic ketene acetal for controlling the NMP of methyl methacrylate and conferring tunable degradability

*Johanna Tran, Elise Guégain, Nada Ibrahim, Simon Harrisson,
Julien Nicolas**



Polymer Chemistry **2016**, 7 (26), 4427-4435

ABSTRACT

Efficient and reliable synthesis of 2-methylene-4-phenyl-1,3-dioxolane (MPDL), a highly effective cyclic ketene acetal for radical ring-opening polymerization, was reported from three different acetal halides and thoroughly characterized by ^1H and ^{13}C NMR spectroscopy, IR spectroscopy, elemental analysis and mass spectrometry. MPDL was then employed as a controlling comonomer for nitroxide-mediated polymerization using methyl methacrylate (MMA) as the principal monomer to produce well-defined, degradable PMMA-rich copolymers ($M_n \sim 20\text{--}30 \text{ kg}\cdot\text{mol}^{-1}$, $D = 1.3\text{--}1.4$) when sufficient MPDL was initially introduced in the monomer feed ($f_{\text{MPDL},0} > 0.2$). Hydrolytic degradation was tuned by varying the amount of MPDL in the monomer feed. Insertion of MPDL into the polymethacrylate backbone only moderately affected the glass transition temperature compared to poly(methyl methacrylate) homopolymer, while giving low molar mass degradation products after hydrolysis.

I. Introduction

A broad range of vinyl polymer-based materials (e.g., nanoparticles, micelles, hydrogels) have been proposed for biomedical applications,¹ but their inherent lack of degradability is a severe drawback. Radical ring-opening polymerization (rROP),² is an attractive strategy for conferring degradability on vinyl polymers, as: (i) different families of cyclic monomers²⁻⁴ can undergo radical ring-opening, leading to main-chain labile groups of different nature (e.g., ester, disulfide, thioester); (ii) these monomers can be copolymerized with traditional vinyl monomers (e.g., vinyl acetate, methacrylic esters) and (iii) the fraction of cleavable linkages in the resulting copolymer can be tuned by adjusting the initial comonomer feed, giving degradation profiles that range from moderate to nearly complete.

Cyclic ketene acetals⁵ are undoubtedly the most extensively studied family of monomers for rROP.² They were the subject of extensive research by Bailey and co-workers in the early 1980s⁶⁻¹³ and have attracted renewed attention over the last decade as comonomers to confer degradability to vinyl polymers, via conventional radical polymerization¹⁴⁻²¹ and reversible deactivation radical polymerization (RDRP) techniques.²²⁻³⁰ This was illustrated by the synthesis of a variety of degradable copolymers designed for biomedical applications including biomaterials, drug delivery and tissue engineering. Two CKAs have been almost exclusively employed for this purpose: 2-methylene-1,3-dioxepane (MDO)³¹ and 5,6-benzo-2-methylene-1,3-dioxepane (BMDO).¹¹ Recently, our group investigated the influence of the nature of the CKA during its nitroxide-mediated copolymerization with oligo(ethylene glycol) methyl ether methacrylate (MeOEGMA) in the presence of a small amount of acrylonitrile (AN), which acts as a controlling comonomer.^{28,29} Addition of even relatively small amounts of MDO or BMDO resulted in very slow polymerizations (nearly inhibited) and loss of control. In the presence of 2-methylene-4-phenyl-1,3-dioxolane (MPDL, also abbreviated MPDO),^{13,32} however, high monomer conversions were reached and well-defined copolymers with adjustable amounts of ester groups in the main chain could be obtained.²⁹ We postulated that the styrene-like structure of the ring-opened radical of MPDL facilitated the cleavage of the MPDL-SG1 macroalkoxyamine, allowing cross-propagation to proceed. In addition, MPDL was able to act as a controlling comonomer for the NMP of MeOEGMA, thus avoiding the use of a small amount of AN.²⁷ As for other controlling comonomers (e.g., styrene,³³ AN,³⁴ 9-(4-vinylbenzyl)-9-H-carbazole³⁵), this is due to the preferential formation of OEGMA-MPDL-SG1 macroalkoxyamines during the polymerization.²⁸ The amount of degradation conferred

by MPDL could be tuned by varying the initial monomer ratio, and neither the copolymer nor its degradation products were cytotoxic to different cell lines.²⁷

The first step of the MPDL synthesis involves transacetalization of styrene glycol with a haloacetaldehyde dimethyl acetal (styrene glycol as well as the bromo and chloro acetaldehydes are commercially available) under acid catalysis.¹³ A few different experimental conditions have been reported for MPDL synthesis.^{13,36-39} However, they turned out to be poorly detailed, difficult to reproduce (even after multiple trials), and required harsh reaction conditions as well as laborious work-up.

Despite these limitations, the unique features of MPDL prompted us to develop a reliable and robust method for its synthesis. We were able to obtain high-purity MPDL from different haloacetaldehyde dimethyl acetals under mild conditions with good overall yields and in a highly reproducible fashion. To demonstrate the applicability of the use of MPDL as a controlling comonomer for NMP of methacrylic esters, MPDL was then successfully copolymerized with methyl methacrylate (MMA) as the principal monomer (Figure 1). It gave access to a small library of well-defined, degradable polymethacrylates with rapid and tunable degradation patterns (from moderate to nearly complete) governed by the initial monomer stoichiometry. The influence of the presence of MPDL units on the thermal properties of the resulting copolymers was also investigated.

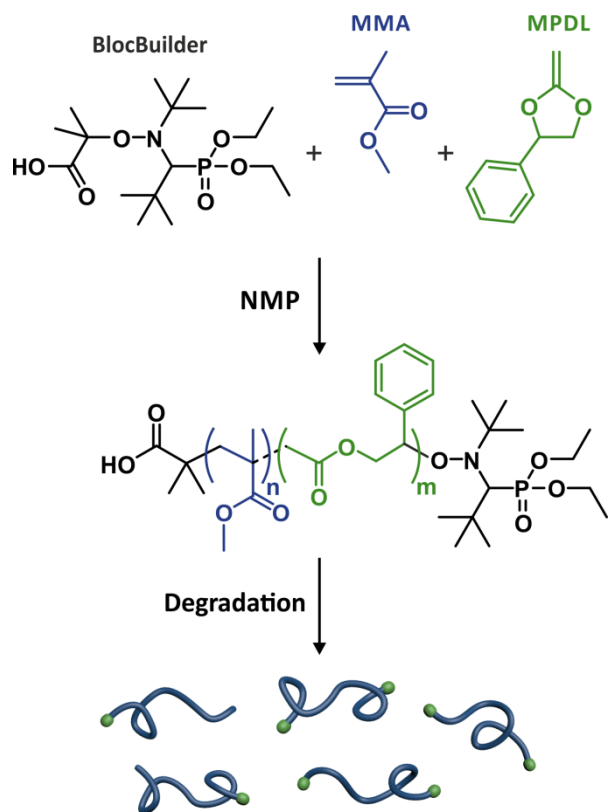


Figure 1. Synthesis of degradable poly[(methyl methacrylate)-*co*-2-methylene-4-phenyl-1,3-dioxolane] by nitroxide-mediated polymerization (NMP) of methyl methacrylate (MMA) and 2-methylene-4-phenyl-1,3-dioxolane (MPDL) using the BlocBuilder alkoxyamine.

II. Experimental Part

a. Materials

Unless otherwise specified, reagents were used as received without further purification. Methyl methacrylate (MMA, Sigma Aldrich, 99%) and acetone (Carlo Erba) were distilled prior to use. Styrene glycol was purchased either from Alfa Aesar (97%) and used as received, or from Sigma Aldrich (97%) and recrystallized from toluene before use. Bromoacetaldehyde dimethyl acetal (97%), chloroacetaldehyde dimethyl acetal (98%), Dowex 50 (H⁺) resin, sodium iodide (98%), Aliquat® 336, potassium *tert*-butoxide (> 98%), anhydrous THF (99.9%) and anhydrous toluene (99.8%) were purchased from Sigma Aldrich. BlocBuilder was kindly supplied by Arkema. THF and diethyl ether were purchased from VWR and all other solvents were purchased from Carlo Erba.

b. Analytical Techniques

Infrared (IR) spectra were obtained from the neat liquids on a Perkin Elmer spectrometer (Spectrum Two, FT-IR). Only significant absorptions are listed. Gas chromatography–mass spectrometry (GC/MS) spectra were recorded on an ITQ900® (Thermo Scientific) spectrometer. Elemental analysis was performed by the Service de microanalyse, Institut de Chimie des Substances Naturelles, Gif-sur-Yvette. Nuclear Magnetic Resonance (NMR) spectra were recorded in 5 mm tubes on a Bruker Avance 300 spectrometer. Chemical shifts of ^1H NMR and ^{13}C NMR are reported in ppm (δ units), and tetramethylsilane (TMS) was used as internal reference. The abbreviations used to designate the multiplicities are: s = singlet, d = doublet, t = triplet, q = quartet, m = multiplet. Size Exclusion Chromatography (SEC) analyses were performed on a Tosoh EcoSEC HLC-8320 GPC with two columns from Polymer Laboratories (PL-gel MIXED-D 300 \times 7.5 mm, beads diameter 5 μm ; linear part 400 to 4 \times 10⁵ g.mol⁻¹). Analyses were performed at 35 °C in chloroform (HPLC grade) at a flow-rate of 1 mL.min⁻¹. Toluene was used as flow-rate marker. Samples were filtered with a 0.2 μm PTFE filter before analysis. The calibration curve was based on poly(methyl methacrylate) (PMMA) standards from Polymer Laboratories. The EcoSEC Analysis software enabled the determination of the number-average molar mass M_n , the weight-average molar mass M_w and the dispersity ($D = M_w/M_n$). Differential scanning calorimetry (DSC) analyses were performed on a TA DSC Q20 using a heat/cool/heat cycle from -90 to +150 °C. After the first heating cycle, samples were kept at 150 °C for 3 min before being cooled to 0 °C and heated again to 150 °C. The heating and cooling rates were 10 °C.min⁻¹. Because the results depend on the sample's thermal history, the first cycle was used to obtain samples with the same thermal history (similar crystallization conditions), thus ensuring reproducibility of the following cycles.

c. Synthetic pathways to 2-methylene-4-phenyl-1,3-dioxolane (MPDL)

Yields refer to isolated and purified products.

General procedure for the transacetalization reaction. A mixture of haloacetaldehyde dimethyl acetal (1 equiv.) and styrene glycol (1 equiv.) with Dowex 50 (H⁺) resin was stirred overnight in a round bottom flask equipped with a distillation apparatus (Vigreux condenser of 10 cm height) at 120 °C. The amount of methanol collected by distillation is variable but had no effect on the outcome of the synthesis. The reaction was allowed to cool to room

temperature. Resin was removed by filtration. The mixture was purified by fractional distillation under reduced pressure using a rotary vane pump ($T_{\text{bath}} = 120\text{ }^{\circ}\text{C}$; $T_{\text{vapor}} = 70\text{ }^{\circ}\text{C}$; $P = 1\text{--}5.10^{-1}\text{ mbar}$).

Cis- and trans-2-chloromethyl-4-phenyl-1,3-dioxolane (2). Based on the general procedure for the transacetalization reaction, a mixture of chloroacetaldehyde dimethyl acetal (2.286 g, 18 mmol) and styrene glycol (2.475 g, 18 mmol) with Dowex 50 (H^+) resin (27 mg) was heated for 15 h at $120\text{ }^{\circ}\text{C}$. After resin was removed, the crude residue was evaporated on a rotary evaporator and purified by fractional distillation under reduced pressure at $120\text{ }^{\circ}\text{C}$ to give 2.3 g of a colorless liquid with 64 % yield. ^1H NMR (300 MHz, CDCl_3) δ 7.45–7.28 (m, 5H, *H* aromatics), 5.50–5.33 (t, $J = 3.9\text{ Hz}$ and t, $J = 3.8\text{ Hz}$, 1H, O-CH-O), 5.16–5.04 (dd, $J = 7.3\text{ Hz}$, 6.5 Hz and t, $J = 7.2\text{ Hz}$, 1H, Ph-CH-O), 4.44–4.24 (dd, $J = 8.1$, 6 Hz and m, 1 H, -CH₂-O), 3.81–3.75 (t, $J = 8.1\text{ Hz}$, 1H, -CH₂-O), 3.72–3.60 (d, $J = 3.6\text{ Hz}$ and m, 2H, CH₂-Cl). ^{13}C NMR (75 MHz, CDCl_3) δ 138.4 and 137.9 (1C), 128.7 and 128.5 and 128.3 (3C), 126.4 and 126.0 (2C), 103.3 and 103.0 (1C), 79.2 and 78.5 (1C), 72.8 and 72.2 (1C), 44.9 and 44.7 (1C). IR (cm^{-1}) $\nu = 2890, 1494, 1428, 1369, 1138, 1043, 1004, 950, 843, 753, 697, 585, 528$. GC/MS-CI (RT_{min} ; m/z %) = 6.91 and 6.97; 197 (100 %) and 199 (55 %) $[\text{M}-\text{H}]^+$. Anal. Calcd for $\text{C}_{10}\text{H}_{11}\text{ClO}_2$: C 60.46, H 5.58. Found: C 60.10, H 5.72.

Cis- and trans-2-bromomethyl-4-phenyl-1,3-dioxolane (3). Based on the general procedure for the transacetalization reaction, a mixture of bromoacetaldehyde dimethyl acetal (5.075 g, 30 mmol) and styrene glycol (4.101 g, 30 mmol) with Dowex 50 (H^+) resin (42 mg) was heated for 15 h at $120\text{ }^{\circ}\text{C}$. After resin was removed, the crude residue was evaporated on a rotary evaporator and it was then purified by fractional distillation under reduced pressure at $120\text{ }^{\circ}\text{C}$ to give 5.7 g of a colorless liquid with 80 % yield. ^1H NMR (300 MHz, CDCl_3) δ 7.44–7.28 (m, 5H, *H* aromatics), 5.50–5.32 (t, $J = 4.1\text{ Hz}$ and t, $J = 3.8\text{ Hz}$, 1H, O-CH-O), 5.19–5.06 (dd, $J = 7.5\text{ Hz}$, 6.3 Hz and t, $J = 7.2\text{ Hz}$, 1H, Ph-CH-O), 4.47–4.25 (dd, $J = 8.1\text{ Hz}$, 6 Hz and dd, $J = 7.7\text{ Hz}$, 6.8 Hz, 1H, -CH₂-O), 3.84–3.74 (m, 1H, -CH₂-O), 3.55–3.47 (d, $J = 3.6\text{ Hz}$ and m, 2H, -CH₂-Br). ^{13}C NMR (75 MHz, CDCl_3) δ 138.3 and 137.8 (1C), 128.7 and 128.6 and 128.4 (3C), 126.5 and 126.1 (2C), 102.9 and 102.5 (1C), 79.4 and 78.6 (1C), 72.9 and 72.3 (1C), 32.8 and 32.7 (1C). IR (cm^{-1}) $\nu = 2884, 1423, 1365, 1136, 1026, 996, 947, 822, 755, 697, 671, 586, 522$. GC/MS-CI (RT_{min} ; m/z %) = 7.69 and 7.75; 241 (100 %) and 243 (70 %) $[\text{M}-\text{H}]^+$. Anal. Calcd for $\text{C}_{10}\text{H}_{11}\text{BrO}_2$: C 49.41, H 4.56. Found: C 49.67, H 4.46.

Cis- and trans-2-iodomethyl-4-phenyl-1,3-dioxolane (4). To a solution of cis- and trans-2-bromomethyl-4-phenyl-1,3-dioxolane (2.000 g, 8 mmol) and acetone (8 mL) in a dry glass

tube, sodium iodide (2.400 g, 16 mmol) was added. The tube was sealed with a screw cap and stirred at 90 °C for 24 h. DCM was added and the mixture was filtered through a fritted glass and evaporated under vacuum. A saturated solution of Na₂S₂O₃ was added, and the mixture was extracted with ethyl acetate. The organic layers were dried over MgSO₄ and concentrated under vacuum. The final product was obtained as yellow liquid (2.1 g) with 88 % yield. ¹H NMR (300 MHz, CDCl₃) δ 7.46–7.29 (m, 5H, *H* aromatics), 5.27–5.03 (m, 2H, Ph-*CH*-O and O-*CH*-O), 4.49–4.25 (dd, *J* = 8.3 Hz, *J* = 6.2 Hz and m, 1H, -*CH*₂-O), 3.86–3.75 (m, 1H, -*CH*₂-O), 3.41–3.33 (d, *J* = 3.6 Hz and m, 2H, -*CH*₂-I). ¹³C NMR (75 MHz, CDCl₃) δ 138.5 and 137.7 (1C), 128.6 and 128.5 and 128.3 (3C), 126.6 and 126.0 (2C), 102.7 and 102.2 (1C), 79.5 and 78.7 (1C), 73.0 and 72.3 (1C), 7.2 and 6.7 (1C). IR (cm⁻¹) ν = 2878, 1416, 1359, 1130, 1024, 979, 942, 754, 697, 626, 586, 523. GC/MS-CI (RT_{min}; *m/z* %) = 8.48 and 8.54; 289 (100 %) [M-H]⁺. Anal. Calcd for C₁₀H₁₁IO₂: C 41.40, H 3.82. Found: C 42.07, H 3.83.

General procedure for the preparation of MPDL (5). In a two-neck round bottom flask was dissolved cyclic iodo, bromo or chloro acetal (1 equiv.) and 2 mol.% of Aliquat® 336 in anhydrous THF. Under inert atmosphere, the mixture was cooled to 0 °C and potassium *tert*-butoxide (2 equiv.) was slowly added through a powder funnel. The reaction mixture was then stirred vigorously at 0 °C for 2 h (unless otherwise mentioned) under inert atmosphere. After the mixture was warmed to room temperature, diethyl ether was added and the resulting precipitated salts were filtered through a glass frit. Unless otherwise mentioned, the product was purified by fractional distillation under reduced pressure using a rotary vane pump (*T*_{bath} = 85 °C; *T*_{vapor} = 50 °C; *P* = 1–5.10⁻¹ mbar).

Synthesis of MPDL from cis- and trans-2-chloromethyl-4-phenyl-1,3-dioxolane. Based on the general procedure for the preparation of MPDL, a mixture of cyclic chloro acetal (10.022 g, 50 mmol) and Aliquat® 336 (0.436 g, 1 mmol) was dissolved in 20 mL of anhydrous THF. Potassium *tert*-butoxide (12.355 g, 110 mmol) was slowly added through a powder funnel. The product was obtained as a colorless liquid (1.86 g) with 23% yield. ¹H NMR (300 MHz, CDCl₃) δ 7.40–7.31 (m, 5H, *CH* aromatics), 5.36–5.31 (t, *J* = 7 Hz, 1H, Ph-*CH*-O), 4.51–4.46 (t, *J* = 7.4 Hz, 1H, -*CH*₂-O), 4.03–3.98 (t, *J* = 7.7 Hz, 1H, -*CH*₂-O), 3.45–3.28 (dd, *J* = 2.8 Hz, 10 Hz, 2H, -*CCH*₂). ¹³C NMR (75 MHz, CDCl₃) δ 164.2 (1C), 137.2 (1C), 128.9 (3C), 126.0 (2C), 79.0 (1C), 72.3 (1C), 54.00 (1C). IR (cm⁻¹) ν = 2894, 1677, 1474, 1456, 1323, 1211, 1198, 1000, 965, 876, 755, 726, 695, 592, 525. GC/MS-CI (RT_{min}; *m/z* %) = 5.48 ; 162 (15 %) [M-H]⁺. Anal. Calcd for C₁₀H₁₀O₂.1/5 H₂O: C 72.45, H 6.32. Found: C

72.40, H 6.19. The deviation from the expected result for C₁₀H₁₀O₂ is due to ~20% of hydrolysis that took place before the elemental analysis.

Synthesis of MPDL from cis- and trans-2-bromomethyl-4-phenyl-1,3-dioxolane. Based on the general procedure for the preparation of MPDL, a mixture of cyclic bromo acetal (10.014 g, 41 mmol) and Aliquat® 336 (0.336 g, 0.8 mmol) was dissolved in 20 mL of anhydrous THF. Potassium *tert*-butoxide (9.729 g, 87 mmol) was slowly added through a powder funnel. The product was obtained as a colorless liquid (5.40 g) with 81% yield.

Synthesis of MPDL from cis- and trans-2-iodomethyl-4-phenyl-1,3-dioxolane. Based on the general procedure for the preparation of MPDL, a mixture of cyclic iodo acetal (1.000 g, 3.4 mmol) and Aliquat® 336 (0.027 g, 0.07 mmol) was dissolved in 6 mL of anhydrous THF. Potassium *tert*-butoxide (0.761 g, 7 mmol) was slowly added through a powder funnel. The mixture was allowed to stir at 0 °C for 1.5 h. Disappearance of the starting compound was monitored by TLC using cyclohexane: ethyl acetate (8:2) as eluent. The product was purified by precipitation of salts in ether, filtered twice, concentrated and then dried under high vacuum. The final compound was obtained as a clear yellow liquid (0.469 g) with 85 % yield.

d. Polymerization reactions

Targeted M_n at 100% MMA conversion was 30 000 g.mol⁻¹.

Synthesis of poly(methyl methacrylate)-*co*-(2-methylene-4-phenyl-1,3-dioxolane) (P(MMA-*co*-MPDL)). A typical solution copolymerization procedure (expt. **4**, $f_{\text{MPDL},0} = 0.7$) is as follows. In a 5 mL vial, fitted with a rubber septum and a magnetic stirrer bar, a mixture of MMA (0.3190 g, 3.19 mmol), MPDL (1.180 g, 7.28 mmol), the BlocBuilder alkoxyamine initiator (4.0 mg, 1.05×10^{-2} mmol) and anhydrous toluene (1.5 g, 1.73 mL) was degassed under stirring by argon bubbling for 15 min at room temperature. The mixture was then immersed in a preheated oil bath at 90 °C. Aliquots were periodically taken to monitor the MMA conversion by ¹H NMR spectroscopy using the methyl protons in α -position to the ester group of MMA and the macromolecular characteristics (M_n and \bar{D}) by SEC. The copolymer was then precipitated once in cold methanol and dried under high vacuum until constant weight was obtained. The same procedure was followed by adapting the amount of the reactants for expt. **0** ($f_{\text{MPDL},0} = 0$) [MMA (1.510 g, 15.1 mmol), BlocBuilder alkoxyamine initiator (19.4 mg, 5.09×10^{-2} mmol)], expt. **1** ($f_{\text{MPDL},0} = 0.1$) [MMA (1.274 g, 12.7 mmol), MPDL (0.236 g, 1.45 mmol), BlocBuilder alkoxyamine initiator (16.5 mg, 4.34×10^{-2}

mmol)], expt. **2** ($f_{\text{MPDL},0} = 0.2$) [MMA (1.063 g, 10.6 mmol), MPDL (0.448 g, 2.77 mmol), BlocBuilder alkoxyamine initiator (13.9 mg, 3.65×10^{-2} mmol)] and expt. **3** ($f_{\text{MPDL},0} = 0.4$) [MMA (0.713 g, 7.13 mmol), MPDL (0.811 g, 5.01 mmol), BlocBuilder alkoxyamine initiator (9.4 mg, 2.46×10^{-2} mmol)].

Synthesis of poly(methyl methacrylate-*co*-styrene) (P(MMA-*co*-S), expt. 0'). In a 5 mL vial, fitted with a rubber septum and a magnetic stirrer bar, a mixture of MMA (1.501 g, 15 mmol), S (0.154 g, 1.48 mmol) and the BlocBuilder alkoxyamine initiator (10.3 mg, 2.70×10^{-2} mmol) was degassed under stirring by argon bubbling for 15 min at room temperature. The mixture was then immersed in a preheated oil bath at 90 °C. After 2 h, the copolymerization was stopped. A sample was taken to estimate the MMA conversion by ^1H NMR spectroscopy and the macromolecular characteristics (M_n and \bar{D}) by SEC. The copolymer was then precipitated once in cold methanol and dried under high vacuum until constant weight was obtained.

e. Hydrolytic degradation

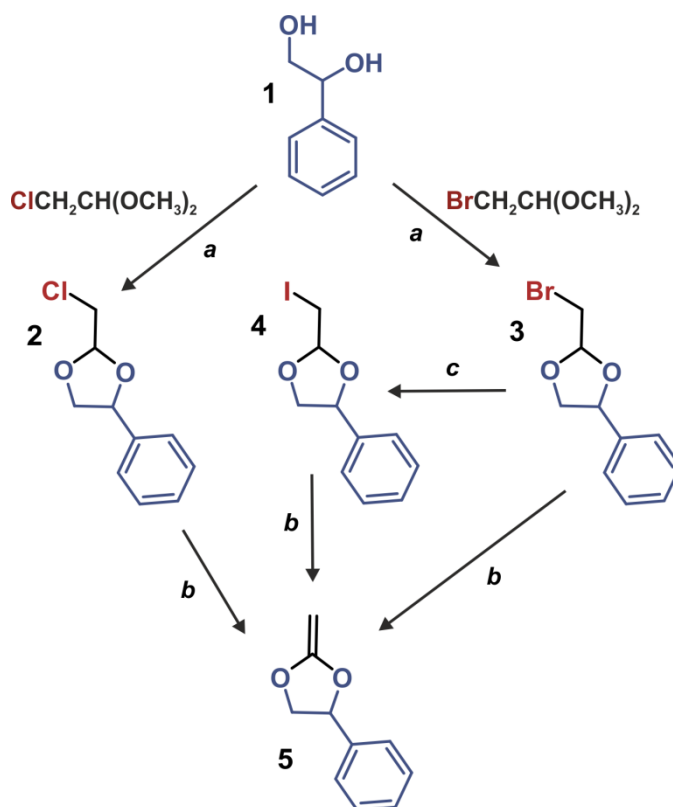
In a 5 mL vial, 50 mg of P(MMA-*co*-MPDL) copolymer was dissolved in 2.5 mL of THF. After solubilization, 2.5 mL of potassium hydroxide solution (KOH, 5%) in methanol was added. The cloudy mixture was stirred at room temperature. Aliquots were periodically taken, immediately dried under vacuum and 2 mL of chloroform were added. Salts were removed by filtration, solvent was removed under reduced pressure and degradation products were analyzed by SEC.

III. Results and Discussion

a. Synthesis of MPDL

Optimized synthetic pathways to MPDL are depicted in Scheme 1. Cyclic chloro- and bromoacetals (**2** and **3**, Scheme 1) were synthesized by transacetalization reaction between styrene glycol (**1**, Scheme 1) and the corresponding haloacetaldehyde dimethyl acetal, using DOWEX H⁺ resin as a catalyst. As the reaction is reversible, distillation of methanol is essential to achieve full conversion of the starting compounds. Although the amount of recovered methanol was not systematically quantitative, no influence was noticed on the

reaction yield. Cyclic chloro- and bromoacetals were obtained in 64 % and 80 % yields, respectively.



Scheme 1. Synthetic pathways to 2-methylene-4-phenyl-1,3-dioxolane (MPDL). Reagents: (a) DOWEX H⁺ ; (b) *tert*-BuOK, Aliquat[®] 336, dry THF ; (c) NaI, dry acetone.

Our early attempts to carry out elimination reaction on cyclic chloroacetal (**2**) at high temperature in *tert*-BuOH, according to previously published work,¹³ met with limited success because of the non-reproducibility of the reaction and the moderate yield (< 40 %). High temperature could also be detrimental to the synthesis of CKAs due to their potential instability and could lead to the formation of byproducts. Moreover, the use of *tert*-BuOH as a solvent is not practical due to its rather high melting point (~25°C), which prevents workup at low temperature. We therefore investigated this reaction at 0°C in the presence of a catalytic amount of Aliquat[®]336 in dry THF, as adapted from an early publication briefly describing the synthesis of different CKA.⁴⁰ We thoroughly revisited this method and applied it to MPDL from three cyclic halogeno acetals (i.e., chloro-, bromo- and iodo-acetadehyde dimethyl acetal) to determine the best alkyl halide precursor for the elimination reaction. The

elimination reaction is a crucial step as the final purity of MPDL has been shown to strongly affect the outcome of the copolymerization.²⁷

Cyclic iodoacetal (**4**, Scheme 1) was synthesized from its brominated analog (**3**) by a Finkelstein reaction in the presence of NaI in acetone. The product was obtained in 88 % yield. The structure of the iodinated compound was determined by ¹H and ¹³C NMR indicating that halogen exchange was successfully achieved. The ¹³C-I resonances of both isomers (at 7.2 and 6.7 ppm) were shifted downfield compared to the ¹³C-Br resonances of the parent compound (at 32.8 and 32.7 ppm) (see experimental part).

When elimination was carried out on chloroacetal (**2**), the yield was very low (23 %), whereas bromoacetal (**3**) afforded the elimination product with 81 % yield within 2 h, and iodoacetal (**4**) gave an 85 % yield of the elimination product within 1.5 h (Scheme 1). In Figures S1 and S2 are given representative ¹H and ¹³C NMR spectra of MPDL. These findings are consistent with the reactivity of the three halogens. Importantly, elimination from the cyclic iodoacetal (**4**), reported here for the first time, gave a very good yield under mild experimental conditions (likely due to the good leaving group) and opens new perspectives regarding the synthesis of other types of CKA from iodoacetal derivatives.

b. Nitroxide-mediated copolymerization with methyl methacrylate

NMP of methyl methacrylate (MMA) was conducted with a variable amount of MPDL ($f_{\text{MPDL},0} = 0-0.7$, expts. **0-4**) and initiated by the SG1-based BlocBuilder alkoxyamine at 90 °C in 50 wt.% toluene. We recently reported that MPDL was a good controlling comonomer in the NMP of MeOEGMA.²⁷ Our current results demonstrated the versatility of this approach by showing that MPDL can also act as a controlling comonomer for the NMP of MMA. As expected,^{41,42} homopolymerization of MMA (expt. **0**) rapidly stopped at low conversion (~20%) due to extensive irreversible termination, and yielded an uncontrolled PMMA ($\bar{D} \sim 1.9$), with no linear evolution of the M_n over monomer conversion (Figure 2). Adding only 10 mol.% MPDL to the monomer feed (expt. **1**) slightly reduced the dispersity ($\bar{D} \sim 1.7-1.8$) of the resulting P(MMA-*co*-MPDL) copolymer and gave a linear evolution of the M_n over 10–30% conversion in the 7 500 to 10 000 g.mol⁻¹ range (Figure 2b). Addition of 20 mol.% MPDL (expt. **2**, $f_{\text{MPDL},0} = 0.2$) showed a first-order kinetics up to 9 h, followed by deviation from linearity. The evolution of experimental M_n with MMA conversion showed a relatively good match with the theoretical M_n , up to 32% conversion where $M_n = 10\,300$ g.mol⁻¹ and $\bar{D} = 1.54$ (Figure 2b). When the initial molar fraction of MPDL was increased to 40 mol.%

(expt. 3, $f_{\text{MPDL},0} = 0.4$) the kinetics was significantly improved and the first-order kinetics was assessed up to 10 h. Lower dispersities ($D \sim 1.36$ – 1.47) were also observed (Figure 2b). Control was further improved with the highest initial amount of MPDL (expt. 4, $f_{\text{MPDL},0} = 0.7$), giving perfect first-order kinetics up to high conversion (Figure 2a) together with linear evolution of M_n with conversion and low dispersities ($D \sim 1.23$ – 1.42) (Figure 2b). Even though addition of MPDL to the monomer the feed decreased the initial polymerization rate within the first hour, it enabled higher conversions to be reached due to a lower amount of irreversible termination reactions.

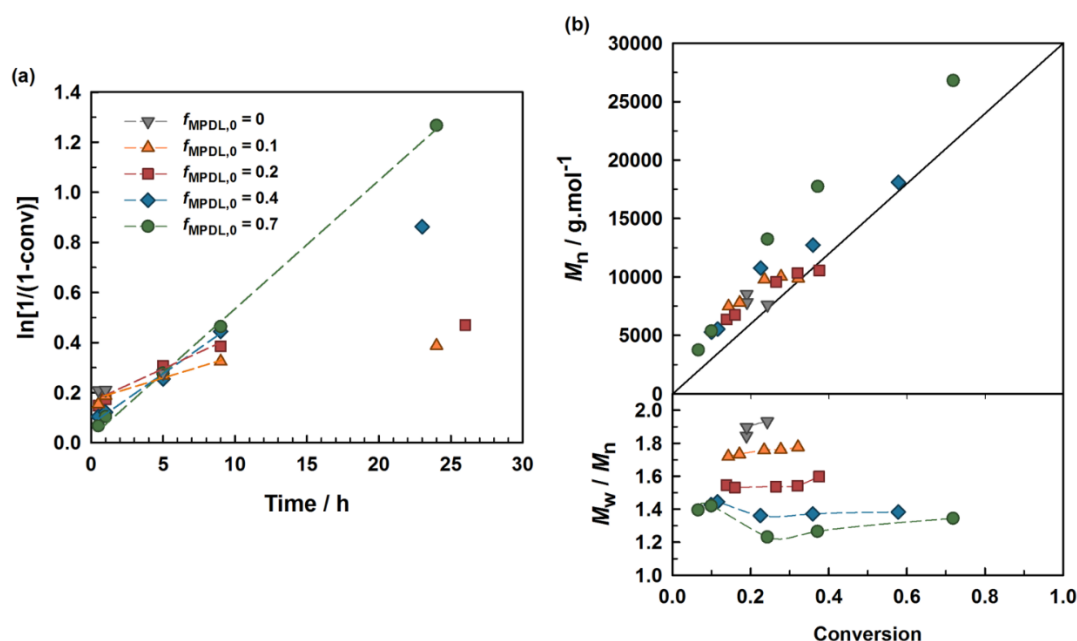


Figure 2. NMP of MMA and MPDL in toluene initiated by the BlocBuilder at 90 °C, as a function of the initial amount of MPDL: ∇ , expt. 0 ($f_{\text{MPDL},0} = 0$); \blacktriangle , expt. 1 ($f_{\text{MPDL},0} = 0.1$); \blacksquare , expt. 2 ($f_{\text{MPDL},0} = 0.2$); \blacklozenge , expt. 3 ($f_{\text{MPDL},0} = 0.4$); \bullet , expt. 4 ($f_{\text{MPDL},0} = 0.7$). (a) $\ln[1/(1-\text{conv})]$ vs. time (conv = MMA conversion). (b) Number-average molar mass, M_n and dispersity, M_w/M_n , vs. conversion. The solid black line represents the theoretical M_n and lines connecting data points are guides for the eye only.

The quality of control was further supported by the evolution of molecular weight distribution with time, notably for expts. 3 and 4 (Figure S3). In summary, the highest amount of MPDL gave the best control over the polymerisation.

c. Structural characterization

A second set of P(MMA-*co*-MPDL) copolymers was prepared by varying $f_{\text{MPDL},0}$ from 0.1 to 0.7 and by targeting a molar mass of 25 000 g.mol⁻¹ (Table 1, expts. **1'**–**4'**). ¹H NMR spectroscopy of the purified copolymers showed all signals expected for a P(MMA-*co*-MPDL) structure (Figure S4). The aromatic protons of the phenyl group of MPDL (signal *b*) were clearly visible and qualitatively confirmed that its level of incorporation in the copolymer could be adjusted by varying its initial concentration in the comonomer feed.

Table 1. Experimental Conditions and Characteristics of the Copolymers Synthesized for the Structural Characterization and for the Hydrolytic Degradation Study.

expt.	$f_{\text{MPDL},0}^a$	F_{MPDL}^b	MMA conv. (%) ^c / time (h)	$M_{n,\text{theo.}}$ (g.mol ⁻¹) ^d	$M_{n,\text{exp.}}$ (g.mol ⁻¹) ^e	M_w/M_n^e	T_g (°C) ^f
0'	0	0	40 / 2	n.d.	32 500	1.38	106.7
1'	0.1	0.03	24 / 8	17 000	21 500	1.58	n.d.
2'	0.2	0.06	26 / 6	15 500	23 200	1.46	100.0
3'	0.4	0.14	26 / 6	15 200	23 200	1.34	97.6
4'	0.7	0.29	36 / 6	18 100	28 300	1.40	73.6

^a Initial molar fraction of MPDL in the monomer feed. ^b Molar fraction of MPDL in the copolymer determined by ¹H NMR, using the methyl protons in α -position to the ester group of MMA unit and the aromatic protons of MPDL unit. ^c Calculated by ¹H NMR. ^d Calculated according to: $M_{n,\text{theo.}} = \text{conversion} \times MW_{\text{MMA}} \times [\text{MMA}]_0 / [\text{alkoxyamine}]_0 + MW_{\text{alkoxyamine}}$. ^e Determined by SEC in chloroform with PMMA standards. ^f Glass transition temperature determined by DSC.

The molar fraction of MPDL in the copolymer (F_{MPDL}) was then calculated by ¹H NMR spectroscopy. F_{MPDL} was equal to 0.03, 0.06, 0.14 and 0.29, for expt. **1'** ($f_{\text{MPDL},0} = 0.1$), expt. **2'** ($f_{\text{MPDL},0} = 0.2$), expt. **3'** ($f_{\text{MPDL},0} = 0.4$) and expt. **4'** ($f_{\text{MPDL},0} = 0.7$), respectively. These values are consistent with reactivity ratios of 0.01 for MPDL, and 4.0 for MMA (Figure S5). The 95% joint confidence interval for the reactivity ratios, evaluated by non-linear least squares fitting of the integrated copolymer composition equation,^{43,44} is shown in Figure S6 and extends from 0 to 0.08 for MPDL, and from 3.4 to 4.9 for MMA. These reactivity ratios are similar to those previously determined for the MPDL/MeOEGMA copolymer pair ($r_{\text{MPDL}} = 0$, $r_{\text{MeOEGMA}} = 6.95$).²⁷ While the amount of MPDL incorporated during copolymerization with MMA is significantly lower than the feed ratio, MPDL is nearly an order of magnitude more reactive towards PMMA radicals than the more commonly used monomer MDO ($r_{\text{MDO}} = 0.057$, $r_{\text{MMA}} = 34$).^{27,45-47}

d. Hydrolytic degradation

In order to examine the degradability of the copolymers, a hydrolytic study was carried out with P(MMA-co-MPDL) copolymers from expts. **1'–4'** (Table 1). Degradation was monitored for 1 h at room temperature under accelerated hydrolytic conditions; that is in THF with 5% KOH in methanol. In all cases, a clear shift of the SEC chromatograms toward low molar masses was observed, proving the fast copolymer degradation into lower molar mass fragments (Figure 3). As expected, the higher the MPDL content in the copolymer, the more pronounced the degradation.

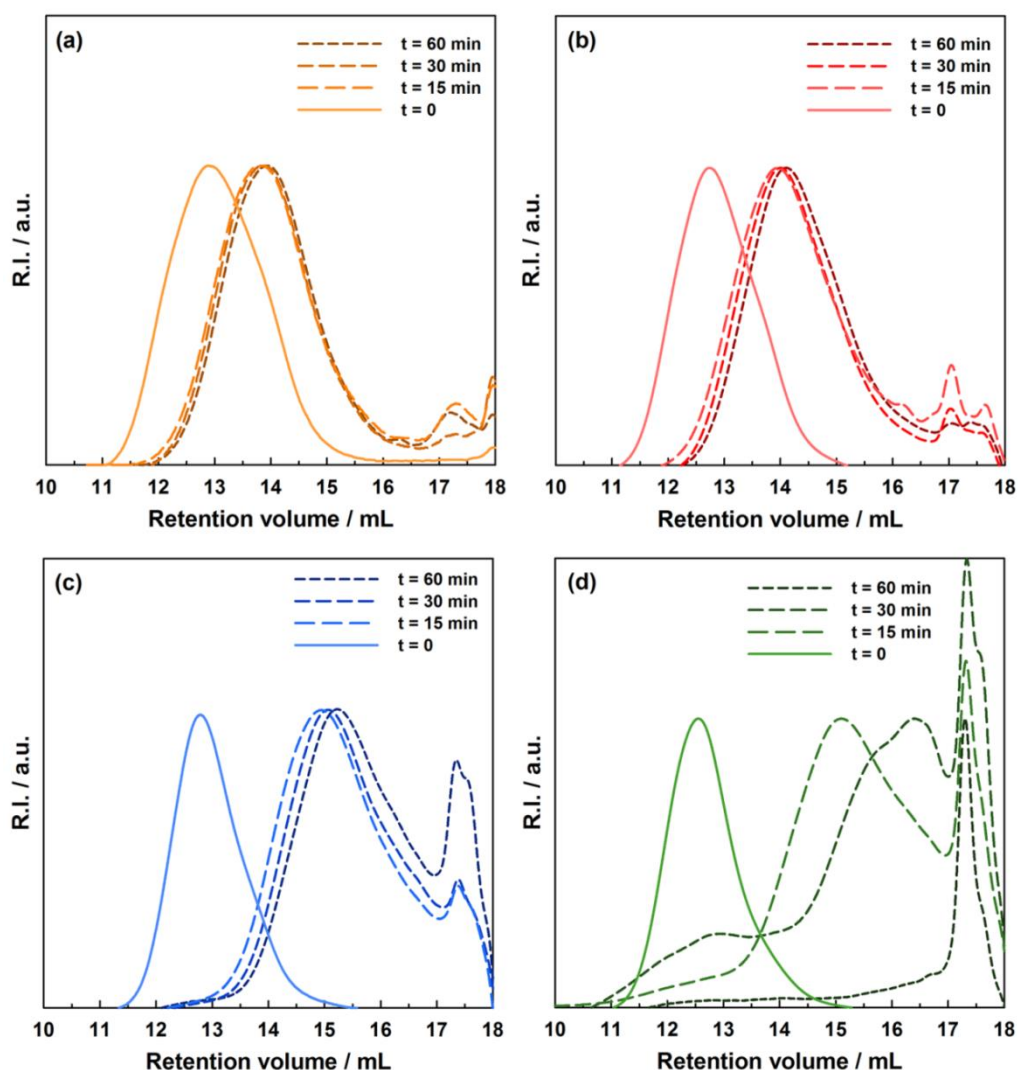


Figure 3. SEC traces taken at different time intervals during the hydrolytic degradation of P(MMA-*co*-MPDL) as a function of the content in MPDL: (a), expt. 1' ($F_{\text{MPDL}} = 0.03$); (b) expt. 2' ($F_{\text{MPDL}} = 0.06$); (c) expt. 3' ($F_{\text{MPDL}} = 0.14$); (d) expt. 4' ($F_{\text{MPDL}} = 0.29$).

The degradation was quantitatively assessed by plotting the evolution of M_n vs. time (Figure 4). Whereas a P(MMA-*co*-S), used as a negative control (expt. 0'), did not show any degradation, the M_n of P(MMA-*co*-MPDL) with $F_{\text{MPDL}} = 0.03$ decreased by 59%, and the P(MMA-*co*-MPDL) with $F_{\text{MPDL}} = 0.14$ gave a 95% decrease. Nearly complete degradation was obtained for $F_{\text{MPDL}} = 0.29$ with a decrease by over 98% in 5 min. An exponential decay fit was then successfully applied to each degradation kinetics, allowing the calculation of M_n reached at equilibrium ($M_{n,\infty}$), the time constant (τ) and the initial degradation rate (Figure 4 and Table 2). These values are of high importance to better characterize our system, and may also be useful for potential benchmarking between different kinds of materials to select the most appropriate one for a specific application.

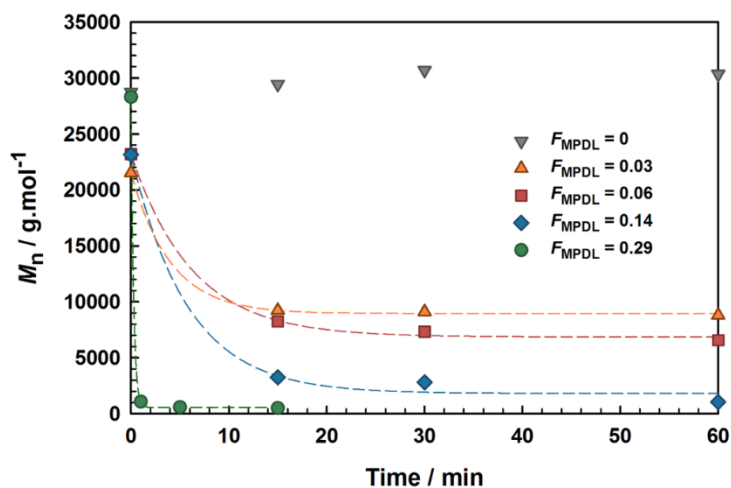


Figure 4. Hydrolytic degradation in THF with 5% KOH in methanol of P(MMA-*co*-MPDL) as a function of the MPDL fraction: ▼, expt. 0' (P(MMA-*co*-S), $F_{\text{MPDL}} = 0$); ▲, expt. 1' ($F_{\text{MPDL}} = 0.03$); ■, expt. 2' ($F_{\text{MPDL}} = 0.06$); ◆, expt. 3' ($F_{\text{MPDL}} = 0.14$); ●, expt. 4' ($F_{\text{MPDL}} = 0.29$). Evolution of the number-average molar mass, M_n , with time. Dashed lines represent the exponential fit, equation plot: $M_n(t) = M_{n,\infty} + a \times \exp(-t/\tau)$.

Table 2. Features of the Hydrolytic Degradation of P(MMA-*co*-MPDL) Copolymers Containing Different Amounts of MPDL.^a

expt.	F_{MPDL}^b	average		experimental $M_{n,\infty}$ (g.mol ⁻¹) ^e	M_n decrease (%) ^f	τ (min) ^e	initial rate (g.mol ⁻¹ .min ⁻¹) ^e
		consecutive MMA units (n) ^c	theoretical $M_{n,\infty}$ (g.mol ⁻¹) ^d				
1'	0.03	32.3	3 400	8 900	-59	4.0	3 100
2'	0.06	15.7	1 700	6 900	-72	6.23	2 600
3'	0.14	6.1	800	1 800	-95	5.74	3 700
4'	0.29	2.7	400	500	-98	0.25	110 000

^a Degradation was performed for 1 h at room temperature in THF with 5% KOH in methanol. ^b Molar fraction of MPDL in the copolymer determined by ¹H NMR. ^c Calculated according to: $(1 - F_{\text{MPDL}})/F_{\text{MPDL}}$. ^d Calculated according to: $n \times \text{MW}_{\text{MMA}} + \text{MW}_{\text{MPDL}}$. ^e Extracted from the exponential decay fit. ^f M_n decrease after hydrolytic degradation of the purified copolymers calculated according to $(M_{n,f} - M_{n,0})/M_{n,0}$.

For the highest MPDL content (expt. 4', $F_{\text{MPDL}} = 0.29$), the initial degradation rate was as high as 110 000 g.mol⁻¹.min⁻¹. However, for lower MPDL contents (expt. 1', $F_{\text{MPDL}} = 0.03$, expt. 2', $F_{\text{MPDL}} = 0.06$ and expt. 3', $F_{\text{MPDL}} = 0.14$), degradations were relatively much slower and reached their steady state in about 15 min. Initial degradation rates were respectively 3 100, 2 600 and 3 700 g.mol⁻¹.min⁻¹. This time constant represents how fast the copolymers respond to a perturbation (in the present study: the degradation conditions). From the exponential decay fits, our systems respond rapidly to hydrolysis, as τ ranged from several minutes (expts. 1'–3') to 15 s (expt. 4').

The final molar mass (experimental $M_{n,\infty}$) was taken as the limit of the exponential decay when time tends to infinity (Table 2). The theoretical $M_{n,\infty}$ was determined by calculating the average polymer length after hydrolysis. As r_{MPDL} is close to zero for the copolymerization with MMA, the probability of finding a sequence of more than one MPDL unit is negligible. The average length of an MMA sequence (n) was calculated from F_{MPDL} according to: $n = (1 - F_{\text{MPDL}})/F_{\text{MPDL}}$ (Table 2). This enabled the calculation of the theoretical $M_{n,\infty}$ according to: $M_{n,\infty} = n \times \text{MW}_{\text{MMA}} + \text{MW}_{\text{MPDL}}$, with MW the molecular weight of the monomer considered (Table 2). After a degradation time of 1 h, a reasonable agreement between the final experimental molar masses and the theoretical values for expts. 4' and 3' were obtained, whereas for expts. 1' and 2', the experimental values, while still low, were

significantly higher than the predicted ones (Table 2). These results confirmed the tunable insertion of ester bond in the main chain of the copolymer during MPDL copolymerization with MMA. They also confirmed that, depending on the MPDL content (F_{MPDL}), the rate of degradation could be tuned, and degradation can proceed almost up to completion.

e. Thermal characterization

In a parallel study, DSC was used to probe the influence of MPDL units on the glass transition temperature⁴⁸ of the resulting P(MMA-*co*-MPDL) copolymers from Table 1 (expts. 2'-4'). All copolymers exhibited a single well-defined T_g as the result of the random incorporation of isolated MPDL units in the PMMA chains (Figure 5). Also, T_g decreased with an increase of the molar fraction of MPDL units in the copolymer due to introduction of flexible MPDL opened structures into the rigid PMMA backbones; with values ranging from 100.0 °C (for $F_{\text{MPDL}} = 0.06$) to 73.6 °C (for $F_{\text{MPDL}} = 0.29$). Interestingly, a P(MMA-*co*-MPDL) containing 6% MPDL (expt. 2') led to a small decrease of T_g (ca. -5%) compared to that of pure PMMA ($T_g \sim 105$ °C)⁴⁹ or of P(MMA-*co*-S) (expt. 0', $T_g = 106.7$ °C), while giving a significant M_n decrease (-72%) upon hydrolytic degradation. These results fit the Fox equation⁵⁰ with an estimated T_g for PMDPL of 45 ± 10 °C (Figure S7).

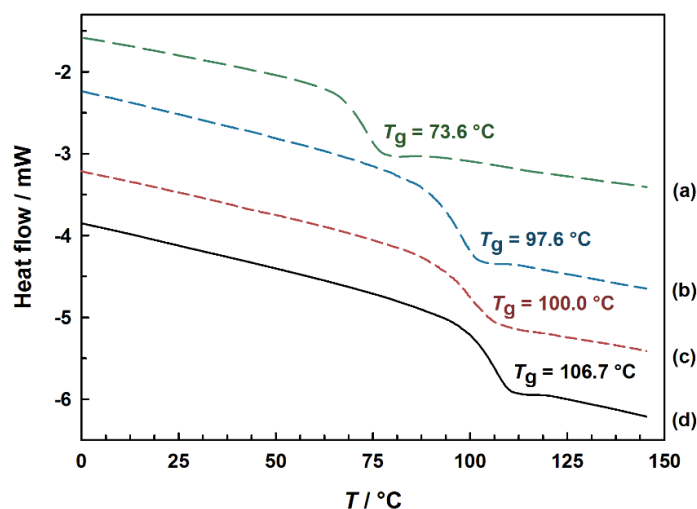


Figure 5. DSC curves of the purified P(MMA-*co*-MPDL) and P(MMA-*co*-S) copolymers (Table 1, expts. 0' and 2'-4') obtained by NMP of MMA and MPDL (or S) in toluene initiated by the BlocBuilder at 90 °C, as a function of the molar fraction of MPDL in the copolymer: (a), expt. 4' ($F_{\text{MPDL}} = 0.29$); (b) expt. 3' ($F_{\text{MPDL}} = 0.14$); (c) expt. 2' ($F_{\text{MPDL}} = 0.06$); (d) expt. 0' (P(MMA-*co*-S), $F_{\text{MPDL}} = 0$).

IV. Conclusion

In this study, we have reported efficient and reliable synthetic pathways to MPDL, a little studied CKA monomer which is able to confer degradability to vinyl polymers prepared by radical ring-opening (co)polymerization. MPDL was obtained in a reproducible manner from the three different acetal halides (bromo-, chloro- and iodoacetal) with high yields and high purity. In a second step, MPDL was shown to act as a controlling comonomer for the nitroxide-mediated copolymerization of MMA. Whereas well-defined copolymers were obtained only for initial molar fractions in MPDL above 20 mol.%, all polymers synthesized showed rapid and significant hydrolytic degradation even for low fractions of inserted MPDL ($F_{\text{MPDL}} \geq 0.03$). For higher MPDL contents ($F_{\text{MPDL}} \geq 0.14$), degradation was nearly complete. It was also shown that insertion of MPDL units into the PMMA backbone up to $F_{\text{MPDL}} = 0.14$ only moderately affected the T_g of the resulting copolymer. This study opens up new pathways towards the design of well-defined and degradable vinyl materials by RDRP techniques for a wide range of (bio)applications.

References

- (1) Delplace, V.; Nicolas, J. *Nature Chem.* **2015**, *7*, 771.
- (2) Agarwal, S. *Polym. Chem.* **2010**, *1*, 953.
- (3) Evans, R. A.; Rizzardo, E. *Macromolecules* **1996**, *29*, 6983.
- (4) Paulusse, J. M. J.; Amir, R. J.; Evans, R. A.; Hawker, C. J. *J. Am. Chem. Soc.* **2009**, *131*, 9805.
- (5) Kopčanský, P.; Tomašovičová, N.; Koneracka, M.; Timko, M.; Závašová, V.; Tomčo, L. *Acta Electrotechnica et Informatica* **2010**, *10*, 10.
- (6) Bailey, W. J. *Makromol. Chem., Suppl.* **1985**, *13*, 171.
- (7) Bailey, W. J. *Polym. J. (Tokyo)* **1985**, *17*, 85.
- (8) Bailey, W. J.; Beam, C. F., Jr.; Cappuccilli, E. D.; Haddad, I.; Volpe, A. A. *ACS Symp. Ser.* **1982**, *195*, 391.
- (9) Bailey, W. J.; Chen, P. Y.; Chen, S. C.; Chiao, W. B.; Endo, T.; Gapud, B.; Lin, Y. N.; Ni, Z.; Pan, C. Y.; et al. *J. Macromol. Sci., Chem.* **1984**, *A21*, 1611.
- (10) Bailey, W. J.; Chou, J. L. *Polym. Mater. Sci. Eng.* **1987**, *56*, 30.
- (11) Bailey, W. J.; Ni, Z.; Wu, S. R. *Macromolecules* **1982**, *15*, 711.
- (12) Bailey, W. J.; Wu, S. R.; Ni, Z. *J. Macromol. Sci., Chem.* **1982**, *A18*, 973.
- (13) Bailey, W. J.; Wu, S. R.; Ni, Z. *Makromol. Chem.* **1982**, *183*, 1913.
- (14) Agarwal, S.; Ren, L. *Macromolecules* **2009**, *42*, 1574.
- (15) Ren, L.; Speyerer, C.; Agarwal, S. *Macromolecules* **2007**, *40*, 7834.
- (16) Undin, J.; Finne-Wistrand, A.; Albertsson, A.-C. *Biomacromolecules* **2013**, *14*, 2095.
- (17) Undin, J.; Illanes, T.; Finne-Wistrand, A.; Albertsson, A.-C. *Polym. Chem.* **2012**, *3*, 1260.
- (18) Undin, J.; Plikk, P.; Finne-Wistrand, A.; Albertsson, A.-C. *J. Polym. Sci., Part A: Polym. Chem.* **2010**, *48*, 4965.
- (19) Wickel, H.; Agarwal, S. *Macromolecules* **2003**, *36*, 6152.
- (20) Wickel, H.; Agarwal, S.; Greiner, A. *Macromolecules* **2003**, *36*, 2397.
- (21) Zhang, Y.; Chu, D.; Zheng, M.; Kissel, T.; Agarwal, S. *Polym. Chem.* **2012**, *3*, 2752.
- (22) Huang, J.; Gil, R.; Matyjaszewski, K. *Polymer* **2005**, *46*, 11698.
- (23) Lutz, J.-F.; Andrieu, J.; Üzgün, S.; Rudolph, C.; Agarwal, S. *Macromolecules* **2007**, *40*, 8540.
- (24) Riachi, C.; Schüwer, N.; Klok, H.-A. *Macromolecules* **2009**, *42*, 8076.
- (25) Siegwart, D. J.; Bencherif, S. A.; Srinivasan, A.; Hollinger, J. O.; Matyjaszewski, K. *J. Biomed. Mater. Res., Part A* **2008**, *87A*, 345.
- (26) Yuan, J.-Y.; Pan, C.-Y. *Eur. Polym. J.* **2002**, *38*, 2069.
- (27) Delplace, V.; Guegain, E.; Harrisson, S.; Gigmes, D.; Guillaneuf, Y.; Nicolas, J. *Chem. Commun.* **2015**, *51*, 12847.
- (28) Delplace, V.; Harrisson, S.; Tardy, A.; Gigmes, D.; Guillaneuf, Y.; Nicolas, J. *Macromol. Rapid Commun.* **2014**, *35*, 484.
- (29) Delplace, V.; Tardy, A.; Harrisson, S.; Mura, S.; Gigmes, D.; Guillaneuf, Y.; Nicolas, J. *Biomacromolecules* **2013**, *14*, 2837.
- (30) Decker, C. G.; Maynard, H. D. *Eur. Polym. J.* **2015**, *65*, 305.
- (31) Bailey, W. J.; Ni, Z.; Wu, S. R. *J. Polym. Sci., Polym. Chem. Ed.* **1982**, *20*, 3021.
- (32) Pan, C.-Y.; Lou, X.-D. *Makromol. Chem. Phys.* **2000**, *201*, 1115.
- (33) Nicolas, J.; Dire, C.; Mueller, L.; Belleney, J.; Charleux, B.; Marque, S. R. A.; Bertin, D.; Magnet, S.; Couvreur, L. *Macromolecules* **2006**, *39*, 8274.
- (34) Nicolas, J.; Brusseau, S.; Charleux, B. *J. Polym. Sci., Part A: Polym. Chem.* **2010**, *48*, 34.

- (35) Lessard, B. H.; Guillaneuf, Y.; Mathew, M.; Liang, K.; Clement, J.-L.; Gignes, D.; Hutchinson, R. A.; Marić, M. *Macromolecules* **2013**, *46*, 805.
- (36) Wu, Z.; Stanley, R. R.; Pittman, C. U. *J. Org. Chem.* **1999**, *64*, 8386.
- (37) Díaz-Ortiz, A.; Prieto, P.; Loupy, A.; Abenhaim, D. *Tetrahedron Lett.* **1996**, *37*, 1695.
- (38) Díez-Barra, E.; de la Hoz, A.; Díaz-Ortiz, A.; Prieto, P. *Synlett* **1992**, 1992, 893.
- (39) Schulze, T.; Letsch, J.; Klemm, E. *J. Polym. Sci., Part A: Polym. Chem.* **1996**, *34*, 81.
- (40) Bailey, W. J.; Zhou, L.-L. *Tetrahedron Lett.* **1991**, *32*, 1539.
- (41) Dire, C.; Belleney, J.; Nicolas, J.; Bertin, D.; Magnet, S.; Charleux, B. *J. Polym. Sci., Part A: Polym. Chem.* **2008**, *46*, 6333.
- (42) Nicolas, J.; Mueller, L.; Dire, C.; Matyjaszewski, K.; Charleux, B. *Macromolecules* **2009**, *42*, 4470.
- (43) Van Den Brink, M.; Van Herk, A. M.; German, A. L. *J. Polym. Sci., Part A: Polym. Chem.* **1999**, *37*, 3793.
- (44) Harrisson, S.; Ercole, F.; Muir, B. W. *Polym. Chem.* **2010**, *1*, 326.
- (45) Takahashi, T. *J. Polym. Sci., Part A: Polym. Chem.* **1970**, *8*, 739.
- (46) Roberts, G. E.; Coote, M. L.; Heuts, J. P. A.; Morris, L. M.; Davis, T. P. *Macromolecules* **1999**, *32*, 1332.
- (47) Harrisson, S.; Davis, T. P.; Evans, R. A.; Rizzardo, E. *Macromolecules* **2001**, *34*, 3869.
- (48) Frisch, M. J.; Trucks, G. W.; Schlegel, H. B.; Scuseria, G. E.; Robb, M. A.; Cheeseman, J. R.; Scalmani, G.; Barone, V.; Mennucci, B.; Petersson, G. A.; Nakatsuji, H.; Caricato, M.; Li, X.; Hratchian, H. P.; Izmaylov, A. F.; Bloino, J.; Zheng, G.; Sonnenberg, J. L.; Hada, M.; Ehara, M.; Toyota, K.; Fukuda, R.; Hasegawa, J.; Ishida, M.; Nakajima, T.; Honda, Y.; Kitao, O.; Nakai, H.; Vreven, T.; Montgomery Jr., J. A.; Peralta, J. E.; Ogliaro, F.; Bearpark, M. J.; Heyd, J.; Brothers, E. N.; Kudin, K. N.; Staroverov, V. N.; Kobayashi, R.; Normand, J.; Raghavachari, K.; Rendell, A. P.; Burant, J. C.; Iyengar, S. S.; Tomasi, J.; Cossi, M.; Rega, N.; Millam, N. J.; Klene, M.; Knox, J. E.; Cross, J. B.; Bakken, V.; Adamo, C.; Jaramillo, J.; Gomperts, R.; Stratmann, R. E.; Yazyev, O.; Austin, A. J.; Cammi, R.; Pomelli, C.; Ochterski, J. W.; Martin, R. L.; Morokuma, K.; Zakrzewski, V. G.; Voth, G. A.; Salvador, P.; Dannenberg, J. J.; Dapprich, S.; Daniels, A. D.; Farkas, Ö.; Foresman, J. B.; Ortiz, J. V.; Cioslowski, J.; Fox, D. J.; Gaussian, Inc.: Wallingford, CT, USA, 2009.
- (49) Brandrup, J.; Immergut, E.; Grulke, E. *Polymer Handbook, 4th Edition*; Wiley Interscience: New-York, 1999.
- (50) Fox, T. G. *Bull. Am. Phys. Soc.* **1956**, *1*, 123.

Supplementary Information

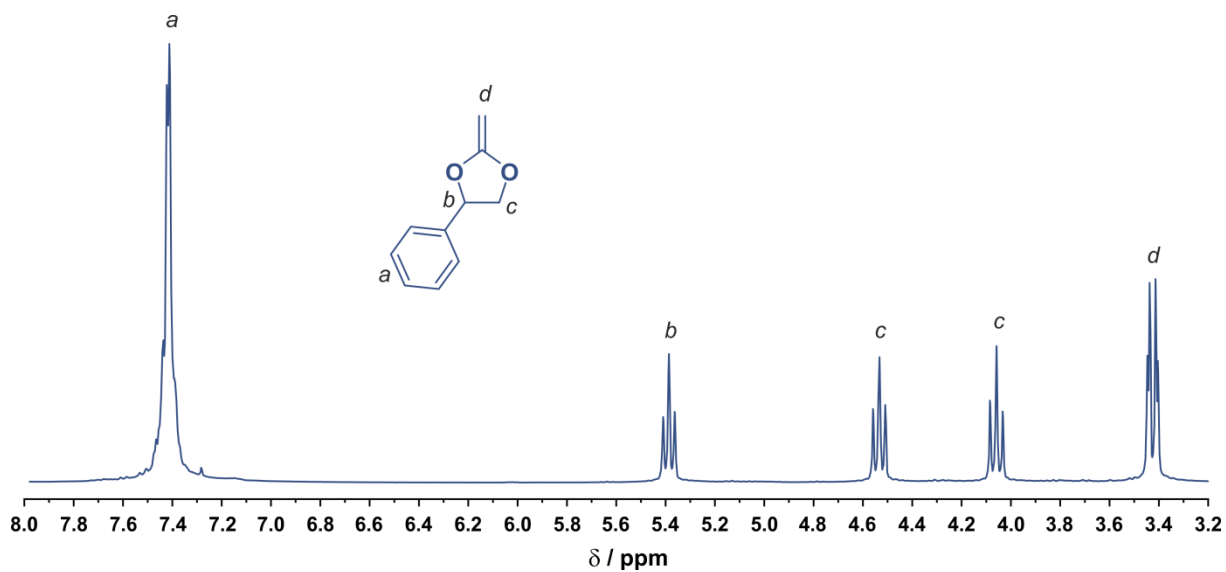


Figure S1. Representative ^1H NMR spectrum in CDCl_3 in the 3.2–8.0 ppm region of MPDL.

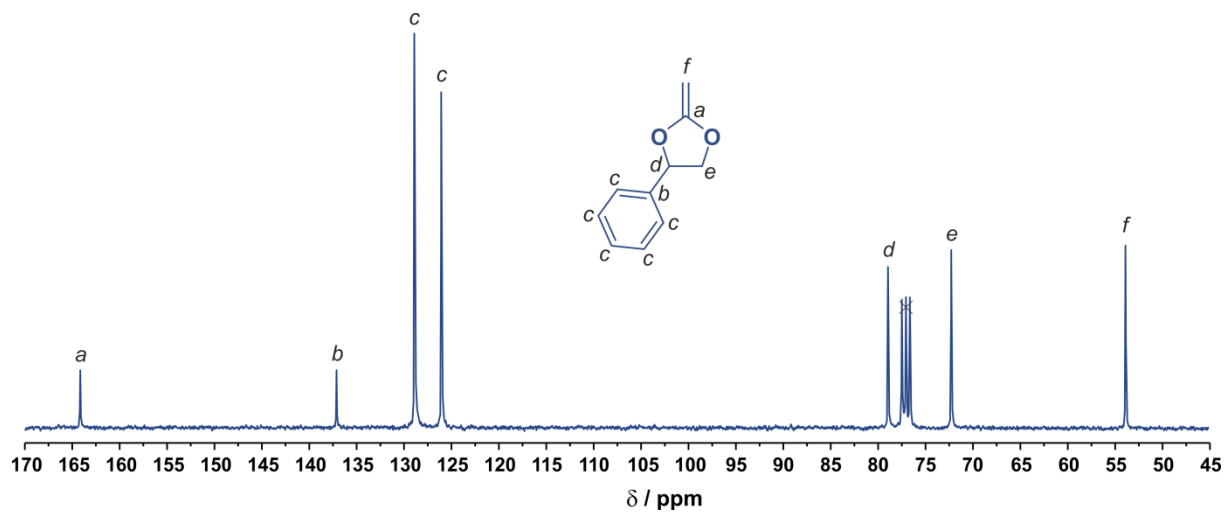


Figure S2. Representative ^{13}C NMR spectrum in CDCl_3 in the 45–170 ppm region of MPDL.

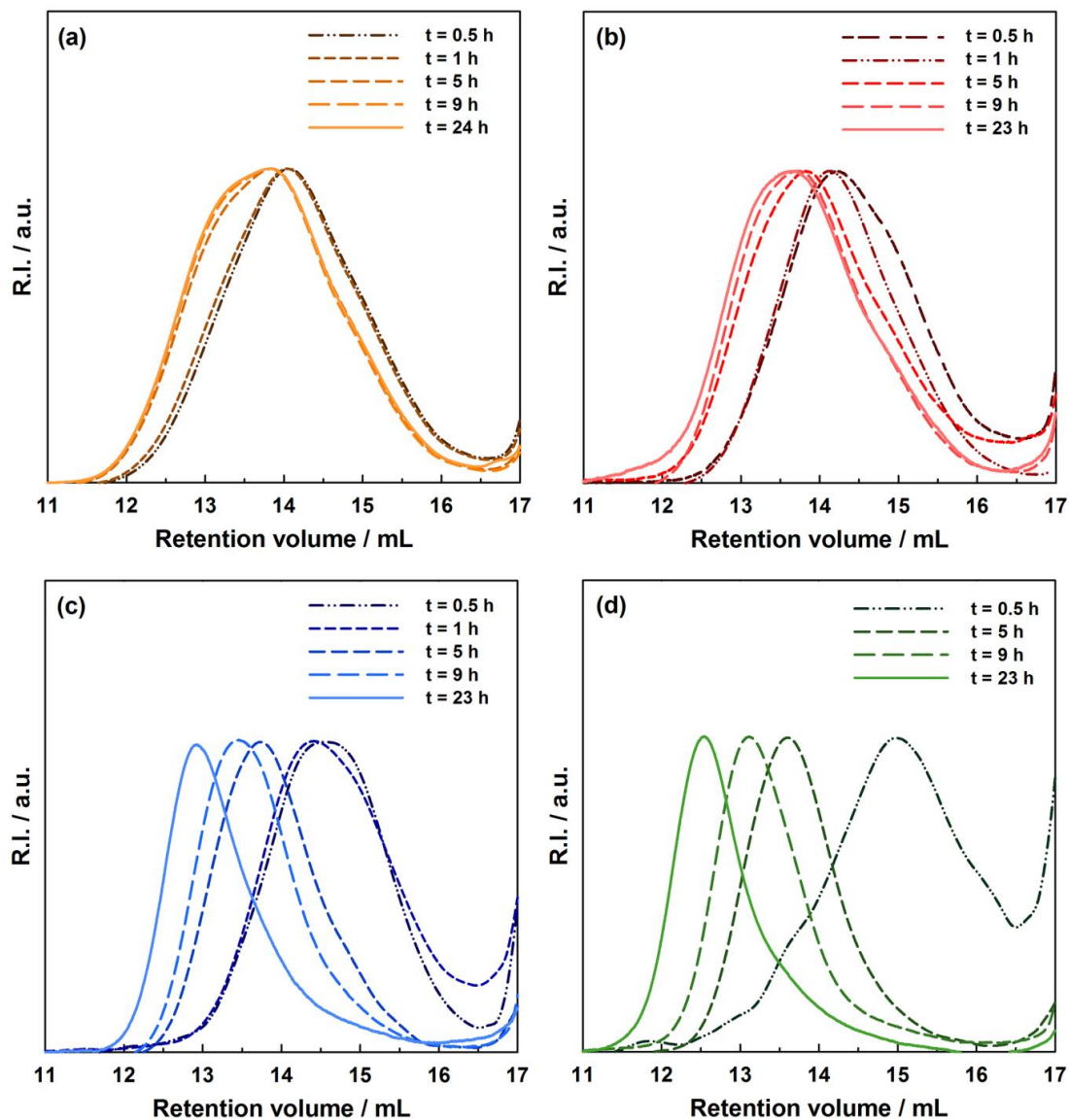


Figure S3. SEC traces taken at different time intervals during the NMP of MMA and MPDL in toluene initiated by the BlocBuilder alkoxyamine at 90 °C, as a function of the initial amount of MPDL: (a) expt. 1 ($f_{\text{MPDL},0} = 0.1$); (b) expt. 2 ($f_{\text{MPDL},0} = 0.2$); (c) expt. 3 ($f_{\text{MPDL},0} = 0.4$); (d) expt. 4 ($f_{\text{MPDL},0} = 0.7$).

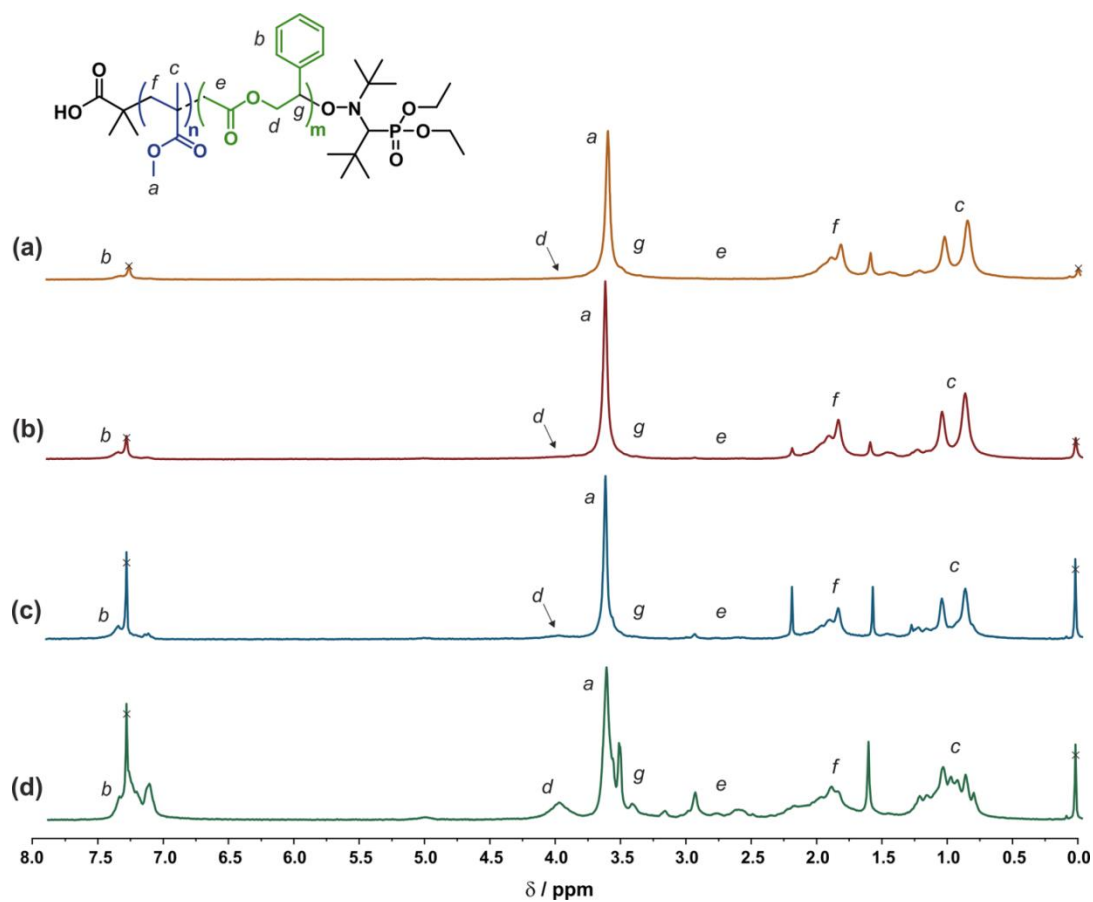


Figure S4. ^1H NMR spectra in CDCl_3 of the purified copolymers resulting from the NMP of MMA and MPDL in toluene initiated by the BlocBuilder alkoxyamine at 90°C , as a function of the initial amount of MPDL: (a) expt. 1' ($f_{\text{MPDL},0} = 0.1$); (b) expt. 2' ($f_{\text{MPDL},0} = 0.2$); (c) expt. 3' ($f_{\text{MPDL},0} = 0.4$); (d) expt. 4' ($f_{\text{MPDL},0} = 0.7$).

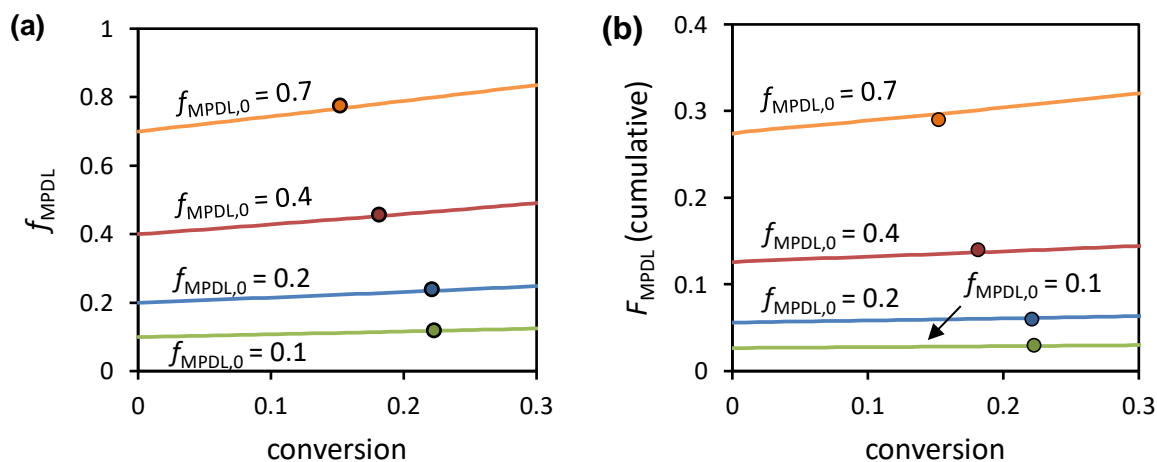


Figure S5. Comparison of modeled and experimental data for (a) the monomer feed ratio and (b) the cumulative copolymer composition as a function of conversion. Modeled data were obtained by nonlinear least squared fitting of the integrated copolymer composition equation to the experimental data, yielding reactivity ratios of $r_{\text{MPDL}} = 0.01$, $r_{\text{MMA}} = 4.0$.

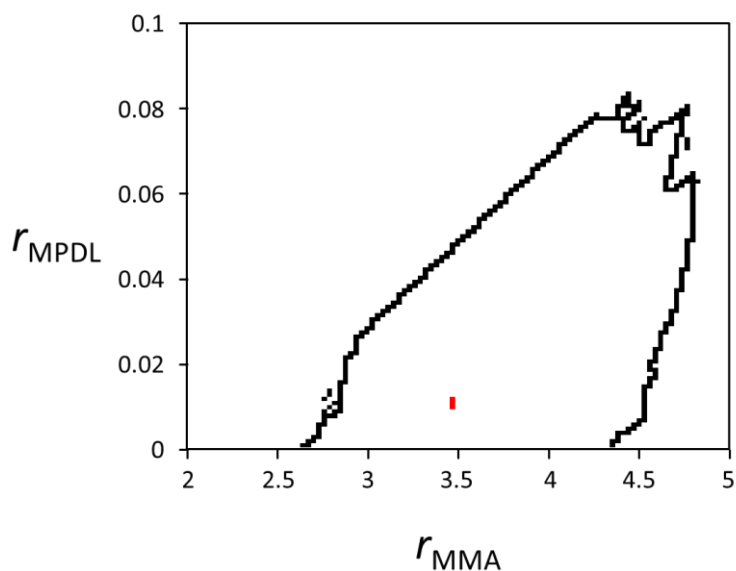


Figure S6. 95% joint confidence region for reactivity ratios of MPDL and MMA, calculated by the ‘visualisation of the sum of least squares space’ method of van den Brink et al.⁴³ The red point represents the best estimate of $r_{\text{MPDL}} = 0.01$, $r_{\text{MMA}} = 4.0$.

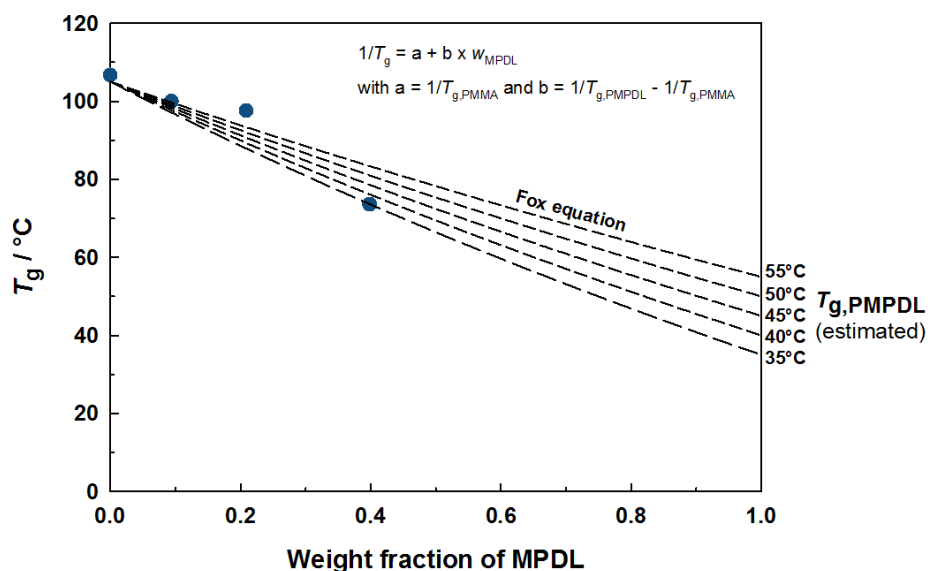


Figure S7. Experimental T_g values of the different copolymers as function of the weight fraction of MPDL in the copolymer, and curve of the Fox equation ($1/T_g = w_{PMPDL}/T_{g,PMPDL} + w_{MMA}/T_{g,PMMA}$, with w and T_g the weight fraction and T_g of each homopolymer) with an estimated T_g for PMDPL of 45 ± 10 °C.

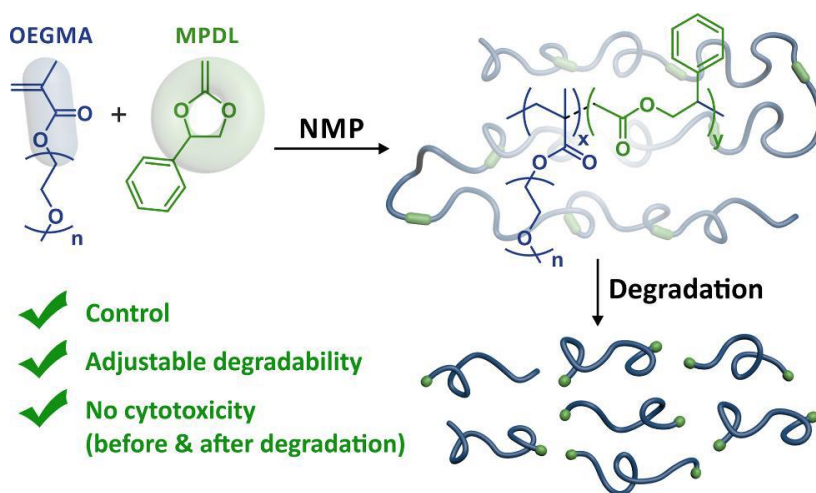
References

1. Van Den Brink, M.; Van Herk, A. M.; German, A. L. *J. Polym. Sci., Part A: Polym. Chem.* **1999**, *37*, 3793-3803.
2. Fox, T. G. *Bull. Am. Phys. Soc.* **1956**, *1*, 123-125.

Chapter 4

A Ring to Rule Them All: A Cyclic Ketene Acetal Comonomer Controls the Nitroxide-Mediated Polymerization of Methacrylates and Confers Tunable Degradability

*Vianney Delplace, Elise Guégain, Simon Harrisson, Didier Gigmes, Yohann Guillaneuf and Julien Nicolas**



Chemical Communications **2015**, 51 (64), 12847-12850

ABSTRACT

2-methylene-4-phenyl-1,3-dioxolane (MPDL) was successfully used as a controlling comonomer in NMP with oligo(ethylene glycol) methyl ether methacrylate (MeOEGMA) to prepare well-defined and degradable PEG-based P(MeOEGMA-*co*-MPDL) copolymers. The level of ester group incorporation is controlled, leading to reductions in molecular weight of up to 95% on hydrolysis. Neither the polymer nor its degradation products displayed cytotoxicity. The method was also successfully applied to methyl methacrylate.

I. Introduction

Reversible deactivation radical polymerization (RDRP) enables the synthesis of well-defined, complex and functional macromolecular architectures.¹⁻⁴ Nitroxide-mediated polymerization (NMP)³ is perhaps the simplest RDRP technique as it does not require addition of a metal catalyst or radical initiator, but relies on reversible thermal activation of a dormant alkoxyamine end-functionality to form propagating radicals and a stable nitroxide free-radical. Although early drawbacks of NMP (e.g., requirement for high temperatures, applicability to a limited number of monomers), have been substantially overcome by the development of second-generation nitroxides such as SG1,^{5,6} the control of methacrylic esters is still a challenge. The high activation-deactivation equilibrium constant (K) of SG1 results in a high concentration of propagating radicals, favoring the occurrence of irreversible termination reactions.⁷ The polymerization stops at low conversion and highly disperse polymers of uncontrolled molecular weight are obtained. Greatly improved control can be obtained by adding a small amount (typically 2-9 mol.%) of a suitable controlling comonomer with favorable kinetic parameters (i.e., low K and low cross-propagation rate constant) such as styrene (S),^{8,9} acrylonitrile (AN)^{10,11} or 9-(4-vinylbenzyl)-9H-carbazole.¹²⁻¹⁴ Most polymer chains were then shown to contain a unit of the controlling comonomer in the terminal position, which explained the high proportion of living chains.⁹

The flexibility and robustness offered by RDRP have led to a recent surge in the design of innovative and sophisticated vinyl monomer-based materials intended to find applications in different bio-related areas such as drug delivery or tissue engineering.^{15,16} However, because their carbon-carbon backbones resist degradation, these materials may cause prohibitive toxicity, which will hamper their translation to clinical settings and eventually to the market. On this basis, innovative strategies to confer different levels of (bio)degradability to vinyl polymers have emerged. Radical ring-opening polymerization (rROP) of cyclic ketene acetals (CKAs) is one of the most efficient strategies for the incorporation of degradable groups in the polymer backbone, enabling its complete degradation.¹⁷ Recent years have seen a resurgence of interest in CKAs, which may be explained by their ability to copolymerize with traditional vinyl monomers by both conventional free-radical polymerization and RDRP techniques. The versatility of this approach has been illustrated by the synthesis of a variety of different copolymer structures,¹⁸⁻²⁷ which are intended for biomedical applications.

Herein, we report the discovery that 2-methylene-4-phenyl-1,3-dioxolane (MPDL), a scarcely studied CKA,²⁸ both acting as a controlling monomer for the NMP of methacrylic esters and confers tunable degradability to the resulting copolymer, leading to non-cytotoxic degradation products (Scheme 1). This was applied to the SG1-mediated polymerization of methyl methacrylate (MMA) and oligo(ethylene glycol) methyl ether methacrylate (MeOEGMA); the latter being a widely-used monomer for the preparation of non-degradable, PEG-based polymers with potential biological applications.^{24,29-31} The choice of NMP is particularly relevant for the preparation of polymer biomaterials as it has been shown that both SG1-terminated polymers and the SG1 nitroxide itself displayed no cytotoxicity over three different mammalian cell lines even at high doses.¹¹

II. Experimental Part

a. Materials

Oligo(ethylene glycol) methyl ether methacrylate (MeOEGMA, $M_n = 300 \text{ g.mol}^{-1}$), styrene (S, 99%), methyl methacrylate (MMA, 99%), diethyl phosphite (DEP, 98%), chloroacetaldehyde dimethyl acetal (99%), (+/-)-1-phenyl-1,2-ethanediol (97%), Dowex® 50WX8 hydrogen form, potassium *tert*-butoxide (95%), *tert*-butanol anhydrous ($\geq 99.5\%$) and toluene anhydrous (99.8%) were purchased from Sigma-Aldrich and used as received (except for MMA which was distilled). Deuterated chloroform (CDCl_3) was obtained from Eurisotop. All other solvents were purchased from Carlo-Erba. 2-methyl-2-[*N-tert*-butyl-*N*-(1-diethoxyphosphoryl-2,2-dimethylpropyl) aminoxy]propionic acid alkoxyamine (BlocBuilder, 99%) and *N-tert*-butyl-*N*-(1-diethylphosphono-2,2-dimethylpropyl) nitroxide (SG1, 85%) were kindly supplied by Arkema.

b. Analytical methods

Nuclear magnetic resonance spectroscopy (NMR). ^1H NMR spectroscopy was performed in 5 mm diameter tubes in CDCl_3 on a Bruker Avance-300 (300 MHz) spectrometer. The chemical shift scale was then calibrated on the basis of the solvent peak ($\delta = 7.26 \text{ ppm}$). ^{31}P NMR spectroscopy was performed in 5 mm diameter tubes in CDCl_3 on a Bruker Avance-400 (400 MHz) spectrometer. Diethylphosphite (DEP) and its characteristic peak ($\delta = 7,1 \text{ ppm}$) was used as internal reference to calibrate the chemical shift scale.

Size exclusion chromatography (SEC). SEC was performed at 30 °C with two columns from Polymer Laboratories (PL-gel MIXED-D; 300 × 7.5 mm; bead diameter, 5 μm; linear part, 400–400 000 g.mol⁻¹) and a differential refractive index detector (Spectrasystem RI-150 from Thermo Electron Corp.), using chloroform (CHCl₃) as eluent, at a flow rate of 1 mL.min⁻¹, and toluene as a flow-rate marker. The conventional calibration curve was based on poly(methyl methacrylate) (PMMA) standards (peak molar masses, $M_p = 625\text{--}625\,500$ g.mol⁻¹) or polystyrene³² standards ($M_p = 162\text{--}523\,000$ g.mol⁻¹) from Polymer Laboratories. This technique allowed M_n (number-average molar mass), M_w (weight-average molar mass), and M_w/M_n (dispersity, D) to be determined.

c. Methods

Synthesis of 2-methylene-4-phenyl-1,3-dioxolane (MPDL). 2-Methylene-4-phenyl-1,3-dioxolane (MPDL) was synthesized in two steps as described by Bailey and co-workers,²⁸ with some modifications.

Synthesis of 2-chloromethyl-4-phenyl-1,3-dioxolane (Cl-MPDL). In a 200 mL round-bottom flask fitted with a magnetic bar and equipped with a distillation system (to collect methanol), a mixture of chloroacetaldehyde dimethyl acetal (25 g, 2.01×10^{-1} mol, 1 eq.), styrene glycol (27.75 g, 2.01×10^{-1} mol, 1 eq.) and Dowex 50 (H⁺) resin (250 mg) was heated at 120 °C overnight. Note that no methanol was collected by distillation. After the reaction mixture was cooled down to ambient temperature, the resin was then removed by filtration. The residual methanol was then removed under reduce pressure and the crude product was purified by vacuum distillation at 115 °C. Yield: 70 % (28 g, 1.4×10^{-1} mol) of a mixture of two diastereoisomers (a white solid and a colorless liquid).

Synthesis of 2-methylene-4-phenyl-1,3-dioxolane (MPDL). In a 200 mL three-neck round bottom flask, fitted with a magnetic bar and equipped with a Vigreux column, a mixture of potassium *tert*-butoxide (10.1 g, 9.02×10^{-2} mol, 1.2 eq.) in 110 mL dry *tert*-butanol was heated to 80 °C under nitrogen atmosphere. Cl-MPDL (15 g, 7.54×10^{-2} mol, 1 eq.) in 40 mL of dry *tert*-butanol were added dropwise to the mixture using an addition funnel. After the addition was completed, the temperature was raised to 100 °C to maintain a gentle reflux overnight. After the reaction mixture was cooled down to ambient temperature, 200 mL of cold diethyl ether were added and the resulting precipitate was removed by filtration. After the solvents were removed under reduce pressure, the residue was purified by vacuum distillation at 85 °C. No pyridine was further added to stabilize the MPDL. Note that the batch of MPDL must be of high purity and fresh before use to avoid the formation of a small

fraction of high molar mass polymer before and/or during the polymerization. Yield: 37% (4.5 g, 2.8×10^{-2} mol) of a colorless liquid (see Figure S1).

Synthesis of poly[oligo(ethylene glycol) methyl ether methacrylate] (PMeOEGMA, expt. 1). In a 5 mL vial, fitted with a rubber septum and a magnetic bar, a mixture of MeOEGMA (1.50 g, 5.00×10^{-3} mol), BlocBuilder alkoxyamine initiator (0.019 g, 5.07×10^{-5} mol) and anhydrous toluene (1.5 g, 1.73 mL) was deoxygenated under stirring by nitrogen bubbling for 15 min at room temperature. The mixture was then immersed in a preheated oil bath at 90 °C, corresponding to the time zero of the reaction (according to the small volume of solution and its quasi-instantaneous heating). Aliquots were periodically taken over a period of 6 h and dried to follow the MeOEGMA conversion by ^1H NMR spectroscopy (using the methylene protons in α -position to the ester group of OEGMA) and the evolution of the molar mass and the dispersity by SEC from PMMA standards.

Synthesis of poly[(oligo(ethylene glycol) methyl ether methacrylate)-*co*-(2-methylene-4-phenyl-1,3-dioxolane)] (P(MeOEGMA-*co*-MPDL). A typical solution copolymerization procedure (expt. 3) is as follows. In a 5 mL vial, fitted with a rubber septum and a magnetic bar, a mixture of MeOEGMA (1.103 g, 3.68×10^{-3} mol), MPDL (0.397 g, 2.45×10^{-3} mol), the BlocBuilder alkoxyamine initiator (0.014 g, 3.73×10^{-5} mol) and anhydrous toluene (1.5 g, 1.73 mL) was deoxygenated under stirring by nitrogen bubbling for 15 min at room temperature. The mixture was then immersed in a preheated oil bath at 90 °C, corresponding to the time zero of the reaction (according to the small volume of solution and its quasi-instantaneous heating). Aliquots were periodically taken and dried to follow the MeOEGMA conversion by ^1H NMR spectroscopy (using the methoxy protons of OEG (CH_3), the methylene protons in α -position to the ester group of OEGMA (CH_2) and the proton in α -position to the aromatic group or MPDL (CH), and following Eq. 1) and the evolution of the molar mass evolution and the dispersity by SEC from PMMA standards (note that the theoretical M_n is based on MeOEGMA).

$$\text{Conv.(\%)} = \frac{[(I_{\text{CH}_3} - 2 \cdot I_{\text{CH}})/3 - I_{\text{CH}_2}/2]}{(I_{\text{CH}_3} - 2 \cdot I_{\text{CH}})/3} \quad \text{Eq. 1}$$

The copolymer was then precipitated once in cold diethyl ether and dried under high vacuum until constant weight. ^1H NMR spectra of the purified copolymer can be found in Supporting Information (Figure S4). The same procedure was followed by adapting the amount of the reactants for expt. 2 [MeOEGMA (1.322 g, 4.41×10^{-3} mol), MPDL (0.178 g, 1.10×10^{-3} mol), BlocBuilder alkoxyamine initiator (0.017 g, 4.45×10^{-5} mol)] and expt. 4 [MeOEGMA (0.664 g, 2.21×10^{-3} mol), MPDL (0.836 g, 5.16×10^{-3} mol), BlocBuilder alkoxyamine

initiator (0.0085 g, 2.23×10^{-5} mol)]. Note that for the hydrolytic degradation study, expt. 4 has been redone but stopped at 44% conversion to yield a lower molar mass copolymer ($M_n = 17200 \text{ g}\cdot\text{mol}^{-1}$, $\bar{D} = 1.38$, $F_{\text{MPDL}} = 0.248$), more comparable to those obtained with expts. 2-3.

Synthesis of polystyrene (PS, expt. 5). In a 5 mL vial, fitted with a rubber septum and a magnetic bar, a mixture of S (4.808 g, 4.62×10^{-2} mol) and BlocBuilder alkoxyamine initiator (0.060 g, 1.56×10^{-4} mol) was deoxygenated under stirring by nitrogen bubbling for 15 min at room temperature. The vial was placed in a preheated oil bath at 120 °C, triggering the polymerization (according to the small volume of solution and its quasi-instantaneous heating). After 2 h, the polymerization was stopped by cooling down the reaction medium. The S conversion was determined by ^1H NMR spectroscopy (using the vinyl protons) and the molar mass and the dispersity was determined by SEC from PS standards. Conv. (2 h) = 53%, $M_{n,\text{SEC}} = 15\,300 \text{ g}\cdot\text{mol}^{-1}$, $M_w/M_n = 1.20$ (raw copolymer).

Synthesis of poly[(methyl methacrylate)-*co*-(2-methylene-4-phenyl-1,3-dioxolane)] (P(MMA-*co*-MPDL), expt. 6). In a 5 mL vial, fitted with a rubber septum and a magnetic bar, a mixture of MMA (0.3138 g, 3.14×10^{-3} mol), MPDL (1.1862 g, 7.32×10^{-3} mol), BlocBuilder alkoxyamine initiator (0.006 g, 1.57×10^{-5} mol) and anhydrous toluene (1.5 g, 1.73 mL) was deoxygenated under stirring by nitrogen bubbling for 15 min at room temperature. The mixture was then immersed in a preheated oil bath at 90 °C, corresponding to the time zero of the reaction (according to the small volume of solution and its quasi-instantaneous heating). After 15 h, the copolymerization was stopped. A sample was taken to estimate the MMA conversion by ^1H NMR spectroscopy and the molar mass and the dispersity were determined by SEC from PMMA standards. The copolymer was precipitated in cold methanol and dried under high vacuum until constant weight. Conv. MMA (15 h) = 40%, $M_{n,\text{SEC}} = 10\,200 \text{ g}\cdot\text{mol}^{-1}$, $M_w/M_n = 1.20$ (Figure S5), $F_{\text{MPDL}} = 0.35$.

Hydrolytic degradation. In a 5 mL vial, 30 mg of copolymer was dissolved in 3 mL of 5% KOH aqueous solution and stirred at room temperature. Aliquots of 1 mL were periodically taken, neutralized with 1 M HCl aqueous solution and lyophilized. 2 mL of chloroform was then added, allowing filtration of the salts. Finally, the solvent was removed under reduced pressure and the degradation products were analyzed by SEC.

d. Cytotoxicity study

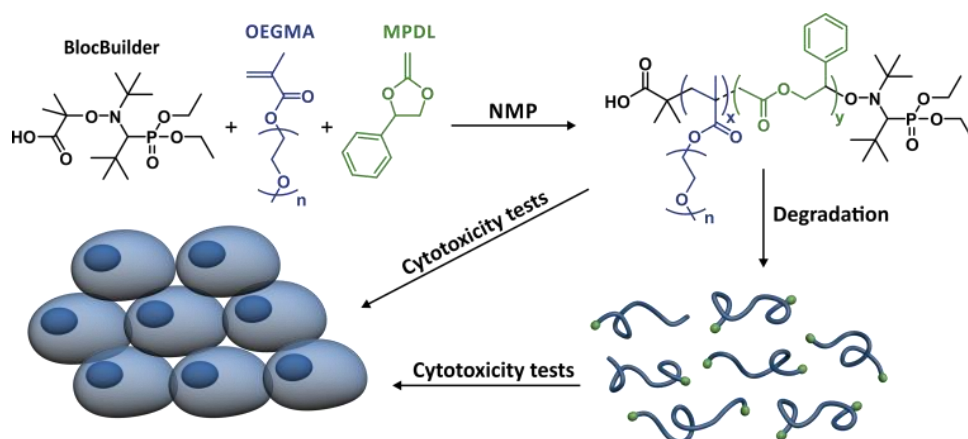
Cell lines and cell culture. The embryonic murine fibroblast (NIH/3T3) was cultured in Dulbecco's Modified Eagle Medium (DMEM, Lonza) supplemented with $50 \text{ U}\cdot\text{mL}^{-1}$ penicillin, $50 \text{ U}\cdot\text{mL}^{-1}$ streptomycin and 10% fetal bovine serum (FBS, Lonza, Belgium). The

J774.A1 murine macrophage-monocyte cell line was cultured in RPMI 1640 medium (Lonza) supplemented with 50 U.mL⁻¹ penicillin, 50 U.mL⁻¹ streptomycin and 10% heat inactivated FBS. Both cell lines were obtained from ATCC and maintained at 37 °C in a humidified 5% CO₂ atmosphere.

Cytotoxicity assay. The *in vitro* cytotoxic activity of chosen copolymers and their degradation products was evaluated on both cell lines, using the 3-[4,5-dimethylthiazol-2-yl]-3,5-diphenyltetrazolium bromide (MTT) test. Cells were seeded in 100 μL of growth medium (NIH/3T3, 3 × 10⁴ cells.mL⁻¹; J774.A1, 6 × 10⁴ cells.mL⁻¹) in 96-well microliter plates (TPP) and preincubated for 24 h. After appropriate dilutions, 100 μL of copolymer solution in cell medium was added over the cells and incubated for 72 h. Initial cell density and incubation time were determined to allow cells to remain in exponential growth and to undergo two cell-doubling times during the assay. At the end of the incubation period, 20 μL of a 5 mg.mL⁻¹ MTT (Sigma-Aldrich) solution in phosphate buffered saline (PBS) was added to each well. After 2 h of incubation, the culture medium was removed and replaced by 200 μL of dimethyl sulfoxide (DMSO), in order to dissolve the formazan crystals. The absorbance of the solubilized dye was measured spectrophotometrically with a microplate reader (LAB System Original Multiscan MS) at 570 nm. The percentage of viable cells for each treatment was calculated from the ratio of the absorbance of the well containing the treated cells versus the average absorbance of the control wells (*i.e.*, untreated cells). All experiments were set up in triplicate to determine means and SDs.

III. Results and Discussion

MPDL is a 5-membered ring CKA which is easier to synthesize than the more widely used CKAs, 2-methylene-1,3-dioxepane (MDO)³³ and 5,6-benzo-2-methylene-1,3-dioxepane (BMDO).³⁴ We recently used MPDL to prepare degradable P(MeOEGMA-*co*-AN-*co*-MPDL) terpolymers.^{18,35} Analysis by ³¹P NMR spectroscopy highlighted the competition between AN and MPDL to be the terminal monomer unit, with most copolymer chains terminated by MPDL-SG1 sequences.³⁵ This set us thinking: could MPDL itself act as a controlling comonomer for the NMP of methacrylic esters and at the same time confer tunable degradability to the resulting copolymers?



Scheme 1 Synthesis, Degradation and Cytotoxicity of Poly[(Oligo(Ethylene Glycol) Methyl Ether Methacrylate)-*co*-(2-Methylene-4-Phenyl-1,3-Dioxolane)] (P(MeOEGMA-*co*-MPDL)) prepared by NMP.

MPDL was obtained after a multigram-scale synthesis (see ESI and Fig. S1).[†] The copolymerization of MeOEGMA with a variable amount of MPDL ($f_{\text{MPDL},0} = 0\text{--}70\text{ mol.}\%$) was initiated by the BlocBuilder alkoxyamine at $90\text{ }^{\circ}\text{C}$ in $50\text{ wt.}\%$ toluene without additional SG1 (Fig. 1). As expected, the homopolymerization of MeOEGMA ($f_{\text{MPDL},0} = 0$) was initially very fast but rapidly stopped, yielding polydisperse PMeOEGMA ($M_n = 12500\text{ g.mol}^{-1}$, $\mathcal{D} = 1.72$) with no control over the molecular weight. When $20\text{ mol.}\%$ of MPDL was added in the comonomer feed, the situation significantly changed. Two kinetic regimes were observed. The polymerization was rapid within the first 2 h before slowing dramatically, likely due to the insufficient amount of MPDL units inserted to prevent irreversible termination. Some evolution of the M_n with the conversion was however noticed, matching quite well the calculated ones, with substantial improvement over the dispersities. \mathcal{D} reached 1.54 at 44% conversion for a 13300 g.mol^{-1} P(MeOEGMA-*co*-MPDL) copolymer. At $f_{\text{MPDL},0} = 0.4$, more rapid establishment of first order kinetics with a greater slope over 10 h were observed, presumably due to earlier insertion of MPDL units. This amount of MPDL was perhaps not enough to prevent the occurrence of irreversible termination reactions in the long run, as seen by the deviation from linearity at 24 h . Nevertheless a linear evolution of M_n with monomer conversion between 7000 and 15000 g.mol^{-1} , and lower \mathcal{D} values (i.e., $1.42\text{--}1.53$) were observed. A further increase in the initial amount of MPDL ($f_{\text{MPDL},0} = 0.7$) resulted in immediate establishment of first order kinetics up to high monomer conversion ($\sim 70\%$) and linear evolution of M_n over a wide range of values ($\sim 4400\text{--}27000\text{ g.mol}^{-1}$). Dispersity was also improved as it reached 1.31 at 39% monomer conversion. In fact, the higher $f_{\text{MPDL},0}$, the lower the dispersities during the polymerization (Fig. 1b). The evolution of molecular weight distribution with time further illustrated the controlled nature of the copolymerizations (Fig.

S2).[†] Two independent batches of MPDL demonstrated very good reproducibility in terms of kinetics and control, confirming the reliability of this strategy (Fig. S3).[†] The copolymers were purified after 30 h by precipitation in cold diethyl ether, giving $M_n = 14700 \text{ g.mol}^{-1}$ and $\mathcal{D} = 1.55$ for expt. 2, $M_n = 20100 \text{ g.mol}^{-1}$ and $\mathcal{D} = 1.44$ for expt. 3, and $M_n = 24500 \text{ g.mol}^{-1}$ and $\mathcal{D} = 1.30$ for expt. 4.

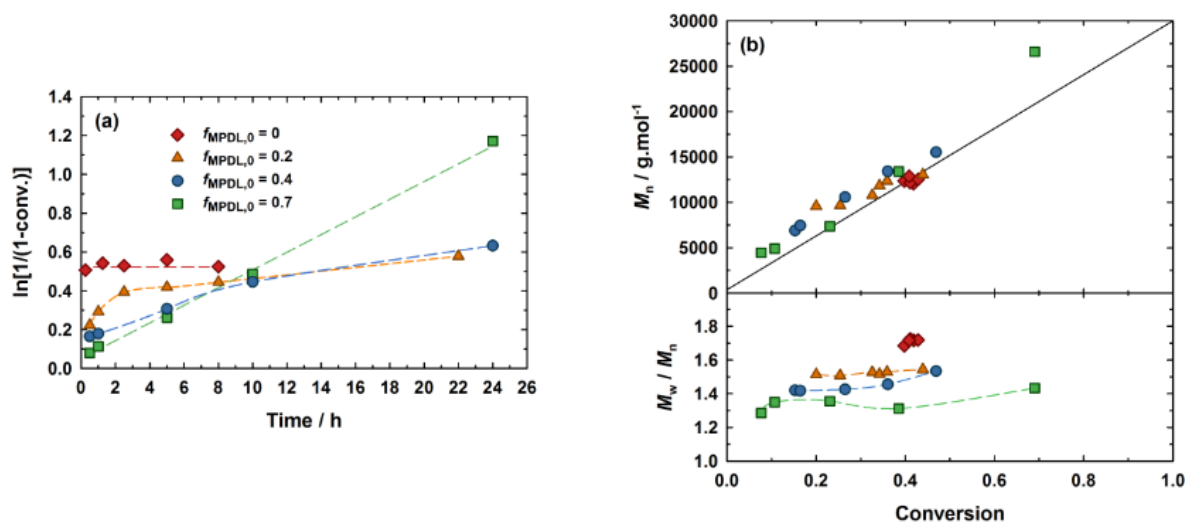


Figure 1. NMP of MeOEGMA and MPDL in toluene initiated by the BlocBuilder alkoxyamine at 90 °C, as a function of the initial amount of MPDL: \blacklozenge , expt. 1 ($f_{\text{MPDL},0} = 0$); \blacktriangle , expt. 2 ($f_{\text{MPDL},0} = 0.2$); \bullet , expt. 3 ($f_{\text{MPDL},0} = 0.4$); \blacksquare , expt. 4 ($f_{\text{MPDL},0} = 0.7$). (a) $\text{Ln}[1/(1-\text{conv.})]$ vs time (conv. = MeOEGMA conversion). (b) Number-average molar mass M_n , and dispersity, M_w/M_n , vs conversion. The full line represents the theoretical M_n (MeOEGMA) and the dashed ones are guides for the eye only.

^1H NMR spectroscopy of the purified P(MeOEGMA-*co*-MPDL) copolymers (expts. 2–4) showed all signals expected for a P(MeOEGMA-*co*-MPDL) structure. (Fig. S4). The aromatic hydrogens of the phenyl group of MPDL (signal *e*) were clearly visible and confirmed that its level of incorporation in the copolymer could be adjusted by varying its initial concentration in the comonomer feed. The preferential formation of the MPDL-SG1 terminal sequence was confirmed by ^{31}P NMR spectroscopy as its spectrum is very similar to that of PS-SG1 (expt. 5), due to the styrene-like ring-opened structure of MPDL (Fig. S5).[†] This analogy in structures between the open radical forms of S and MPDL explains the ability of MPDL to act as a controlling comonomer. The copolymerization was also successfully performed with MMA, a representative methacrylate monomer. Under similar experimental conditions, a well-defined P(MMA-*co*-MPDL) copolymer (expt. 6, conv. MMA (15 h) = 40%, $M_n = 10200 \text{ g.mol}^{-1}$, $\mathcal{D} = 1.20$) was prepared (Fig. S6). ^{31}P NMR spectroscopy performed in the presence

of a known amount of diethyl phosphite as internal reference gave a living chain fraction as high as 85% (Fig. S7),[†] which is similar to those obtained using S or AN as a comonomers, thus establishing the efficiency of MPDL as a controlling comonomer.

The molar fraction of MPDL in the copolymer, F_{MPDL} , with respect to MeOEGMA was determined by ¹H NMR spectroscopy to be 3.6, 11.3 and 24.8 mol.% for expt. **2** ($f_{\text{MPDL},0} = 0.2$), expt. **3** ($f_{\text{MPDL},0} = 0.4$) and expt. **4** ($f_{\text{MPDL},0} = 0.7$), respectively. As for the vast majority of CKAs, unfavorable reactivity ratios impose high concentrations of MPDL in the comonomer feed in order to achieve substantial incorporation in the resulting copolymer. The reactivity ratios were determined by fitting the integrated form of the copolymer composition equation to the monomer feed composition vs conversion data using the visualization of the sum of squares method,³⁶ assuming non-negligible errors in both variables. This procedure gave a point estimate of 6.95 for r_{MeOEGMA} and 0 for r_{MPDL} , with a 95% joint confidence region spanning the range of 6.3–7.9 for r_{MeOEGMA} and 0–0.038 for r_{MPDL} (Fig. S8).[†] The values obtained are typical for copolymerizations of methacrylate monomers with ring-opening monomers such as MDO ($r_{\text{MMA}} = 34$, $r_{\text{MDO}} = 0.057$),³⁷ 1,1-dichloro-2-vinylcyclopropane ($r_{\text{MMA}} = 11$, $r_{\text{VCP}} = 0.07$)³⁸ and 7-methylene-2-methyl-1,5-dithiacyclooctane ($r_{\text{MMA}} = 6.3$, $r_{\text{MDTO}} = 0.52$),³⁹ and reflect the lack of radical-stabilizing substituents on the double bond of the CKA.

To assess the degradability, hydrolytic degradation of the copolymers was performed in accelerated conditions (i.e., 5% KOH aqueous solution) and monitored over a period of 24 h to estimate the kinetics of hydrolysis (Fig. 2a). Adjustable incorporation of MPDL in the copolymer enabled fine tuning of the level of degradation, which typically reached its steady state after 5 h. While the copolymer with the lowest amount of MPDL (expt. **2**) led to modest degradation (~30% decrease in M_n for $F_{\text{MPDL}} = 0.036$), significant (even complete) degradation was observed for greater amounts of MPDL. When $F_{\text{MPDL}} = 0.113$ (expt. **3**), the decrease in M_n was 81% whereas it reached 95% for $F_{\text{MPDL}} = 0.248$ (expt. **4**). The complete hydrolysis of the latter was confirmed by size exclusion chromatograms which shifted toward lower molar masses (Fig. 2b). Note that the polymer without MPDL (expt. **1**) was perfectly stable, thus ruling out reduction in molecular weight due to ester side chain hydrolysis.

The theoretical decrease in M_n of these copolymers can be calculated from the average sequence length of PMeOEGMA blocks in each copolymer. This can be directly estimated from the copolymer composition, as due to the very low r_{MPDL} , the probability of finding a sequence of two or more MPDL units is negligible. From the MPDL content of the polymers it corresponds to, on average, 1 MPDL unit for every 26.8 (expt. **2**), 7.8 (expt. **3**) and 3.0

(expt. 4) MeOEGMA units. These lengths correspond to M_n of 8210, 2530 and 1080 $\text{g}\cdot\text{mol}^{-1}$, respectively. These values are in rather good agreement with those obtained for the degraded polymers (12600, 3500 and 800 $\text{g}\cdot\text{mol}^{-1}$, respectively), especially the one with the highest amount of MPDL, thus confirming the near-complete hydrolysis of the main chain ester groups.

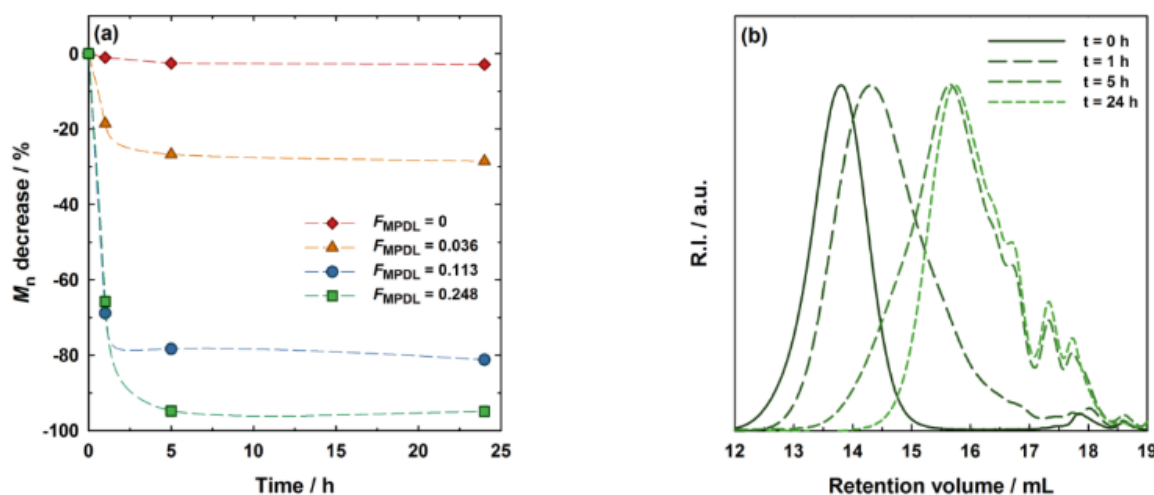


Figure 2. Hydrolytic degradation in 5% KOH of P(MeOEGMA-*co*-MPDL) as a function of the content in MPDL: \blacklozenge , expt. 1 ($F_{\text{MPDL},0} = 0$); \blacktriangle , expt. 2 ($F_{\text{MPDL},0} = 0.036$); \bullet , expt. 3 ($F_{\text{MPDL},0} = 0.113$); \blacksquare , expt. 4 ($F_{\text{MPDL},0} = 0.248$) (a) Evolution of the number-average molar mass, M_n with time. Dashed lines are guides for the eye only. (b) Evolution of the SEC chromatograms at different time for expt. 4 during degradation.

Conferring PEG-based polymers with the ability to be degraded in a hydrolytic environment is a significant advance compared to traditional linear or comb-like PEGs that are resistant to degradation. However, neither the degradation products nor the polymer itself should be cytotoxic in an optimized product. This point is crucial as it will determine the ultimate biocompatibility of the materials. The potential toxicity of different copolymers has been tested on two representative mammalian cell types: murine fibroblasts (NIH/3T3) and murine macrophages (J774.A1). Whereas NIH/3T3 cells are one of the most commonly used fibroblast cell lines, J774.A1 cells, which play a key role in phagocytosis, were chosen to highlight possible toxicity of the copolymers after being engulfed by macrophages. The cytotoxicity was evaluated in vitro by MTT assay at two copolymer concentrations (0.1 and 1 $\text{mg}\cdot\text{mL}^{-1}$) (Fig. 3). Incubation of undegraded P(MeOEGMA-*co*-MPDL) copolymer (expt. 3, $F_{\text{MPDL},0} = 0.113$) with both cell lines resulted in >95% cell viability at 0.1 $\text{mg}\cdot\text{mL}^{-1}$. At 1 $\text{mg}\cdot\text{mL}^{-1}$ cells viabilities were still high; 83% with NIH/3T3 cells and 72% with J774.A1

cells. More importantly, MTT assays revealed no cytotoxicity from the degradation products whatever the cell line and the copolymer concentration. Cell viabilities were in the 97–99% range at $0.1 \text{ mg}\cdot\text{mL}^{-1}$ and 86–92% at $1 \text{ mg}\cdot\text{mL}^{-1}$. These results indicate the absence of obvious toxicity from the copolymer and from the products, which is a very encouraging indication of their biocompatibility and their safe use as biomaterial building blocks.

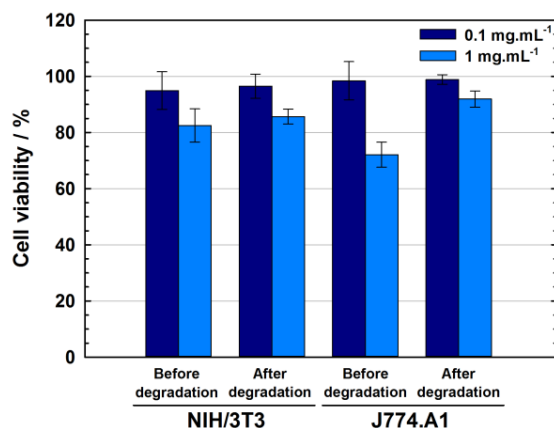


Figure 3. Cell viability (MTT assay) after incubation of NIH/3T3 cells and J774.A1 cells with P(MeOEGMA-*co*-MPDL) copolymer (expt. 3, $F_{\text{MPDL},0} = 0.113$) at 0,1 and 1 $\text{mg}\cdot\text{mL}^{-1}$. Results were expressed as percentages of absorption of treated cells (\pm SD) in comparison to that of untreated ones as a control.

IV. Conclusion

In conclusion, we have demonstrated that MPDL, a little-studied CKA, can both act as a controlling comonomer for the SG1-mediated polymerization of methacrylic esters and confer tunable degradability to the resulting copolymer. By adjusting the comonomer feed, up to complete degradation was observed. No significant toxicity was shown, either from P(MeOEGMA-*co*-MPDL) or from its degradation products. Not only does this broaden the range of suitable controlling comonomers for the NMP of methacrylic esters, but it adds significant value to the copolymerization approach due to the degradability of the resulting copolymer. Additionally, this study opens up exciting perspectives in the design of new controlling comonomers and NMP-derived degradable architectures with a wide range of potential (bio)applications. For instance, nanoparticles or therapeutic proteins decorated with degradable PEG segments should show reduced toxicity and persistence compared to their nondegradable PEGylated analogues.

References

- (1) Kamigaito, M.; Ando, T.; Sawamoto, M. *Chem. Rev.* **2001**, *101*, 3689.
- (2) Moad, G.; Rizzardo, E.; Thang, S. H. *Aust. J. Chem.* **2009**, *62*, 1402.
- (3) Nicolas, J.; Guillaneuf, Y.; Lefay, C.; Bertin, D.; Gigmès, D.; Charleux, B. *Prog. Polym. Sci.* **2013**, *38*, 63.
- (4) Perrier, S.; Takolpuckdee, P. *J. Polym. Sci., Part A: Polym. Chem.* **2005**, *43*, 5347.
- (5) Benoit, D.; Chaplinski, V.; Braslau, R.; Hawker, C. J. *J. Am. Chem. Soc.* **1999**, *121*, 3904.
- (6) Benoit, D.; Grimaldi, S.; Robin, S.; Finet, J.-P.; Tordo, P.; Gnanou, Y. *J. Am. Chem. Soc.* **2000**, *122*, 5929.
- (7) Dire, C.; Belleney, J.; Nicolas, J.; Bertin, D.; Magnet, S.; Charleux, B. *J. Polym. Sci., Part A: Polym. Chem.* **2008**, *46*, 6333.
- (8) Charleux, B.; Nicolas, J.; Guerret, O. *Macromolecules* **2005**, *38*, 5485.
- (9) Nicolas, J.; Dire, C.; Mueller, L.; Belleney, J.; Charleux, B.; Marque, S. R. A.; Bertin, D.; Magnet, S.; Couvreur, L. *Macromolecules* **2006**, *39*, 8274.
- (10) Nicolas, J.; Brusseau, S.; Charleux, B. *J. Polym. Sci., Part A: Polym. Chem.* **2010**, *48*, 34.
- (11) Chenal, M.; Mura, S.; Marchal, C.; Gigmès, D.; Charleux, B.; Fattal, E.; Couvreur, P.; Nicolas, J. *Macromolecules* **2010**, *43*, 9291.
- (12) Lessard, B.; Ling, E. J. Y.; Morin, M. S. T.; Marić, M. *J. Polym. Sci., Part A: Polym. Chem.* **2011**, *49*, 1033.
- (13) Lessard, B. H.; Ling, E. J. Y.; Marić, M. *Macromolecules* **2012**, *45*, 1879.
- (14) Lessard, B. H.; Guillaneuf, Y.; Mathew, M.; Liang, K.; Clement, J.-L.; Gigmès, D.; Hutchinson, R. A.; Marić, M. *Macromolecules* **2013**, *46*, 805.
- (15) Delplace, V.; Couvreur, P.; Nicolas, J. *Polym. Chem.* **2014**, *5*, 1529.
- (16) Elsabahy, M.; Wooley, K. L. *Chem. Soc. Rev.* **2012**, *41*, 2545.
- (17) Agarwal, S. *Polym. Chem.* **2010**, *1*, 953.
- (18) Delplace, V.; Tardy, A.; Harriison, S.; Mura, S.; Gigmès, D.; Guillaneuf, Y.; Nicolas, J. *Biomacromolecules* **2013**, *14*, 2837.
- (19) Lutz, J.-F.; Andrieu, J.; Üzgün, S.; Rudolph, C.; Agarwal, S. *Macromolecules* **2007**, *40*, 8540.
- (20) Undin, J.; Finne-Wistrand, A.; Albertsson, A.-C. *Biomacromolecules* **2013**, *14*, 2095.
- (21) Undin, J.; Illanes, T.; Finne-Wistrand, A.; Albertsson, A.-C. *Polym. Chem.* **2012**, *3*, 1260.
- (22) Maji, S.; Zheng, M.; Agarwal, S. *Macromol. Chem. Phys.* **2011**, *212*, 2573.
- (23) Zhang, Y.; Chu, D.; Zheng, M.; Kissel, T.; Agarwal, S. *Polym. Chem.* **2012**, *3*, 2752.
- (24) Riachi, C.; Schüwer, N.; Klok, H.-A. *Macromolecules* **2009**, *42*, 8076.
- (25) Chung, I. S.; Matyjaszewski, K. *Macromolecules* **2003**, *36*, 2995.
- (26) Siegwart, D. J.; Bencherif, S. A.; Srinivasan, A.; Hollinger, J. O.; Matyjaszewski, K. *J. Biomed. Mater. Res., Part A* **2008**, *87A*, 345.
- (27) Zhang, Y.; Aigner, A.; Agarwal, S. *Macromol. Biosci.* **2013**, *13*, 1267.
- (28) Bailey, W. J.; Wu, S. R.; Ni, Z. *Makromol. Chem.* **1982**, *183*, 1913.
- (29) Le Droumaguet, B.; Nicolas, J. *Polym. Chem.* **2010**, *1*, 563.
- (30) Lutz, J.-F. *J. Polym. Sci., Part A: Polym. Chem.* **2008**, *46*, 3459.
- (31) Nicolas, J.; Mantovani, G.; Haddleton, D. M. *Macromol. Rapid Commun.* **2007**, *28*, 1083.
- (32) Deng, L.; Furuta, P. T.; Garon, S.; Li, J.; Kavulak, D.; Thompson, M. E.; Fréchet, J. M. J. *Chemistry of Materials* **2006**, *18*, 386.
- (33) Bailey, W. J.; Ni, Z.; Wu, S. R. *J. Polym. Sci., Polym. Chem. Ed.* **1982**, *20*, 3021.

- (34) Bailey, W. J.; Ni, Z.; Wu, S. R. *Macromolecules* **1982**, *15*, 711.
- (35) Delplace, V.; Harrisson, S.; Tardy, A.; Gimes, D.; Guillaneuf, Y.; Nicolas, J. *Macromol. Rapid Commun.* **2014**, *35*, 484.
- (36) Van Den Brink, M.; Van Herk, A. M.; German, A. L. *J. Polym. Sci., Part A: Polym. Chem.* **1999**, *37*, 3793.
- (37) Roberts, G. E.; Coote, M. L.; Heuts, J. P. A.; Morris, L. M.; Davis, T. P. *Macromolecules* **1999**, *32*, 1332.
- (38) Takahashi, T. *Journal of Polymer Science Part A-1: Polymer Chemistry* **1970**, *8*, 739.
- (39) Harrisson, S.; Davis, T. P.; Evans, R. A.; Rizzardo, E. *Macromolecules* **2001**, *34*, 3869.

Supplementary Information

Table S1. Experimental Conditions and Results of the Different (Co)polymerizations.

Expt.	Main monomer	$f_{\text{MPDL},0}^{(a)}$	T (°C)	Toluene (wt.%)	Conv (%) / time (h)	$M_n^{(b)}$ (g.mol ⁻¹)	$D^{(b)}$	$F_{\text{MPDL}}^{(c)}$
1	MeOEGMA	-	90	50	41 / 8	12 500 ^d	1.72 ^d	-
2	MeOEGMA	0.2	90	50	44 / 22	13 300 ^d	1.54 ^d	0.036
3	MeOEGMA	0.4	90	50	47 / 24	15 500 ^d	1.53 ^d	0.113
4	MeOEGMA	0.7	90	50	69 / 24	26 600 ^d	1.43 ^d	0.248
5	S	-	120	-	53 / 2	15 300	1.20	-
6	MMA	0.7	90	50	40 / 15	10 200	1.20	0.35

^aInitial molar fraction of MPDL in the monomer feed. ^bDetermined by size exclusion chromatography (SEC). ^cMolar fraction of MPDL in the final copolymer. ^dData for the raw (co)polymers.

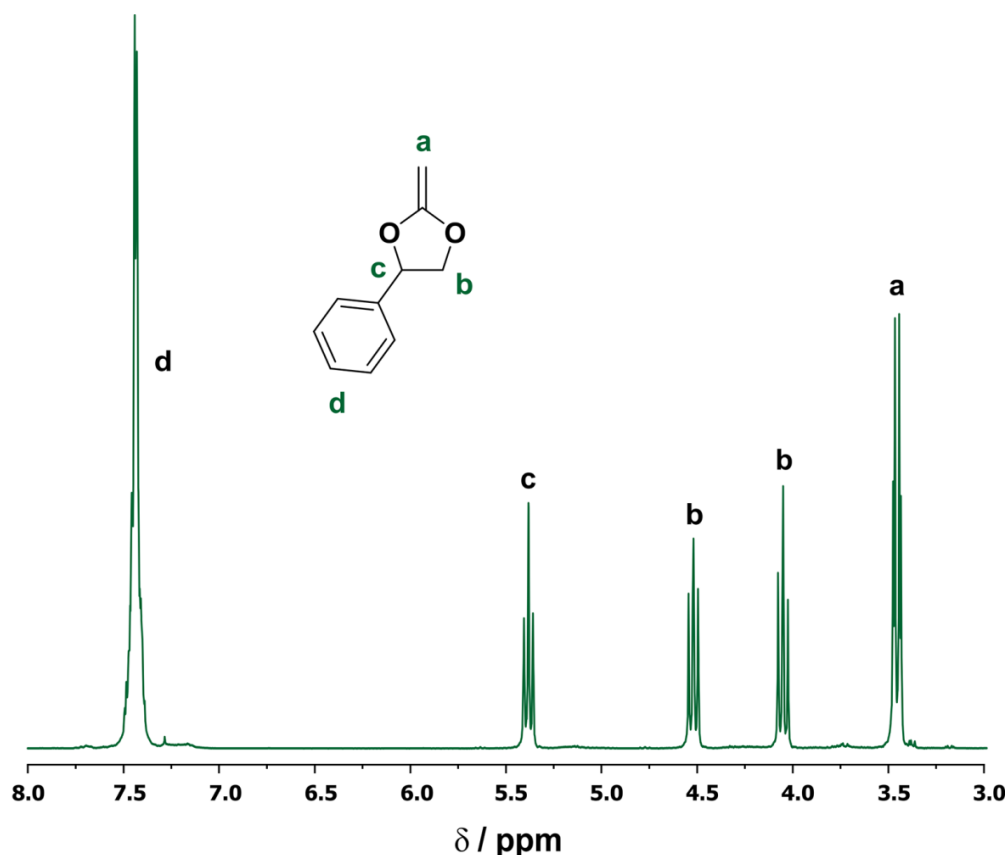


Figure S1. ¹H NMR spectrum of 2-methylene-4-phenyl-1,3-dioxolane (MPDL) in the 3.0–8.0 region in CDCl₃.

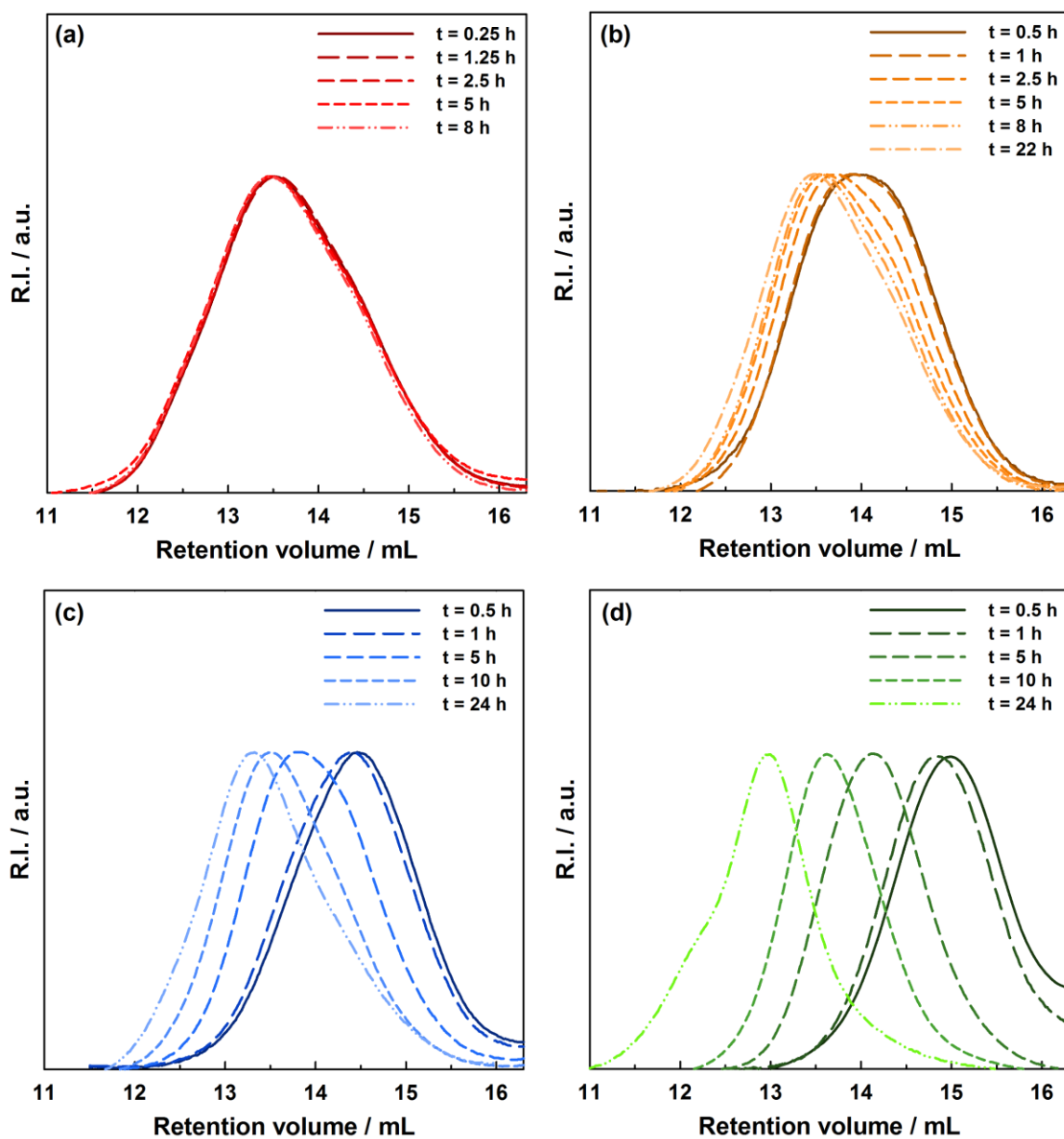


Figure S2. SEC traces taken at different time intervals during the NMP of oligo(ethylene glycol) methyl ether methacrylate (MeOEGMA) and 2-methylene-4-phenyl-1,3-dioxolane (MPDL) in toluene initiated by the BlocBuilder alkoxyamine at 90 °C, as a function of the initial amount of MPDL: (a) expt. 1 ($f_{\text{MPDL},0} = 0$); (b) expt. 2 ($f_{\text{MPDL},0} = 0.2$); (c) expt. 3 ($f_{\text{MPDL},0} = 0.4$); (d) expt. 4 ($f_{\text{MPDL},0} = 0.7$).

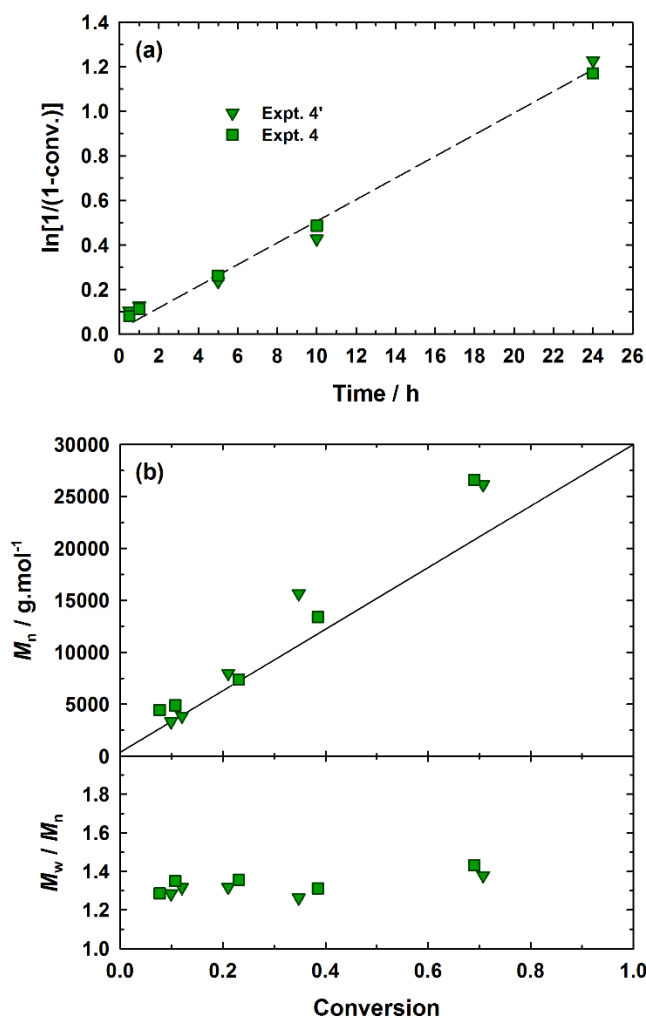


Figure S3. Reproducibility of the NMP of oligo(ethylene glycol) methyl ether methacrylate (MeOEGMA) and 2-methylene-4-phenyl-1,3-dioxolane (MPDL) in toluene initiated by the BlocBuilder alkoxyamine at 90 °C for $f_{\text{MPDL},0} = 0.7$. (a) $\ln[1/(1-\text{conv.})]$ vs time (conv. = MeOEGMA conversion). (b) Number-average molar mass M_n , and dispersity, M_w/M_n , vs conversion. The full line represents the theoretical M_n and the dashed ones are guides for the eye only.

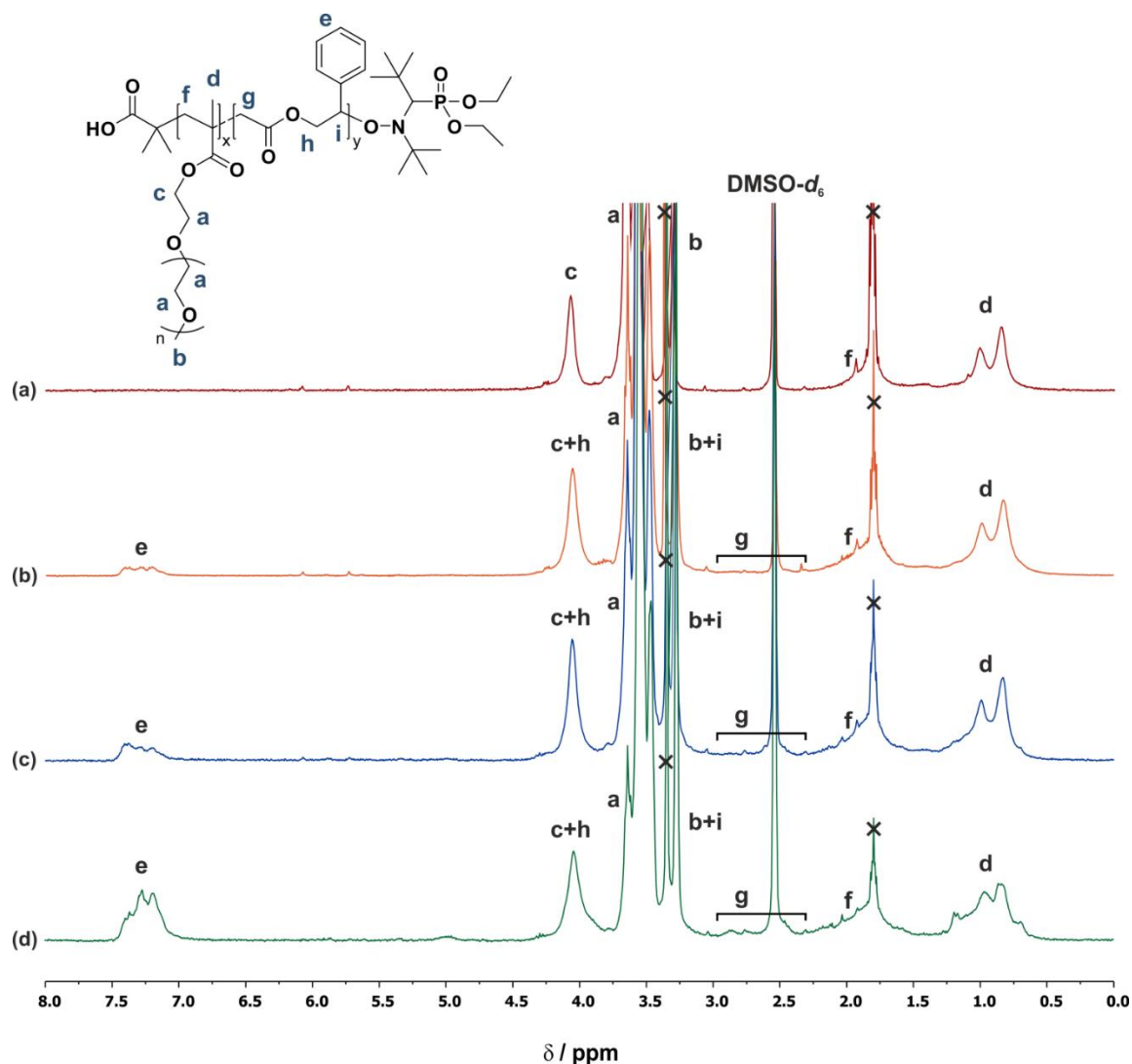


Figure S4. ^1H NMR spectra in $\text{DMSO-}d_6$ of the purified (co)polymers resulting from the NMP of oligo(ethylene glycol) methyl ether methacrylate (MeOEGMA) and 2-methylene-4-phenyl-1,3-dioxolane (MPDL) in toluene initiated by the BlocBuilder alkoxyamine at $90\text{ }^\circ\text{C}$, as a function of the initial amount of MPDL: (a) expt. 1 ($f_{\text{MPDL},0} = 0$); (b) expt. 2 ($f_{\text{MPDL},0} = 0.2$); (c) expt. 3 ($f_{\text{MPDL},0} = 0.4$); (d) expt. 4 ($f_{\text{MPDL},0} = 0.7$).

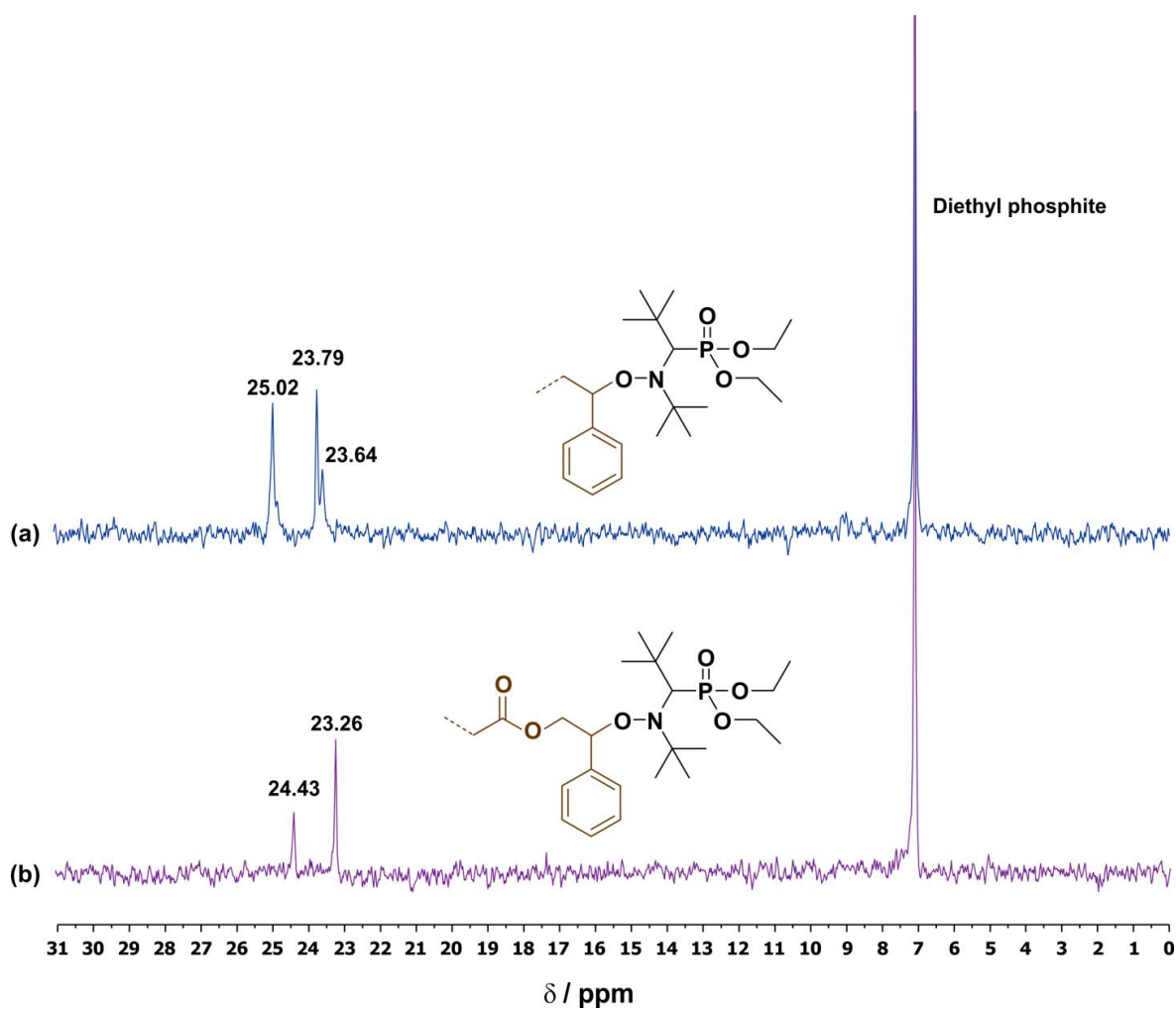


Figure S5. ^{31}P NMR spectra in CDCl_3 of: (a) PS-SG1 (expt. 5) and (b) P(MeOEGMA-co-MPDL)-SG1 ($f_{\text{MPDL},0} = 0.4$, expt. 3).

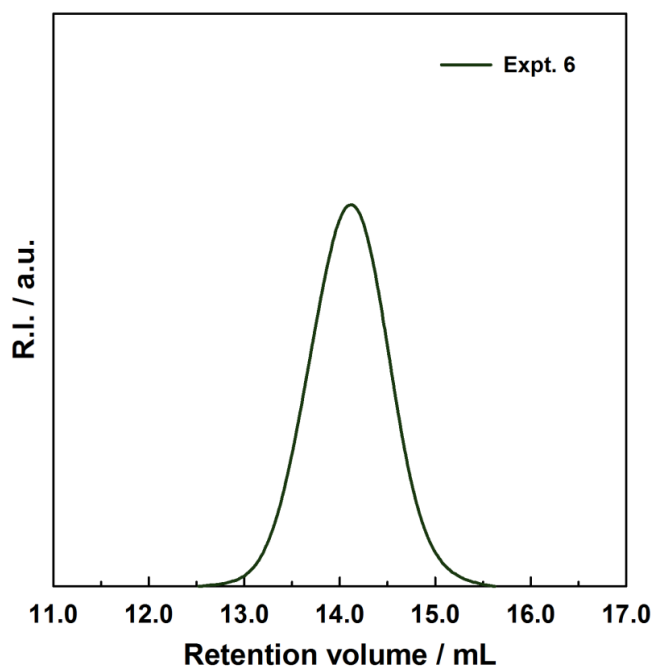


Figure S6. SEC traces of the purified P(MMA-*co*-MPDL) copolymer (expt. 6).

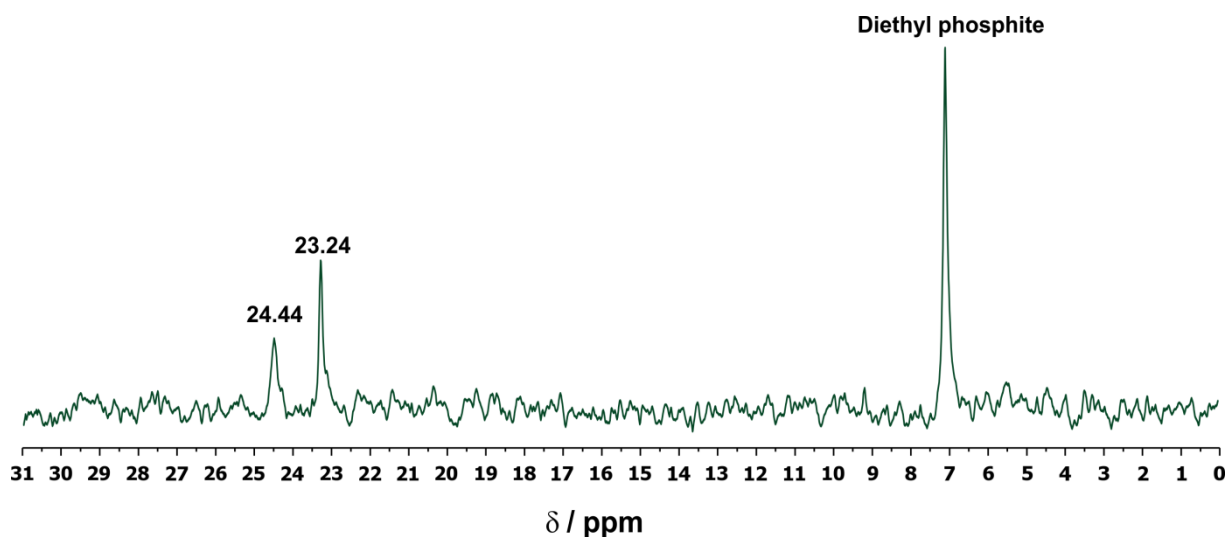


Figure S7. ¹H NMR spectra in DMSO-*d*₆ of the purified copolymer resulting from the NMP of methyl methacrylate (MMA) and 2-methylene-4-phenyl-1,3-dioxolane (MPDL) in toluene initiated by the BlocBuilder alkoxyamine at 90 °C (expt. 6).

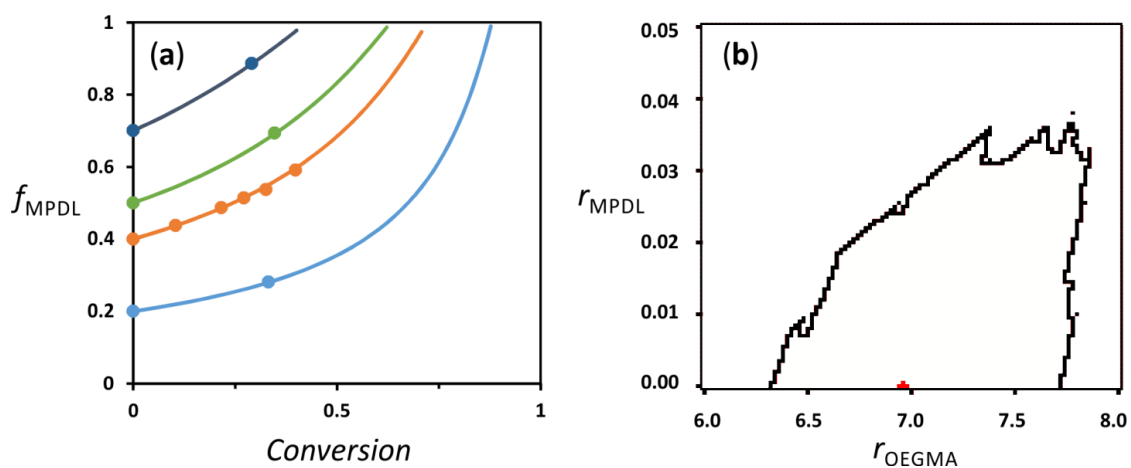
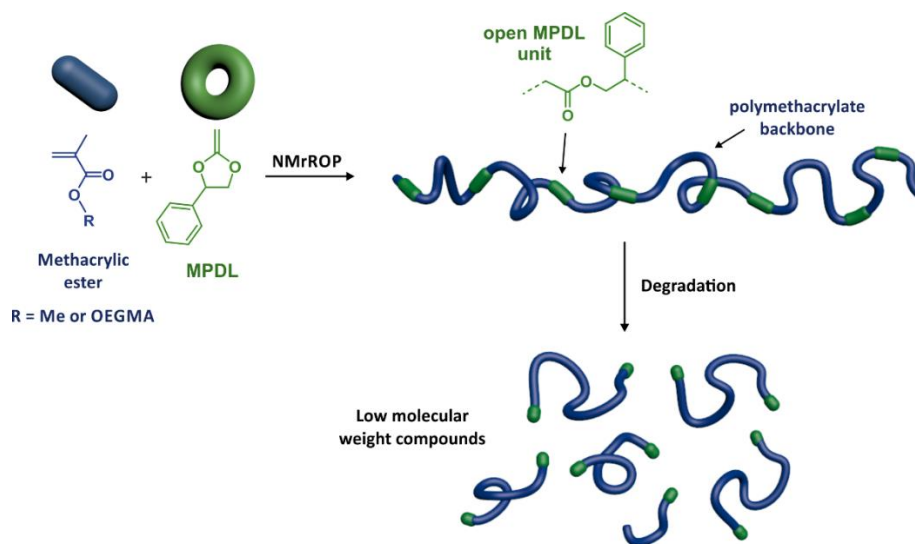


Figure S8. (a) Mole fraction of MPDL in the monomer feed as a function of conversion. Circles represent experimental data and lines are the predictions of the copolymer composition using the copolymer composition equation with reactivity ratios of $r_{\text{MPDL}} = 0$, $r_{\text{MeOEGMA}} = 6.95$. (b) 95% joint confidence region (JCR) for reactivity ratios of MeOEGMA and MPDL calculated by the ‘visualization of the sum of least squares space’ method of van den Brink et al. (M. van den Brink, A. M. van Herk and A. L. German, *J. Polym. Sci., Part A: Polym. Chem.*, 1999, 37, 3793).

Chapter 5

Degradation of Copolymers Prepared by Nitroxide-Mediated Radical Ring-Opening Polymerization and Point-by-Point Comparison with Traditional Polyesters

*Elise Guégain, Jean-Philippe Michel, Tanguy Boissenot, Julien Nicolas**



To be submitted

ABSTRACT

Two libraries of well-defined, degradable vinyl copolymers of opposite solubility, based either on methyl methacrylate or on oligo(ethylene glycol) methyl ether methacrylate (OEGMA), and containing various amount of 2-methylene-4-phenyl-1,3-dioxolane (MPDL), were synthesized by nitroxide-mediated polymerization. A comprehensive degradation study (long-term hydrolytic degradation, degradation of thick and thin films, water uptake, enzymatic degradation) was then performed and results were compared with those from traditional aliphatic polyesters (PLGA, PLA and PCL). It appeared that P(MMA-*co*-MPDL) copolymers slowly degraded in PBS with degradation kinetics slower than that of PCL whereas P(OEGMA-*co*-MPDL) copolymers led to significant degradation, in between that of PLA and PCL, depending the amount of MPDL, but without leading to a dramatic drop of pH as for PLGA and PLA. Whereas P(MMA-*co*-MPDL) copolymers might be well-suited for biomaterials intended for long-term use (e.g., devices, implants), faster degrading P(OEGMA-*co*-MPDL) copolymers might be envisioned for short- or mid-term applications such as nanoscale drug-delivery systems and meet a need for hydrophilic degradable materials with tunable degradation kinetics.

I. Introduction

The development of (bio)degradable polymers is currently the focus of great attention given their use in a wide range of applications including ¹medicine, microelectronics and environmental protection.²⁻⁴ Polymers intended for biomedical applications are indeed of extreme importance for drug delivery or tissue engineering applications and should usually meet the following criteria: (i) biodegradability (mainly for administered materials) and biocompatibility (to avoid toxic side-effects); (ii) uniformity in polymer chain length and composition to ensure a reproducible biological response and (iii) functionalizability with biologically active (macro)molecules (e.g., drugs, targeting ligands) and fluorescent probes for therapeutic and diagnostic/tracing purposes, respectively.

Among the different classes of biodegradable polymers, aliphatic polyesters synthesized by ring-opening polymerization (ROP) of cyclic monomers (e.g., lactide, glycolide, caprolactone, etc.) are certainly the most studied materials for biomedical applications, including the manufacture of resorbable sutures, tissue engineering scaffolds and drug delivery systems.⁵ Importantly, polycaprolactone (PCL), polylactide (PLA), polyglycolide (PGA) and their copolymers (poly(lactide-*co*-glycolide), PLGA) have gained Food and Drug Administration (FDA) approval for use in humans as a result of their biocompatibility and biodegradability.^{6,7} Other degradable polymers rapidly emerged as promising candidates such as synthetic polypeptides, polyanhydrides, poly(alkyl cyanoacrylates), poly(ortho esters), polyamides, etc.⁸

Vinyl polymers are very attractive materials and present numerous benefits compared to traditional polyesters owing to their ease of synthesis and their broad diversity of architectures, compositions and functionalities. For instance, these features have enabled the design of highly sophisticated and innovative polymer-protein/peptide bioconjugates or nanocarriers for drug delivery. These achievements were made possible in particular since the advent of reversible deactivation radical polymerization (RDRP) techniques, such as nitroxide mediated polymerization (NMP),⁹ atom-transfer radical polymerization (ATRP)¹⁰ and reversible addition-fragmentation chain transfer polymerization (RAFT).¹¹ However, given their carbon-carbon backbones, they are extremely resistant to degradation and this property strongly limits their application in the biomedical field because potential bioaccumulation in the organism may cause toxicity. This is unfortunate in regards to the massive amount of work devoted to vinyl polymer-based systems intended for biomedical applications.

This critical situation and the general need for more environmentally friendly plastic materials further stimulated the development of degradable vinyl polymers. Among the different strategies, radical ring-opening polymerization (rROP) represents one of the most promising approaches because it combines the advantages of a radical mechanism, thus being fully compatible with free-radical polymerization and RDRP methods, and it enables insertion of labile groups (e.g., ester, disulfide, etc.) in the polymer backbone to ensure degradation.¹² Different classes of cyclic monomers undergoing a radical ring-opening mechanism have been developed and among them, cyclic ketene acetals^{13, 14, 15} originally developed by Bailey in the 80's, are perhaps the most used monomers for rROP. Interestingly, CKA can be copolymerized with certain traditional vinyl monomers, mainly (meth)acrylic esters and vinyl acetate,¹⁶⁻²³ allowing for tunable insertion of ester groups in the resulting copolymers. For instance, a variety of different copolymers based on 2-methylene-1,3-dioxepane (MDO) or 5,6-benzo-2-methylene-1,3-dioxepane (BMDO), which represent the two main CKA used in the literature, have been reported for potential applications in drug delivery, tissue engineering, hydrophobic coatings, or as other kinds of structural biomaterials.

Recently, our group revisited the use of 2-methylene-4-phenyl-1,3-dioxolane (MPDL) by optimizing its synthesis²⁴ and using it as a comonomer during the NMP of either OEGMA²⁵ or MMA²⁴ to make degradable PEG-based or PMMA-rich materials, respectively (Figure 1). Even though NMP of methacrylic esters is known to be relatively difficult to achieve, the styrene-like open radical structure of MPDL allowed good control and high living chain fractions to be achieved during its copolymerization with methacrylic esters by acting as a so-called 'controlling' comonomer. Interestingly, conversely to the use of BMDO or MDO under identical experimental conditions, MPDL enabled high monomer conversions to be reached and tunable insertion in the copolymers, thus leading to adjustable degradation; from moderate to nearly complete. Also, neither the resulting P(OEGMA-*co*-MPDL) copolymers nor their degradation products were cytotoxic up to high concentration on three representative cell lines. As for P(MMA-*co*-MPDL) copolymers, insertion of MPDL only moderately affected the glass transition temperature compared to pure PMMA, while giving low molar mass degradation products after hydrolysis.

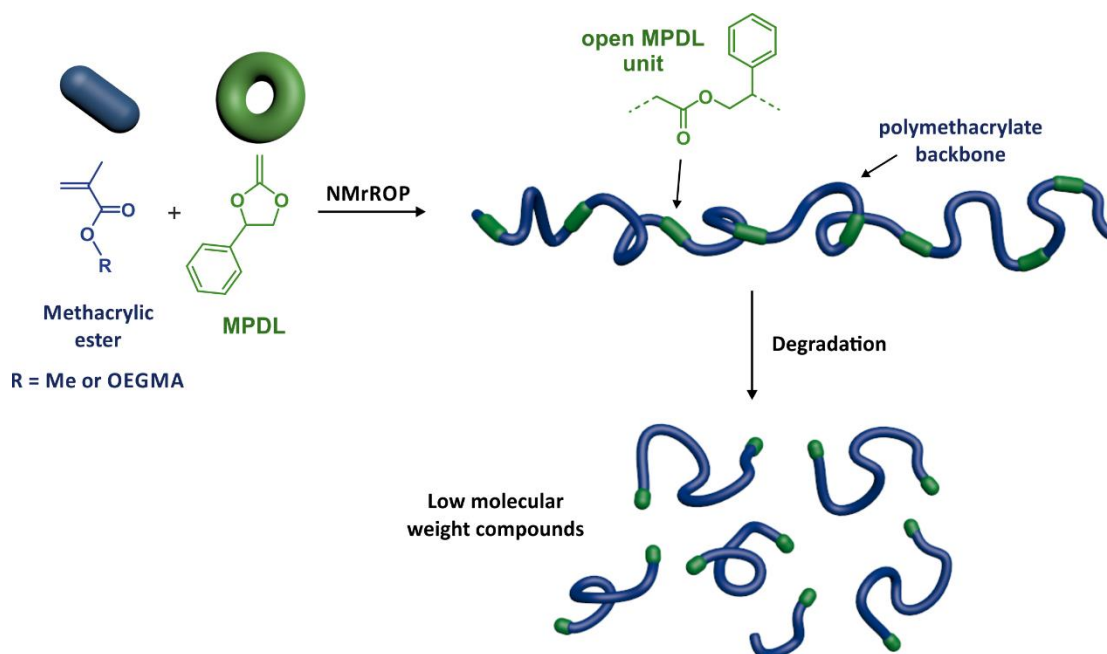


Figure 1. Synthesis of degradable copolymers by nitroxide-mediated radical ring-opening copolymerization (NMrROP) between methacrylic esters and 2-methylene-4-phenyl-1,3-dioxolane (MPDL) as ester bound precursor in the copolymer backbone.

In these studies, copolymer degradation was performed under accelerated conditions to probe the presence of open CKA units; in aqueous 5% KOH for OEGMA-based copolymers and in THF/MeOH solution with 5% KOH for MMA-based counterparts. Degradation kinetics were rapid (from minutes to hours) and allowed to confirm the presence of labile groups in the copolymer backbones. However, even though these harsh degradation conditions are usually used for such a purpose, they do not reflect the physiological conditions and are thus poorly predictive of the materials fate in a biological environment. Also, to the best of our knowledge, degradation of CKA-based materials under physiological conditions have never been benchmarked with traditional aliphatic polyesters such as PLGA, PLA and PCL, which still represent gold standards in terms of degradable polymers for biomedical applications. Only degradation in the presence of enzymes are sometimes reported. This missing information is crucial for designing the right materials having the degradation pattern that match with the target application.

Herein, we performed a comprehensive degradation study of two distinct libraries of CKA-containing copolymers, namely hydrophilic P(OEGMA-*co*-MPDL) and hydrophobic P(MMA-*co*-MPDL), under conditions mimicking the physiological environment (Figure 2). In particular, we simultaneously investigated: (i) the long term hydrolytic degradation in PBS

at different pH; (ii) the physical erosion of thick and thin polymer films and (iii) the enzymatic degradation. A point-by-point comparison under identical conditions was also performed with the three representative aliphatic polyesters (i.e., PLGA, PLA and PCL, Figure 2), allowing the different materials to be compared and some preliminary structure-degradation relationships to be established.

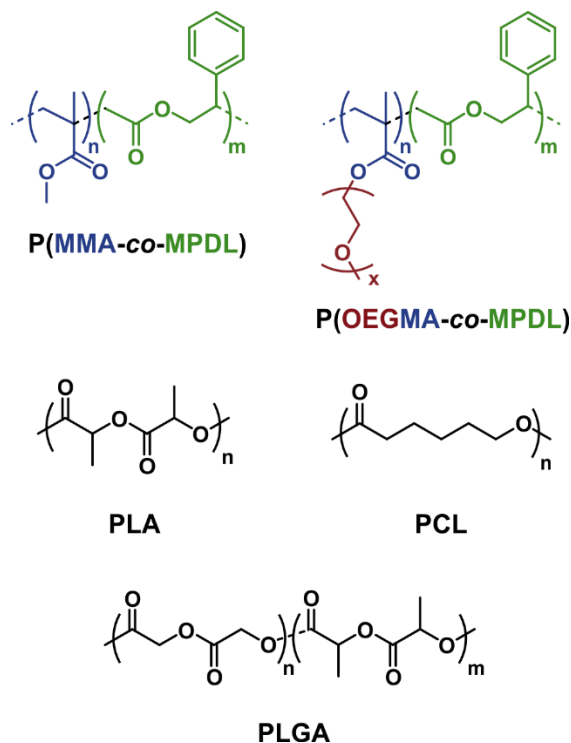


Figure 2. Chemical structure of the different polyesters employed in this study: poly[(methyl methacrylate)-*co*-(2-methylene-4-phenyl-1,3-dioxolane)] (P(MMA-*co*-MPDL)), poly[(oligo(ethylene glycol) methyl ether methacrylate)-*co*-(2-methylene-4-phenyl-1,3-dioxolane)] (P(OEGMA-*co*-MPDL)), poly(D,L-lactide-*co*-glycolide) (PLGA), poly(D,L-lactide) (PLA) and polycaprolactone (PCL).

II. Experimental part

a. Materials

Oligo(ethylene glycol) methyl ether methacrylate (OEGMA, $M_n = 300 \text{ g}\cdot\text{mol}^{-1}$), styrene (S, 99%), methyl methacrylate (MMA, 99%), anhydrous toluene (99.8%), lipase B from *Candida Antartica* immobilized on imobead (4019 U/g) were purchased from Sigma-Aldrich and used as received (except for MMA which was distilled under reduced pressure). BlocBuilder™ alkoxyamine and the SG1 nitroxide were kindly provided by Arkema.

Poly(D,L-lactide-*co*-glycolide) (Resomer[®] RG 503, lactide:glycolide 50:50, ester terminated, $M_w = 24\ 000\text{--}38\ 000\ \text{g}\cdot\text{mol}^{-1}$), poly(D,L-lactide) (Resomer[®] R 203 S, ester terminated, $M_w = 18\ 000\text{--}28\ 000\ \text{g}\cdot\text{mol}^{-1}$) and polycaprolactone (average $M_n = 45\ 000\ \text{g}\cdot\text{mol}^{-1}$) were obtained from Sigma-Aldrich. 2-Methylene-4-phenyl-1,3-dioxolane (MPDL) monomer was prepared according to a previously published method.²⁴ All other materials were purchased from Sigma-Aldrich at the highest available purity and used as received. Phosphate buffer saline (PBS 0.1 M, with 0.9 % NaCl and 0.02 % NaN₃, pH 7.4) and acetate buffer (0.1 M, with .02 % NaN₃, pH 5.5) were prepared in the lab. Deuterated chloroform (CDCl₃) was obtained from Eurisotop. All other solvents were purchased from Carlo-Erba.

b. Analytical methods

Nuclear Magnetic Resonance Spectroscopy (NMR). NMR spectroscopy was performed in 5 mm diameter tubes in CDCl₃ at 25 °C. ¹H spectroscopy was performed on a Bruker Avance 300 spectrometer at 300 MHz. The chemical shift scale was calibrated on the basis of the internal solvent signals.

Size exclusion chromatography (SEC). SEC was performed at 30 °C with two columns from Polymer Laboratories (PL-gel MIXED-D; 300 × 7.5 mm; bead diameter, 5 μm; linear part, 400–400 000 g·mol⁻¹) and a differential refractive index detector (Spectrasystem RI-150 from Thermo Electron Corp.), using chloroform as eluent, at a flow rate of 1 mL·min⁻¹, and toluene as a flow-rate marker. The conventional calibration curve was based on poly(methyl methacrylate) (PMMA) standards (peak molar masses, $M_p = 625\text{--}625\ 500\ \text{g}\cdot\text{mol}^{-1}$) or polystyrene²⁶ standards ($M_p = 162\text{--}523\ 000\ \text{g}\cdot\text{mol}^{-1}$) from Polymer Laboratories. This technique allowed M_n (number-average molar mass), M_w (weight-average molar mass), and M_w/M_n (dispersity, D) to be determined.

Atomic force microscopy (AFM). AFM experiments were performed using the Nanowizard 3 Ultra Speed from JPK Instruments (Berlin, Germany, www.jpk.com), installed on an air-buffered table coupled to a dynamic anti-vibration device, and enclosed in an acoustic box. Imaging of the polymer thin film surface morphology was performed in air in AC or HyperDrive[®] mode, with gold-coated silicon cantilevers PPP-NCHAuD of $30 \pm 10\ \text{N}\cdot\text{m}^{-1}$ spring constant and $290 \pm 5\ \text{kHz}$ resonance frequency (Nanosensors, Neuchatel, Switzerland). The pyramid-shaped tips had a radius of curvature less than 10 nm. A free amplitude oscillation of 15 nm (1 nm) was chosen in AC mode (in HyperDrive mode) allowing the best

resolution of the imaged surface. In AC mode, setpoints ranging between 50% and 80% of the free amplitude were used depending on the polymer surface. Images were taken at scan rates of 1 or 2 Hz. Image processing (flatten, plane fit, edge and hole detection) was performed with the JPK Data Processing software (JPK Instruments). At least three different areas of each sample were scanned and typical images were presented. Average values of height and lateral dimensions of surface features were determined with all pictures.

Scanning electron microscopy²⁷. Scanning Electron Microscopy²⁷ was performed using a MERLIN microscope (Carl Zeiss) and operating at 3 kV with a filament current of about 0.5 mA. Liquid samples were deposited on a carbon conductive double-sided tape (Euromedex, France). They were coated with a palladium-platinum layer of about 3 nm using a Cressington sputter-coater 208HR with a rotary-planetary-tilt stage, equipped with a MTM-20 thickness controller.

c. Polymer synthesis

Synthesis of poly[(methyl methacrylate)-*co*-(styrene)] (P(MMA-*co*-S), P1). In a 20 mL vial, fitted with a rubber septum and a magnetic bar, a mixture of MMA (12.00 g, 1.20×10^{-1} mol), S (1.235 g, 1.19×10^{-2} mol) and the BlocBuilder alkoxyamine initiator (0.084 g, 2.20×10^{-4} mol) and free SG1 (0.002 g, 5.85×10^{-6} mol) was deoxygenated under stirring by nitrogen bubbling for 15 min at room temperature. The mixture was then immersed in a preheated oil bath at 90 °C, corresponding to the time zero of the reaction. After 2 h, the polymerization was stopped by cooling down to ambient temperature. The MMA conversion was calculated by ¹H NMR spectroscopy and the macromolecular characteristics of the copolymer (M_n and Đ) were determined by SEC (using a calibration based on PMMA standards). The copolymer was then precipitated once in cold MeOH and dried under high vacuum until constant weight.

Synthesis of poly[(methyl methacrylate)-*co*-(2-methylene-4-phenyl-1,3-dioxolane)] (P(MMA-*co*-MPDL), P2–P4). A typical solution copolymerization procedure (P2) is as follows. In a 40 mL vial, fitted with a rubber septum and a magnetic bar, a mixture of MMA (12.100 g, 1.21×10^{-1} mol), MPDL (4.900 g, 3.02×10^{-2} mol), the BlocBuilder alkoxyamine initiator (0.061 g, 1.60×10^{-4} mol) and anhydrous toluene (17.0 g, 19.61 mL) was deoxygenated under stirring by nitrogen bubbling for 15 min at room temperature. The mixture was then immersed in a preheated oil bath at 90 °C, corresponding to the time zero of the reaction. After 8 h, the polymerization was stopped by cooling down to ambient

temperature. The MMA conversion was calculated by ^1H NMR spectroscopy and the macromolecular characteristics of the copolymer (M_n and Đ) were determined by SEC (using a calibration based on PMMA standards). The copolymer was then precipitated once in cold MeOH and dried under high vacuum until constant weight. The same procedure was followed by adapting the amount of reactants for **P3** [MMA (8.652 g, 8.65×10^{-2} mol), MPDL (9.348 g, 5.77×10^{-2} mol), BlocBuilder alkoxyamine initiator (0.0414 g, 1.09×10^{-4} mol)] and **P4** [MMA (3.766 g, 3.77×10^{-2} mol), MPDL (14.234 g, 8.79×10^{-2} mol), BlocBuilder alkoxyamine initiator (0.020 g, 5.35×10^{-5} mol)]. Final compositions of the copolymers were determined by comparing the methyl protons in α -position to the ester group of MMA (at 3.7 ppm) to the aromatic protons of MPDL (at 7.2 ppm).

Synthesis of poly[(oligo(ethylene glycol) methyl ether methacrylate)-*co*-(styrene)] (P(OEGMA-*co*-S), P5). In a 20 mL vial, fitted with a rubber septum and a magnetic bar, a mixture of OEGMA (6.000 g, 2.00×10^{-2} mol), S (0.206 g, 1.98×10^{-3} mol), the BlocBuilder alkoxyamine initiator (0.024 g, 6.23×10^{-5} mol) and free SG1 (0.002 g, 5.85×10^{-6} mol) was deoxygenated under stirring by nitrogen bubbling for 15 min at room temperature. The mixture was then immersed in a preheated oil bath at 90 °C, corresponding to the time zero of the reaction. After 30 min, polymerization was stopped by cooling down to ambient temperature. The OEGMA conversion was calculated by ^1H NMR spectroscopy and the macromolecular characteristics of the copolymer (M_n and Đ) were determined by SEC (using a calibration based on PMMA standards). The copolymer was then precipitated once in a mixture of cold cyclohexane/petroleum ether (1/1, v/v) and dried under high vacuum until constant weight.

Synthesis of poly[(oligo(ethylene glycol) methyl ether methacrylate)-*co*-(2-methylene-4-phenyl-1,3-dioxolane)] (P(OEGMA-*co*-MPDL), P6–P8). A typical solution copolymerization procedure (**P6**) is as follows. In a 20 mL vial, fitted with a rubber septum and a magnetic bar, a mixture of OEGMA (2.643 g, 8.81×10^{-3} mol), MPDL (0.357 g, 2.20×10^{-3} mol), the BlocBuilder alkoxyamine initiator (0.014 g, 3.78×10^{-5} mol) and anhydrous toluene (3.0 g, 3.46 mL) was deoxygenated under stirring by nitrogen bubbling for 15 min at room temperature. The mixture was then immersed in a preheated oil bath at 90 °C, corresponding to the time zero of the reaction. After 8 h, the polymerization was stopped by cooling down to ambient temperature. The OEGMA conversion was calculated by ^1H NMR spectroscopy and the macromolecular characteristics of the copolymer (M_n and Đ) were determined by SEC (using a calibration based on PMMA standards). The copolymer was then precipitated once in a mixture of cold cyclohexane/petroleum ether (1/1, v/v) and dried under

high vacuum until constant weight. The same procedure was followed by adapting the amount of the reactants for **P7** [OEGMA (2.206 g, 7.35×10^{-3} mol), MPDL (0.794 g, 4.90×10^{-3} mol), BlocBuilder alkoxyamine initiator (0.012 g, 3.10×10^{-5} mol)] and **P8** [OEGMA (1.328 g, 4.43×10^{-3} mol), MPDL (1.673 g, 1.03×10^{-3} mol), BlocBuilder alkoxyamine initiator (0.0085 g, 2.20×10^{-5} mol)]. Final compositions of the copolymers were determined by comparing the terminal methoxy protons of OEG (at 3.4 ppm) to the ester group of MMA (at 3.7 ppm) to the aromatic protons of MPDL (at 7.2 ppm).

d. Degradation experiments

All the degradation experiments were performed in an orbital shaker (IKA KS4000i control) oven set at 150 rpm and 37 °C.

Long-term hydrolytic degradation in PBS. 200 mg of copolymer was poured into 20 mL of PBS and mechanically stirred in an orbital shaker thermostated at 37 °C. Aliquots of 2 mL were withdrawn at different intervals (i.e., 4, 6 and 12 months) and lyophilized. 2 mL of chloroform were then added, allowing removal of buffer salts by filtration. Finally, the solvent was removed under reduced pressure and the degradation products were analyzed by SEC.

Hydrolytic degradation of thick polymer films. Films of ~1 mm thickness, 150 mg in mass and 1 cm² surface area were prepared using a solvent casting method. The copolymer was solubilized in chloroform at a concentration of 200 mg.mL⁻¹. 0.75 mL of copolymer solution was poured into plastic mold of 1 cm². The mold was covered with aluminum foil and the solvent was slowly evaporated in air at room temperature for 3 days to prevent bubble formation. The resulting copolymer film was then further dried under high vacuum for one day to evaporate remaining solvent. After weighing, films were placed in individual vials containing 10 mL of PBS and mechanically stirred in an orbital shaker thermostated at 37 °C. Films were withdrawn at different intervals (i.e., 4, 6, 12 and 18 months). Water uptake and mass loss were evaluated by weighing using the following equation: water uptake = $\frac{m_0 - m_w}{m_0}$ where m_0 and m_w are the initial mass and the mass of the wet film after degradation (quickly wiped with paper), respectively and masse loss = $\frac{m_0 - m_d}{m_0}$ where m_d is the mass of the dried film after degradation.

Hydrolytic degradation of thin polymer films. Thin films of 10 mg in mass and ~0.5 mm² surface area were prepared using a solvent casting method. The copolymer was solubilized in

chloroform, with a concentration of 200 mg.mL⁻¹. 50 µL were dropped on a mica slide. The films were covered with aluminum foil and the solvent was evaporated slowly in air at room temperature for 2 days to prevent bubbles formation. The resulting (co)polymer film was then annealed above the melting temperature of each (co)polymer; that is at 180 °C, 115 °C and 80 °C for PMMA-based, PLA/PLGA and PCL films, respectively. When the annealing temperature was reached, thin films were dried under vacuum for 20 h. Films were then placed in 10 mL of PBS and mechanically stirred in an orbital shaker thermostated at 37 °C. After selected intervals (i.e., 1, 6 and 12 months), films were withdrawn. Before imaging by SEM and AFM, they were washed with distilled water to remove salts that may be responsible for low image quality.

Enzymatic degradation. Copolymers were poured in PBS at a concentration of 0.5 mg.mL⁻¹ by the nanoprecipitation technique. 50 mg of copolymer were solubilized in 2.5 mL of THF and added dropwise to 10 mL of PBS. THF was evaporated and lipase from *Candida Antartica* (100 U.mL⁻¹) was added to the mixture (250 mg). After one week of incubation under stirring at 40 °C, the mixture was lyophilized and 2 mL of chloroform were added allowing removal of buffer salts by filtration. The degradation products were then analyzed by SEC.

e. Intravenous injections and preliminary toxicity to mice

Six-to-eight-week-old female athymic nude mice were purchased from Harlan Laboratory. All animals were housed in appropriate animal care facilities during the experimental period and handled according to the principles of laboratory animal care and legislation in force in France (authorization No. 03803.02). Mice (~20 g) were randomly divided into 7 groups of 5 mice and each group received a single injection in the tail vein with either copolymers (**P7** and **P8**) with concentrations from 0.8 to 2.4 g.kg⁻¹ or PBS as control. The injected volume was 10 µL per gram of body weight. Mice were regularly monitored for changes in weight and behavior, and were humanely sacrificed 20 days after the injection.

III. Results and Discussion

a. Synthesis and characterization of degradable copolymers

Two libraries of degradable copolymers with targeted M_n of $\sim 25\,000$ – $35\,000\text{ g}\cdot\text{mol}^{-1}$ and comprising variable amounts of MPDL units were prepared by NMrROP. Copolymerizations between MPDL and MMA (**P1–P4**) or OEGMA (**P5–P8**) were initiated by the BlocBuilder alkoxyamine to yield either degradable hydrophobic or hydrophilic copolymers, respectively (Figure 3, Table 1). For both libraries, the initial molar fraction of MPDL, $f_{\text{MPDL},0}$, was varied from 0.2 to 0.7 to adjust the amount of MPDL inserted in the copolymer and therefore its degree of degradation. Copolymers without MPDL were also synthesized by using styrene (S) as a ‘controlling’ comonomer, given the structural similarity of the styrenic radical with the open radical structure of MPDL (**P1** and **P5**).

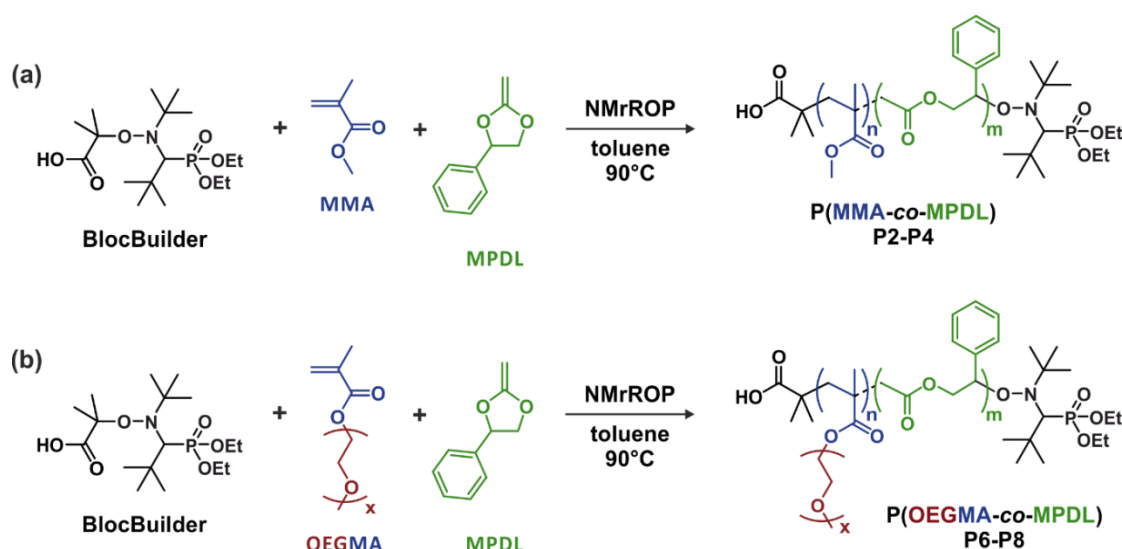


Figure 3. Synthesis of (a) poly[(methyl methacrylate)-*co*-(2-methylene-4-phenyl-1,3-dioxolane)] (P(MMA-*co*-MPDL)) and (b) poly[(oligo(ethylene glycol) methyl ether methacrylate)-*co*-(2-methylene-4-phenyl-1,3-dioxolane)] (P(OEGMA-*co*-MPDL)) by nitroxide-mediated radical ring-opening copolymerization (NMrROP) of MMA (or OEGMA) and MPDL.

Table 1. Experimental Conditions and Macromolecular Characteristics of the Degradable Copolymers Used In This Study.

Expt.	Methacrylic ester	$f_{\text{MPDL},0}$	Conv. ^a (%) / time (h)	M_n^b (g/mol)	\bar{D}^b	F_{MPDL}^c
P1	MMA	0	40 / 2.5	32 500	1.19	0
P2	MMA	0.2	25 / 8	30 500	1.62	0.08
P3	MMA	0.4	35 / 8	32 600	1.55	0.12
P4	MMA	0.7	35 / 8	35 000	1.32	0.27

P5	OEGMA	0	29 / 0.5	22 900	1.24	0
P6	OEGMA	0.2	42 / 8	31 600	1.35	0.09
P7	OEGMA	0.4	46 / 8	33 100	1.32	0.15
P8	OEGMA	0.7	36 / 8	28 300	1.19	0.27

^aMethacrylic ester conversion determined by ¹H NMR spectroscopy. ^bDetermined by SEC after purification. ^cDetermined by ¹H NMR spectroscopy.

Because MPDL acts as a ‘controlling’ comonomer during the NMP of methacrylic esters, the higher $f_{\text{MPDL},0}$, the better the control of the copolymerization (Table 1). P(MMA-*co*-MPDL) copolymers exhibited decreasing dispersities from 1.62 to 1.32 by gradually increasing the initial amount of MPDL from 0.2 to 0.7. A similar trend was observed with P(OEGMA-*co*-MPDL) copolymers whose dispersities ranged from 1.35 to 1.19 under identical experimental conditions. Both series of copolymers were also in the good targeted range of M_n .

The molar fraction of MPDL inserted in the copolymers was determined by ¹H NMR spectroscopy. Because of unfavorable reactivity ratios of MPDL/MMA ($r_{\text{MPDL}} = 0.01$ and $r_{\text{MMA}} = 4.0^{24}$) and MPDL/OEGMA ($r_{\text{MPDL}} = 0$ and $r_{\text{OEGMA}} = 6.95^{25}$) monomer pairs, the final amounts of MPDL in the copolymers, F_{MPDL} , were significantly lower than the initial amounts of MPDL in the comonomer feed. However, it was still possible to fine-tune F_{MPDL} by varying $f_{\text{MPDL},0}$. It led, on average, to copolymers containing ~8% (**P2** and **P6**), ~14% (**P3** and **P7**) and ~27% (**P4** and **P8**) for $f_{\text{MPDL},0} = 0.2, 0.4$ and 0.7 , respectively (Table 1). As for control P(MMA-*co*-S) **P1** and P(OEGMA-*co*-S) **P5** copolymers without MPDL, they were nicely controlled with low dispersities (1.19 and 1.24, respectively).

b. Long-term hydrolytic degradation in PBS

Long-term hydrolytic degradation of the different copolymers was first investigated in PBS (100 mM, pH 7.4) at 37 °C to mimic physiological conditions. All copolymers were poured in PBS and incubated under orbital-shaking at 150 rpm and thermostated at 37°C. MMA-based copolymers and traditional aliphatic polyesters were insoluble in water and thus dispersed in PBS whereas OEGMA-based copolymers were soluble in water (Figure S1). The evolution of the M_n was monitored by SEC for 12 months by withdrawing samples at different intervals (i.e., 4, 6 and 12 months).

Degradation of P(MMA-*co*-MPDL) was very slow and led to a decrease in M_n of ~20 % after 12 months (Figure 4a and S2). Conversely to our expectations, no effect of the MPDL content was noticed on the degradation. It was indeed anticipated that increasing the MPDL content would have resulted in an increase of the degradation. Despite constant stirring by

orbital shaking, P(MMA-*co*-MPDL) copolymers poorly dispersed in water, leaving a persistent insoluble fraction at the water/air interface even after 12 months (Figure S1c). Conversely, P(OEGMA-*co*-MPDL) led to significant hydrolytic degradation under identical experimental conditions (Figure 4b and S3). The decrease in M_n was governed by the MPDL fraction in the copolymer; the higher F_{MPDL} , the more significant the degradation. After 12 months, the M_n decrease indeed reached -38, -55 and -72 % for $F_{\text{MPDL}} = 0.09, 0.15$ and 0.27 , respectively.

The different degradation patterns of P(MMA-*co*-MPDL) and P(OEGMA-*co*-MPDL) copolymers can be explained by their different solubility in water. Whereas water-solubility of P(OEGMA-*co*-MPDL) is ensured by its OEG side chains, thus allowing water molecules to access to the ester groups in the main chain and cause degradation, P(MMA-*co*-MPDL) is too hydrophobic and exhibited poor water uptake that prevented significant degradation. This aspect will be further discussed in the *Hydrolytic degradation of polymer films* section. Both control copolymers **P1** and **P5** led to minimal degradation (~14 %) after 12 months, presumably because of partial hydrolysis of MMA and OEGMA units, respectively. Either hydrolysis is significant and the decrease in M_n is caused by loss of multiple methyl or OEG groups, or it is marginal but the few resulting carboxylic acid groups lead to interaction with SEC columns, thus affecting the retention time.²⁸ This last hypothesis seems predominant since ¹H NMR spectra of P(MMA-*co*-MPDL) and P(OEGMA-*co*-MPDL) did not show any noticeable change of integration for the signals of the methyl/methylene hydrogens in the α -position to the ester bond.

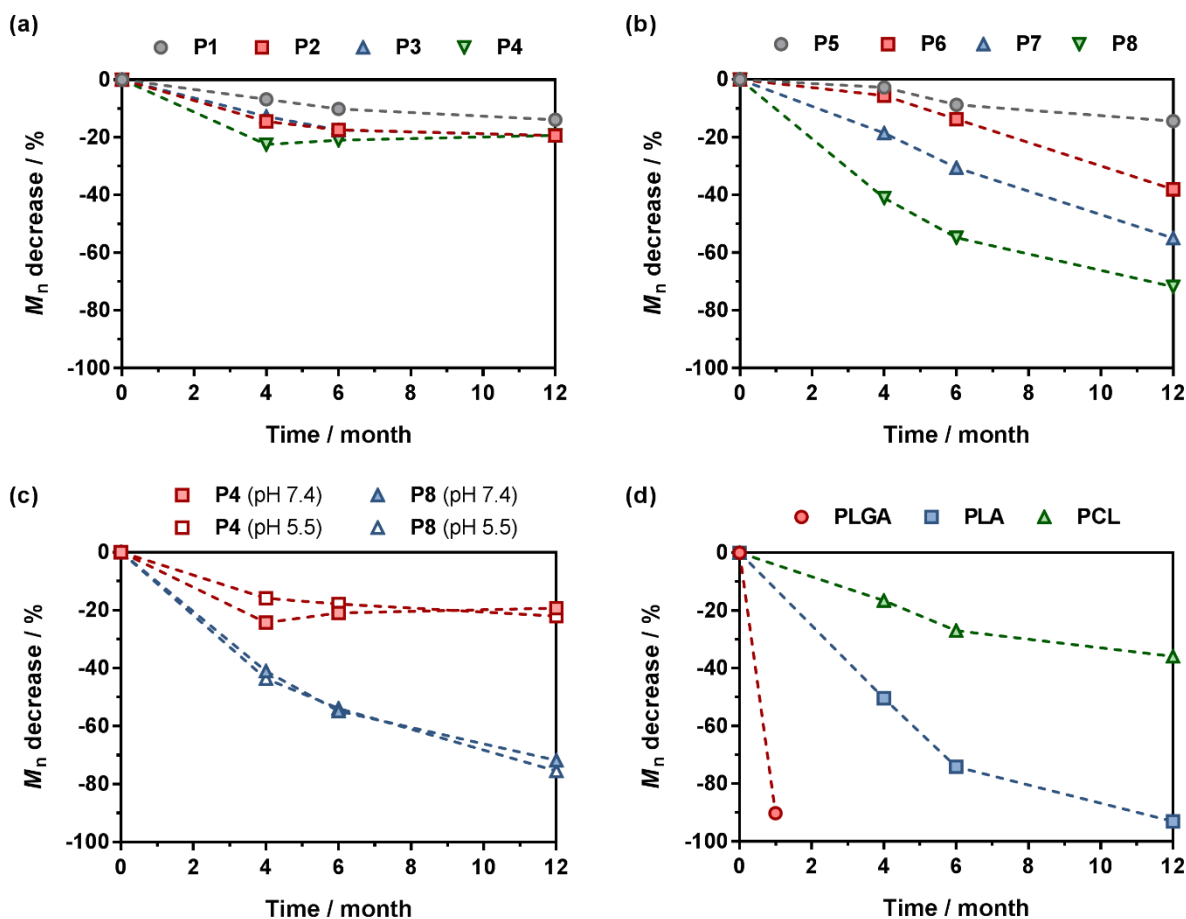


Figure 4. Evolution of the number-average molar mass, M_n , with time of the different copolymers during the hydrolytic degradation in PBS at 37 °C. (a) P(MMA-*co*-MPDL): P1 ($F_{MPDL} = 0$); P2 ($F_{MPDL} = 0.08$); P3 ($F_{MPDL} = 0.12$); P4 ($F_{MPDL} = 0.27$). (b) P(OEGMA-*co*-MPDL): P5 ($F_{MPDL} = 0$); P6 ($F_{MPDL} = 0.09$); P7 ($F_{MPDL} = 0.15$); P8 ($F_{MPDL} = 0.27$). (c) Influence of the pH: P4 (pH 7.4 or 5.5); P8 (pH 7.4 or 5.5). (d) Aliphatic polyesters (pH 7.4).

Evolution with time of the M_n of P(OEGMA-*co*-MPDL), and in particular of the slope of the curves, suggested that even though hydrolytic degradation did not reach completion after 12 months, lower M_n will likely be obtained if the degradation is prolonged for a longer period of time (Figure 4b). However, the final theoretical M_n after complete degradation can be estimated from the final composition of the copolymers, providing nearly statistical incorporation of MPDL all along the copolymer chain. Given the unfavorable reactivity ratio of MPDL, it was assumed that the number of consecutive MPDL units was negligible. Thus, the average number of OEGMA units between two MPDL units was calculated according to $1/F_{MPDL} - 1$ and was equal to 10, 6 and 3 for $F_{MPDL} = 0.09$ (**P6**), 0.15 (**P7**) and 0.27 (**P8**), respectively, corresponding to residual M_n of 3200, 1900 and 1000 g.mol⁻¹.

Influence of pH on degradation was then investigated. One copolymer from each library, **P4** and **P8**, was subjected to degradation in acetate buffer (pH 5.5) for 12 months and the degradation pattern was compared to that obtained in PBS (pH 7.4). However, no noticeable effect was observed on the degradation rate as shown by a nearly perfect overlay of M_n values at each time point (Figure 4c).

A key aspect of the study was whether our materials could be competitive in terms of degradation under physiological conditions, with traditional aliphatic polyesters. The two series of MPDL-containing copolymers were therefore benchmarked with PLGA, PLA and PCL. Identical degradation conditions (PBS, 100 mM, pH 7.4) were applied and evolution of M_n after different periods of time was reported on Figure 4d and S4. As previously reported, degradation of PLGA was the fastest, leading to complete degradation after 1 month.²⁹ As expected, since PLA is more sterically hindered than PLGA, its complete degradation took a longer time, approximately 12 months,³⁰ whereas degradation of PCL was the slowest leading to a decrease in M_n of only 36 % after 12 months.³¹ As for MPDL-containing copolymers, P(MMA-*co*-MPDL) **P2–P4** exhibited slightly slower degradation rates than that of PCL. However, hydrolytic degradation of P(OEGMA-*co*-MPDL) **P6–P8** was comprised between that of PLA and PCL. It is a very important result showing that hydrolytic degradation of properly designed CKA-containing vinyl copolymers can be in the same order of magnitude than degradation of PCL and PLA, which are extensively used FDA-approved biodegradable polymers.

pH was monitored over time during hydrolytic degradation at pH 7.4 of OEGMA-based copolymers **P5–P8**, and of PLGA, PLA and PCL (Figure 5). Hydrolytic degradation of polyester leads to carboxylic acid chain-end frequently associated with a drop in pH.^{32,33} pH of PLGA and PLA dispersions indeed decreased from 7.4 to 5.5 after 1 and 12 months, respectively, which is in good agreement with what is usually observed.^{32,33} This drop in pH may be a strong limitation as it was shown that local acidification produced by the degradation products of PLGA/PLA usually resulted in detrimental local inflammatory response.^{32,33} Because of the minimal degradation of PCL over this period of time, no drop in pH was observed. Remarkably, pH of the different P(OEGMA-*co*-MPDL) solutions was stable and remain > 6.8 even after 1 year, as for P(OEGMA-*co*-S) used as a control copolymer. This high pH stability is very relevant and represents a meaningful advantage compared to aliphatic polyesters as their *in vivo* degradation may not lead to local acidification and probably to local toxicity.

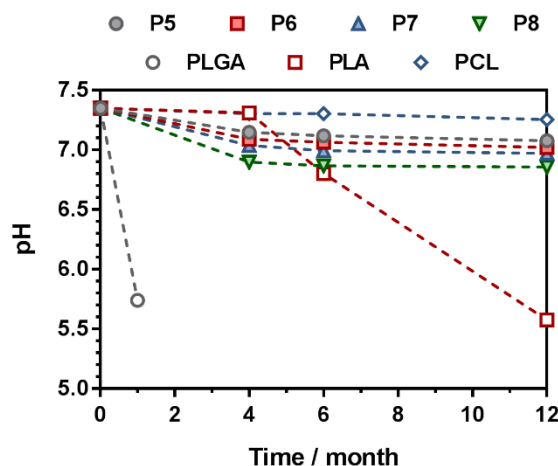


Figure 5. Evolution of pH with time during hydrolytic degradation in PBS (pH 7.4, 37°C) of OEGMA-based copolymers: ●, **P5** ($F_{\text{MPDL}} = 0$); ■, **P6** ($F_{\text{MPDL}} = 0.09$); ▲, **P7** ($F_{\text{MPDL}} = 0.15$); ▼, **P8** ($F_{\text{MPDL}} = 0.27$) and aliphatic polyesters.

c. Hydrolytic degradation of polymer films

Films of approximately 150 mg in mass, 1 mm thickness and 1 cm² surface area (Figure S5) were prepared by the solvent casting method from hydrophobic (co)polymers: P(MMA-*co*-MPDL) **P2–P4**, PLA, PLGA, and PCL. Hydrolytic degradation was carried out in PBS (100 mM, pH 7.4) stirred in an orbital shaker thermostated at 37 °C. Erosion of hydrophobic polymers occurs through surface or bulk erosion^{34,35} and the balance between the kinetics of diffusion of water inside the polymer matrix and the hydrolysis rate of the polymer's labile groups defines the erosion mechanism. If water diffusion is faster than the labile group hydrolysis, the material degrades through bulk erosion. On the contrary, if the chain cleavage is faster than water diffusion, the material undergoes surface erosion. Water uptake and mass loss were monitored for 12 months. In parallel, thin films (~10 mg in mass, 0.5 mm² surface area) were prepared on mica surface for further scanning electron microscopy²⁷ and atomic force microscopy (AFM) observations to gain some insight into the degradation mechanism of our copolymers.

The water uptake ability of thick polymer films was first determined by comparing their weight in wet and dry states (Figure 6a). Water uptake of PLGA and PLA films was fast and reached values as high as ~210 % after 1 month for PLGA and ~500 % after 4 months for PLA. This behavior confirmed that water significantly diffused inside PLGA/PLA matrix, in agreement with their relatively fast degradation rates (Figure 4d). PCL and P(MMA-*co*-

MPDL) **P2–P4** films gave less than 8 % of water uptake. These results were consistent with long-term hydrolytic degradation experiments that showed very slow degradation of dispersed P(MMA-*co*-MPDL) copolymers.

Although the strong hydrophobicity of P(MMA-*co*-MPDL) copolymers may explain their poor water uptake, influence of their glass transition temperature (i.e., segmental mobility) cannot be ruled out. T_{gs} of PLGA and PLA are about 44–48 °C and 48–52 °C, respectively,³⁶ so relatively close to the experimental temperature (37 °C). Therefore, although glassy, polymer chains still have some segmental flexibility, favoring water penetration in the polymer matrix.³⁷ For PCL, the situation was more complicated. Even if its T_g (-60 °C) is significantly lower than the experimental temperature, the crystallinity of the polymer strongly hampered water uptake.³⁸ Conversely, T_{gs} of P(MMA-*co*-MPDL) are equal to 107 °C for **P1**, 100 °C for **P2**, 98 °C for **P3** and 74 °C for **P4**,²⁴ so much higher than those of PLGA and PLA. Consequently, not only P(MMA-*co*-MPDL) copolymers were hydrophobic but also very rigid and highly compact, thus preventing water molecules to extensively diffuse into the polymer matrix to induce degradation.^{37,39}

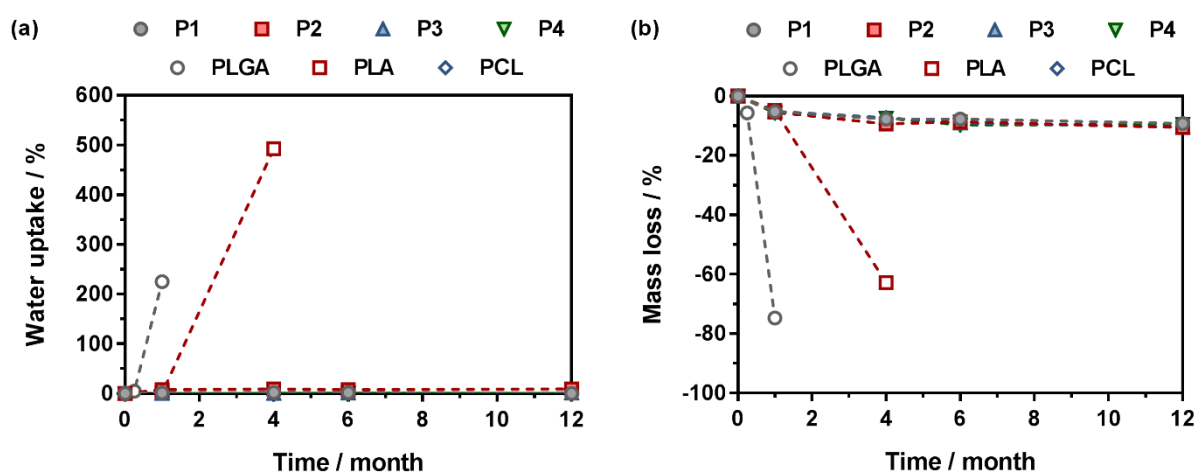


Figure 6. (a) Water uptake and (b) mass low of thick films during hydrolytic degradation in PBS (pH 7.4, 37°C) of MMA-based copolymers: ●, **P1** ($F_{MPDL} = 0$); ■, **P2** ($F_{MPDL} = 0.08$); ▲, **P3** ($F_{MPDL} = 0.12$); ▼, **P4** ($F_{MPDL} = 0.27$) and aliphatic polyesters.

Similarly to water uptake, mass loss of PLGA and PLA thick films in PBS under identical degradation conditions was fast (Figure 6b). PLGA films lost ~75 % of their mass after 1 month and PLA lost ~63 % after 4 months. In contrast, MMA-based copolymers **P2–P4** and PCL had similar behavior, with a mass loss around ~10 % after 12 months. As water hardly

entered into the polymer matrix, only the surface of film was likely subjected to degradation, which left the bulk intact. Photographs of P(MMA-*co*-MPDL) **P4**, PLGA, PLA and PCL films before and after 12 months in PBS (Figure S5) further illustrated the rapid degradation of PLGA and PLA films as opposed to the nearly hydrolytic stability of films from **P4** and PCL. These data supported that P(MMA-*co*-MPDL) and PCL films³⁸ were degraded through a surface erosion mechanism.

SEM (Figure 7) and AFM (height images in Figure 8, cross section in Figure S6 and phase images in Figure S7) were then used to gain insight into surface erosion of thin polymer films from P(MMA-*co*-S) **P1**, P(MMA-*co*-MPDL) **P2–P4**, PLGA, PLA and PCL. Note that all thin film surfaces before hydrolysis (0 month) were not perfectly smooth at the nanometric scale and exhibited either several clusters of a few tens of nanometers high or roughness of the same range. Importantly, as the degree of hydrolysis reached an advanced stage (6 or 12 months), all films underwent drastic changes in their surface morphology with increased roughness or with the apparition of pores. The apparition of a tip effect on pictures was characteristic of degraded surface and mean that transfer of matter from the degraded surface to the AFM tip occurred during imaging. This matter modified the tip geometry and resulted in altered resolution in AFM imaging.

PLGA thin films were totally degraded after 1 month. SEM images showed highly porous micrometric cavities. This micrometric roughness added to a softening of the material prevented us from obtaining AFM pictures of PLGA film surface. For PLA film, erosion was slower and SEM pictures showed a PLA film surface of increasing porosity with time. Several micrometric holes were formed after 1-month hydrolysis, reaching tens of micrometers after 12 months. However, these porous structures were less visible by AFM. After 6 months, surface became rougher and small holes appeared, whereas after 12 months, the morphology of the surface changed drastically and large cavities of 30 nm deep appeared. For PCL, SEM pictures showed numerous holes after 1 month which were turned into large and porous cavities after 12 months. By AFM, the surface of the film before hydrolysis was rough, with a difference in height of 50 nm. After 1 month, the surface seemed to flatten and for the 6-months hydrolysis, larger holes with a depth of 100 nm appeared. The 12 months film was too rough and porous to be observed by AFM with good resolution.

As expected, P(MMA-*co*-S) **P1** did not show drastic modification of morphology. By AFM, clusters seemed to erode with time, although this was less obvious by SEM. AFM observation of the copolymer with the lowest MPDL content (**P2**, $F_{\text{MPDL}} = 0.08$) showed a surface becoming more rugged and the clusters disappeared after 1 month. After 6 months,

porosity started with a depth of 10 to 20 nm and after 12 months, holes became more numerous and their size and deep increased. The AFM pictures after 12 months of hydrolysis showed a drastic change in morphology, associated with advanced hydrolysis of the material. SEM images confirmed the apparition of numerous small holes on the surface of the films. For MPDL molar fraction of 0.12 (**P3**), the material became porous (20 to 40 nm deep) within only 1 month and the size and number of pores increased with time. The modification in morphology characteristic of film erosion was observed by AFM after 12 months. By SEM, many small holes similar to those observed with **P3** were observed and bigger cavities of few micrometers appeared after 6 months. For the highest MPDL content (**P4**, $F_{\text{MPDL}} = 0.27$), several holes appeared on the surface after one month and the change in morphology occurred after only 6 months. After 12 months, large (few hundreds of nm) and deep (few tens nm) holes were observed on the surface by SEM. One can note that in all cases, AFM phase imaging pointed out the softening of the material with time (Figure S7), which became more viscoelastic while hydrolysis proceeded.

Altogether, these data indicated that films composed of P(MMA-*co*-MPDL) undergo surface erosion, similarly to PCL films. Because of the strong hydrophobicity and rigidity of the copolymers, water uptake was rather modest (< 10 %), thus preventing bulk hydrolysis. Although slow, surface erosion was confirmed by both AFM and SEM and the kinetic of porosity formation on the surface of the film was affected by the MPDL content: the higher the MPDL content, the earlier the holes formation.

Chapter 5 – Degradation of Copolymers Prepared by Nitroxide-Mediated Radical Ring-Opening Polymerization and Point-by-Point Comparison with Traditional Polyesters

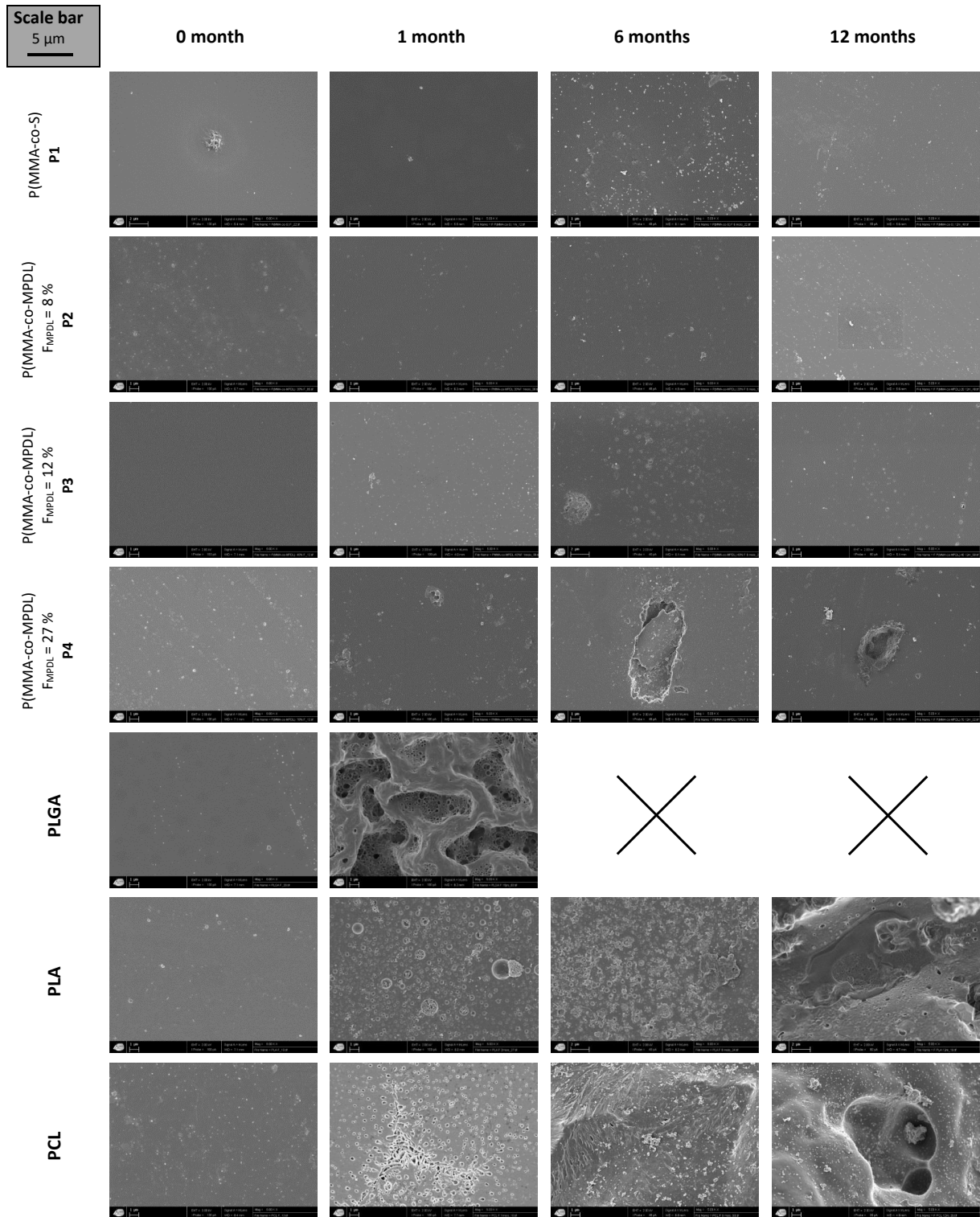


Figure 7. SEM images (Mag = 5 KX) showing the evolution of thin film surfaces of MMA-based copolymers **P1–P4**, PLGA, PLA and PCL during hydrolytic degradation in PBS (100 mM, pH 7.4, 37 °C). The scale is indicated at the top left of the table (black bar).

Chapter 5 – Degradation of Copolymers Prepared by Nitroxide-Mediated Radical Ring-Opening Polymerization and Point-by-Point Comparison with Traditional Polyesters

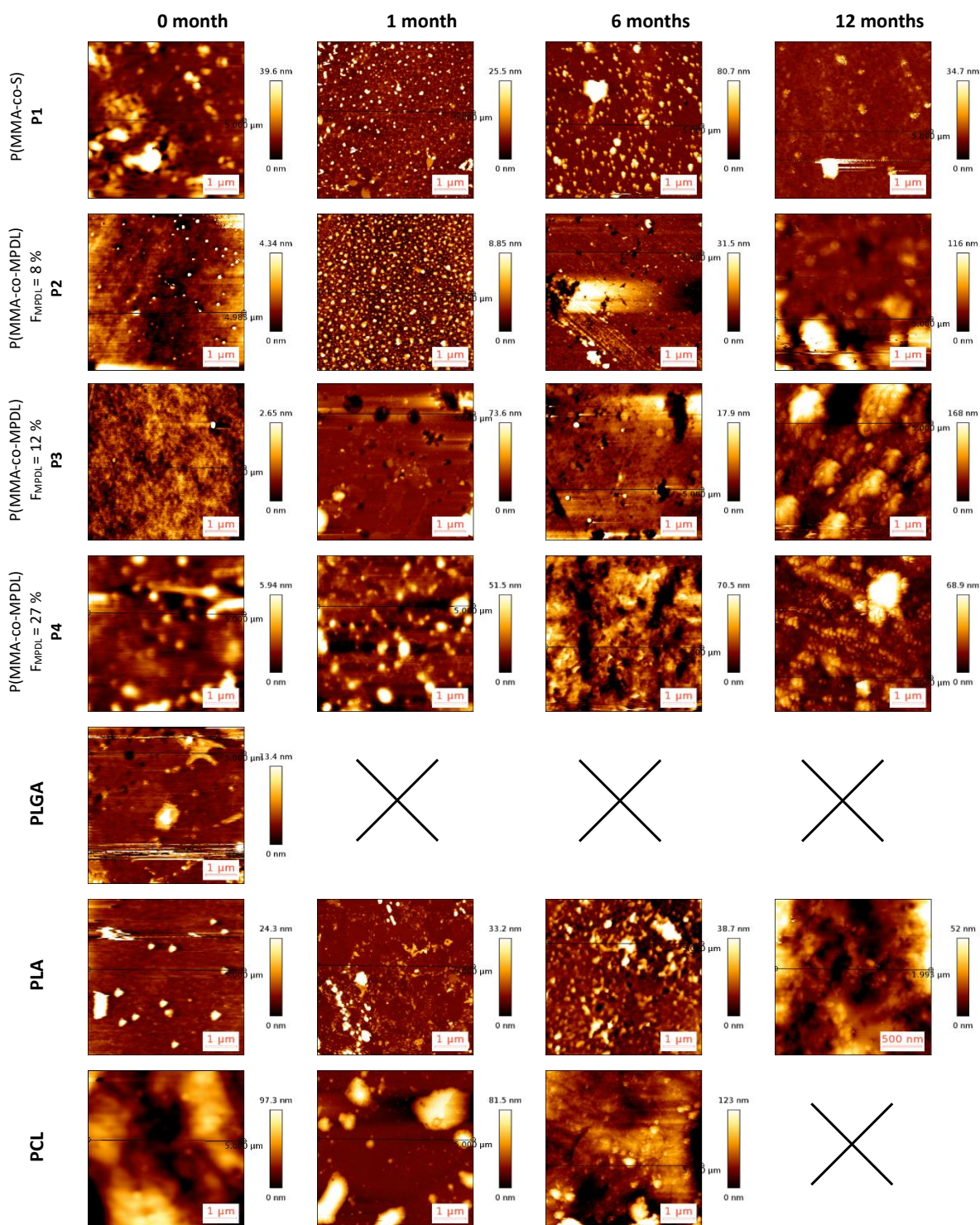


Figure 8. AFM height images obtained in AC mode during hydrolytic degradation in PBS (100 mM, pH 7.4, 37 °C) of MMA-based copolymers **P1–P4**, PLGA, PLA and PCL (5 μm \times 5 μm , except for PLA 12 months, 2 μm \times 2 μm). The scale is indicated on the right side of each image (colored bar).

d. Enzymatic degradation

Hydrolytic degradation is of utmost importance while considering polyester family, as it is considered to be the main degradation mechanism in vivo.⁴⁰ However, enzymatic degradation of P(MMA-*co*-MPDL) and P(OEGMA-*co*-MPDL) copolymers was still attempted to probe their sensitivity to action of lipases, a sub-class of the esterases. Incubation of the different copolymers was performed in PBS at 37 °C for one week in the presence of lipases from *Candida Antartica*, one enzyme already used in the literature for such a purpose.^{17,41,42} Enzymatic cleavage is known to be specific and to catalyze hydrolysis, enzymes need to interact with their substrate (*i.e.*, the ester bond of the polymer).⁴³⁻⁴⁵ Consequently, the affinity between the polymer main chain and the enzyme as well as the environment of the ester bond strongly affect the efficacy of the enzyme.

Negligible degradation was observed with P(MMA-*co*-MPDL) copolymers (**P1–P4**, Table 2), as illustrated by nearly perfect overlay of the SEC chromatograms all along the experiment (Figure S8). Conversely, P(OEGMA-*co*-MPDL) (**P4–P8**) displayed moderate degradation (6–15%) while the control copolymer without MPDL (**P5**) was perfectly inert (Table 2, Figure S9).

Table 2. Evolution Of The Number-Average Molar Mass⁴⁶ Of P(MMA-*co*-MPDL) and P(OEGMA-*co*-MPDL) Copolymers After Enzymatic Degradation.

Expt.	Methacrylic ester	F_{MPDL}^a (mol. %)	M_n decrease ^b (%)
P1	MMA	0	2
P2	MMA	8	3
P3	MMA	12	2
P4	MMA	27	1
P5	OEGMA	0	<1
P6	OEGMA	9	15
P7	OEGMA	15	13
P8	OEGMA	27	6

^aDetermined by ¹H NMR spectroscopy. ^bDetermined by SEC

We assumed that hydrophobicity of the P(MMA-*co*-MPDL) copolymer backbone prevented interaction between the enzyme active site and ester functions, whereas the relatively water-solubility of P(OEGMA-*co*-MPDL) copolymers enabled at least partial enzymatic cleavage. However, we suspected the detrimental influence of hydrophobic MPDL units on enzyme

accessibility to ester moieties as the higher the MPDL content in the copolymer, the lower the M_n decrease: -15 % for **P6** ($F_{\text{MPDL}} = 0.09$), -13 % for **P7** ($F_{\text{MPDL}} = 0.15$) and -6 % for **P8** ($F_{\text{MPDL}} = 0.27$). In addition, high aromatic group contents may result in interaction between aromatic rings (π -stacking) from MPDL units and induce specific conformation of the polymer chains^{47,48} that would further reduce accessibility to ester functions. Also, given PEG is known to induce steric repulsion of proteins, one can question, even though they are relatively small, the adverse effect of OEG side chains on enzyme accessibility to the ester groups. Although enzymatic degradation was modest, it could likely be improved as it has been shown that performing the degradation on a longer timescale (35 days) and replacing the degradation medium every 24 h enabled extensive degradation of MPDL-containing materials.⁴⁹

e. Preliminary in vivo toxicity

Although OEGMA-based materials are considered to be non-toxic and potentially stealth,^{17,50-59} inserting multiple MPDL units group could modify the toxicity of the resulting copolymers. Even though innocuousness of P(OEGMA-*co*-MPDL) copolymers was previously demonstrated on two representative mammalian cell types,²⁵ in vivo toxicity has never been investigated.

P(OEGMA-*co*-MPDL) copolymers containing 15 and 27 % MPDL (**P7** and **P8**, respectively) were injected intravenously (single injection) in mice with concentrations ranging from 0.8 to 2.4 g.kg⁻¹. The body weight and the mice behavior were monitored for 20 days. In all cases, despite a slight weight decrease during the first 6 days (ranging from -0.5 to -5 %), in general for the highest copolymer concentrations, evolution of body weight was nearly constant with time, similarly to untreated mice (Figure 9). Except for **P8** at 0.8 mg.kg⁻¹, the higher the copolymer concentration, the higher the body weight loss. However, no mortality neither noticeable modification in terms of feeding and behavior was observed, suggesting the safety of the treatment.

Interestingly, the median lethal dose (LD₅₀) of traditional hydrophobic polyesters was equal to 0.22 g.kg⁻¹ for PLGA nanoparticles¹³ and 1.47 g.kg⁻¹ for PEG-*b*-PCL nanoparticles⁶⁰ and PEG-*b*-PLA nanoparticles were well tolerated up to 0.44 g.kg⁻¹.⁶¹ Despite the fact that P(OEGMA-*co*-MPDL) copolymers are water-soluble and not under the form of nanoparticles, their innocuousness in vivo, even at high concentration (2.4 g.kg⁻¹), makes them promising building block for the design of biocompatible and biodegradable polymers. Interestingly, in

vivo toxicity of non-degradable, hydrophilic polymers, such as PEG, was also weak and LD₅₀ ranged from 8.6 g.kg⁻¹ for $M_{n,PEG} = 400 \text{ g.mol}^{-1}$ to 16.0 g.kg⁻¹ for $M_{n,PEG} = 4000 \text{ g.mol}^{-1}$.^{62,63}

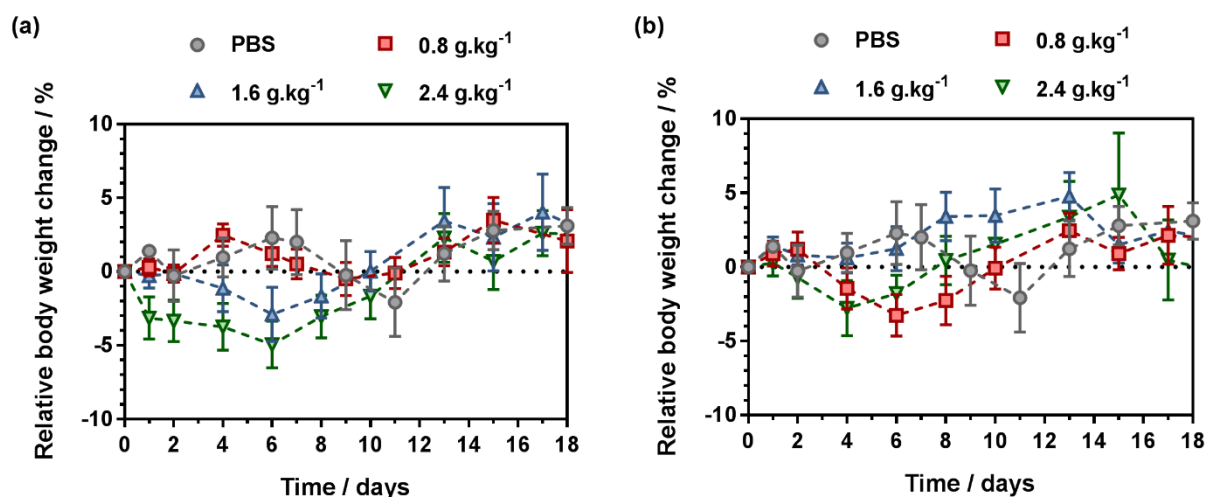


Figure 9. Relative body weight change of mice, as a function of time after intravenous injections of PBS or P(OEGMA-*co*-MPDL) (a) **P7** and (b) **P8**.

IV. Conclusion

Comprehensive degradation study of MPDL-containing polymethacrylates copolymers of opposite solubility (either based on MMA or OEGMA) synthesized by NMrROP, by means of long-term hydrolytic degradation, degradation of thick and thin films together with enzymatic degradation, all achieved in PBS (pH 7.4, 37 °C), was performed and point-by-point comparison with traditional aliphatic polyesters (PLGA, PLA and PCL) was established for benchmarking purposes.

It was shown that P(MMA-*co*-MPDL) copolymers slowly degraded in PBS with degradation kinetics slower than that of PCL. P(MMA-*co*-MPDL) film erosion suggested that combination of copolymer hydrophobicity and rigidity prevented bulk erosion and thus a slow surface erosion was observed by SEM and AFM. As expected, no decrease in M_n was obtained after enzymatic degradation.

Conversely, water-soluble P(OEGMA-*co*-MPDL) copolymers led to significant degradation under long term hydrolysis in PBS. The degradation kinetics was finely tuned by varying the MPDL content, which enabled to obtain degradation performances in between those of PLA and PCL, thus representing an important result. However, P(OEGMA-*co*-MPDL) copolymers were only moderately degraded by enzymes, likely because of a combination between a too high hydrophobicity of MPDL units, potential conformation of the

copolymer chain because of hydrophobic interaction and steric repulsion of OEG side chains, thus preventing optimal cleavage by the enzyme.

On one hand, as they remained rather stable under hydrolytic and enzymatic conditions, P(MMA-*co*-MPDL) copolymers might be well-suited for biomaterials intended for long-term use, such as devices or implants.^{8,64-66} On the other hand, P(OEGMA-*co*-MPDL) demonstrated promising degradation rate under hydrolytic conditions and might thus be envisioned for short- or mid-term applications such as nanoscale drug-delivery systems and meet a need for hydrophilic degradable materials with tunable degradation kinetics.

References

- (1) Benoit, D.; Grimaldi, S.; Robin, S.; Finet, J.-P.; Tordo, P.; Gnanou, Y. *Journal of the American Chemical Society* **2000**, *122*, 5929.
- (2) Gross, R. A.; Kalra, B. *Science* **2002**, *297*, 803.
- (3) Siracusa, V.; Rocculi, P.; Romani, S.; Dalla Rosa, M. *Trends Food Sci. Technol.* **2008**, *19*, 634.
- (4) Tian, H.; Tang, Z.; Zhuang, X.; Chen, X.; Jing, X. *Prog. Polym. Sci.* **2012**, *37*, 237.
- (5) Frazza, E.; Schmitt, E. *J Biomed Mater Res A* **1971**, *5*, 43.
- (6) Nair, L. S.; Laurencin, C. T. *Prog. Polym. Sci.* **2007**, *32*, 762.
- (7) Anderson, J. M.; Shive, M. S. *Adv. Drug Delivery Rev.* **2012**, *64*, 72.
- (8) Ulery, B. D.; Nair, L. S.; Laurencin, C. T. *J. Polym. Sci. Pol. Phys.* **2011**, *49*, 832.
- (9) Tardy, A.; Delplace, V.; Siri, D.; Lefay, C.; Harrisson, S.; Pereira, B. d. F. A.; Charles, L.; Gigmes, D.; Nicolas, J.; Guillauneuf, Y. *Polym. Chem.* **2013**, *4*, 4776.
- (10) Matyjaszewski, K.; Xia, J. *Chem. Rev.* **2001**, *101*, 2921.
- (11) Moad, G.; Rizzardo, E.; Thang, S. H. *Aust. J. Chem.* **2009**, *62*, 1402.
- (12) Tardy, A.; Nicolas, J.; Gigmes, D.; Lefay, C.; Guillauneuf, Y. *Chem. Rev.* **2017**, *117*, 1319.
- (13) Kopčanský, P.; Tomašovičová, N.; Koneracka, M.; Timko, M.; Závašová, V.; Tomčo, L. *Acta Electrotechnica et Informatica* **2010**, *10*, 10.
- (14) Bailey, W. J.; Ni, Z.; Wu, S. R. *J. Polym. Sci. Pol. Chem.* **1982**, *20*, 3021.
- (15) Bailey, W. J.; Ni, Z.; Wu, S. R. *Macromolecules* **1982**, *15*, 711.
- (16) Chung, I. S.; Matyjaszewski, K. *Macromolecules* **2003**, *36*, 2995.
- (17) Lutz, J.-F.; Andrieu, J.; Üzgün, S.; Rudolph, C.; Agarwal, S. *Macromolecules* **2007**, *40*, 8540.
- (18) Agarwal, S.; Ren, L. *Macromolecules* **2009**, *42*, 1574.
- (19) Kobben, S.; Ethirajan, A.; Junkers, T. *Journal of Polymer Science Part A: Polymer Chemistry* **2014**, *52*, 1633.
- (20) Huang, J.; Gil, R.; Matyjaszewski, K. *Polymer* **2005**, *46*, 11698.
- (21) Hedir, G. G.; Bell, C. A.; Jeong, N. S.; Chapman, E.; Collins, I. R.; O'Reilly, R. K.; Dove, A. P. *Macromolecules* **2014**, *47*, 2847.
- (22) Ganda, S.; Jiang, Y.; Thomas, D. S.; Eliezar, J.; Stenzel, M. H. *Macromolecules* **2016**, *49*, 4136.
- (23) d'Ayala, G. G.; Malinconico, M.; Laurienzo, P.; Tardy, A.; Guillauneuf, Y.; Lansalot, M.; D'Agosto, F.; Charleux, B. *Journal of Polymer Science Part A: Polymer Chemistry* **2014**, *52*, 104.
- (24) Tran, J.; Guegain, E.; Ibrahim, N.; Harrisson, S.; Nicolas, J. *Polym. Chem.* **2016**.
- (25) Delplace, V.; Guégain, E.; Harrisson, S.; Gigmes, D.; Guillauneuf, Y.; Nicolas, J. *Chem. Commun.* **2015**, *51*, 12847.
- (26) Deng, L.; Furuta, P. T.; Garon, S.; Li, J.; Kavulak, D.; Thompson, M. E.; Fréchet, J. M. J. *Chemistry of Materials* **2006**, *18*, 386.
- (27) Frisch, M. J.; Trucks, G. W.; Schlegel, H. B.; Scuseria, G. E.; Robb, M. A.; Cheeseman, J. R.; Scalmani, G.; Barone, V.; Mennucci, B.; Petersson, G. A.; Nakatsuji, H.; Caricato, M.; Li, X.; Hratchian, H. P.; Izmaylov, A. F.; Bloino, J.; Zheng, G.; Sonnenberg, J. L.; Hada, M.; Ehara, M.; Toyota, K.; Fukuda, R.; Hasegawa, J.; Ishida, M.; Nakajima, T.; Honda, Y.; Kitao, O.; Nakai, H.; Vreven, T.; Montgomery Jr., J. A.; Peralta, J. E.; Ogliaro, F.; Bearpark, M. J.; Heyd, J.; Brothers, E. N.; Kudin, K. N.; Staroverov, V. N.; Kobayashi, R.; Normand, J.; Raghavachari, K.; Rendell, A. P.; Burant, J. C.; Iyengar, S. S.; Tomasi, J.; Cossi, M.; Rega, N.; Millam, N. J.; Klene, M.; Knox, J. E.; Cross, J. B.; Bakken, V.; Adamo, C.; Jaramillo,

- J.; Gomperts, R.; Stratmann, R. E.; Yazyev, O.; Austin, A. J.; Cammi, R.; Pomelli, C.; Ochterski, J. W.; Martin, R. L.; Morokuma, K.; Zakrzewski, V. G.; Voth, G. A.; Salvador, P.; Dannenberg, J. J.; Dapprich, S.; Daniels, A. D.; Farkas, Ö.; Foresman, J. B.; Ortiz, J. V.; Cioslowski, J.; Fox, D. J.; Gaussian, Inc.: Wallingford, CT, USA, 2009.
- (28) Specht, C. H.; Frimmel, F. H. *Environmental science & technology* **2000**, *34*, 2361.
- (29) Zolnik, B. S.; Burgess, D. J. *J. Control. Rel.* **2007**, *122*, 338.
- (30) Tsuji, H.; Ikarashi, K. *Biomaterials* **2004**, *25*, 5449.
- (31) Castilla-Cortázar, I.; Más-Estellés, J.; Meseguer-Dueñas, J.; Ivirico, J. E.; Marí, B.; Vidaurre, A. *Polym. Degrad. Stab.* **2012**, *97*, 1241.
- (32) Taylor, M.; Daniels, A.; Andriano, K.; Heller, J. *J Appl Biomater* **1994**, *5*, 151.
- (33) Ignatius, A.; Claes, L. E. *Biomaterials* **1996**, *17*, 831.
- (34) Göpferich, A. *Biomaterials* **1996**, *17*, 103.
- (35) von Burkersroda, F.; Schedl, L.; Göpferich, A. *Biomaterials* **2002**, *23*, 4221.
- (36) data provided by Sigma Aldrich
- (37) Breitenbach, A.; Pistel, K.; Kissel, T. *Polymer* **2000**, *41*, 4781.
- (38) Lam, C. X.; Hutmacher, D. W.; Schantz, J. T.; Woodruff, M. A.; Teoh, S. H. *J Biomed Mater Res A* **2009**, *90*, 906.
- (39) Dušková-Smrčková, M.; Dušek, K. *J. Mater. Sci.* **2002**, *37*, 4733.
- (40) Vert, M.; Li, S.; Spenlehauer, G.; Guérin, P. *J. Mater. Sci.: Mater. Med.* **1992**, *3*, 432.
- (41) Undin, J.; Illanes, T.; Finne-Wistrand, A.; Albertsson, A.-C. *Polym. Chem.* **2012**, *3*, 1260.
- (42) He, F.; Li, S.; Vert, M.; Zhuo, R. *Polymer* **2003**, *44*, 5145.
- (43) Liederer, B. M.; Borchardt, R. T. *J. Pharm. Sci.* **2006**, *95*, 1177.
- (44) Lienhard, G. E. *Science* **1973**, *180*, 149.
- (45) Fersht, A. *Proceedings of the Royal Society of London B: Biological Sciences* **1974**, *187*, 397.
- (46) Liu, J.; Liu, W.; Weitzhandler, I.; Bhattacharyya, J.; Li, X.; Wang, J.; Qi, Y.; Bhattacharjee, S.; Chilkoti, A. *Angewandte Chemie International Edition* **2015**, *54*, 1002.
- (47) Gazit, E. *Chem. Soc. Rev.* **2007**, *36*, 1263.
- (48) Ilhan, F.; Gray, M.; Blanchette, K.; Rotello, V. M. *Macromolecules* **1999**, *32*, 6159.
- (49) Zhang, Y.; Zheng, M.; Kissel, T.; Agarwal, S. *Biomacromolecules* **2012**, *13*, 313.
- (50) Ozer, I.; Tomak, A.; Zareie, H. M.; Baran, Y.; Bulmus, V. *Biomacromolecules* **2017**, *18*, 2699.
- (51) Chenal, M.; Boursier, C.; Guillaneuf, Y.; Taverna, M.; Couvreur, P.; Nicolas, J. *Polym. Chem.* **2011**, *2*, 1523.
- (52) Chenal, M.; Mura, S.; Marchal, C.; Gignes, D.; Charleux, B.; Fattal, E.; Couvreur, P.; Nicolas, J. *Macromolecules* **2010**, *43*, 9291.
- (53) Louguet, S.; Verret, V.; Bédouet, L.; Servais, E.; Pascale, F.; Wassef, M.; Labarre, D.; Laurent, A.; Moine, L. *Acta Biomater.* **2014**, *10*, 1194.
- (54) Bontempo, D.; Maynard, H. D. *J. Am. Chem. Soc.* **2005**, *127*, 6508.
- (55) Pasut, G.; Veronese, F. M. *Adv. Drug Delivery Rev.* **2009**, *61*, 1177.
- (56) Lutz, J. F. *J. Polym. Sci. Pol. Chem.* **2008**, *46*, 3459.
- (57) Ryan, S. M.; Mantovani, G.; Wang, X.; Haddleton, D. M.; Brayden, D. J. *Expert Opin. Drug Deliv.* **2008**, *5*, 371.
- (58) Harris, J. M.; Chess, R. B. *Nat. Rev. Drug Discov.* **2003**, *2*, 214.
- (59) Jokerst, J. V.; Lobovkina, T.; Zare, R. N.; Gambhir, S. S. *Nanomedicine* **2011**, *6*, 715.
- (60) Kim, S. Y.; Lee, Y. M.; Baik, D. J.; Kang, J. S. *Biomaterials* **2003**, *24*, 55.
- (61) Plard, J.-P.; Bazile, D. *Colloids Surf. B* **1999**, *16*, 173.

Chapter 5 – Degradation of Copolymers Prepared by Nitroxide-Mediated Radical Ring-Opening
Polymerization and Point-by-Point Comparison with Traditional Polyesters

- (62) Rowe, R.; Sheskey, P.; Quinn, M. *London, England* **2009**, 637.
- (63) Smyth, H. F.; Carpenter, C. P.; Weil, C. S. *J. Pharm. Sci.* **1950**, 39, 349.
- (64) Middleton, J. C.; Tipton, A. J. *Biomaterials* **2000**, 21, 2335.
- (65) Sabir, M. I.; Xu, X.; Li, L. *J. Mater. Sci.* **2009**, 44, 5713.
- (66) Yao, D.; Smith, A.; Nagarajan, P.; Vasquez, A.; Dang, L.; Chaudhry, G. R. *Journal of Biomedical Materials Research Part B: Applied Biomaterials* **2006**, 77, 287.

Supplementary Information

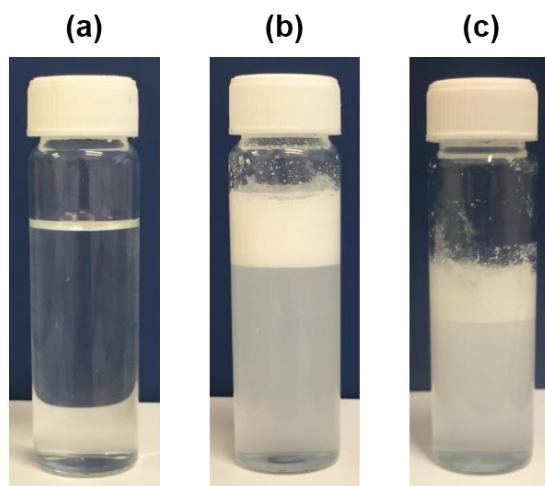


Figure S1. Pictures of the copolymer solutions or dispersion in PBS before degradation: (a) P(OEGMA-*co*-MPDL) copolymer solution (**P8**); (b) P(MMA-*co*-MPDL) copolymer dispersion (**P4**) and after degradation (12 months) and (c) P(MMA-*co*-MPDL) copolymer dispersion (**P4**).

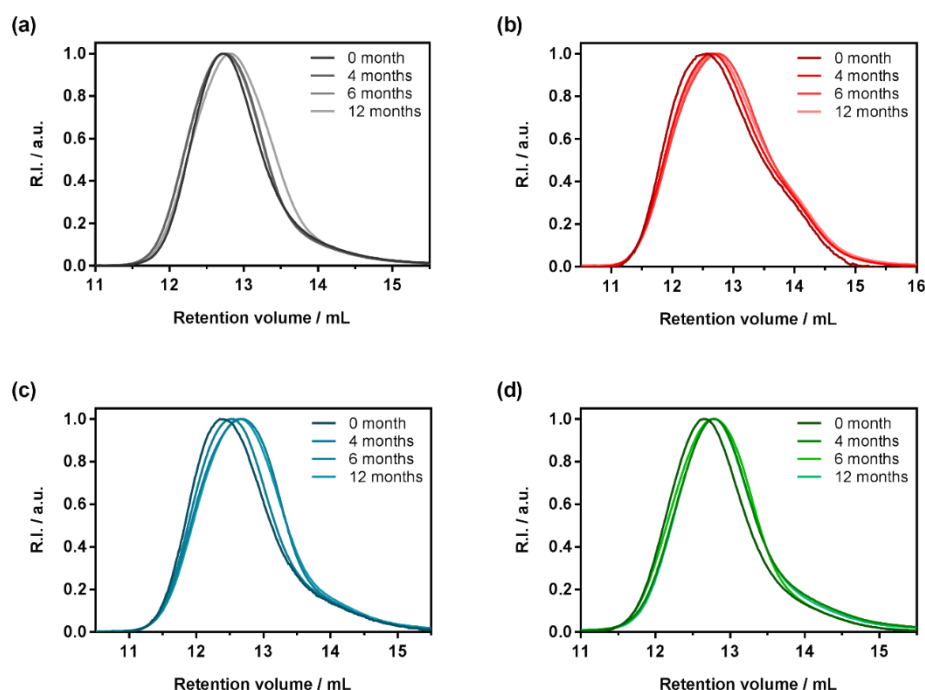


Figure S2. Evolution of the SEC chromatograms of P(MMA-*co*-MPDL) copolymers at different time during hydrolytic degradation in PBS (pH 7.4, 37 °C) as a function of the MPDL fraction. (a) **P1** ($F_{\text{MPDL}} = 0$); (b) **P2** ($F_{\text{MPDL}} = 0.08$); (c) **P3** ($F_{\text{MPDL}} = 0.12$); (d) **P4** ($F_{\text{MPDL}} = 0.27$).

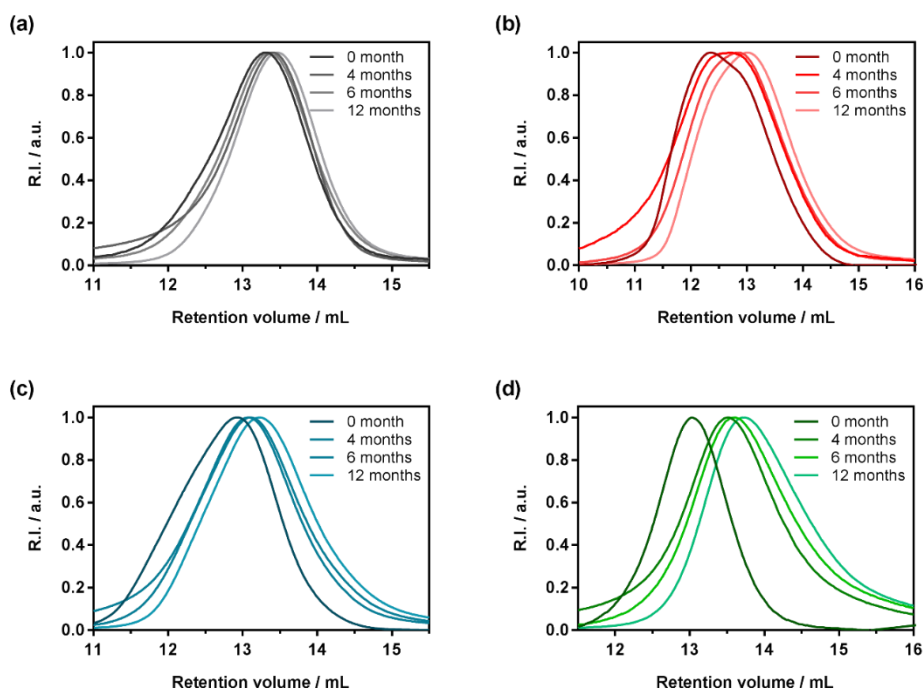


Figure S3. Evolution of the SEC chromatograms of P(OEGMA-*co*-MPDL) copolymers at different time during hydrolytic degradation in PBS (pH 7.4, 37 °C) as a function of the MPDL fraction. (a) **P5** ($F_{\text{MPDL}} = 0$); (b) **P6** ($F_{\text{MPDL}} = 0.09$); (c) **P7** ($F_{\text{MPDL}} = 0.15$); (d) **P8** ($F_{\text{MPDL}} = 0.27$).

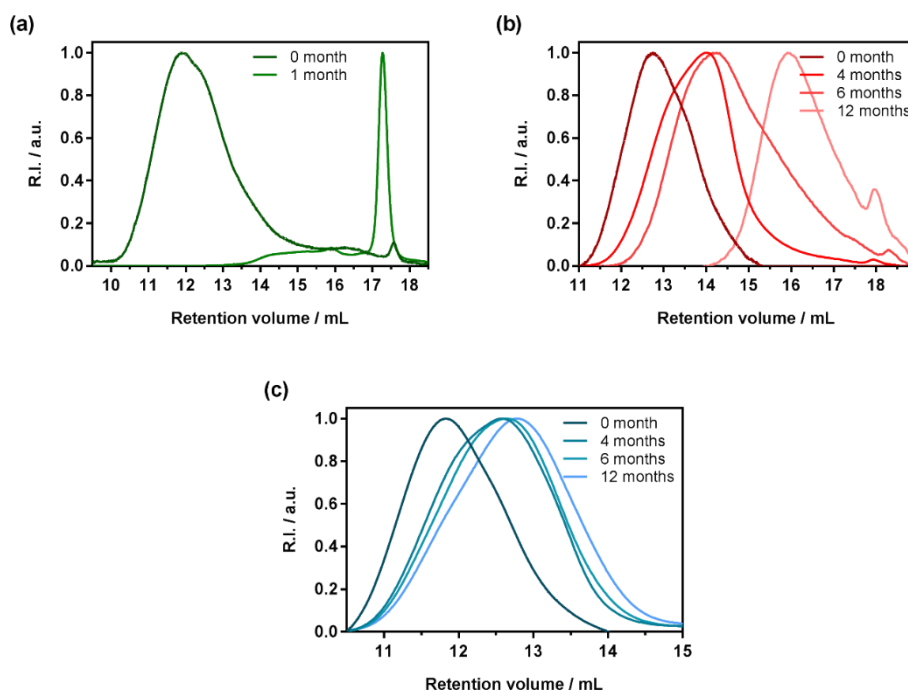


Figure S4. Evolution of the SEC chromatograms of traditional aliphatic polyesters at different time during hydrolytic degradation in PBS (pH 7.4, 37 °C). (a) PLGA; (b) PLA; (c) PCL.

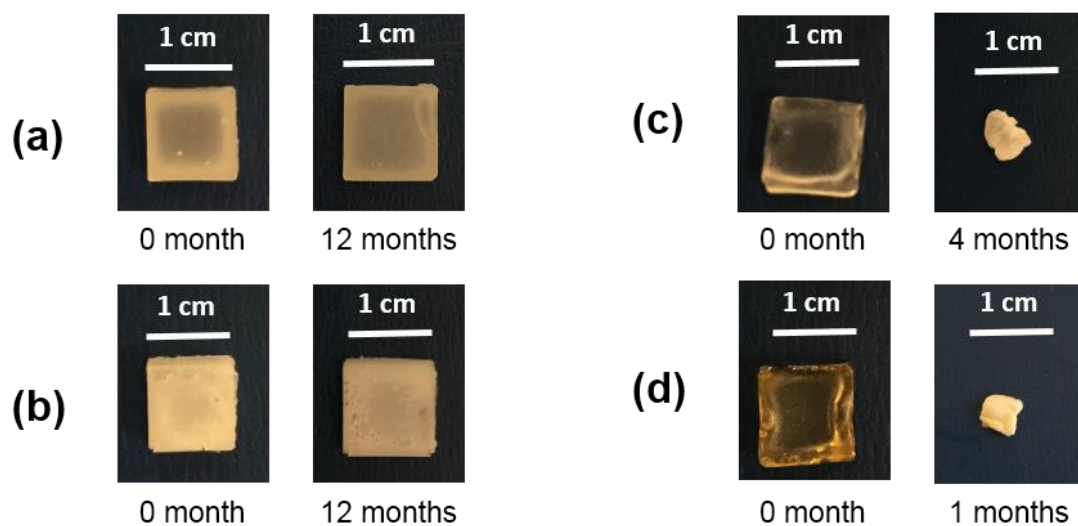


Figure S5. Pictures of the polymer films before and after hydrolytic degradation in PBS (pH 7.4, 37 °C). (a) P(MMA-co-MPDL) P4; (b) PCL; (c) PLA; (d) PLGA.

Chapter 5 – Degradation of Copolymers Prepared by Nitroxide-Mediated Radical Ring-Opening
Polymerization and Point-by-Point Comparison with Traditional Polyesters

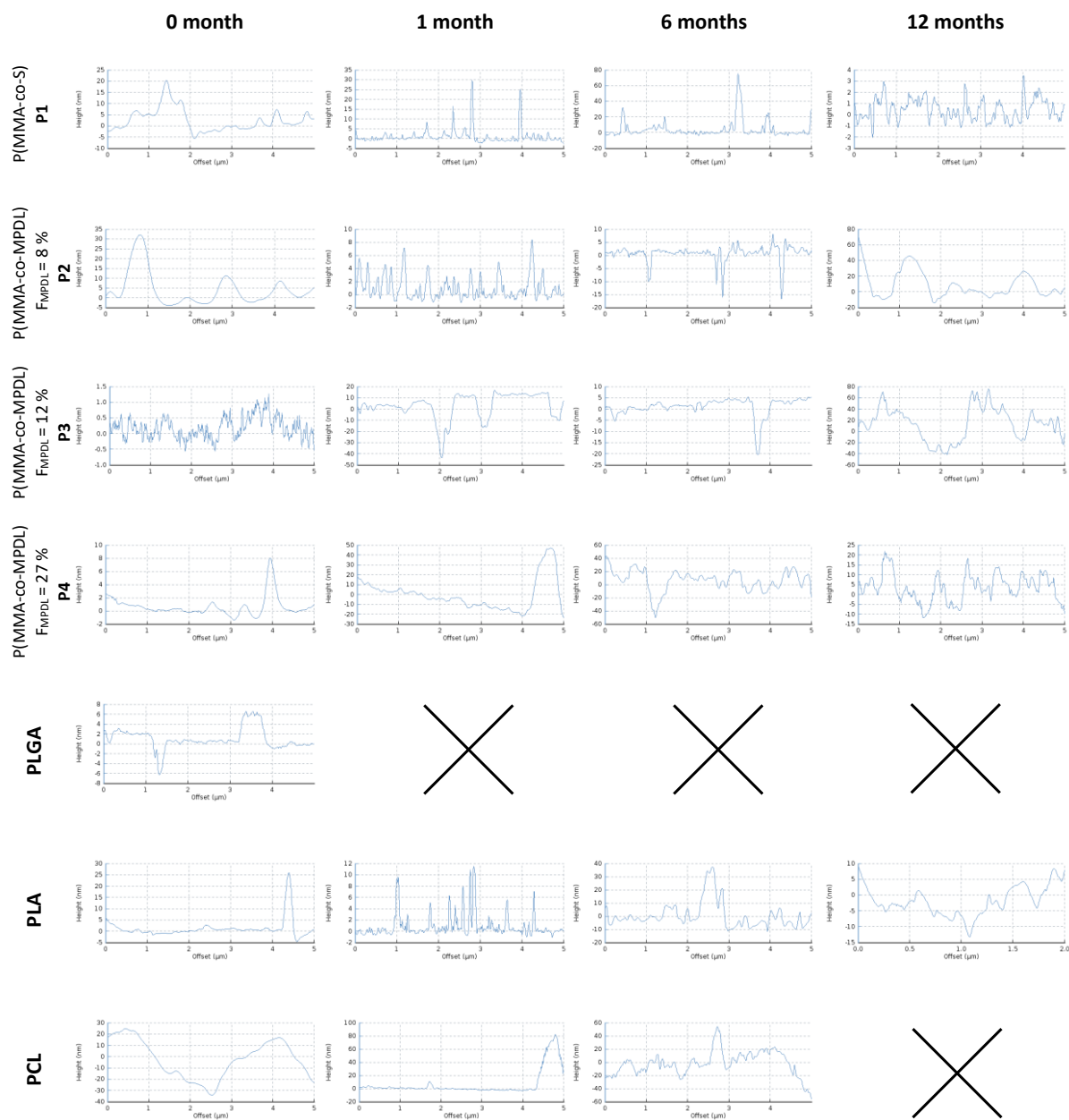


Figure S6. AFM cross section obtained in AC mode during hydrolytic degradation in PBS (100 mM, pH 7.4, 37 °C) of MMA-based copolymers P1–P4, PLGA, PLA and PCL. Cross section recorded along the line drawn on the height images in Figure 8.

Chapter 5 – Degradation of Copolymers Prepared by Nitroxide-Mediated Radical Ring-Opening
Polymerization and Point-by-Point Comparison with Traditional Polyesters

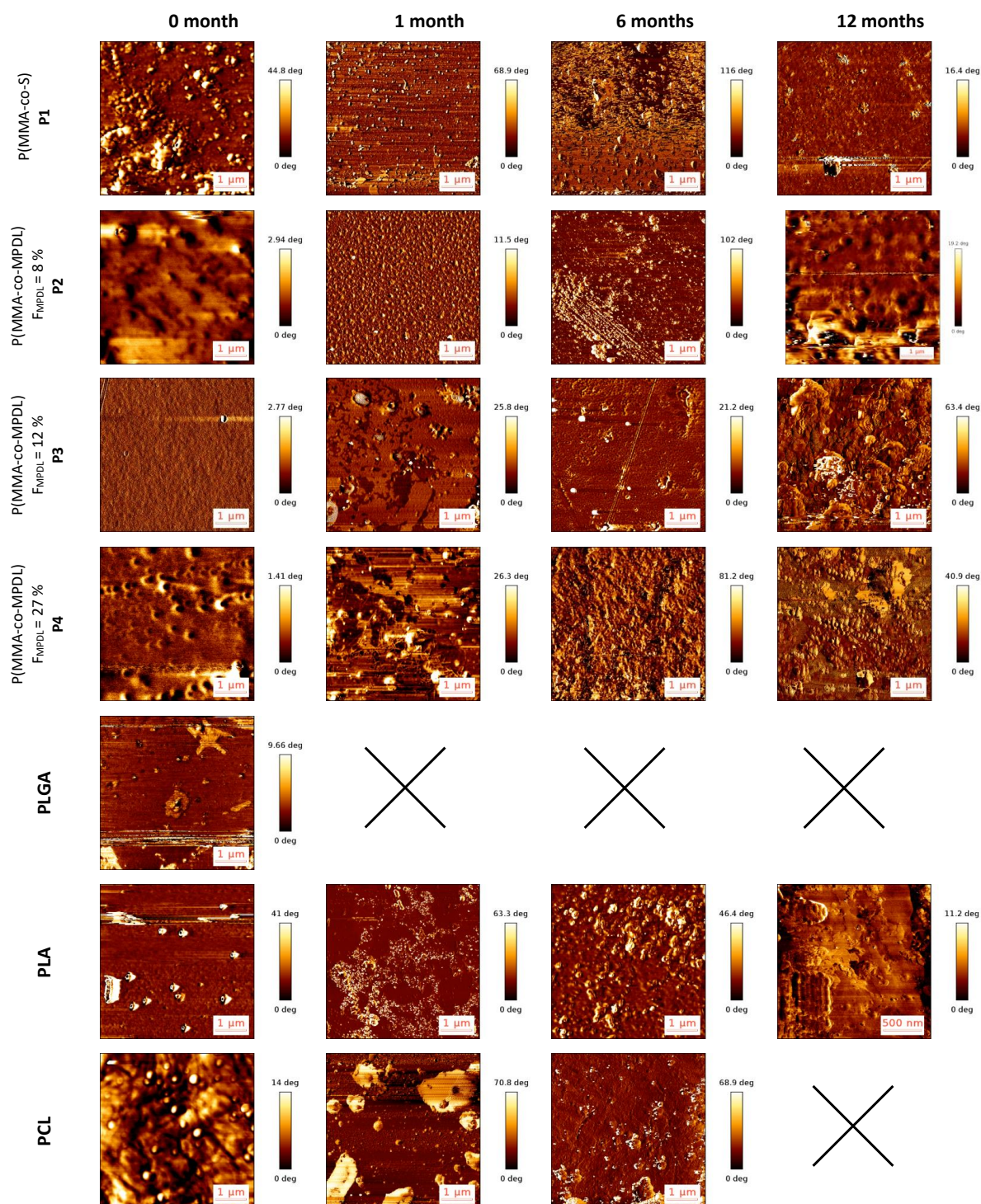


Figure S7. AFM phase images ($5 \times 5 \mu\text{m}$, except for PLA 12 months, $2 \times 2 \mu\text{m}$) obtained in AC mode during hydrolytic degradation in PBS (100 mM, pH 7.4, 37 °C) of MMA-based copolymers **P1–P4**, PLGA, PLA and PCL thin films. The scale is indicated on the right side of each image (colored bar).

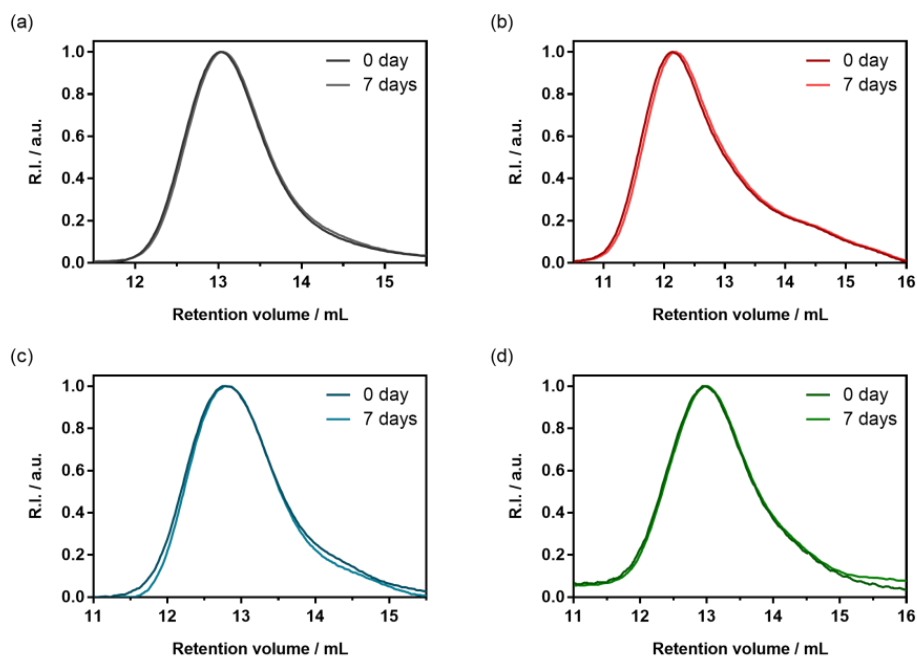


Figure S8. Evolution of the SEC chromatograms of P(MMA-*co*-MPDL) copolymers at different time during enzymatic degradation (lipases) as a function of the MPDL fraction. (a) **P1** ($F_{\text{MPDL}} = 0$); (b) **P2** ($F_{\text{MPDL}} = 0.08$); (c) **P3** ($F_{\text{MPDL}} = 0.12$); (d) **P4** ($F_{\text{MPDL}} = 0.27$).

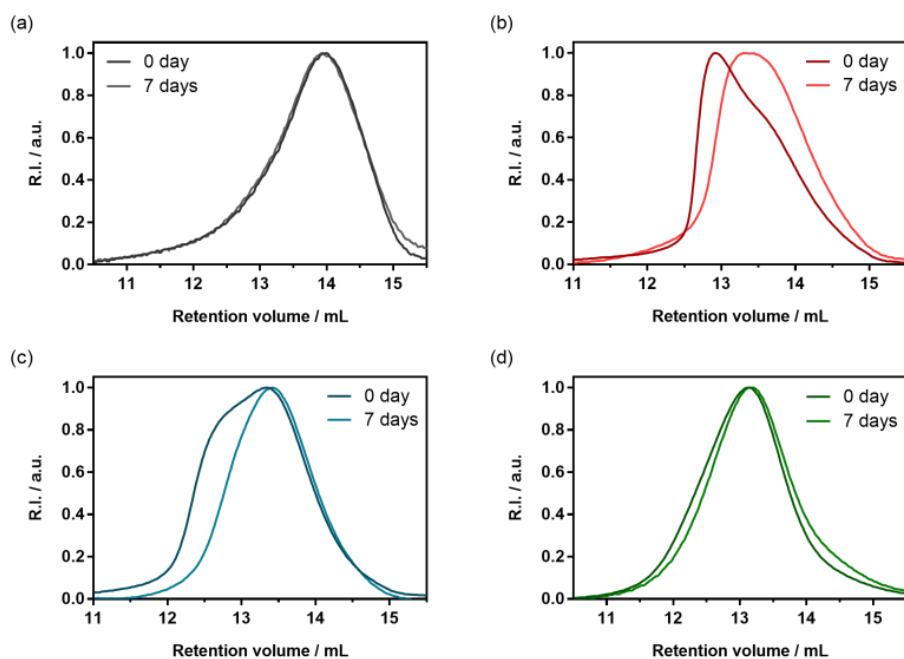
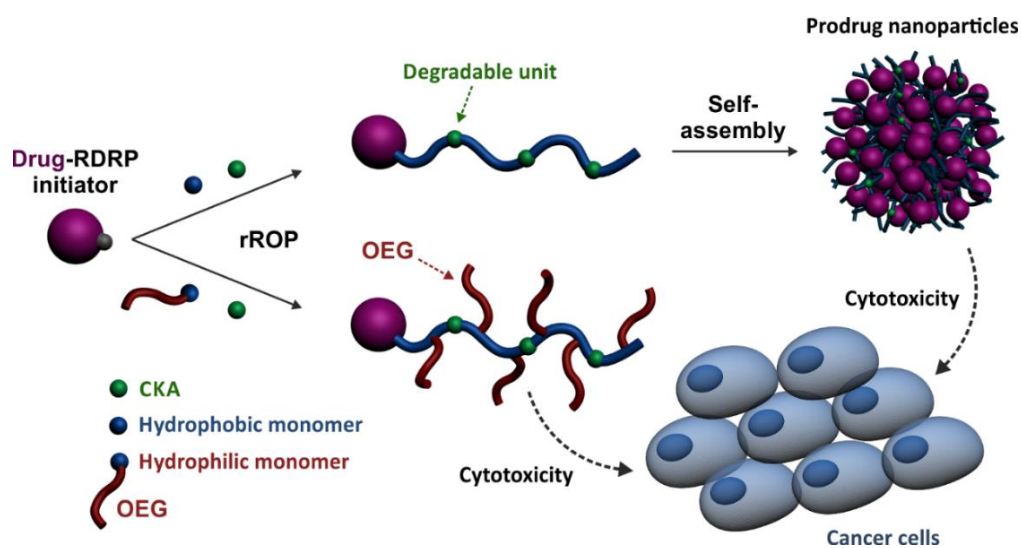


Figure S9. Evolution of the SEC chromatograms of P(OEGMA-*co*-MPDL) copolymers at different time during enzymatic degradation (lipases) as a function of the MPDL fraction. (a) **P5** ($F_{\text{MPDL}} = 0$); (b) **P6** ($F_{\text{MPDL}} = 0.08$); (c) **P7** ($F_{\text{MPDL}} = 0.12$); (d) **P8** ($F_{\text{MPDL}} = 0.27$).

Chapter 6

Degradable Polymer Prodrugs with Adjustable Activity from Drug-Initiated Radical Ring-Opening Copolymerization

*Elise Guégain, Johanna Tran, Quentin Deguettes, Julien Nicolas**



To be submitted

ABSTRACT

Degradable polymer prodrugs based on gemcitabine (Gem) as an anticancer drug were synthesized by 'drug-initiated' nitroxide-mediated radical ring-opening copolymerization (NMrROP) of methacrylic esters and 2-methylene-4-phenyl-1,3-dioxolane (MPDL). Different structural parameters were varied to determine the best biological performances: the nature of the monomer [i.e., oligo(ethylene glycol) methacrylate (OEGMA) or methyl methacrylate (MMA)], the nature of the Gem-polymer linker (i.e., amide or amide + diglycolate) and the MPDL content in the copolymer. Depending on the nature of the methacrylate monomer, a small library of water-soluble copolymer prodrugs or nanoparticles was obtained ($M_n \sim 10000 \text{ g.mol}^{-1}$, $D = 1.1\text{--}1.5$), that exhibited tunable hydrolytic degradation under accelerated conditions governed by the MPDL content. Drug-release profiles in human serum and *in vitro* anticancer activity on different cell lines enabled to establish preliminary structure-activity relationships. It was demonstrated that the cytotoxicity was independently governed by: (i) the MPDL content –the lower the MPDL content, the greater the cytotoxicity; (ii) the nature of the linker –the presence of a labile diglycolate linker enabled a greater Gem release compared to a simple amide bond and (iii) the hydrophilicity of the methacrylate monomer –OEGMA enabled a greater anticancer activity to be obtained compared to MMA-based polymer prodrugs. Remarkably, the optimal structural parameters enabled to reach the cytotoxic activity of the parent (free) drug.

I. Introduction

In the field of nanomedicine, drug-loaded polymer nanocarriers is considered as a promising strategy to improve the efficacy of drugs such as chemotherapeutics.^{1,2} Traditionally, drugs are physically encapsulated during the nanocarrier formulation and thus simply entrapped into the polymer matrix. These drug delivery systems lead to protection of the drug from rapid metabolization, to longer circulation time, to lower toxicity toward healthy cells/tissues and open the door to active targeting by their surface-functionalization by biologically active ligands. Despite major advances and encouraging results, important limitations remain that may explain the small number of marketed nanomedicines and recent clinical trial disappointments: (i) the “burst-release”; that is the quick and uncontrolled release of a significant fraction of the drug post-injection; (ii) the poor drug-loadings, usually only a few percent and (iii) the crystallization of some drugs into the polymer matrix. These three different events can lead to prohibitive toxicity and/or colloidal instability of the nanocarriers.

The prodrug strategy, which consists in coupling the drug to the nanocarrier, can be used to circumvent, or at least alleviate, the above-mentioned issues.³ Among the different synthetic pathways to produce polymer prodrug nanocarriers, the most used are certainly the “grafting to” and “grafting from” approaches that consist in functionalization of preformed polymer or monomer, respectively. The emerging “grafting through” strategy (also called “drug-initiated”), that relies on the controlled growth of a short polymer chain from a drug, used as a initiator, possesses compelling benefits:⁴ (i) the synthesis and purification are simple because a few synthetic steps are necessary; (ii) the resulting materials has a simple, well-defined structure (one drug attached at the extremity of each polymer chain); (iii) high drug loadings can be easily reached by targeting short polymer chains; (iv) this approach can be applied to different pathologies simply by changing the nature of the drug and (v) the properties of the resulting polymer prodrug can be finely tuned by changing the nature and the composition of the growing polymer.

The robustness of the drug-initiated method has been illustrated by its application to the synthesis of a variety of different polymer prodrugs constructed by either ring-opening polymerization (ROP)⁵⁻⁹ or reversible-deactivation radical polymerization (RDRP),¹⁰⁻¹⁷ including nitroxide-mediated radical polymerization (NMP)¹⁸ or reversible addition-fragmentation chain transfer (RAFT)¹⁹ polymerization. Whereas ROP generated degradable polyester prodrugs nanocarriers, they exhibited poor colloidal stability and required post-stabilization by means of macromolecular surfactants, which is a major drawback. Also, no in

vivo anticancer activity has been reported from those systems. On the other hand, RDRP-constructed polymer prodrugs gave promising anticancer efficacy in vivo, relied on simpler polymerization methods (e.g., no stringent conditions, commercially available controlling agents) and offered much more versatility regarding the nature of the polymer used. However, they are not degradable because of the carbon-carbon backbone of the vinyl polymer chains. This represents an important issue because non-degradable materials may accumulate in the body, leading to prohibitive toxicity in case chronic/repeated administration is envisioned. A global strategy combining both advantages of ROP and RDRP for the design of efficient polymer prodrugs by the “*drug-initiated*” approach is thus highly desirable.

Conferring degradability to vinyl materials is currently the focus of intensive work.²⁰ This research topic is crucial given the numerous systems based on vinyl polymers devoted to biomedical applications regularly being reported in the literature. Among the different synthetic strategies, radical ring-opening polymerization (rROP) appears to be the method of choice for incorporating labile groups into the polymer backbone and enabling significant degradation.^{21,22} Thanks to its radical ring-opening mechanism, rROP possesses both the versatility and simplicity of radical polymerization, together with the ability to introduce functional groups into the polymer backbone. Among the different classes of monomers that have been polymerized by rROP, cyclic ketene acetals²³ are the most-studied family. Although their homopolymerization have been extensively studied in the 80s,²⁴⁻²⁷ they aroused renewed interest over the past decade as comonomers to confer degradability to vinyl polymers via insertion of ester groups from either free-radical copolymerization²⁸⁻³⁴ or RDRP.^{32,35-46} A second family of monomers, cyclic allylic sulfides^{47,48} have also been used to incorporate cleavable ester, thioester, and disulfide functionalities into the polymer backbone through RAFT copolymerization with traditional vinyl monomers.⁴¹ Despite several applications of rROP-designed materials for biomedical applications, their use in the field of prodrug nanocarriers has never been reported.

Herein, we report for the first time on a general approach that combines the best of two worlds; that is the drug-initiated synthesis of degradable polymer prodrug by rROP. We demonstrated that well-defined, degradable vinyl copolymers can be synthesized from an anticancer drug-bearing RDRP initiator by rROP, leading to nanocarriers, either water-soluble conjugates or nanoparticles (Figure 1), with adjustable anticancer activity depending on the nature of both the drug-polymer linkage and of the grown copolymer together with its composition. Not only this new class of polymer prodrugs overcame a significant obstacle in

the field but it also disclosed important insights into the relevant parameters that govern the drug release kinetics and eventually the anticancer activity.

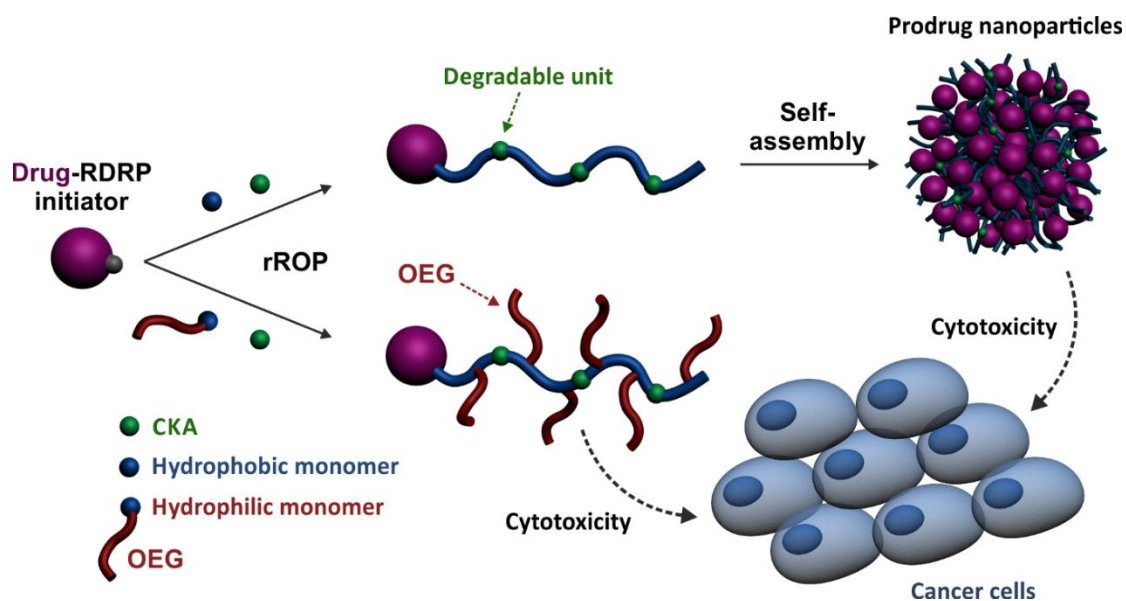


Figure 1. Synthetic strategy for the design of degradable Gemcitabine-based polymer prodrugs by ‘drug-initiated’ nitroxide-mediated radical ring-opening copolymerization (NMrROP).

II. Experimental section

a. Material

Gemcitabine (> 98%) was purchased from Carbosynth Limited (UK). *N-tert-butyl-N*-[1-diethylphosphono-(2,2-dimethylpropyl)] nitroxide (SG1, 85%) was kindly supplied from Arkema (France). Oligo(ethylene glycol) methyl ether methacrylate (MeOEGMA, $M_n = 300 \text{ g}\cdot\text{mol}^{-1}$), styrene (S, 99%), methyl methacrylate (MMA, 99%) and toluene (anhydrous, 99.8%) were purchased from Sigma-Aldrich (France) and used as received (except for MMA which was distilled under reduced pressure). 2-Methylene-4-phenyl-1,3-dioxolane (MPDL),⁴⁹ 4-amino-1-[4-(*tert*-butyl-dimethylsilyloxy)-5-(*tert*-butyl-dimethyl-silyloxymethyl)-3,3-difluorotetrahydro-furan-2-yl]-1H-pyrimidin-2-one (TBDMS-Gem),¹¹ and alkoxyamines Gem-AMA-SG1¹⁰ and AMA-digly⁵⁰ were prepared as reported previously. Tetrabutylammonium fluoride (TBAF) was purchased from Alfa Aesar (A Johnson Matthey Co., France). Perfluoro-15-Crown-5-Ether (PFCE) was obtained from FluoroChem (UK). All other reactants were purchased from Sigma-Aldrich at the highest available purity and used as

received. Deuterated chloroform (CDCl_3) was obtained from Eurisotop. All other solvents were purchased from Carlo-Erba. Dulbecco's modified eagle's medium (DMEM) and fetal bovine serum (FBS) were purchased from Dulbecco (Invitrogen, France). Penicillin and streptomycin were obtained from Lonza (Verviers, Belgium). The 2-methyl-2-[*N*-*tert*-butyl-*N*-(1-diethoxyphosphoryl-2,2-dimethylpropyl) aminoxy]propionic acid alkoxyamine (BlocBuilder MA, 99%) and the *N*-*tert*-butyl-*N*-(1-diethylphosphono-2,2-dimethylpropyl) nitroxide (SG1, 85%) were kindly supplied by Arkema.

b. Analytical method

Nuclear magnetic resonance (NMR) spectroscopy. NMR spectroscopy was performed in 5 mm diameter tubes in CDCl_3 at 25 °C. ^1H NMR or ^{13}C NMR spectroscopy were performed on a Bruker Avance 300 spectrometer at 300 MHz or 75 MHz, respectively. The chemical shift scale was calibrated based on the internal solvent signals. ^{19}F NMR spectra were recorded on a Bruker Avance 400 at 376.5 MHz. The chemical shift scale was calibrated relative to an internal standard (PFCE, $\delta = -88$ ppm).

Mass Spectrometry (MS). Mass spectra were recorded with a Bruker Esquire-LC instrument. High-resolution (HR) mass spectra (electron spin ionization, ESI) were recorded on a ESI/TOF (LCT, Waters) LC-spectrometer. Elemental analyses were performed by the Service de microanalyse, Centre d'Etudes Pharmaceutiques, Châtenay-Malabry, France, with a PerkinElmer 2400 analyzer.

Size exclusion chromatography (SEC). SEC was performed at 30 °C with two columns from Polymer Laboratories (PL-gel MIXED-D; 300×7.5 mm; bead diameter, 5 μm ; linear part, $400\text{--}400\,000$ $\text{g}\cdot\text{mol}^{-1}$) and a differential refractive index detector (Spectrasystem RI-150 from Thermo Electron Corp.), using chloroform (CHCl_3) as eluent at a flow rate of 1 $\text{mL}\cdot\text{min}^{-1}$. Toluene was used as a flow-rate marker. The conventional calibration curve was based on poly(methyl methacrylate) (PMMA) standards (peak molar masses, $M_p = 625\text{--}625\,500$ $\text{g}\cdot\text{mol}^{-1}$) from Polymer Laboratories. This technique allowed M_n (number-average molar mass), M_w (weight-average molar mass), and M_w/M_n (dispersity, D) to be determined.

Dynamic light scattering (DLS) and zeta potential. Nanoparticle diameters (D_z) and zeta potentials (ζ) were measured by dynamic light scattering (DLS) with a Nano ZS from Malvern (173° scattering angle) at a temperature of 25 °C. The surface charge of the nanoparticles was determined by ζ -potential (mV) measurement at 25 °C after dilution with 1 mM NaCl, using the Smoluchowski equation.

Cryogenic transmission electron microscopy (cryo-TEM). The morphology of the nanoassemblies was observed by cryo-TEM. Briefly, 5 μL of the nanoparticle suspension (0.5 $\text{mg}\cdot\text{mL}^{-1}$) was deposited on a Lacey Formvar/carbon 300 mesh copper microscopy grid (Ted Pella). Most of the drop was removed with a blotting filter paper and the residual thin film remaining within the holes was vitrified by plunging into liquid ethane. Samples were then observed using a JEOL 2100HC microscope.

c. Synthetic procedures

Synthesis of Gem-digly-AMA-SG1. TBDMS-Gem (3.0 g, 6.1 mmol), AMA-digly (2.5 g, 4.7 mmol) and benzotriazol-1-yl-oxytripyrrolidinophosphonium hexafluorophosphate (PyBOP, 3.2 g, 6.1 mmol) were dissolved in 30 mL of dry DMF. *N,N*-Diisopropylethylamine (DIPEA, 2.2 mL, 12.4 mmol) was added dropwise. After stirring at 30 °C for 24 h under nitrogen atmosphere, the mixture was poured into 200 mL of EtOAc. The organic phase was washed with 1 M HCl, sat. NaHCO_3 aqueous solution, and brine before being dried over MgSO_4 . The residue was concentrated under reduced pressure and purified by flash chromatography (SiO_2 , gradient elution from EtOAc/petroleum ether = 1/1, v/v to EtOAc) to give 2.01 g of Gem-digly-AMA-SG1 as a white/slightly orange solid (Figure S1). Yield = 42 %. ^1H NMR (CDCl_3 , 300 MHz): *Major diastereomer*: δ = 8.11 (1H, s, H_6), 7.41 (1H, s, H_5), 6.36 (1H, s, $\text{H}_{1'}$), 4.60 (1H, q, H_b), 3.75-4.50 (16H, m, H_a , H_g , $\text{H}_{3'}$, $\text{H}_{4'}$, $\text{H}_{5'}$), 3.26 (1H, d, H_f), 1.48 (3H, d, H_c), 1.29 (6H, t, H_h), 1.10 (18H, s, H_e), 0.90 (18H, s, H_i), 0.13 (12H, s, H_j) ppm. *Minor diastereomer*: δ = 8.10 (1H, s, H_6), 7.43 (1H, s, H_5), 6.34 (1H, s, $\text{H}_{1'}$), 4.60 (1H, q, H_b), 3.75-4.50 (16H, m, H_a , H_g , $\text{H}_{3'}$, $\text{H}_{4'}$, $\text{H}_{5'}$), 3.35 (1H, d, H_f), 1.50 (3H, d, H_c), 1.29 (6H, t, H_h), 1.15 (18H, s, H_e), 0.95 (18H, s, H_i), 0.10 (12H, s, H_j) ppm. ^{13}C NMR (CDCl_3 , 75 MHz): *Major diastereomer*: δ = 173.6 (s, C_d), 169.4 (s, C_k), 169.2 (s, C_j), 161.8 (s, C_4), 154.9 (s, C_2), 144.3 (s, C_6), 121.9 (s, $\text{C}_{2'}$), 96.5 (s, C_5), 84.9 (d, $\text{C}_{1'}$), 82.3 (s, C_b), 81.4 (s, $\text{C}_{4'}$), 70.9 (s, C_a), 70.2 (t, $\text{C}_{3'}$), 68.0 (s, C_a), 63.0 (s, $\text{C}_{5'}$), 61.7 (t, C_g), 60.0 (s, C_a), 58.9 (d, C_g), 35.5 (d, C_l), 29.6 (d, C_g), 27.9 (s, C_e), 25.7 (d, C_e), 19.3 (s, C_c), 18.3 (s, C_i), 17.9 (s, C_m), 16.5 (d, C_h) ppm. *Minor diastereomer*: δ = 172.6 (s, C_d), 169.3 (s, C_k), 169.1 (s, C_j), 161.9 (s, C_4), 154.9 (s, C_2), 144.2 (s, C_6), 121.9 (s, $\text{C}_{2'}$), 96.6 (s, C_5), 84.4 (d, $\text{C}_{1'}$), 82.3 (s, C_b), 81.5 (s, $\text{C}_{4'}$), 70.9 (s, C_a), 69.5 (t, $\text{C}_{3'}$), 68.3 (s, C_a), 63.0 (s, $\text{C}_{5'}$), 62.0 (t, C_g), 60.0 (s, C_a), 59.1 (d, C_g), 35.2 (d, C_l), 30.1 (d, C_g), 28.0 (s, C_e), 25.7 (d, C_e), 19.3 (s, C_c), 18.3 (s, C_i), 18.0 (s, C_m), 16.2 (d, C_h) ppm. ^{19}F NMR (CDCl_3 , 376.5 MHz): δ = - 117 ppm. MS (ESI⁻): m/z = 999.5 (M-H)⁻. Calc. for $\text{C}_{43}\text{H}_{79}\text{F}_2\text{N}_4\text{O}_{14}\text{PSi}_2$: 1001.

Synthesis of Gem-poly[(oligo(ethylene glycol) methyl ether methacrylate)-*co*-(2-methylene-4-phenyl-1,3-dioxolane)] (Gem-P(OEGMA-*co*-MPDL)). A typical solution copolymerization procedure ($f_{\text{MPDL},0} = 0.2$, Expt. 1) is described as follows. In a 5 mL vial fitted with a rubber septum and a magnetic stirring bar, a mixture of OEGMA (1.3214 g, 4.40 mmol, $M_n = 300 \text{ g}\cdot\text{mol}^{-1}$), MPDL (0.1786 g, 1.10 mmol), Gem-AMA-SG1 (28.0 mg, 4.58×10^{-2} mmol), SG1 (1.5 mg, 4.39×10^{-3} mmol) and anhydrous toluene (1.5 g, 1.73 mL) was degassed under stirring by argon bubbling for 15 min at room temperature. The mixture was then immersed in a preheated oil bath at 90 °C, corresponding to the time zero of the reaction (according to the small volume of solution and its quasi-instantaneous heating). Aliquots were periodically taken to monitor the OEGMA conversion by ^1H NMR spectroscopy and the macromolecular characteristics (M_n and \bar{D}) by SEC. The copolymer was then precipitated twice in a mixture of cold cyclohexane/petroleum ether (1/1, v/v) and dried under high vacuum until constant weight. The same procedure was followed by adapting the amount of the reactants for $f_{\text{MPDL},0} = 0.4$ (Expt. 2) [OEGMA (1.1028 g, 3.68 mmol), MPDL (0.3972 g, 2.45 mmol), Gem-AMA-SG1 (23.0 mg, 3.76×10^{-2} mmol) and SG1 (1.3 mg, 3.80×10^{-3} mmol)] and $f_{\text{MPDL},0} = 0.7$ (Expt. 3) [OEGMA (0.6633 g, 2.21 mmol), MPDL (0.8367 g, 5.17 mmol), Gem-AMA-SG1 (13.8 mg, 2.31×10^{-2} mmol) and SG1 (0.8 mg, 2.34×10^{-3} mmol)].

Synthesis of Gem-digly-poly[(oligo(ethylene glycol) methyl ether methacrylate)-*co*-(2-methylene-4-phenyl-1,3-dioxolane)] (Gem-digly-P(OEGMA-*co*-MPDL)). A typical solution copolymerization procedure ($f_{\text{MPDL},0} = 0.2$, Expt. 1d) is as follows. In a 5 mL vial, fitted with a rubber septum and a magnetic stirring bar, a mixture of OEGMA (1.3214 g, 4.40 mmol), MPDL (0.1786 g, 1.10 mmol), Gem-digly-AMA-SG1 (45.0 mg, 4.50×10^{-2} mmol), SG1 (1.5 mg, 4.39×10^{-3} mmol) and anhydrous toluene (1.5 g, 1.73 mL) was degassed under stirring by argon bubbling for 15 min at room temperature. The mixture was then immersed in a preheated oil bath at 90 °C. Samples were periodically taken to monitor the OEGMA conversion by ^1H NMR spectroscopy and the macromolecular characteristics (M_n and \bar{D}) by SEC. The copolymer was then precipitated twice in a mixture of cold cyclohexane/petroleum ether (1/1, v/v) and dried under high vacuum until constant weight. The same procedure was followed by adapting the amount of the reactants for $f_{\text{MPDL},0} = 0.4$ (Expt. 2d) [OEGMA (1.1028 g, 3.68 mmol), MPDL (0.3972 g, 2.45 mmol), Gem-digly-AMA-SG1 (38.0 mg, 3.80×10^{-2} mmol) and SG1 (1.3 mg, 3.80×10^{-3} mmol)] and $f_{\text{MPDL},0} = 0.7$ (Expt. 3d) [OEGMA (0.6633 g, 2.21 mmol), MPDL (0.8367 g, 5.17 mmol), Gem-digly-AMA-SG1 (23.0 mg, 2.30×10^{-2} mmol) and SG1 (0.8 mg, 2.34×10^{-3} mmol)].

Synthesis of Gem-poly[(methyl methacrylate)-*co*-(2-methylene-4-phenyl-1,3-dioxolane)] (Gem-P(MMA-*co*-MPDL)). A typical solution copolymerization procedure ($f_{\text{MPDL},0} = 0.2$, Expt. 4) is as follows. In a 5 mL vial, fitted with a rubber septum and a magnetic stirring bar, a mixture of MMA (1.0673 g, 10.67 mmol), MPDL (0.4327 g, 2.67 mmol), Gem-AMA-SG1 (22.0 mg, 3.59×10^{-2} mmol), SG1 (1.3 mg, 3.80×10^{-3} mmol) and anhydrous toluene (1.5 g, 1.73 mL) was degassed under stirring by argon bubbling for 15 min at room temperature. The mixture was then immersed in a preheated oil bath at 90 °C. Samples were periodically taken to monitor the MMA conversion by ^1H NMR spectroscopy and the macromolecular characteristics (M_n and \bar{D}) by SEC. The copolymer was then precipitated twice in cold MeOH and dried under high vacuum until constant weight. The same procedure was followed by adapting the amount of the reactants for $f_{\text{MPDL},0} = 0.4$ (Expt. 5) [MMA (0.7215 g, 7.22 mmol), MPDL (0.7785 g, 4.81 mmol), Gem-AMA-SG1 (15.0 mg, 2.45×10^{-2} mmol) and SG1 (0.9 mg, 2.49×10^{-3} mmol)] and $f_{\text{MPDL},0} = 0.7$ (Expt. 6) [MMA (0.3135 g, 3.14 mmol), MPDL (1.1865 g, 7.32 mmol), Gem-AMA-SG1 (6.5 mg, 1.06×10^{-2} mmol) and SG1 (0.4 mg, 1.02×10^{-3} mmol)].

Synthesis of Gem-digly-poly[(methyl methacrylate)-*co*-(2-methylene-4-phenyl-1,3-dioxolane)] (Gem-digly-P(MMA-*co*-MPDL)). A typical solution copolymerization procedure ($f_{\text{MPDL},0} = 0.2$, Expt. 4d) is as follows. In a 5 mL vial, fitted with a rubber septum and a magnetic stirring bar, a mixture of MMA (1.0673 g, 10.67 mmol), MPDL (0.4327 g, 2.67 mmol), Gem-digly-AMA-SG1 (36.0 mg, 3.60×10^{-2} mmol), SG1 (1.3 mg, 3.80×10^{-3} mmol) and anhydrous toluene (1.5 g, 1.73 mL) was degassed under stirring by argon bubbling for 15 min at room temperature. The mixture was then immersed in a preheated oil bath at 90 °C. Samples were periodically taken to monitor the MMA conversion by ^1H NMR spectroscopy and the macromolecular characteristics (M_n and \bar{D}) by SEC. The copolymer was then precipitated twice in cold MeOH and dried under high vacuum until constant weight. The same procedure was followed by adapting the amount of the reactants for $f_{\text{MPDL},0} = 0.4$ (Expt. 5d) [MMA (0.7215 g, 7.22 mmol), MPDL (0.7785 g, 4.81 mmol), Gem-digly-AMA-SG1 (25.0 mg, 2.5×10^{-2} mmol) and SG1 (0.9 mg, 2.49×10^{-3} mmol)] and $f_{\text{MPDL},0} = 0.7$ (Expt. 6d) [MMA (0.3135 g, 3.14 mmol), MPDL (1.1865 g, 7.32 mmol), Gem-digly-AMA-SG1 (10.5 mg, 1.05×10^{-2} mmol) and SG1 (0.4 mg, 1.02×10^{-3} mmol)].

Synthesis of low molar mass Gem-poly[(oligo(ethylene glycol) methyl ether methacrylate)-*co*-(2-methylene-4-phenyl-1,3-dioxolane)] (Gem-P(OEGMA-*co*-MPDL)). Copolymers with targeted M_n of $\sim 10\,000 \text{ g}\cdot\text{mol}^{-1}$ were prepared by following a similar procedure as for Expt. 1 but with a polymerization time of 8 h. Experimental conditions were

as follows: **P1** ($f_{\text{MPDL},0} = 0.2$) [OEGMA (1.7618 g, 5.87 mmol), MPDL (0.2382 g, 1.47 mmol), Gem-AMA-SG1 (200.0 mg, 3.27×10^{-1} mmol), SG1 (12 mg, 3.51×10^{-2} mmol) and anhydrous toluene (2.0 g, 2.31 mL)], **P2** ($f_{\text{MPDL},0} = 0.4$) [OEGMA (1.4704 g, 4.90 mmol), MPDL (0.5296 g, 3.27 mmol), Gem-AMA-SG1 (205.0 mg, 3.35×10^{-1} mmol), SG1 (12 mg, 3.51×10^{-2} mmol) and anhydrous toluene (2.0 g, 2.31 mL)] and **P3** ($f_{\text{MPDL},0} = 0.7$) [OEGMA (0.8862 g, 2.95 mmol), MPDL (1.1138 g, 6.88 mmol), Gem-AMA-SG1 (65.0 mg, 1.06×10^{-1} mmol), SG1 (3.6 mg, 1.05×10^{-2} mmol) and anhydrous toluene (2.0 g, 2.31 mL)]. Final composition of the prodrug was determined by comparing the methoxy protons of OEG from OEGMA (at 3.4 ppm) to the aromatic protons of MPDL (at 7.2 ppm). The presence of Gem was quantitatively confirmed by ^{19}F NMR by comparing the integration of the fluorine atoms of the internal standard PFCE ($\delta = -88$ ppm) and of Gem ($\delta = -117$ ppm).

Synthesis of low molar mass Gem-digly-poly[(oligo(ethylene glycol) methyl ether methacrylate)-co-(2-methylene-4-phenyl-1,3-dioxolane)] (Gem-digly-P(OEGMA-co-MPDL)). Copolymers with targeted M_n of $\sim 10\,000$ g.mol $^{-1}$ were prepared by following a similar procedure as for Expt. 1 but with a polymerization time of 8 h. Experimental conditions were as follows: **P1d** ($f_{\text{MPDL},0} = 0.2$) [OEGMA (0.8805 g, 2.93 mmol), MPDL (0.1195 g, 0.74 mmol), Gem-digly-AMA-SG1 (266.6 mg, 2.66×10^{-1} mmol), SG1 (9 mg, 2.63×10^{-2} mmol) and toluene (1.0 g, 1.15 mL)], for **P2d** ($f_{\text{MPDL},0} = 0.4$) [OEGMA (0.7375 g, 2.46 mmol), MPDL (0.2660 g, 1.64 mmol), Gem-digly-AMA-SG1 (93.3 mg, 9.32×10^{-2} mmol), SG1 (3.2 mg, 9.36×10^{-3} mmol) and toluene (1.0 g, 1.15 mL)] and for **P3d** ($f_{\text{MPDL},0} = 0.7$) [OEGMA (0.4420 g, 1.47 mmol), MPDL (0.5580 g, 3.44 mmol), Gem-digly-AMA-SG1 (53.3 mg, 5.33×10^{-2} mmol), SG1 (1.7 mg, 4.89×10^{-3} mmol) and toluene (1.0 g, 1.15 mL)]. Final composition of the prodrug was determined by comparing the methoxy protons of OEG from OEGMA (at 3.4 ppm) to the aromatic protons of MPDL (at 7.2 ppm). The presence of Gem was quantitatively confirmed by ^{19}F NMR by comparing the integration of the fluorine atoms of the internal standard PFCE ($\delta = -88$ ppm) and of Gem ($\delta = -117$ ppm).

Synthesis of low molar mass poly[(oligo(ethylene glycol) methyl ether methacrylate)-co-styrene] (P(OEGMA-co-S)). Polymer prodrug without MPDL with targeted M_n of $\sim 10\,000$ g.mol $^{-1}$ were prepared by following a similar procedure as for Expt. 1 but with a polymerization time of 8 h. Experimental conditions were as follows: OEGMA (1.4436 g, 4.81 mmol), S (0.0563 g, 5.41×10^{-1} mmol), Gem-AMA-SG1 (7.0 mg, 1.14×10^{-1} mmol), and anhydrous toluene (1.5 g, 1.73 mL). SEC: $M_n = 10300$ g.mol $^{-1}$, $M_w/M_n = 1.29$.

Synthesis of low molar mass poly[(oligo(ethylene glycol) methyl ether methacrylate)-co-(2-methylene-4-phenyl-1,3-dioxolane)] (P(OEGMA-co-MPDL)). Copolymers without

Gem **P7** with targeted M_n of $\sim 10\,000\text{ g}\cdot\text{mol}^{-1}$ and $f_{\text{MPDL},0} = 0.4$ were prepared by following a similar procedure as for Expt. **1** but with a polymerization time of 8 h. Experimental conditions were as follows: OEGMA (1.1028 g, 3.68 mmol), MPDL (0.3972 g, 2.45 mmol), BlocBuilder MA (15.0 mg, 3.94×10^{-2} mmol), and anhydrous toluene (1.5 g, 1.73 mL). Final composition of the copolymer was determined by comparing the terminal methoxy protons of pendant OEG for OEGMA (at 3.4 ppm) to the aromatic hydrogens of MPDL (at $\delta = 7.2$ ppm). SEC: $M_n = 12100\text{ g}\cdot\text{mol}^{-1}$, $M_w/M_n = 1.30$. ^1H NMR: $F_{\text{MPDL}} = 0.13$.

Synthesis of low molar mass Gem-poly[(methyl methacrylate)-co-(2-methylene-4-phenyl-1,3-dioxolane)] (Gem-P(MMA-co-MPDL)). Copolymers with targeted M_n of $\sim 10\,000\text{ g}\cdot\text{mol}^{-1}$ were prepared by following a similar procedure as for Expt. **4** but with a polymerization time of 5 h. Experimental conditions were as follows: **P4** ($f_{\text{MPDL},0} = 0.2$) [MMA (1.0673 g, 10.67 mmol), MPDL (0.4327 g, 2.67 mmol), Gem-AMA-SG1 (340.0 mg, 5.56×10^{-1} mmol), SG1 (18.1 mg, 5.29×10^{-2} mmol) and anhydrous toluene (1.5 g, 1.73 mL)], for **P5** ($f_{\text{MPDL},0} = 0.4$) [MMA (0.7215 g, 7.22 mmol), MPDL (0.7785 g, 4.81 mmol), Gem-AMA-SG1 (230 mg, 3.76×10^{-1} mmol), SG1 (12.3 mg, 3.60×10^{-2} mmol) and anhydrous toluene (1.5 g, 1.73 mL)] and for **P6** ($f_{\text{MPDL},0} = 0.7$) [MMA (0.3135 g, 3.14 mmol), MPDL (1.1865 g, 7.32 mmol), Gem-AMA-SG1 (30.0 mg, 4.90×10^{-2} mmol), SG1 (1.6 mg, 4.69×10^{-3} mmol) and anhydrous toluene (1.5 g, 1.73 mL)]. Final composition of the prodrug was determined by comparing the methyl protons in α -position to the ester group of MMA (at 3.7 ppm) to the aromatic hydrogens of MPDL (at $\delta = 7.2$ ppm). The presence of Gem was quantitatively confirmed by ^{19}F NMR by comparing the integration of the fluorine atoms of the internal standard PFCE ($\delta = -88$ ppm) and of Gem ($\delta = -117$ ppm).

Synthesis of low molar mass Gem-digly-poly(methyl methacrylate)-co-(2-methylene-4-phenyl-1,3-dioxolane) (Gem-digly-P(MMA-co-MPDL)). Copolymers with targeted M_n of $\sim 10\,000\text{ g}\cdot\text{mol}^{-1}$ were prepared by following a similar procedure as for Expt. **4** but with a polymerization time of 5 h. Experimental conditions were as follows: **P4d** ($f_{\text{MPDL},0} = 0.2$) [MMA (1.0673 g, 10.67 mmol), MPDL (0.4327 g, 2.67 mmol), Gem-digly-AMA-SG1 (152.0 mg, 1.52×10^{-1} mmol), SG1 (5.2 mg, 1.52×10^{-2} mmol) and anhydrous toluene (1.5 g, 1.73 mL)] for **P5d** ($f_{\text{MPDL},0} = 0.4$) [MMA (0.7215 g, 7.22 mmol), MPDL (0.7785 g, 4.81 mmol), Gem-digly-AMA-SG1 (100.0 mg, 9.99×10^{-2} mmol), SG1 (3.4 mg, 9.95×10^{-3} mmol) and anhydrous toluene (1.5 g, 1.73 mL)] and for **P6d** ($f_{\text{MPDL},0} = 0.7$) [MMA (0.3135 g, 3.14 mmol), MPDL (1.1865 g, 7.32 mmol), Gem-digly-AMA-SG1 (25 mg, 2.50×10^{-2} mmol), SG1 (0.9 mg, 2.63×10^{-3} mmol) and anhydrous toluene (1.5 g, 1.73 mL)]. Final composition of the prodrug was determined by comparing the methyl protons in α -position to the ester

group of MMA (at 3.7 ppm) to the aromatic hydrogen of MPDL (at $\delta = 7.2$ ppm). The presence of Gem was quantitatively confirmed by ^{19}F NMR by comparing the integration of the fluorine atoms of the internal standard PFCE ($\delta = -88$ ppm) and of Gem ($\delta = -117$ ppm).

Synthesis of low molar mass poly[(methyl methacrylate)-*co*-(2-methylene-4-phenyl-1,3-dioxolane)] (P(MMA-*co*-MPDL)). Copolymers without Gem **P8** with targeted M_n of $\sim 10\,000$ g.mol $^{-1}$ and $f_{\text{MPDL},0} = 0.7$ were prepared by following a similar procedure as for Expt. **4** but with a polymerization time of 5 h. Experimental conditions were as follows: MMA (0.3604 g, 3.60 mmol), MPDL (0.4010 g, 2.47 mmol), BlocBuilder MA (16.0 mg, 4.20×10^{-2} mmol), and anhydrous toluene (0.77 g, 0.89 mL). Final composition of the copolymer was determined by comparing the methyl protons in α -position to the ester group of MMA (at 3.7 ppm) to the aromatic hydrogen of MPDL (at $\delta = 7.2$ ppm). SEC: $M_n = 9100$ g.mol $^{-1}$, $M_w/M_n = 1.26$. ^1H NMR: $F_{\text{MPDL}} = 0.17$.

Synthesis of low molar mass poly[(methyl methacrylate)-*co*-styrene] (P(MMA-*co*-S)). Polymer prodrug without MPDL with targeted M_n of $\sim 10\,000$ g.mol $^{-1}$ were prepared by following a similar procedure as for Expt. **4** but with a polymerization time of 5 h. Experimental conditions were as follows: MMA (1.3393 g, 13.39 mmol), S (0.1607 g, 15.45 mmol), Gem-AMA-SG1 (2.81 mg, 4.59×10^{-2} mmol), and anhydrous toluene (1.5 g, 1.73 mL). SEC: $M_n = 9751$ g.mol $^{-1}$, $M_w/M_n = 1.33$.

d. Deprotection of the copolymers

Deprotection of Gem-digly-P(OEGMA-*co*-MPDL). The TBDMS-protected Gem-digly-P(OEGMA-*co*-MPDL) copolymer (100 mg) was dissolved in 0.5 mL THF and TBAF (1 M in THF, 50 μL) was added. The solution was allowed to stir for 30 min and the solvent was removed under reduced pressure. After solubilization in 2 mL of DCM, the organic phase was washed twice with brine, precipitated in a mixture of cold cyclohexane/petroleum ether (1/1, v/v) and dried under reduced pressure. The copolymers were analyzed by ^1H NMR and SEC. NMR analysis showed complete disappearance of TBDMS protecting groups (Figure S2) and ^{19}F NMR confirmed the quantitative presence of Gem.

Deprotection of Gem-digly-P(MMA-*co*-MPDL). The TBDMS-protected copolymer Gem-digly-P(MMA-*co*-MPDL) (100 mg) was dissolved in 0.5 mL THF and TBAF (1 M in THF, 50 μL) was added. The solution was allowed to stir for 30 min before pouring into 10 mL of MeOH. The copolymer was then precipitated cold MeOH and dried under high vacuum. Polymers were analyzed by ^1H NMR and SEC. NMR analysis showed complete

disappearance of TBDMS protecting groups (Figure S3) and ^{19}F NMR confirmed the quantitative presence of Gem.

e. Hydrolytic degradation

Hydrolytic degradation of Gem-P(OEGMA-*co*-MPDL). In a 5-mL vial, 50 mg of copolymer was dissolved in 5 mL of 5% KOH aqueous solution and stirred at room temperature. Samples (1 mL) were periodically taken, neutralized with 1 M HCl aqueous solution and lyophilized. 2 mL of chloroform was then added, allowing the salts to be filtrated off. Finally, the solvent was removed under reduced pressure and the degradation products were analyzed by SEC.

Hydrolytic degradation of Gem-P(MMA-*co*-MPDL). In a 5-mL vial, 50 mg of copolymer was dissolved in 2.5 mL of THF. After solubilization, 2.5 mL of potassium hydroxide solution (KOH, 5%) in methanol was added. The cloudy mixture was stirred at room temperature. Samples (1 mL) were periodically taken, immediately dried under vacuum and 2 mL of chloroform were added, allowing salts filtration. Finally, solvent was removed under reduced pressure and degradation products were analyzed by SEC. Note that the carboxylic acid chain ends after degradation can be responsible for aggregation of polymer chains during SEC analysis, resulting in larger apparent M_n . This problem was resolved by adding 0.1 % (w/w) of TFA in both the eluent and the sample.

f. Nanoparticle preparation

Nanoparticles were prepared by the nanoprecipitation technique.⁵¹ **For** Gem-P(MMA-*co*-MPDL) and Gem-digly-P(MMA-*co*-MPDL), 2 mg of copolymer was dissolved in 2 mL of THF, and added dropwise to 4 mL MilliQ water under stirring. For Gem-P(OEGMA-*co*-MPDL) and Gem-digly-P(OEGMA-*co*-MPDL), 2.5 mg of copolymer was dissolved in 0.5 mL of THF, and added dropwise to 1 mL MilliQ water under stirring. In all cases, THF was evaporated at ambient temperature using a Rotavapor. Average diameter (D_z) and zeta potential (ζ) measurements were carried out in triplicate.

g. Nanoprecipitation yield

The amount of Gem-P(OEGMA-*co*-MPDL) nanoparticles formed by nanoprecipitation was determined as followed. A minimal amount of 4 mL of nanoparticle suspension (corresponding at least to 10 mg of copolymer) were ultracentrifugated (40 000 rpm, 4 h, 4 °C). The supernatant and the pellet were separated and freeze-dried. The weight fraction of nanoparticles formed after nanoprecipitation was calculated according to: $w_{\text{nanoparticles}} = m_{\text{pellet}} / (m_{\text{pellet}} + m_{\text{supernatant}})$.

h. Drug release kinetics

To determine the release kinetics of Gem, 1.5 mL of Gem-P(OEGMA-*co*-MPDL) **P1–P3** and **P1d–P3d** (0.5 mg.mL⁻¹) or Gem-P(MMA-*co*-MPDL) **P4–P6** and **P4d–P6d** (0.5 mg.mL⁻¹) nanoparticles were added to 1.5 mL of human serum solution supplemented with 200 µg.mL⁻¹ tetrahydrouridine (THU).^{52,53} The mixture was incubated at 37 °C and aliquots (600 µL) of incubation medium were withdrawn at different time points (1, 4, 8 and 24 h), spiked with 60 µL of 10 µM. Theophylline (Internal Standard, IS) before addition of 1 mL of a mixture of acetonitrile/methanol (90/10, v/v) and ultracentrifugated (15000 g, 20 min, 4 °C). The supernatant was then evaporated to dryness under a nitrogen flow at 30 °C. The released drug was quantified by reverse-phase HPLC (Waters, Milford, MA 01757, USA) with a C18 column. Briefly, the chromatographic system consisted of a Waters 1525 Binary HPLC pump, a Waters 2707 Autosampler, a C18 Uptisphere column (3 µm, 150 × 4.6 mm; Interchim), HPLC column temperature controllers (model 7950 column heater and chiller; Jones Chromatography, Lakewood, CO), and a Waters 2998 programmable photodiode-array detector. The HPLC column was maintained at 30 °C and detection was monitored at 270 nm. The HPLC mobile phase consisted of a mixture of methanol and water with 0.05 M sodium acetate (pH 5.0, eluent A: 5/95, v/v; eluent B 97/3, v/v). The residues were dissolved in 100 µL of eluent A. Elution was performed at a flow rate of 0.8 mL.min⁻¹ isocratically for 8 min with eluent A followed by a linear gradient (1 min) to 100% eluent B. This was followed by a 15-min hold at eluent B and a 1 min linear gradient back to 100% eluent A. The system was held for 6 min for equilibration back to initial conditions.

i. Biological Evaluation

Cell lines and cell culture. Human pancreatic cancer cell line MiaPaCa-2 and human lung carcinoma cell line A549 were obtained from the American Type Culture Collection. All cell lines were maintained as recommended. Briefly, A549 and MiaPaCa-2 cells were grown in Dulbecco's minimal essential medium (DMEM). All media were supplemented with 10% heat-inactivated FBS (56 °C, 30 min), penicillin (100 U.mL⁻¹) and streptomycin (100 µg.mL⁻¹). Medium for MiaPaCa-2 cell line was supplemented with 2.5% heat-inactivated (56 °C, 30 min) horse serum (Gibco). Cells were maintained in a humid atmosphere at 37 °C with 5% CO₂.

In vitro anticancer activity. MTT [3-(4,5-dimethylthiazol-2-yl)-2,5-diphenyl tetrazolium bromide] was used to evaluate the cytotoxicity of the different polymer prodrugs. Briefly, cells (5 × 10³/well) were seeded in 96-well plates. After overnight incubation, the cells were then exposed to a series of concentration of polymer prodrugs, control polymers or free Gem for 72 h (A549 cells) or 120 h (MiaPaCa-2 cells). 20 µL of MTT solution (5 mg.mL⁻¹ in PBS) were then added for each well. The plates were incubated for 1 h at 37 °C and the medium was removed. 200 µL of DMSO were then added to each well to dissolve the precipitates. Absorbance was measured at 570 nm using a plate reader (Metertech Σ 960, Fisher Bioblock, Illkirch, France). The percentage of surviving cells was calculated as the absorbance ratio of treated to untreated cells. The inhibitory concentration 50% (IC₅₀) of the treatments was determined from the dose-response curve. All experiments were set up in sextuplicate to determine means and SDs.

III. Results and Discussions

a. Synthetic strategy

To illustrate our approach, gemcitabine (Gem, 2'-deoxy-2',2'-difluorocytidine) was selected as an anticancer drug. Gem is a nucleoside analog approved for the treatment of various solid tumors including lung, pancreatic, breast, or ovarian cancers.⁵⁴ However, severe limitations restrict its clinical use and drastically reduce its efficacy: (i) short plasma half-life and rapid renal excretion due to rapid deamination by deoxycytidine deaminase, (ii) induction of resistances owing to inhibition of transmembrane transporter nucleoside, and (iii) severe side effects as a result of frequent administration schedule. Therefore, new prodrug strategies applied to Gem are of high importance in the field of nanomedicine.

This new class of polymer prodrugs was synthesized by nitroxide-mediated radical ring-opening copolymerization (NMrROP) between a methacrylic ester and 2-methylene-4-phenyl-1,3-dioxolane (MPDL) as a CKA, from a Gem-functionalized alkoxyamine initiator (Figure 1). This synthetic pathway was built upon our previous findings showing that MPDL, a 5-membered CKA, is a very attractive monomer that can be easily obtained and efficiently incorporated into a polymethacrylate backbone by NMrROP, resulting in well-defined copolymers with tunable level of ester group insertion and up to nearly complete degradation upon hydrolysis.^{49,55}

To establish structure-activity relationships and to obtain structures with the highest activity against cancer cells, various structural parameters were varied such as the nature of the methacrylic ester, the composition of the copolymer and the nature of the drug-copolymer linker (Figure 2). More specifically, two different methacrylic ester monomers were copolymerized with MPDL: either oligo(ethylene glycol) methyl ether methacrylate (OEGMA) as a hydrophilic monomer or methyl methacrylate (MMA) as a hydrophobic one (Figure 2a and c). Copolymerizations were initiated by two different alkoxyamines based on the SG1 nitroxide, which only differed in the nature of the linker between Gem and the alkoxyamine moiety: an amide bond (Gem-AMA-SG1) or an amide bond connected to a labile diglycolate linker (Gem-digly-AMA-SG1) (Figure 2b). Variable initial amounts of MPDL were also investigated to confer the resulting polymer prodrugs with distinct levels of degradability.

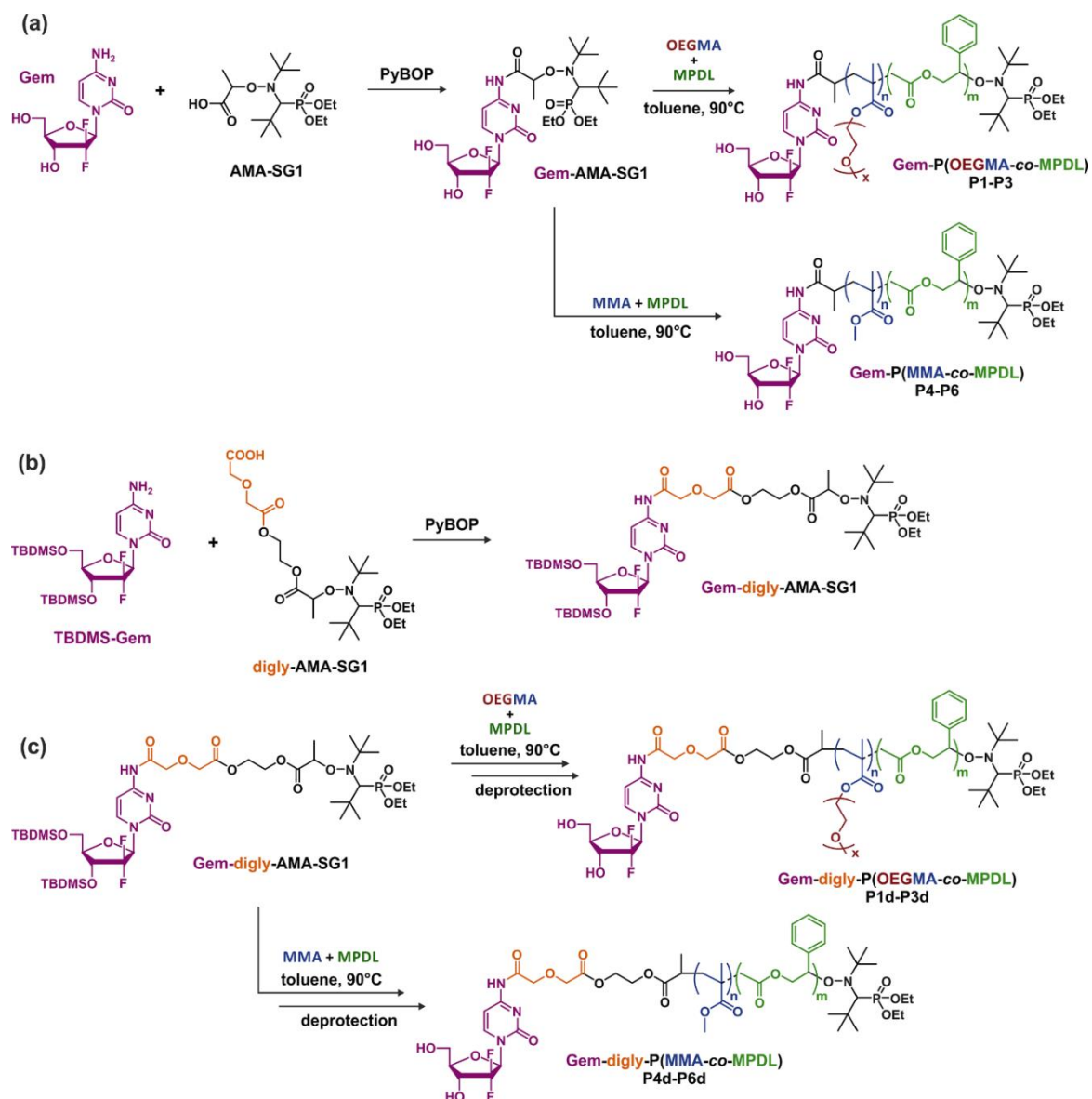


Figure 2. Synthesis of (a) Gem-P(OEGMA-co-MPDL) **P1–P3** and Gem-P(MMA-co-MPDL) **P4–P6** by NMrROP in toluene at 90°C, (b) Gem-digly-AMA-SG1 by PyBOP-assisted coupling between TBDMS-Gem and digly-AMA-SG1 and (c) Gem-digly-P(OEGMA-co-MPDL) **P1d–P3d** and Gem-digly-P(MMA-co-MPDL) **P4d–P6d** by NMrROP in toluene at 90°C, followed by TBDMS group removal.

b. Synthesis of Gem-based alkoxyamine initiators

Given its susceptibility to deamination,⁵⁶ Gem was derivatized through its C-4 amino group. Gem-AMA-SG1 was synthesized by direct coupling between unprotected Gem and AMA-SG1 using PyBOP as a coupling agent.¹⁰ For Gem-digly-AMA-SG1, best conditions were obtained via protection of the two hydroxyl group with TBDMSCl,¹¹ followed by PyBOP-

assisted coupling of the resulting TBDMSGem with AMA-digly-SG1 (Figure 2b). The expected product (Figure S1) was obtained with a coupling yield of 63%.

c. Copolymerization kinetics

A comprehensive kinetic study was first performed to investigate the influence of the different parameters on the control of the copolymerization. Gem-AMA-SG1 or Gem-digly-AMA-SG1 alkoxyamines were used to initiate the NMrROP of OEGMA (expts. **1–3** and **1d–3d**, Figure 3) or MMA (expts. **4–6** and **4d–6d**, Figure 4) in presence of variable initial fraction of MPDL ($f_{\text{MPDL},0} = 0.2\text{--}0.7$) at 90 °C in 50 wt.% toluene. In all cases, the higher the initial fraction of MPDL, the better the control of the copolymerization. For $f_{\text{MPDL},0} = 0.2$, regardless of methacrylic ester used (expts. **1**, **1d**, **4** and **4d**), the copolymerizations did not exhibit a first order kinetics while M_n values hardly increased with conversion and were much higher than the theoretical ones with rather high dispersities after 50% conversion, thus indicating a partial control. Such a low initial amount of MPDL was therefore not sufficient for efficient insertion of MPDL in the copolymer (according to the reactivity ratios) to prevent irreversible termination reactions. For $f_{\text{MPDL},0} = 0.4$, (expts. **2**, **2d**, **5** and **5d**), the control over the polymerization was significantly improved, leading to nearly first order kinetics, linear increase of M_n with conversion, exhibiting values closer to the theoretical ones, and lower dispersities even at high conversion for expts. **4–6** and **4d–6d**. Control was further enhanced for $f_{\text{MPDL},0} = 0.7$ (expt. **3**, **3d**, **6** and **6d**).

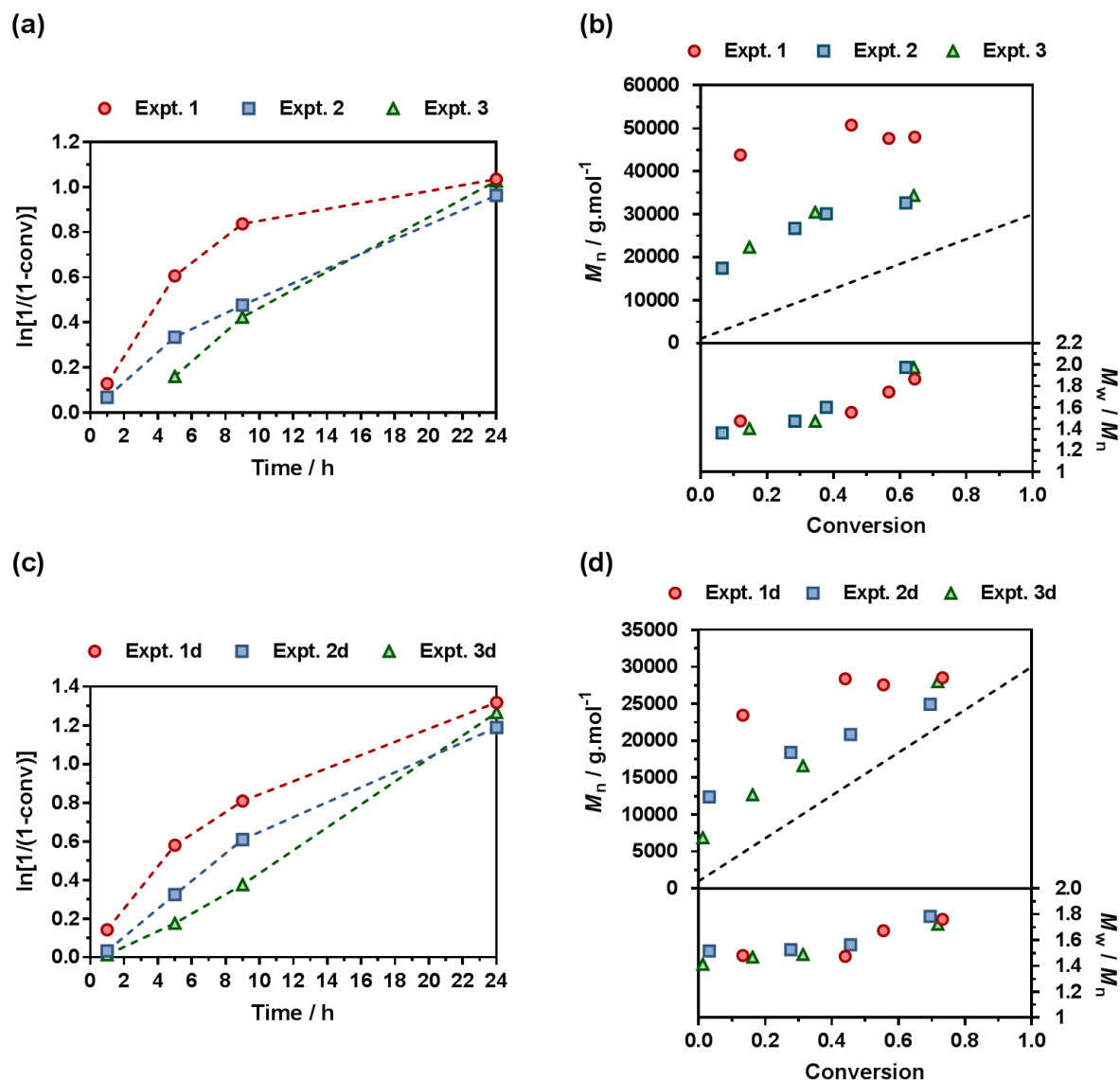


Figure 3. NMRROP of OEGMA and MPDL in 50 wt.% toluene at 90 °C as a function of the nature of the alkoxyamine initiator [(a) and (b) Gem-AMA-SG1, (c) and (d) Gem-digly-AMA-SG1] and the initial fraction of MPDL: \square expts. **1** and **1d** ($f_{MPDL,0} = 0.2$), \blacksquare expts. **2** and **2d** ($f_{MPDL,0} = 0.4$), \blacktriangle expts. **3** and **3d** ($f_{MPDL,0} = 0.7$). (a) and (c) $\ln[1/(1-conv)]$ vs. time ($conv =$ OEGMA conversion). Dashed lines connecting data points are guides for the eye only. (b) and (d) Number-average molar mass, M_n and dispersity, M_w/M_n , vs. conversion. The dashed black line represents the theoretical M_n .

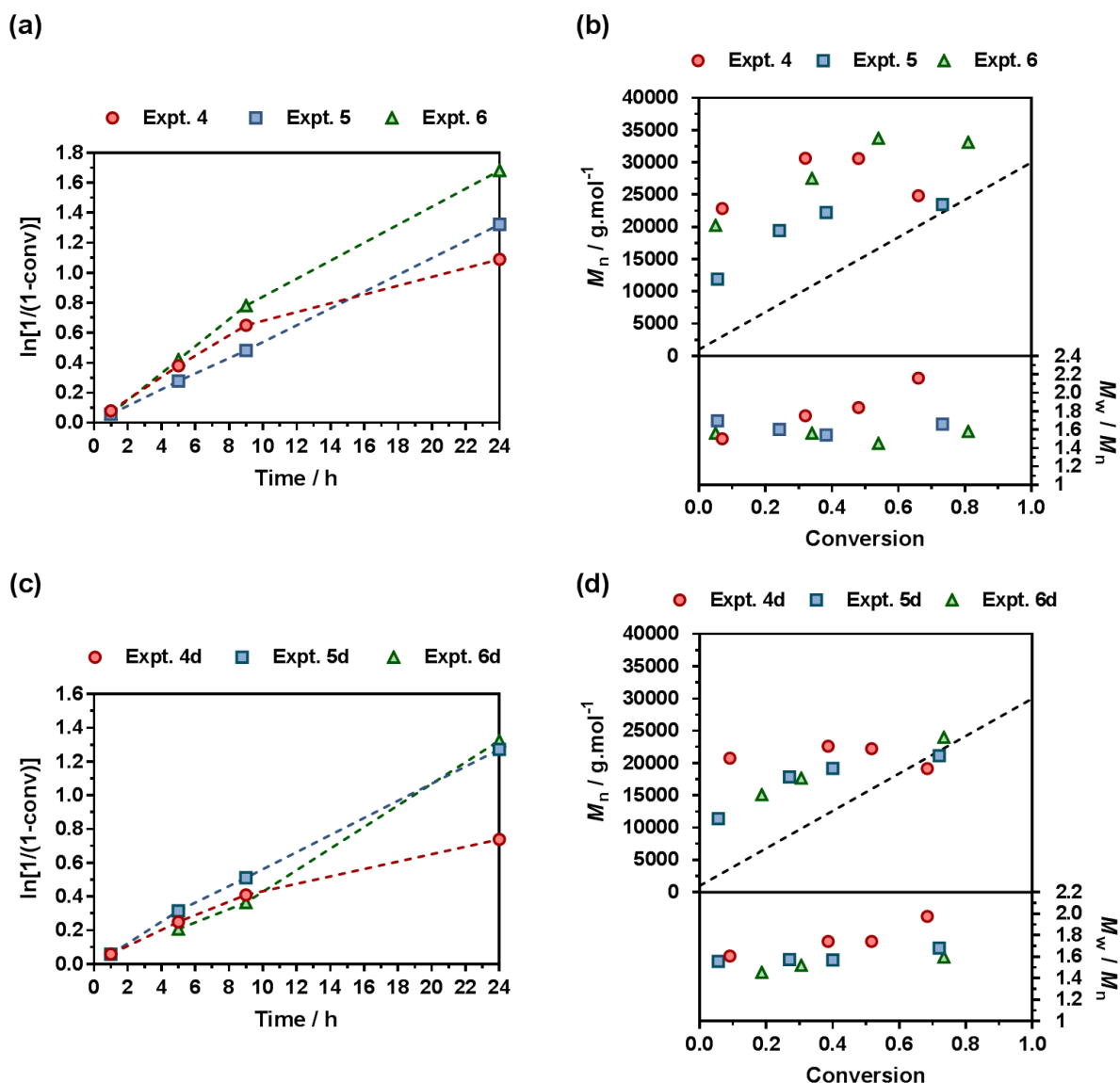


Figure 4. NMRROP of MMA and MPDL in 50 wt.% toluene at 90 °C as a function of the nature of the alkoxyamine initiator [(a) and (b) Gem-AMA-SG1, (c) and (d) Gem-digly-AMA-SG1] and the initial fraction of MPDL: \square expts. **4** and **4d** ($f_{\text{MPDL},0} = 0.2$), \blacksquare expts. **5** and **5d** ($f_{\text{MPDL},0} = 0.4$), \blacktriangle expts. **6** and **6d** ($f_{\text{MPDL},0} = 0.7$). (a) and (c) $\ln[1/(1-\text{conv})]$ vs. time (conv = MMA conversion). Dashed lines connecting data points are guides for the eye only. (b) and (d) Number-average molar mass, M_n and dispersity, M_w/M_n , vs. conversion. The dashed black line represents the theoretical M_n .

Interestingly, the control was generally better when the copolymerizations were initiated by Gem-digly-AMA-SG1 compared to those initiated by Gem-AMA-SG1. M_n values and dispersities at high conversions were indeed systematically lower with Gem-digly-AMA-SG1. This trend can be explained by the structure of the alkoxyamines and its influence on the

dissociation rate and subsequently on the control of the polymerization. Conversely to Gem-digly-AMA-SG1, Gem-AMA-SG1 is prone to intramolecular hydrogen-bonding (IHB) between the hydrogen of the amide from the propagating radical and the nitroxide fragment.⁵⁷ Therefore, a new bond to cleave during dissociation is generated and consequently, the dissociation kinetic is hindered, leading to a less efficient control.

d. Synthesis of low molar mass polymer prodrugs for biological evaluations

One of the main benefits of the drug-initiated method is the facile tuning of the drug loading simply by varying the M_n of the polymer, which is of great importance for further biological evaluation. Herein, we targeted lower molar mass polymer prodrugs ($M_n \sim 10\,000 \text{ g}\cdot\text{mol}^{-1}$) to obtain a drug loading of $\sim 2.5 \text{ wt.}\%$ by adapting the reaction conditions (e.g., lower reaction times and/or lower targeted M_n , see experimental part). Four libraries of well-defined copolymer prodrugs from each series were prepared (Table 1 and Figure S4): Gem-P(OEGMA-*co*-MPDL) (**P1–P3**), Gem-digly-P(OEGMA-*co*-MPDL) (**P1d–P3d**), Gem-P(MMA-*co*-MPDL) (**P4–P6**) and Gem-digly-P(MMA-*co*-MPDL) (**P4d–P6d**). A lower reaction time also enabled improving the control by avoiding high monomer conversion and thus extensive occurrence of irreversible termination reactions. Overall, dispersities of the resulting copolymers ranged from 1.1–1.4, except for **P1** which control was difficult to achieve given the very low amount of inserted MPDL and the use of the less efficient alkoxyamine (as detailed in the previous section). ¹H NMR spectroscopy of the purified copolymers (and deprotected for **P1d–P6d**) showed all signals expected for each structure (Figures S5–S8) and ¹⁹F NMR spectroscopy confirmed the quantitative presence of Gem at the extremity of the copolymers.

Table 1. Experimental Conditions and Macromolecular Properties of Gem-based P(OEGMA-*co*-MPDL) and P(MMA-*co*-MPDL) polymer prodrugs.

Prodrug	Alkoxyamine	Methacrylic ester	$f_{\text{MPDL},0}$	Conv. ^a (%) / Temps (h)	M_n^b (g/mol)	D^b	F_{MPDL}^c
P1	Gem-AMA-SG1	OEGMA	0.2	40 / 8	15 500	1.54	0.06
P2	Gem-AMA-SG1	OEGMA	0.4	28 / 8	10 200	1.39	0.12
P3	Gem-AMA-SG1	OEGMA	0.7	18 / 8	10 000	1.37	0.25

P1d	Gem-digly-AMA-SG1	OEGMA	0.2	61 / 8	11 500	1.24	0.07
P2d	Gem-digly-AMA-SG1	OEGMA	0.4	36 / 8	13 200	1.24	0.11
P3d	Gem-digly-AMA-SG1	OEGMA	0.7	22 / 8	11 200	1.13	0.22
P4	Gem-AMA-SG1	MMA	0.2	35 / 5	13 200	1.27	0.10
P5	Gem-AMA-SG1	MMA	0.4	34 / 5	9 900	1.28	0.19
P6	Gem-AMA-SG1	MMA	0.7	23 / 5	10 300	1.21	0.29
P4d	Gem-digly-AMA-SG1	MMA	0.2	56 / 8	15 400	1.34	0.07
P5d	Gem-digly-AMA-SG1	MMA	0.4	55 / 8	12 400	1.29	0.12
P6d	Gem-digly-AMA-SG1	MMA	0.7	33 / 8	10 900	1.20	0.29

^a Methacrylic ester conversion determined by ¹H NMR. ^b Determined by SEC after precipitation. ^c Determined by ¹H NMR.

Despite unfavorable reactivity ratios of the different monomer pairs ($r_{\text{MPDL}} = 0$ and $r_{\text{OEGMA}} = 6.95$,⁵⁵ and $r_{\text{MPDL}} = 0.01$ and $r_{\text{MMA}} = 4.0$ ⁴⁹), the molar fraction of MPDL in the copolymer (F_{MPDL}) was finely tuned by varying the initial molar fraction of MPDL in the comonomer feed (Table 1) to induce different levels of degradability. On average, F_{MPDL} was ~ 0.07 for $f_{\text{MPDL},0} = 0.2$, ~ 0.13 for $f_{\text{MPDL},0} = 0.4$ and ~ 0.26 for $f_{\text{MPDL},0} = 0.7$.

e. Hydrolytic degradation of the prodrugs

The degradation of the different copolymer prodrugs was then evaluated under accelerated conditions to probe the presence of ester group in the polymer backbone; that is at room temperature in 5 % KOH, either in water for OEGMA-based copolymers (**P1–P3**) or in a THF/MeOH (50:50, v/v) mixture for MMA-based copolymers (**P4–P6**). As expected, control copolymers without MPDL ($F_{\text{MPDL}} = 0$), Gem-P(OEGMA-co-S) and Gem-P(MMA-co-S), gave no sign of degradation as shown by their constant M_n over time. Conversely, MPDL-containing copolymer prodrugs led to adjustable degradation in direct relationship with their MPDL content, as shown by the shifts of the SEC chromatograms towards lower M_n values (Figure S9–S10). Whatever the nature of the methacrylic ester, the higher the MPDL content, the greater the degradation. The M_n decrease (Figure 5) spanned from 10–30% for copolymers with the lowest MPDL contents (**P1** and **P4**) to $\sim 70\%$ for those with the highest amounts of MPDL (**P3** and **P6**). These results confirmed the significant insertion of open MPDL units in the main chain of the copolymers and the possibility to fine-tune their degradation by adjusting the initial comonomer stoichiometry.

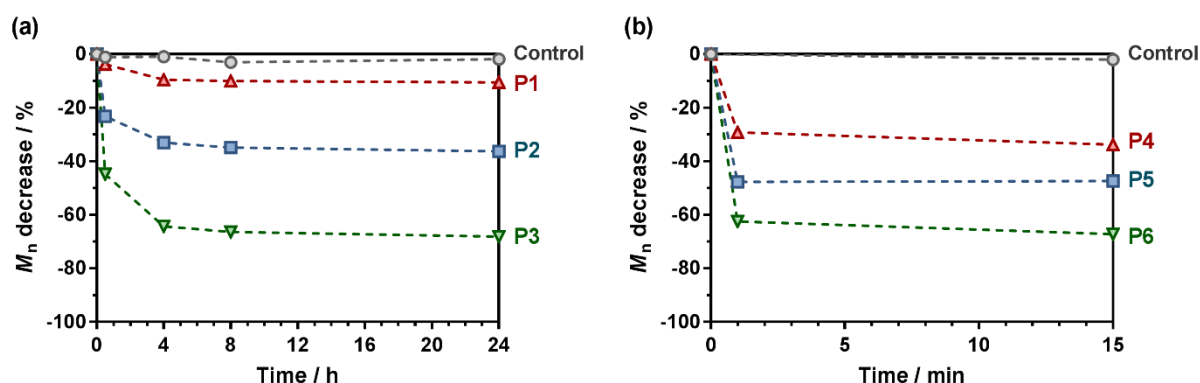


Figure 5. Hydrolytic degradation under accelerated conditions (5% KOH) of the different degradable polymer prodrugs as a function of the MPDL fraction and the nature of the methacrylic ester monomer: (a) Gem-P(OEGMA-co-MPDL); ●, control ($F_{\text{MPDL}} = 0$); ▲, **P1** ($F_{\text{MPDL}} = 0.06$); ■, **P2** ($F_{\text{MPDL}} = 0.12$); ▼, **P3** ($F_{\text{MPDL}} = 0.25$). (b) Gem-P(MMA-co-MPDL); ●, control ($F_{\text{MPDL}} = 0$); ▲, **P4** ($F_{\text{MPDL}} = 0.10$); ■, **P5** ($F_{\text{MPDL}} = 0.19$); ▼, **P6** ($F_{\text{MPDL}} = 0.29$). Dashed lines are guides for the eye only.

f. Physicochemical properties

Given their hydrophobic backbone and the water-solubility of Gem, Gem-P(MMA-co-MPDL) (**P4–P6**) and Gem-digly-P(MMA-co-MPDL) (**P4d–P6d**) prodrugs were formulated into nanoparticles in water. They displayed an average diameter (D_z) in the 110–200 nm range, along with narrow particle size distributions (PSD, Table 2).

Table 2. Characterization of Gem-P(MMA-co-MPDL) and Gem-digly-P(MMA-co-MPDL) Nanoparticles.

Prodrug	D_z^a 58	PSD ^a	ζ^b (mV)	%Gem ^c (wt. %)
P4	196	0.09	-55	2.0
P5	162	0.10	-57	2.6
P6	174	0.09	-55	2.5
P4d	109	0.13	-37	1.7
P5d	110	0.11	-38	2.1
P6d	117	0.10	-46	2.4

^a Determined by DLS. ^b Zeta potential, determined by the DLS apparatus. ^c Determined according to: %Gem = $MW_{\text{Gem}}/M_{n,\text{SEC}}$.

Interestingly, nanoparticles prepared from **P4d–P6d** were significantly smaller than **P4–P6**, possibly because of the additional hydrophilicity provided by the diglycolate linker, promoting Gem positioning at the surface of the nanoparticles and thus inducing a more efficient stabilization. Representative Cryo-TEM images showed spherical morphologies in good agreement with DLS data (Figure 6a and 6b). All nanoparticles exhibited great colloidal stability over time as shown by their constant size and size distributions for at least 25 days after nanoprecipitation (Figure 6c). Such an efficient colloidal stability is likely the result of an efficient electrostatic stabilization, as shown by significantly negative zeta potential measurements (Table 2).

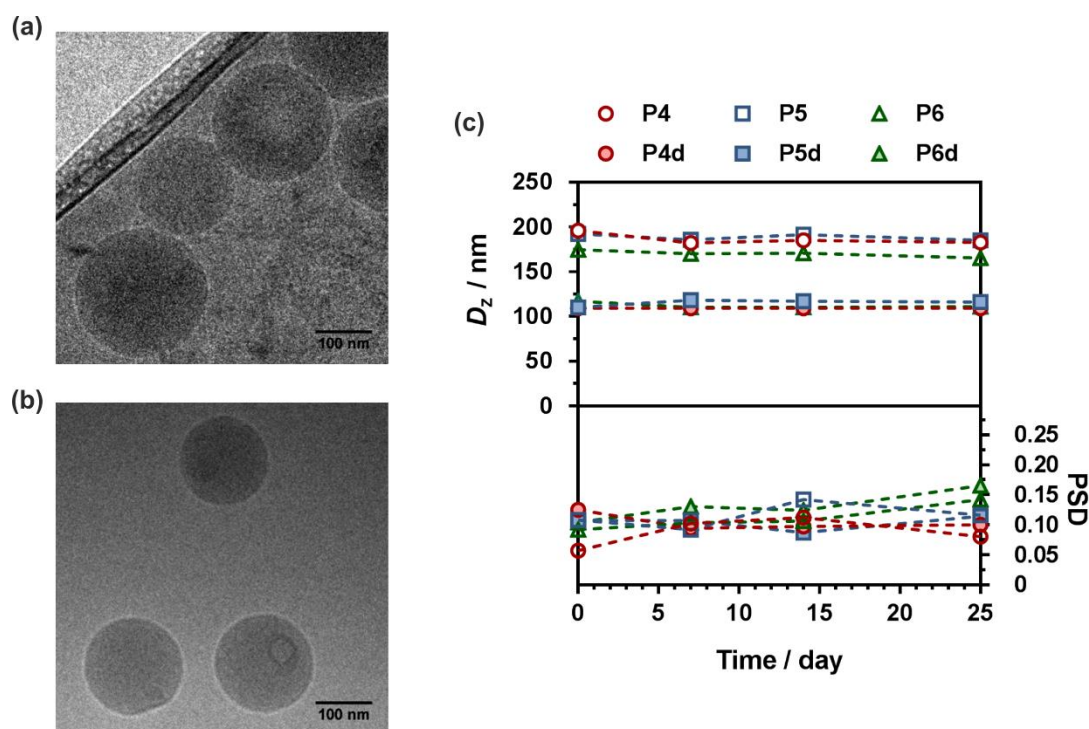


Figure 6. Representative Cryo-TEM images of (a) Gem-P(MMA-co-MPDL) **P6** and (b) Gem-digly-P(MMA-co-MPDL) **P6d** nanoparticles. (c) Evolution with time of the average diameter and the particle size distribution (PSD) of Gem-P(MMA-co-MPDL) (**P4–P6**) and Gem-digly-P(MMA-co-MPDL) (**P4d–P6d**) nanoparticles in water determined by DLS.

Given the relatively moderate F_{MPDL} values for P(OEGMA-co-MPDL) copolymers, water-solubility of OEGMA was expected to dominate over hydrophobicity from MPDL units, and thus preferentially lead to fully water-soluble polymer prodrugs. To validate this hypothesis, Gem-P(OEGMA-co-MPDL) prodrugs with increasing contents of MPDL (**P1–P3**) were

nanoprecipitated in water and the amount of nanoparticles was quantified by measurement of the dry content after ultracentrifugation (see experimental part and Table S1). The weight fraction of nanoparticles was estimated to maximum 16 wt.% for the copolymer containing the highest amount of MPDL ($F_{\text{MPDL}} = 0.25$) to less than 1 wt.% for the one with the lowest amount ($F_{\text{MPDL}} = 0.06$).

g. Drug release in human serum

The Gem release kinetics from the two different classes of polymer prodrugs was evaluated in human serum to mimic the biological environment of the human body. For Gem-P(OEGMA-*co*-MPDL) **P1–P3**, the total Gem release gradually increased from ~7 to ~25 % when decreasing F_{MPDL} from 0.25 to 0.06 (Figure 7a). Analogous copolymers with the diglycolate linker (**P1d–P3d**) led to the same trend but with a significantly higher Gem release; from ~33 % for $F_{\text{MPDL}} = 0.22$ to ~70 % for $F_{\text{MPDL}} = 0.07$ (Figure 7b). Replacing OEGMA by MMA in the polymer prodrug structures (**P4–P6** and **P4d–P6d**) led to the exact same trend but with significantly lower Gem release contents. Gem-P(MMA-*co*-MPDL) nanoparticles **P4–P6** led to nearly no Gem release (< 2 %) whereas Gem-digly-P(MMA-*co*-MPDL) nanoparticles (**P4d–P6d**) allowed final Gem release contents to reach 7–13 % (Figure 7c and d). This may be explained not only by the detrimental effect of hydrophobic MMA units nearby the Gem-polymer linker, but also by the nanoparticulate nature of the polymer prodrug itself, both preventing water uptake and/or enzyme access.

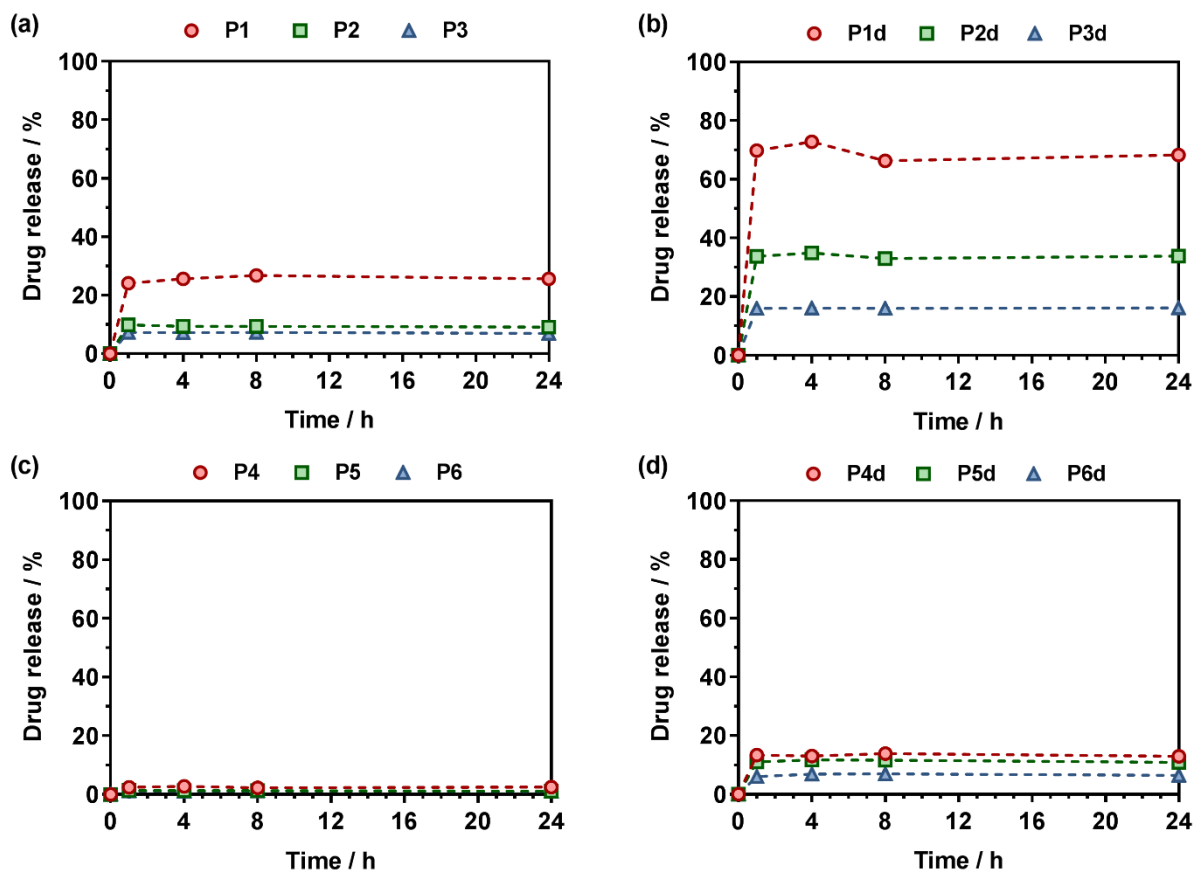


Figure 7. Gem release profiles at 37 °C in human serum from (a) Gem-P(OEGMA-*co*-MPDL) (**P1-P3**), (b) Gem-digly P(OEGMA-*co*-MPDL) (**P1d-P3d**), (c) Gem-P(MMA-*co*-MPDL) (**P4-P6**) and (d) Gem-digly-P(MMA-*co*-MPDL) (**P4d-P6d**).

Alltogether, these results showed that Gem release was independently governed by: (i) the MPDL content –the lower the MPDL content, the greater the Gem release; (ii) the nature of the linker –the presence of the diglycolate linker enabled a greater Gem release compared to a simple amide bond and (iii) the hydrophilicity of the methacrylate monomer –OEGMA enabled a greater Gem release compared to MMA. It is therefore suggested that increasing the hydrophilicity nearby the drug-polymer linkage, by using OEGMA and/or from decreasing the MPDL fraction in the copolymer, had a beneficial influence on the Gem release. Regarding the diglycolate linker, its beneficial impact may be explained by: (i) its higher lability compared to a single amide bond that may enable its rapid cleavage and (ii) its connection to the amide bond that may promote the amide bond accessibility to enzymes.

h. *In vitro* anticancer activity

A crucial question is whether the above-mentioned drug release trends observed in human serum directly correlate with anticancer activity of the polymer prodrug. To answer this question, the cell viability of two cancer cell lines corresponding to clinically relevant cancer models for Gem, human lung carcinoma (A549) and human pancreatic cancer (MiaPaCa-2), was determined after incubation with the different polymer prodrugs at various concentrations.

Gem-free control copolymers, P(OEGMA-*co*-MPDL) **P7** and P(MMA-*co*-MPDL) **P8**, were not cytotoxic for all concentrations tested while free Gem exhibited half maximal inhibitory concentrations (IC₅₀) of 4 nM and 14 nM for A549 and MiaPaCa-2 cells, respectively. When increasing the MPDL fraction, IC₅₀ values of Gem-P(OEGMA-*co*-MPDL) **P1–P3** increased from 0.30 to 2.14 μM for A549 cells and from 0.13 to 1.07 μM for MiaPaCa-2 cells (Figure 8). As expected from drug release experiments, diglycolate-containing polymer prodrugs (**P1d–P3d**) gave the same trend but were significantly more cytotoxic, leading to IC₅₀ values 5-8-fold lower for A549 cells (Figure 8a and 8b) to 3–4-fold lower for MiaPaCa-2 cells (Figure 8c and 8d) compared to those obtained from **P1–P3**.

Also in agreement with drug release experiments, Gem-P(MMA-*co*-MPDL) **P4–P6** and Gem-digly-P(MMA-*co*-MPDL) **P4d–P6d** polymer prodrug nanoparticles (Figure 9) were always less cytotoxic than OEGMA-based counterparts. Importantly, whatever the cell line, no decrease in cell viability was obtained for **P4–P6** even at the highest concentrations, whereas the use of the diglycolate linker led the corresponding prodrugs to be cytotoxic, especially for those containing less MPDL (**P5d** and **P6d**, see Figure 9b and 9d). As suggested from drug release experiments, this trend may be correlated with a too high hydrophobicity nearby the Gem-polymer linker, but also to the nanoparticulate nature of the polymer prodrugs that, conversely to fully water-soluble counterparts, were less accessible to water/enzymes, thus preventing efficient release of Gem (only surface exposed Gem-digly moieties were likely accessible for cleavage). Note that, in general, higher cytotoxicity was observed against MiaPaCa-2 cells, with nearly complete cell death. This is explained by the fact that A549 cells are known to exhibit some resistance against Gem, as evidenced by a plateau at 20 % of cell viability.⁵⁹

In a nutshell, the results on both cell lines were in excellent agreement with those obtained from drug release experiments: (i) polymer prodrugs based on P(OEGMA-*co*-MPDL) were more cytotoxic than those based on P(MMA-*co*-MPDL); (ii) increasing the MPDL fraction in the copolymers led to a decrease in cytotoxicity and (iii) polymer prodrugs based on the diglycolate linker were significantly more cytotoxic than those based on a single

amide linkage (See Table S2 for all IC_{50} values). Remarkably, the best candidates, Gem-digly-P(OEGMA-*co*-MPDL) **P1d** enabled to reach the cytotoxic activity of free Gem.

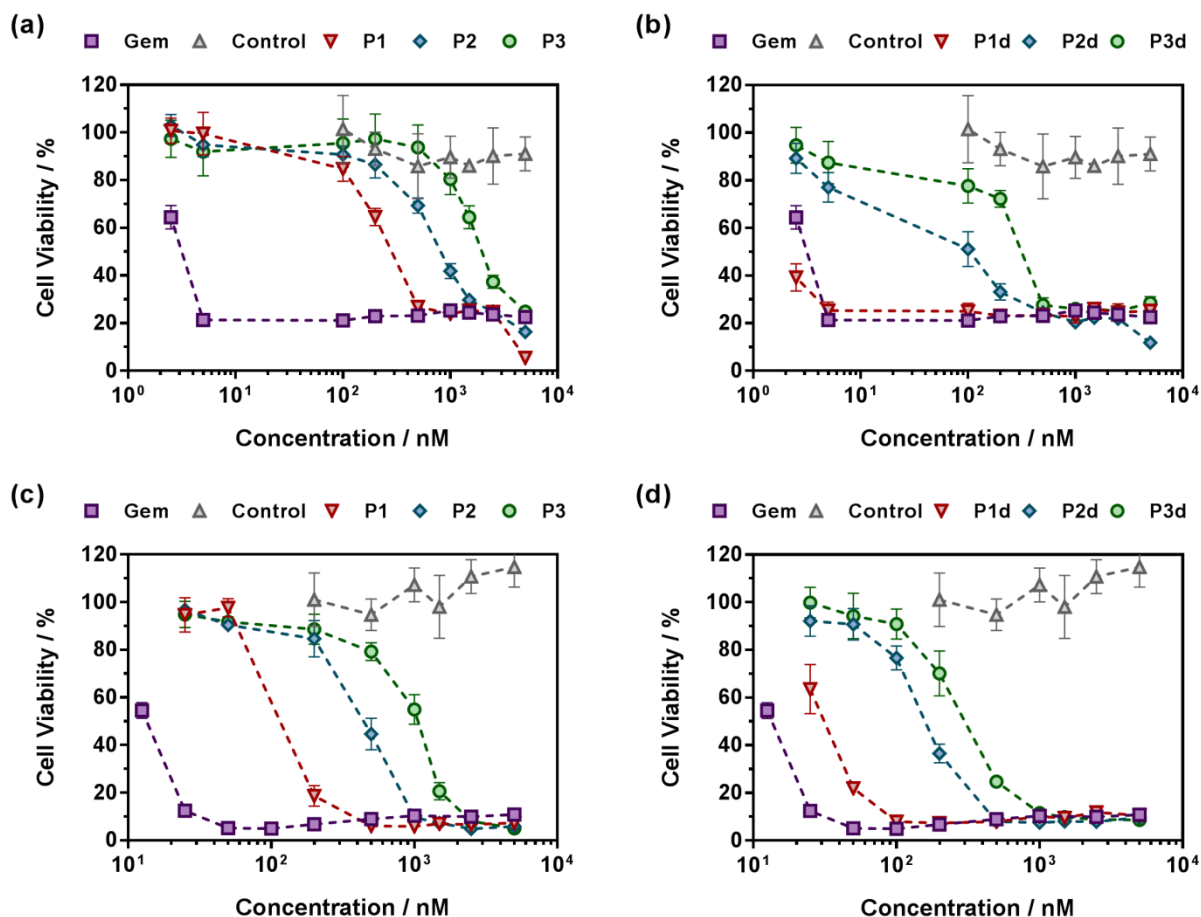


Figure 8. Cell viability (MTT test) with increasing concentrations of (a, c) Gem-P(OEGMA-*co*-MPDL) (**P1–P3**) or (b, d) Gem-digly-P(OEGMA-*co*-MPDL) (**P1d–P3d**) on (a, b) A549 cells and (c, d) MiaPaCa-2 cells.

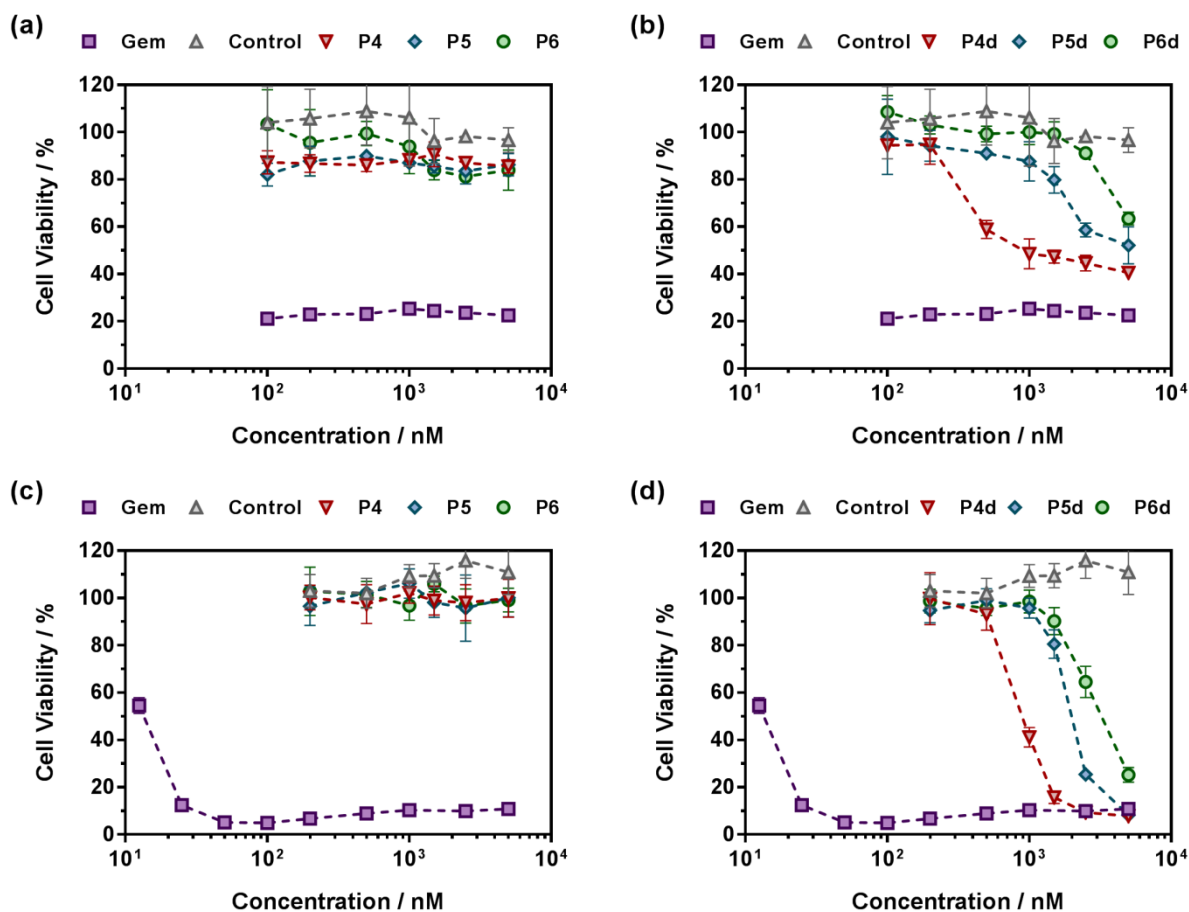


Figure 9. Cell viability (MTT test) with increasing concentrations of (a, c) Gem-P(MMA-co-MPDL) (P4–P6) or (b, d) Gem-digly-P(MMA-co-MPDL) (P4d–P6d) on (a, b) A549 cells and (c, d) MiaPaCa-2 cells.

IV. Conclusion

Degradable vinyl polymer prodrugs were designed by “*drug-initiated*” NMrROP of a methacrylic ester monomer with MPDL from an alkoxyamine derivatized with Gem as an anticancer drug. Two libraries of polymer prodrugs differing by the nature of the methacrylic ester monomer (OEGMA or MMA), the nature of the drug-polymer linker and the MPDL content were prepared. Whereas MMA-based prodrugs formed highly stable nanoparticles upon nanoprecipitation, OEGMA-based prodrugs were water-soluble. The degradation of the copolymer prodrugs was proved under accelerated conditions (i.e., basic hydrolysis) and the degradation level was finely tuned by adjusting the MPDL content. Drug-release profiles in human serum and in vitro anticancer activity against two different cancer cell lines helped to establish structure/activity relationships and select the most favorable structural parameters for having the best activity. We demonstrated that three structural parameters independently

governed the anticancer activity: (i) soluble OEGMA-based prodrugs were more cytotoxic than MMA-based counterpart; (ii) the lower the MPDL content, the greater the anticancer activity and (iii) a diglycolate linker gave a greater activity compared to a simple amide bond. Interestingly, this versatile approach could be extended to other pathologies by using different drugs and to other molecules (e.g., fluorescent dye, imaging agent) for theranostic applications.

References

- (1) Nicolas, J.; Mura, S.; Brambilla, D.; Mackiewicz, N.; Couvreur, P. *Chem. Soc. Rev.* **2013**, *42*, 1147.
- (2) Farokhzad, O. C.; Langer, R. *ACS Nano* **2009**, *3*, 16.
- (3) Delplace, V.; Couvreur, P.; Nicolas, J. *Polym. Chem.* **2014**, *5*, 1529.
- (4) Nicolas, J. *Chem. Mater.* **2016**, *28*, 1591.
- (5) Tong, R.; Cheng, J. *Angew. Chem.* **2008**, *120*, 4908.
- (6) Tong, R.; Cheng, J. *J. Am. Chem. Soc.* **2009**, *131*, 4744.
- (7) Tong, R.; Cheng, J. *Bioconjugate Chem.* **2009**, *21*, 111.
- (8) Tong, R.; Cheng, J. *Macromolecules* **2012**, *45*, 2225.
- (9) Yin, Q.; Tong, R.; Xu, Y.; Baek, K.; Dobrucki, L. W.; Fan, T. M.; Cheng, J. *Biomacromolecules* **2013**, *14*, 920.
- (10) Harrisson, S.; Nicolas, J.; Maksimenko, A.; Bui, D. T.; Mouglin, J.; Couvreur, P. *Angewandte Chemie International Edition* **2013**, *52*, 1678.
- (11) Trung Bui, D.; Maksimenko, A.; Desmaële, D.; Harrisson, S.; Vauthier, C.; Couvreur, P.; Nicolas, J. *Biomacromolecules* **2013**, *14*, 2837.
- (12) Bao, Y.; Boissenot, T.; Guégain, E.; Desmaële, D.; Mura, S.; Couvreur, P.; Nicolas, J. *Chem. Mater.* **2016**, *28*, 6266.
- (13) Bao, Y.; Guégain, E.; Nicolas, V.; Nicolas, J. *Chem. Commun.* **2017**.
- (14) Bao, Y.; Nicolas, J. *Polym. Chem.* **2017**.
- (15) Williams, C. C.; Thang, S. H.; Hantke, T.; Vogel, U.; Seeberger, P. H.; Tsanaktsidis, J.; Lepenies, B. *ChemMedChem* **2012**, *7*, 281.
- (16) Louage, B.; Nuhn, L.; Risseeuw, M. D.; Vanparijs, N.; De Coen, R.; Karalic, I.; Van Calenbergh, S.; De Geest, B. G. *Angewandte Chemie International Edition* **2016**, *55*, 11791.
- (17) Louage, B.; van Steenberg, M. J.; Nuhn, L.; Risseeuw, M. D.; Karalic, I.; Winne, J.; Van Calenbergh, S.; Hennink, W. E.; De Geest, B. G. *ACS Macro Letters* **2017**, *6*, 272.
- (18) Nicolas, J.; Guillaneuf, Y.; Lefay, C.; Bertin, D.; Gigmès, D.; Charleux, B. *Prog. Polym. Sci.* **2013**, *38*, 63.
- (19) Moad, G.; Rizzardo, E.; Thang, S. H. *Aust. J. Chem.* **2009**, *62*, 1402.
- (20) Delplace, V.; Nicolas, J. *Nature Chem.* **2015**, *7*, 771.
- (21) Tardy, A.; Nicolas, J.; Gigmès, D.; Lefay, C.; Guillaneuf, Y. *Chem. Rev.* **2017**, *117*, 1319.
- (22) Agarwal, S. *Polym. Chem.* **2010**, *1*, 953.
- (23) Kopčanský, P.; Tomašovičová, N.; Koneracka, M.; Timko, M.; Závěšová, V.; Tomčo, L. *Acta Electrotechnica et Informatica* **2010**, *10*, 10.
- (24) Bailey, W. J.; Wu, S. R.; Ni, Z. *Die Makromolekulare Chemie* **1982**, *183*, 1913.
- (25) Bailey, W. J.; Ni, Z.; Wu, S. R. *Journal of Polymer Science: Polymer Chemistry Edition* **1982**, *20*, 3021.
- (26) Bailey, W. J.; Ni, Z.; Wu, S. R. *Macromolecules* **1982**, *15*, 711.
- (27) Bailey, W. J.; Zhou, L.-L. *Tetrahedron Lett.* **1991**, *32*, 1539.
- (28) Seema, A.; Liqun, R. *Macromolecules* **2009**, *42*, 1574.
- (29) Ren, L.; Speyerer, C.; Agarwal, S. *Macromolecules* **2007**, *40*, 7834.
- (30) Undin, J.; Finne-Wistrand, A.; Albertsson, A.-C. *Biomacromolecules* **2013**, *14*, 2095.
- (31) Undin, J.; Illanes, T.; Finne-Wistrand, A.; Albertsson, A.-C. *Polym. Chem.* **2012**, *3*, 1260.
- (32) Wickel, H.; Agarwal, S. *Macromolecules* **2003**, *36*, 6152.
- (33) Wickel, H.; Agarwal, S.; Greiner, A. *Macromolecules* **2003**, *36*, 2397.

- (34) Shi, Y.; Schmalz, H.; Agarwal, S. *Polym. Chem.* **2015**, *6*, 6409.
- (35) Huang, J.; Gil, R.; Matyjaszewski, K. *Polymer* **2005**, *46*, 11698.
- (36) Lutz, J.-F.; Andrieu, J.; Üzgün, S.; Rudolph, C.; Agarwal, S. *Macromolecules* **2007**, *40*, 8540.
- (37) Riachi, C.; Schüwer, N.; Klok, H.-A. *Macromolecules* **2009**, *42*, 8076.
- (38) Siegwart, D. J.; Bencherif, S. A.; Srinivasan, A.; Hollinger, J. O.; Matyjaszewski, K. *Journal of Biomedical Materials Research Part A* **2008**, *87*, 345.
- (39) Yuan, J.-Y.; Pan, C.-Y. *Eur. Polym. J.* **2002**, *38*, 2069.
- (40) Hedir, G. G.; Bell, C. A.; Jeong, N. S.; Chapman, E.; Collins, I. R.; O'Reilly, R. K.; Dove, A. P. *Macromolecules* **2014**, *47*, 2847.
- (41) Paulusse, J. M.; Amir, R. J.; Evans, R. A.; Hawker, C. J. *J. Am. Chem. Soc.* **2009**, *131*, 9805.
- (42) Smith, Q.; Huang, J.; Matyjaszewski, K.; Loo, Y.-L. *Macromolecules* **2005**, *38*, 5581.
- (43) Ganda, S.; Jiang, Y.; Thomas, D. S.; Eliezar, J.; Stenzel, M. H. *Macromolecules* **2016**, *49*, 4136.
- (44) Kobben, S.; Ethirajan, A.; Junkers, T. *Journal of Polymer Science Part A: Polymer Chemistry* **2014**, *52*, 1633.
- (45) Hedir, G. G.; Bell, C. A.; O'Reilly, R. K.; Dove, A. P. *Biomacromolecules* **2015**, *16*, 2049.
- (46) Hedir, G.; Arno, M.; Langlais, M.; Husband, J.; O'Reilly, R.; Dove, A. *Angewandte Chemie International Edition* **2017**.
- (47) Evans, R. A.; Rizzardo, E. *Macromolecules* **1996**, *29*, 6983.
- (48) Harrisson, S.; Davis, T. P.; Evans, R. A.; Rizzardo, E. *Macromolecules* **2001**, *34*, 3869.
- (49) Tran, J.; Guegain, E.; Ibrahim, N.; Harrisson, S.; Nicolas, J. *Polym. Chem.* **2016**.
- (50) Bao, Y.; Boissenot, T.; Guégain, E.; Desmaële, D.; Mura, S.; Couvreur, P.; Nicolas, J. *Chem. Mater.* **2016**.
- (51) Fessi, H.; Puisieux, F.; Devissaguet, J. P.; Ammoury, N.; Benita, S. *Int. J. Pharm.* **1989**, *55*, R1.
- (52) Mura, S.; Buchy, E.; Askin, G.; Cayre, F.; Mougín, J.; Gouazou, S.; Sobot, D.; Valetti, S.; Stella, B.; Desmaele, D. *Biochimie* **2016**, *130*, 4.
- (53) Maksimenko, A.; Mougín, J.; Mura, S.; Sliwinski, E.; Lepeltier, E.; Bourgaux, C.; Lepêtre, S.; Zouhiri, F.; Desmaële, D.; Couvreur, P. *Cancer Lett.* **2013**, *334*, 346.
- (54) Hertel, L. W.; Boder, G. B.; Kroin, J. S.; Rinzel, S. M.; Poore, G. A.; Todd, G. C.; Grindey, G. B. *Cancer Res.* **1990**, *50*, 4417.
- (55) Delplace, V.; Guégain, E.; Harrisson, S.; Gigmès, D.; Guillaneuf, Y.; Nicolas, J. *Chem. Commun.* **2015**, *51*, 12847.
- (56) Heinemann, V.; Xu, Y.-Z.; Chubb, S.; Sen, A.; Hertel, L. W.; Grindey, G. B.; Plunkett, W. *Cancer Res.* **1992**, *52*, 533.
- (57) Guégain, E.; Delplace, V.; Trimaille, T.; Gigmès, D.; Siri, D.; Marque, S. R.; Guillaneuf, Y.; Nicolas, J. *Polym. Chem.* **2015**, *6*, 5693.
- (58) Hu, X.; Hu, J.; Tian, J.; Ge, Z.; Zhang, G.; Luo, K.; Liu, S. *Journal of the American Chemical Society* **2013**, *135*, 17617.
- (59) Ikeda, R.; Vermeulen, L. C.; Lau, E.; Jiang, Z.; Sachidanandam, K.; Yamada, K.; Kolesar, J. M. *Int. J. Oncol.* **2011**, *38*, 513.

Supplementary Information

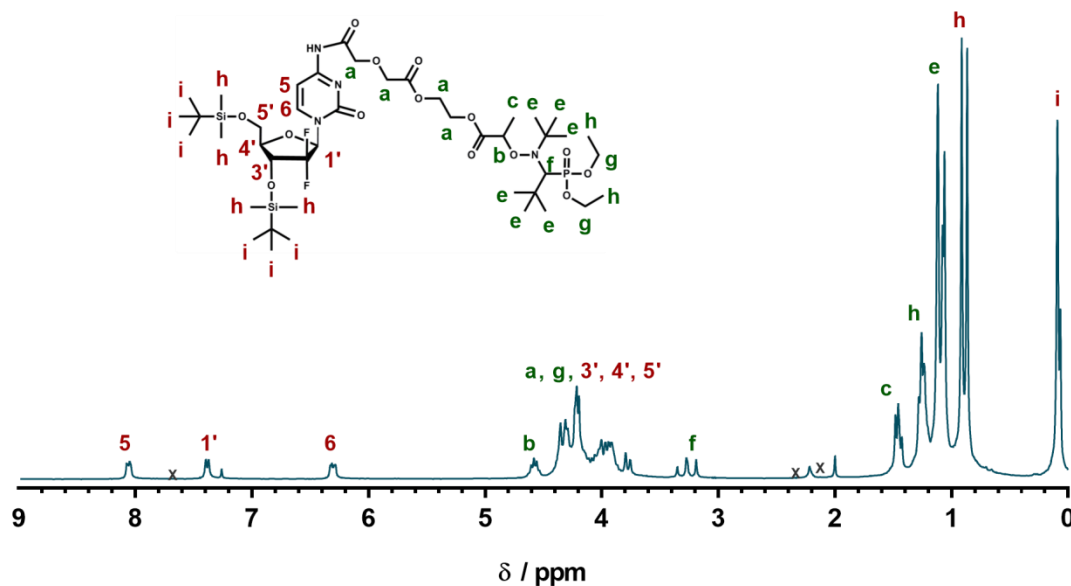


Figure S2. ^1H NMR spectrum in CDCl_3 in the 0–8.5 ppm region of Gem-digly-AMA-SG1.

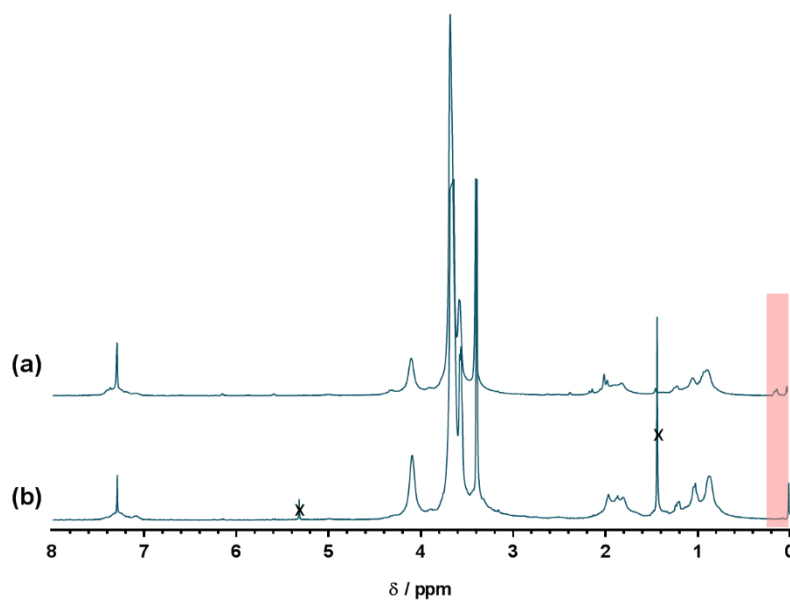


Figure S2. ^1H NMR spectrum in CDCl_3 in the 0–8 ppm region of Gem-digly-P(OEGMA-co-MPDL) **P2d** ($f_{\text{MPDL},0} = 0.4$), (a) after one precipitation and before deprotection and (b) after deprotection. The colored area shows the TBDMS group and its removal after deprotection.

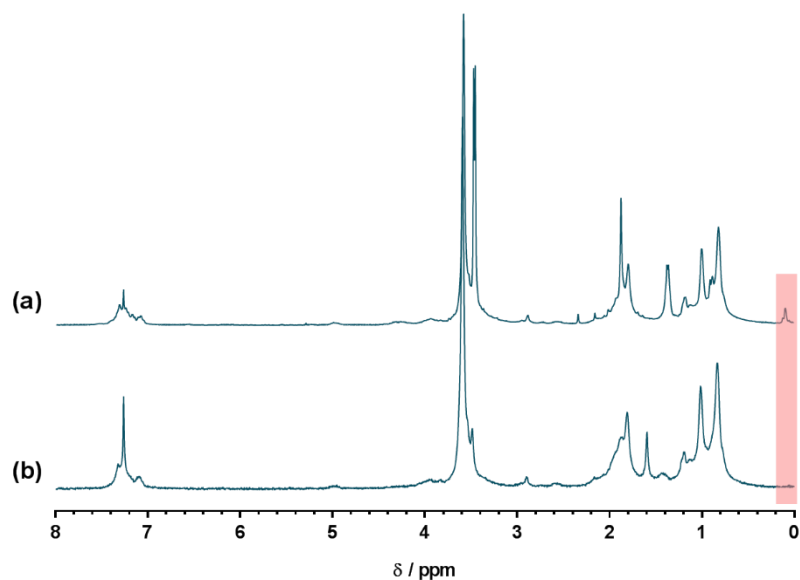


Figure S3. ^1H NMR spectrum in CDCl_3 in the 0–8 ppm region of Gem-digly-P(MMA-*co*-MPDL) **P5d** ($f_{\text{MPDL},0} = 0.4$), (a) after one precipitation and before deprotection and (b) after deprotection. The colored area shows the TBDMS group and its removal after deprotection.

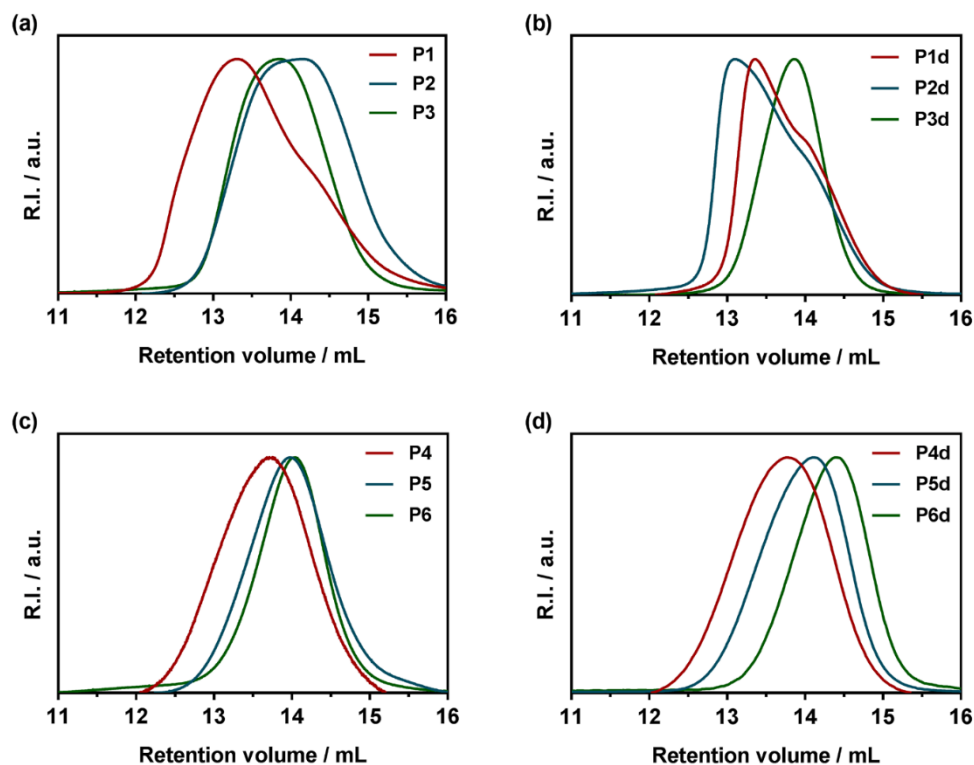


Figure S4. Size exclusion chromatograms (CHCl_3 eluent, $1 \text{ mL}\cdot\text{min}^{-1}$) of (a) Gem-P(OEGMA-*co*-MPDL), **P1–P3**, (b) Gem-digly-P(OEGMA-*co*-MPDL), **P1d–P3d**, (c) Gem-P(MMA-*co*-MPDL), **P4–P6** and (d) Gem-digly-P(MMA-*co*-MPDL), **P4d–P6d**.

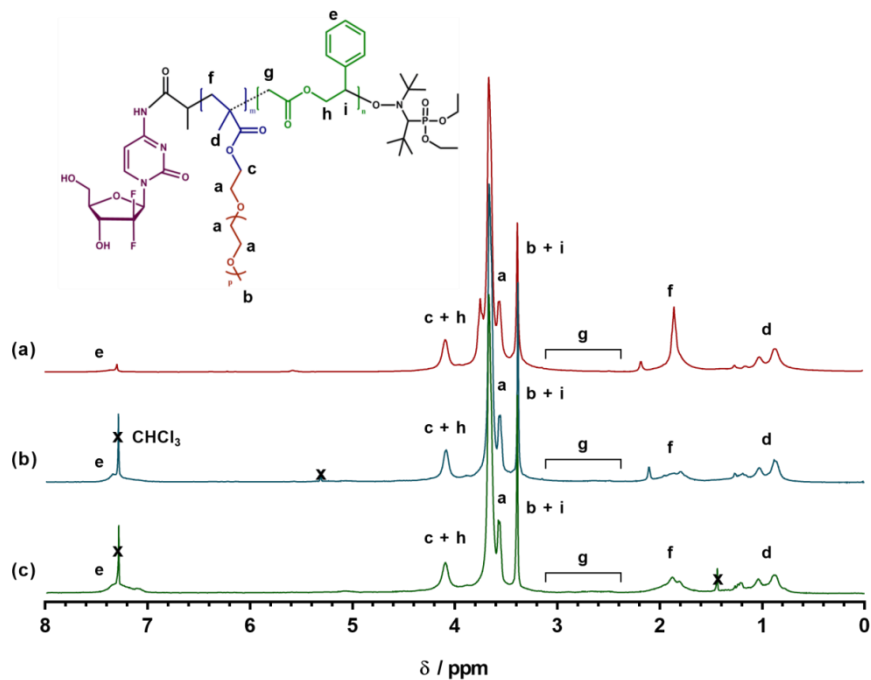


Figure S5. ^1H NMR spectra in CDCl_3 in the 0–8 ppm region of Gem-P(OEGMA-*co*-MPDL) with (a) **P1** ($f_{\text{MPDL},0} = 0.2$); (b) **P2** ($f_{\text{MPDL},0} = 0.4$); (c) **P3** ($f_{\text{MPDL},0} = 0.7$).

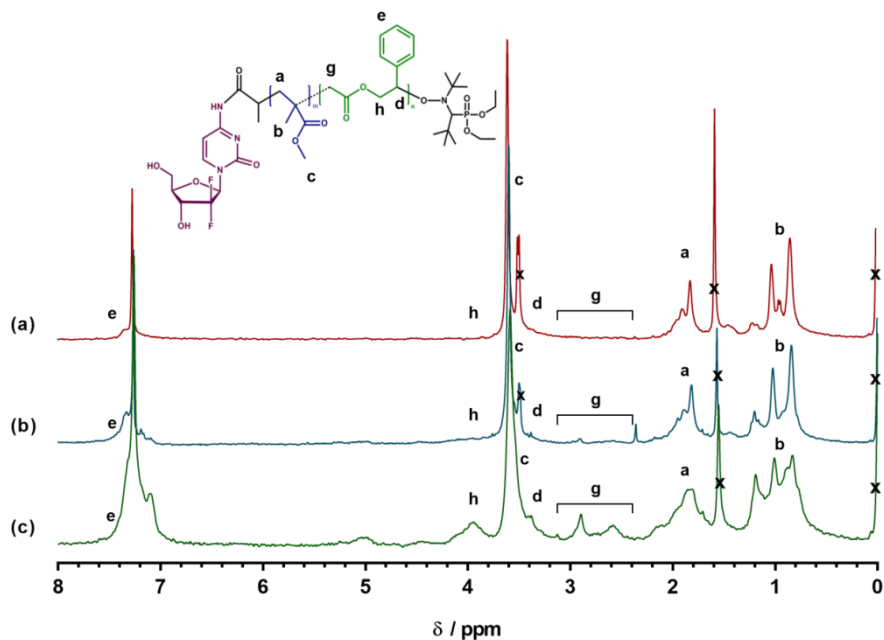


Figure S6. ^1H NMR spectra in CDCl_3 in the 0–8 ppm region of Gem-P(MMA-*co*-MPDL) with (a) **P4** ($f_{\text{MPDL},0} = 0.2$); (b) **P5** ($f_{\text{MPDL},0} = 0.4$); (c) **P6** ($f_{\text{MPDL},0} = 0.7$).

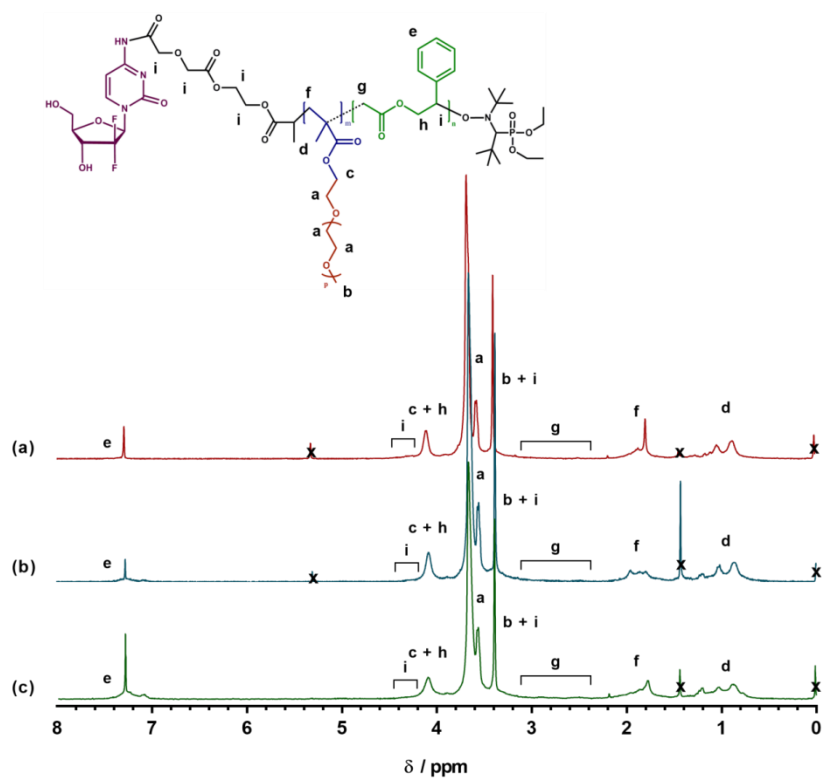


Figure S7. ^1H NMR spectra in CDCl_3 in the 0–8 ppm region of Gem-digly-P(OEGMA-co-MPDL) with (a) **P1d** ($f_{\text{MPDL},0} = 0.2$); (b) **P2d** ($f_{\text{MPDL},0} = 0.4$); (c) **P3d** ($f_{\text{MPDL},0} = 0.7$).

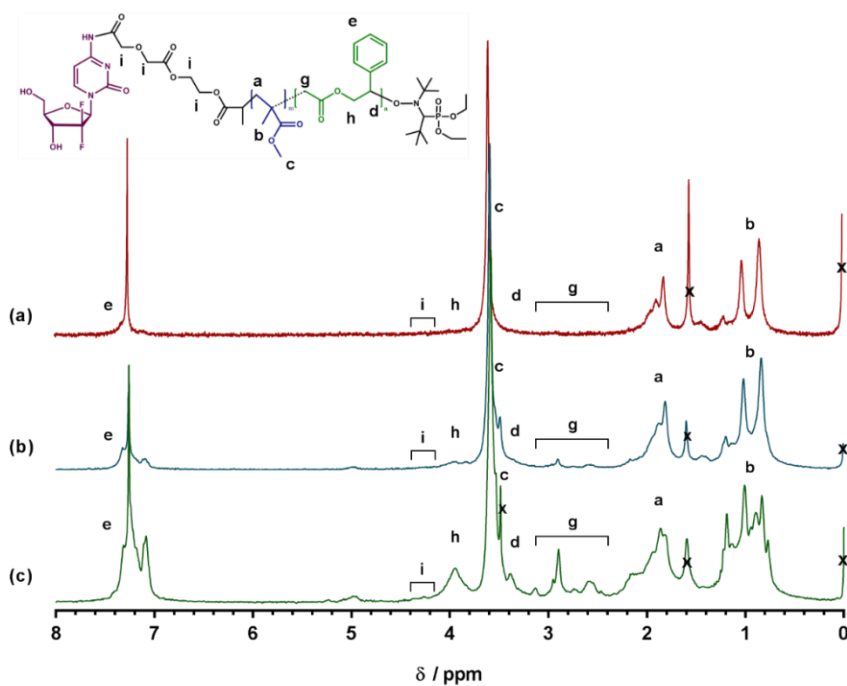


Figure S8. ^1H NMR spectra in CDCl_3 in the 0–8 ppm region of Gem-digly-P(MMA-co-MPDL) with (a) **P4d** ($f_{\text{MPDL},0} = 0.2$); (b) **P5d** ($f_{\text{MPDL},0} = 0.4$); (c) **P6d** ($f_{\text{MPDL},0} = 0.7$).

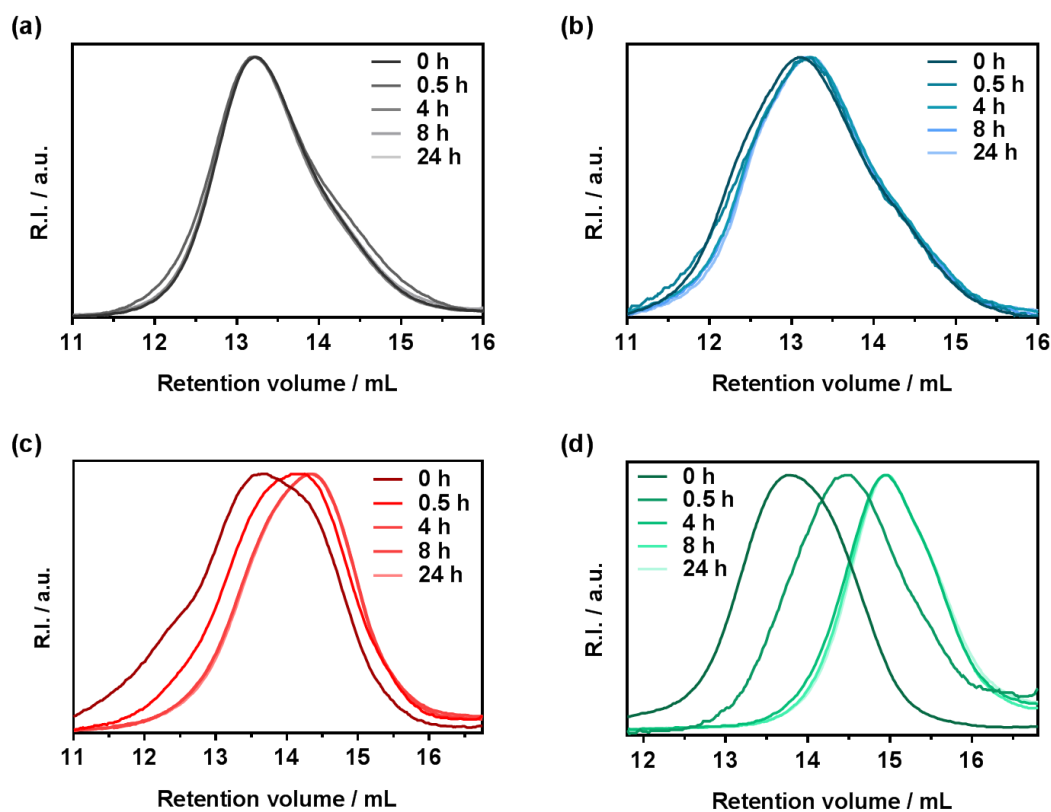


Figure S9. (a) Evolution of the SEC chromatograms at different time during the hydrolytic degradation under accelerated conditions (KOH 5%) of Gem-P(OEGMA-*co*-MPDL) as function of the MPDL content: (a) ●, control ($F_{\text{MPDL}} = 0$); (b) ▲, **P1** ($F_{\text{MPDL}} = 0.06$); (c) ■, **P2** ($F_{\text{MPDL}} = 0.12$); (d) ▼, **P3** ($F_{\text{MPDL}} = 0.25$).

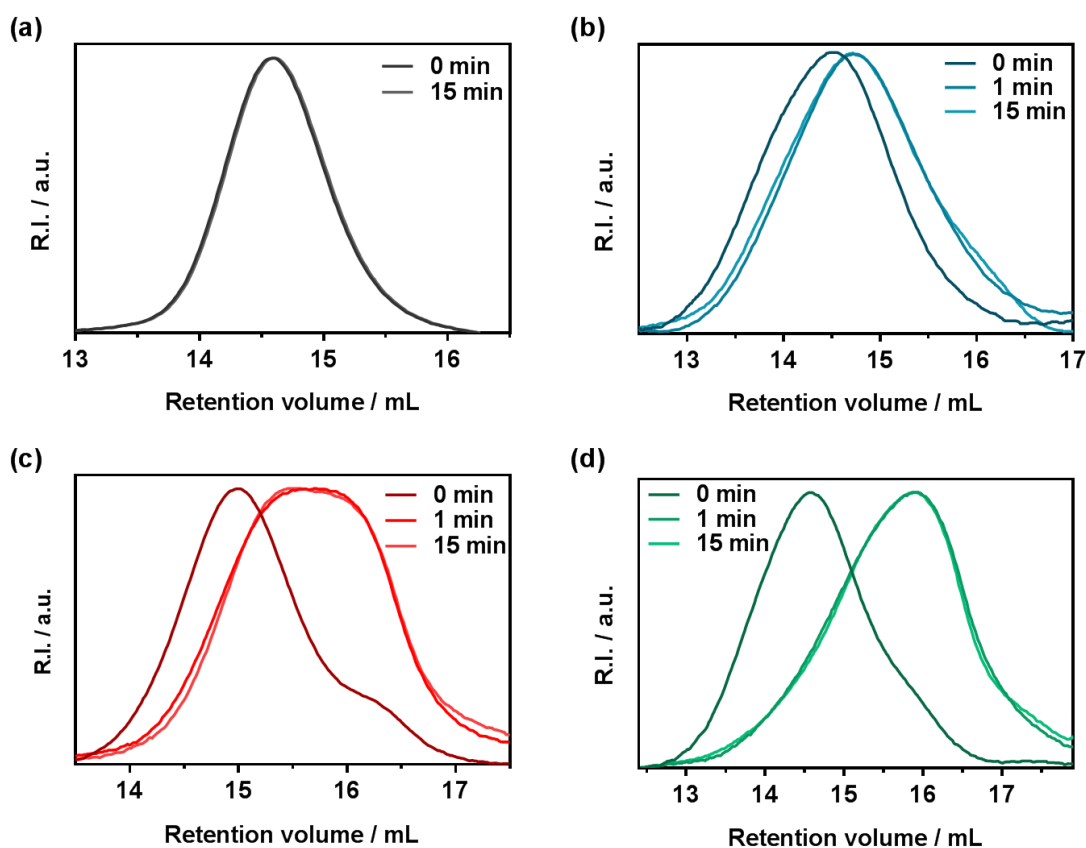


Figure S10. (a) Evolution of the SEC chromatograms at different time during the hydrolytic degradation under accelerated conditions (KOH 5%) of Gem-P(OEGMA-*co*-MPDL) as function of the MPDL content: (a) ●, control ($F_{\text{MPDL}} = 0$); (b) ▲, **P1** ($F_{\text{MPDL}} = 0.06$); (c) ■, **P2** ($F_{\text{MPDL}} = 0.12$); (d) ▼, **P3** ($F_{\text{MPDL}} = 0.25$).

Table S1. Characterization of Gem-P(OEGMA-*co*-MPDL) Nanoparticles.

Prodrug	D_z 1	PSD	%NP (wt. %)
P1	166	0.51	< 1
P2	146	0.13	8
P3	163	0.19	16

Table S2. In Vitro Cytotoxicity (IC_{50}) of Gem-Based Polymer Prodrugs Against A549 and MiaPaCa-2 Cancer Cells.

Prodrug	F_{MPDL} (mol. %)	A549 IC_{50} (μM)	MiaPaCa-2 IC_{50} (μM)
---------	-------------------------------	-------------------------------------	--

Chapter 6 - Degradable Polymer Prodrugs with Adjustable Activity from Drug-Initiated Radical Ring-Opening Copolymerization

P1	6	0.30	0.13
P2	12	0.88	0.45
P3	25	2.14	1.07
P1d	7	0.04	0.03
P2d	11	0.11	0.17
P3d	22	0.40	0.34
P4	10	-	-
P5	19	-	-
P6	29	-	-
P4d	7	~1	0.92
P5d	12	-	2.11
P6d	29	-	3.55

Chapter 7

General Discussion

In a nutshell, the main goal of my PhD thesis was to combine two distinct approaches: the radical ring-opening copolymerization (rROP) of cyclic ketene acetals with traditional vinyl monomers, for the design of (bio)degradable polymers and the “*drug-initiated*” strategy as a way to synthesize vinyl polymer prodrugs for cancer therapy. Therefore, the overall objective was to design new degradable polymer prodrugs from the “*drug initiated*” strategy for anticancer therapy. This goal was progressively reached, by targeting intermediates objectives:

- First, we aimed at determining the impact of functionalization on the controlling ability of various alkoxyamine based on the SG1 nitroxide.
- We then developed a new class of degradable vinyl copolymers (either hydrophobic or hydrophilic) based on 2-methylene-4-phenyl-1,3-dioxolane (MPDL) as a CKA, whose synthesis was optimized.
- We thoroughly investigated their hydrolytic degradation under physiological conditions together with their preliminary toxicity to healthy cells.
- Finally, degradable polymer prodrugs with adjustable anticancer activity were prepared from the previously-developed copolymers and evaluated in vitro on different cancer cells.

However, all research projects come along with unexpected problems and unpleasant results. And this thesis project was no exception. However, it is difficult to point out the problems encountered during the experimental work when writing a thesis based on published articles. For that reason, we will also endeavor to relate the twist and turns faced during those three years (in grey boxes).

I. Structure-Control Relationship of Amide-Functionalized SG1-Based Alkoxyamines

Carboxylic acid-terminated SG1-based alkoxyamines, such as the tertiary BlocBuilder alkoxyamine or its secondary counterpart, the AMA-SG1 alkoxyamine (Figure 1), can be functionalized with primary amines by direct coupling of small molecules, such as drugs¹⁻³ or imaging probes.⁴ Such pre-functionalization of polymerization initiator is called “*grafting from*” or “*drug-initiated*” strategy. Although convenient (e.g., high coupling efficiency due to low steric hindrance and easy purification compared to the so-called “*grafting to*” strategy), the “*grafting from*” approach modifies the chemical structure of the alkoxyamine. Given that control over polymerization by NMP is governed by the dissociation rate constant of the alkoxyamine⁵ and that k_d depends on the alkoxyamine structure (combination of polar, steric and stabilization effects),^{6,7} pre-functionalization could therefore alter the dissociation of the alkoxyamine compared to the unfunctionalized counterpart.

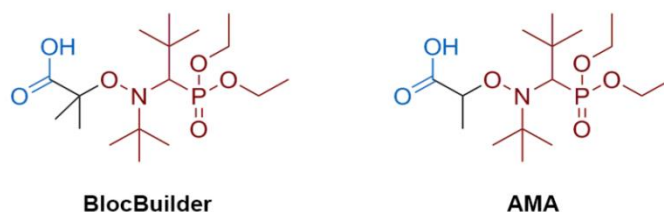


Figure 3. Structures of the BlocBuilder and AMA-SG1 alkoxyamines (the SG1 structure is indicated in red)

a. Pre-functionalization of secondary alkoxyamine with primary amine: toward a slower dissociation rate constant?

The activation energy (E_a , Table 1) of the C-ON bond dissociation of various SG1-based alkoxyamines was measured and the influence of functionalization on the dissociation was evidenced. First, independently of the amine-functionalization, one can mention the effect of the stabilization of the leaving alkyl radical on the dissociation.^{6,7} The alkyl radical of the tertiary BlocBuilder alkoxyamine was more stabilized than that of the secondary AMA alkoxyamine. Thus, the BlocBuilder alkoxyamine was more labile and exhibited a lower dissociation rate constant than its secondary counterpart (Table 1). Despite a less effective control, AMA-based alkoxyamines were selected for derivatization during my PhD thesis

because they usually gave higher coupling yields due to their less hindered structures nearby the carboxylic acid.⁸

Table 1. Experimental activation energy of the C-ON bond dissociation for various alkoxyamines

Alkoxyamine	E_a (kJ.mol ⁻¹)
BlocBuilder	112
AMA	131–133
AMA-NHS	127
AMA-Gem	131

Interestingly, the nature of the nitrogen in the amide function strongly impacts the dissociation rate of the alkoxyamine. Those containing a disubstituted amine displayed dissociation ability similar to their parent alkoxyamine. The situation is however more complicated with alkoxyamines containing monosubstituted amines. They preferentially adopt the *Z* diastereoisomer conformation due to the steric hindrance of the *E* diastereoisomer conformation (Figure 2a). However, the *Z* configuration induced intramolecular hydrogen bonding (IHB) between the alkyl fragment and the nitroxide fragment (Figure 2b) and this new bond to cleave during the dissociation caused an increase of the activation energy by ~10 kJ.mol⁻¹.

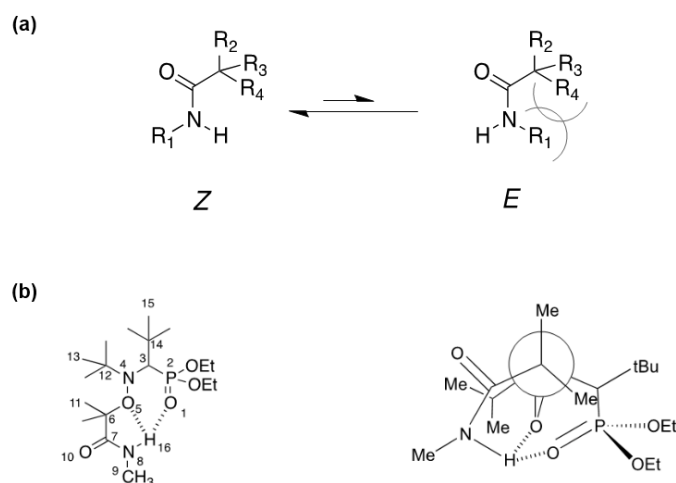


Figure 4. (a) Structure of the *Z* and *E* diastereoisomer configurations for amide-functionalized SG1-based alkoxyamines, and (b) Representation of the multiple intramolecular hydrogen-bonding interactions.

To achieve the synthesis of degradable prodrugs, gemcitabine (Gem) was selected as model anticancer drug. After administration, the half-life of Gem is very short due to rapid deamination (< 1 h).⁹ Therefore, Gem was derivatized with the secondary alkoxyamine AMA-SG1 through its C-4 amino group. To modulate the drug release kinetics and consequently the cytotoxicity, two alkoxyamines bearing different linkers in between Gem and the alkoxyamine moiety: either an amide bond (Gem-AMA-SG1, also called AMA-Gem), or a labile diglycolate linker connected to the amide bond (Gem-digly-AMA-SG1) (Figure 3).

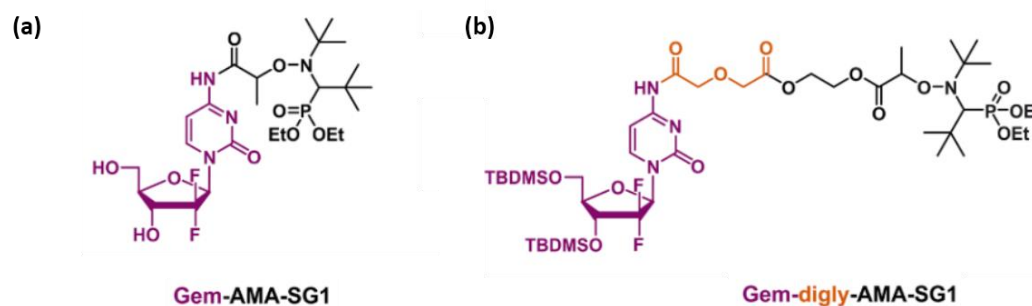


Figure 3. Structures of Gem-AMA-SG1 and Gem-digly-AMA-SG1 alkoxyamines.

The amide-functionalized Gem-AMA-SG1, should be prone to IHB. However, influence of IHB was counter-balanced by the presence of the polar cytosine ring and its activation energy was equal to that of the parent AMA-SG1. Conversely, the ester-functionalized Gem-digly-AMA-SG1 should not be subjected to IHB and should exhibit a lower E_a than Gem-AMA-SG1 and thus better dissociation ability (*refer to section III.1*).

b. Determination of the best polymerization conditions for the NMP of methyl methacrylate from secondary alkoxyamines

Ability of three representative secondary alkoxyamines to induce successful NMP of traditional vinyl monomers (styrene, *n*-butyl acrylate and methyl methacrylate in the presence of a small amount of acrylonitrile as a controlling comonomer) was evaluated: (i) the AMA alkoxyamine, bearing a carboxylic group; (ii) its NHS derivative (AMA-NHS) and (iii) Gem-AMA-SG1 (also called AMA-Gem).

Since our work was focused on the design of degradable copolymers based on methacrylic esters, ability of these alkoxyamines to control the copolymerization of MMA was of great help in determining the most suitable conditions for further copolymerization

with cyclic ketene acetals¹⁰ from Gem-functionalized alkoxyamines. As previously discussed in the introduction part (Chapter 0 & 1), NMP of methacrylic esters exhibits high activation-deactivation rate constant (i.e., leading to high concentration of propagating radical) that favors irreversible termination reactions. The addition of a small amount of controlling comonomer, such as acrylonitrile (AN) or styrene (S), is mandatory to favorably shift the activation-deactivation equilibrium toward the formation of dormant species and to enable the synthesis of well-defined copolymers. In such a context, having a controlled NMP of methacrylate monomers with secondary alkoxyamines that exhibit relatively low decomposition rate constants is not straightforward.

Copolymerizations were performed at 100 °C in toluene (50 wt.%) with 9 mol.% of AN as controlling comonomer. As predicted by the activation energy values of these alkoxyamines, the control of the polymerization was better with AMA-NHS, as shown by closer M_n values to the theoretical ones and lower dispersities than for AMA-Gem and AMA-SG1 (Figure 4).

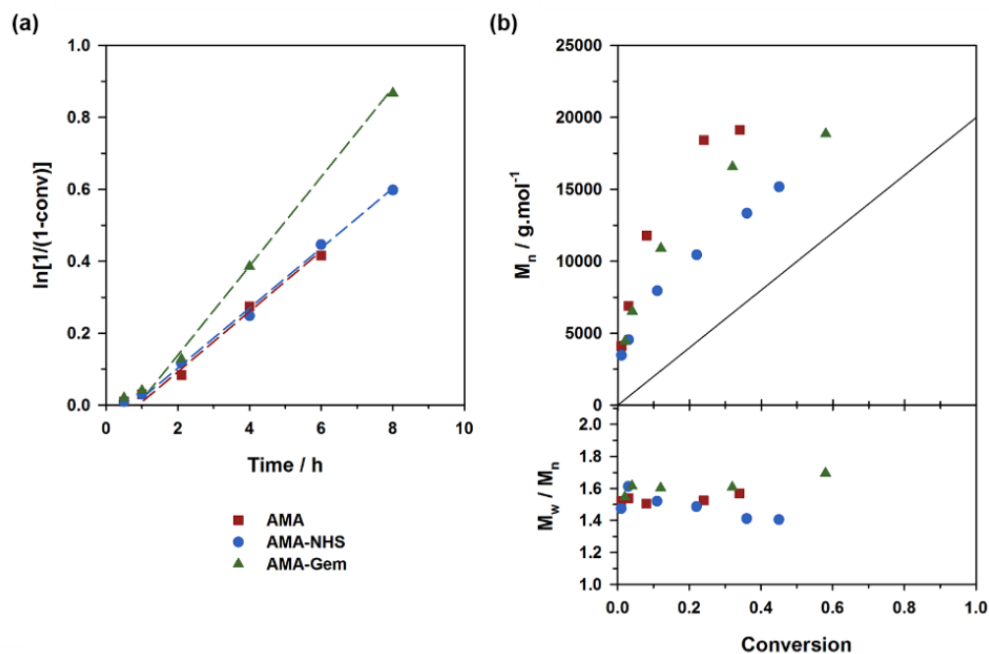


Figure 4. Solution NMP at 100°C of methyl methacrylate (MMA) with 9 mol.% of acrylonitrile (AN) initiated by different SG1-based alkoxyamines. (a) Evolution of $\ln[1/(1-\text{conv})]$ with time; (b) evolution of the number-average molar mass¹¹ and dispersity (\mathcal{D}) with conversion. The full lines represent the theoretical M_n and lines connecting data points are guides for the eye only.

However, since the carbon-carbon backbone of vinyl materials resists degradation, which may lead to polymer accumulation in the organism and induce prohibitive toxicity, the next step was to develop a new class of degradable vinyl copolymers.

II. New Degradable Copolymers Based on Nitroxide-Mediated Radical Ring-Opening Copolymerization of 2-Methylene-4-Phenyl-1,3-Dioxolane (MPDL) and Methacrylic Esters

This work came at the end of the PhD of Vianney Delplace¹² who investigated the synthesis of degradable copolymers prepared by NMrROP initiated by the BlocBuilder alkoxyamine of oligo ethylene glycol methyl ether methacrylate (OEGMA) and 2-methylene-4-phenyl-1,3-dioxolane (MPDL), a CKA acting as ester bond precursor, with a small amount of AN as controlling comonomer.¹³ The terpolymerization yielded well-defined copolymers containing adjustable amount of MPDL and exhibited tunable degradability. Interestingly, chain-end investigation by ³¹P NMR revealed that MPDL competed with AN to be the terminal unit and terpolymers were mainly terminated by MPDL-SG1 sequences.¹⁴ These results suggested that MPDL could act as controlling comonomer and replace AN during the polymerization and prompted us to investigate the copolymerization of MPDL and methacrylate monomers without AN.

a. Synthesis of MPDL: a new reliable and robust method

CKA are relatively sensitive monomers and the synthesis and purification of MPDL was initially quite complicated. In the presence of protic species, the two oxygens atoms of the acetal functionality strongly delocalize the doublets of the carbon-carbon double bond and make the β carbon strongly nucleophilic. Consequently, CKA monomers are highly sensitive to traces of water or acidic compounds.¹⁵

In the 80's, Bailey developed a two-step synthetic route for the synthesis of MPDL:¹⁶ (i) synthesis of chloroacetal by the transacetalization reaction between styrene glycol and chloroacetaldehyde dimethyl acetal and (ii) β -elimination of alkyl chloride using *tert*-butoxide as base. This latter step led to poor reproducibility (due to instability of MPDL) and low

yields (< 30 %). In addition, the use of *tert*-butanol (melting point ~25 °C) to solubilize *tert*-butoxide prevented to work at low temperature which is problematic as the required temperature (80 °C) favored the formation of by-products.

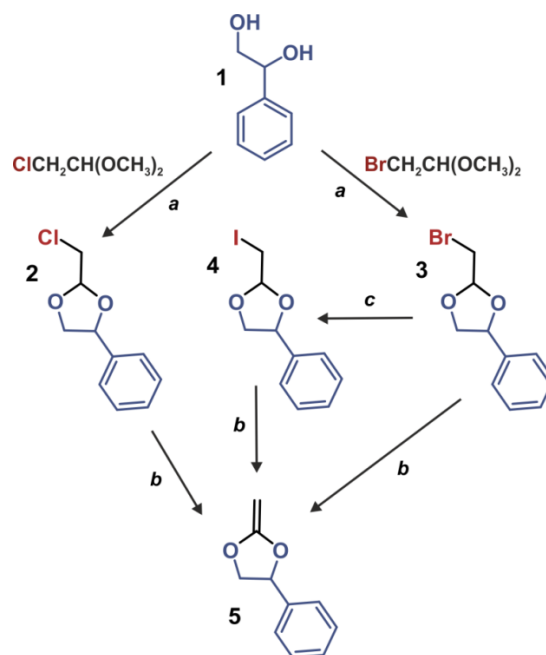


Figure 5. Synthetic routes to 2-methylene-4-phenyl-1,3-dioxolane (MPDL). Reagents: (a) DOWEX H+; (b) *tert*-BuOK, Aliquat® 336, dry THF; (c) NaI, dry acetone.

Therefore, in collaboration with Johanna Tran (another PhD in the group), we thoroughly revisited this method, taking inspiration from another method applied to different CKA that was based on the elimination from bromoacetals with solid-liquid phase-transfer catalysis (Aliquat® 336) in mild conditions (0 °C in THF) (Figure 5). To determine the most suitable halide for the elimination reaction, we extended the method to different cyclic halogeno acetals (i.e., chloro-, bromo- and iodo-acetaldehyde dimethyl acetal). Because of variable leaving group ability ($I > Br > Cl$), the elimination performed on chloroacetal gave the lowest yield (23 %) compared to bromo- and iodoacetals (> 80 %) and the pathway through bromoacetals was preferred (as it required one less step).

b. MPDL: the first degradable, controlling comonomer for the NMP of methacrylates

Copolymerizations of MPDL with either OEGMA or MMA were carried out with variable comonomer ratio ($f_{\text{MPDL},0} = 0.2\text{--}0.7$), with two objectives: (i) evaluate the impact of MPDL

content on the control and (ii) modulate the degradability of the resulting copolymers (Figure 6). Overall, we demonstrated that MPDL was the first degradable controlling comonomer for the NMP of methacrylates monomers. This ability was attributed to the similarity of the opened radical structure of MPDL with the propagating styrenic radical, a well-known controlling comonomer for the NMP of methacrylic esters.^{17,18}

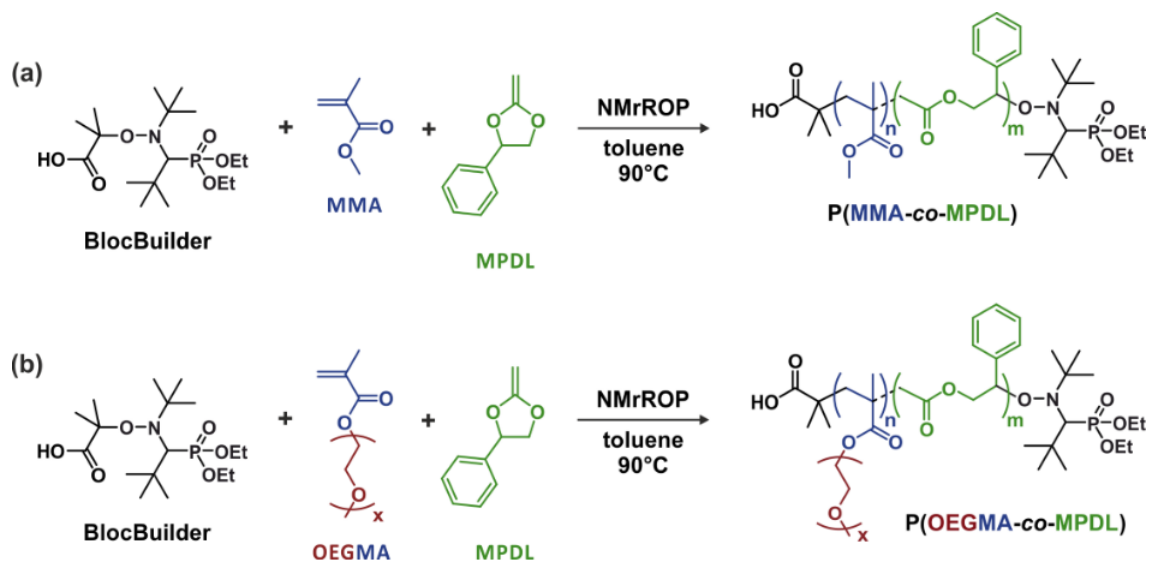


Figure 6. Synthesis of (a) P(MMA-co-MPDL) and (b) P(OEGMA-co-MPDL) by NMrROP.

Nevertheless, because of the low reactivity of MPDL, initial content above 20 mol.% were required to induce sufficient incorporation of MPDL in the final copolymer and to significantly decrease the average activation-deactivation equilibrium constant ($\langle K \rangle$), that is necessary to obtain a satisfying control. Indeed, the higher the initial MPDL content, the better the control of the polymerization (Figure 7). Dispersities ranged from 1.6 to 1.7 for the lowest MPDL contents to 1.2-1.3 for the highest MPDL contents.

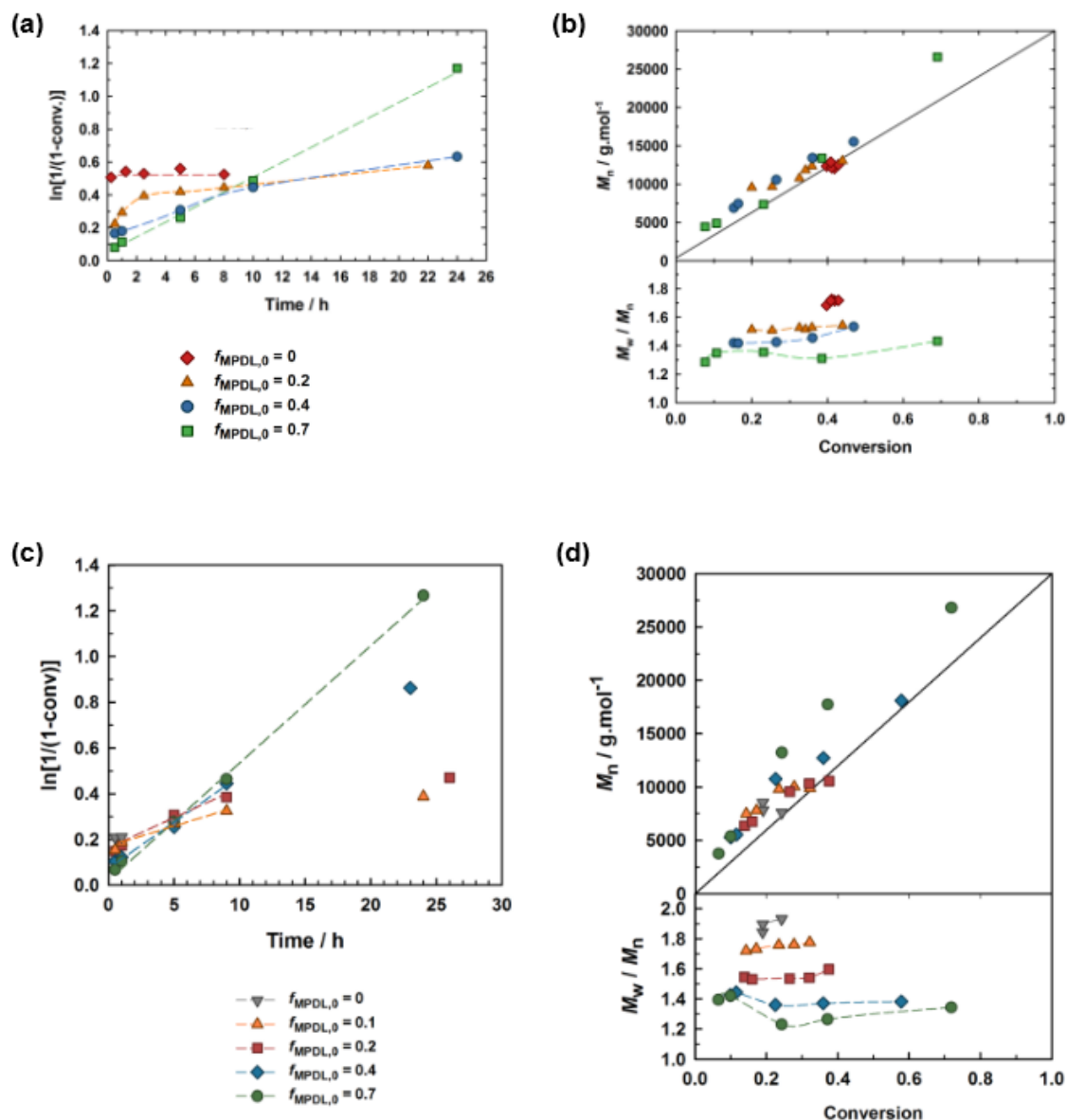


Figure 7. (a) and (b) NMP of OEGMA and MPDL in toluene initiated by the BlocBuilder alkoxyamine at 90 °C, as a function of the initial amount of MPDL: \blacklozenge , $f_{\text{MPDL},0} = 0$; \blacktriangle , $f_{\text{MPDL},0} = 0.2$; \bullet , $f_{\text{MPDL},0} = 0.4$; \blacksquare , $f_{\text{MPDL},0} = 0.7$. (a) $\ln[1/(1-\text{conv.})]$; (c) and (d) NMP of MMA and MPDL in toluene initiated by the BlocBuilder at 90 °C, as a function of the initial amount of MPDL: \blacktriangledown , $f_{\text{MPDL},0} = 0$; \blacktriangle , $f_{\text{MPDL},0} = 0.1$; \blacksquare , $f_{\text{MPDL},0} = 0.2$; \blacklozenge , $f_{\text{MPDL},0} = 0.4$; \bullet , $f_{\text{MPDL},0} = 0.7$. (a) and (c) $\ln[1/(1-\text{conv.})]$ vs. time (conv = methacrylate conversion). (b) and (d) Number-average molar mass, M_n and dispersity, M_w/M_n , vs. conversion. The solid black line represents the theoretical M_n and lines connecting data points are guides for the eye only.

c. Degradation of methacrylic ester-based copolymers under various conditions

To fine-tune the degradability, copolymers containing variable amounts of MPDL (F_{MPDL}), ranging from ~5 % for $f_{\text{MPDL},0} = 0.2$ to ~27 % for $f_{\text{MPDL},0} = 0.7$, were synthesized. Degradability of the two families of copolymers (MMA- and OEGMA-based) was first assessed by hydrolytic degradation under accelerated conditions; that is at room temperature in 5 % KOH, either in water for OEGMA-based copolymers or in a THF/MeOH (50:50, v/v) mixture for MMA-based copolymers. Notably, although fast for OEGMA-based copolymers, faster hydrolysis as well as higher degree of degradation were reached for MMA-based copolymers, likely due to a better solubilization in organic solvents. As expected, the more pronounced degradation was achieved for the copolymers containing the highest MPDL fractions (Figure 8).

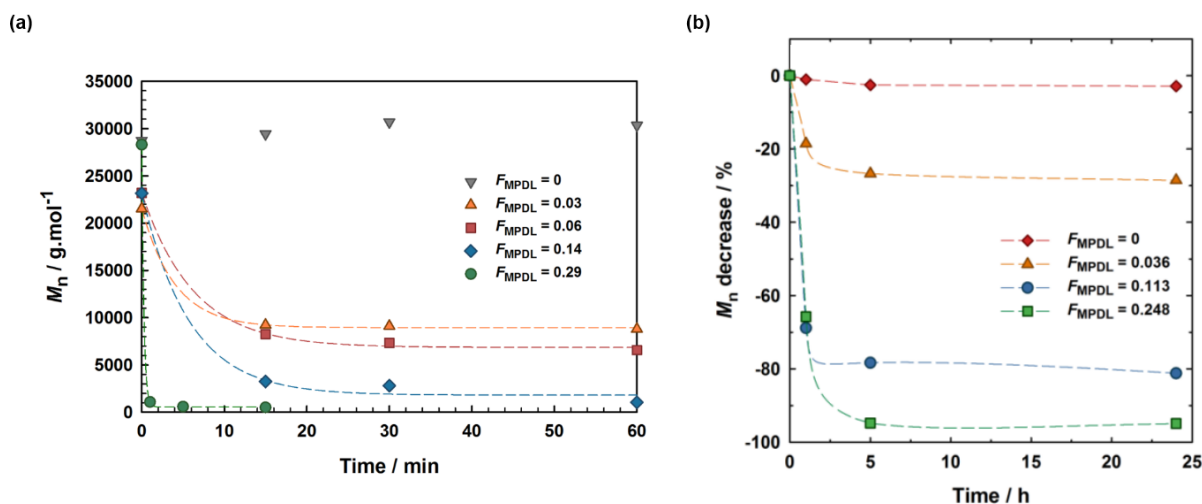


Figure 8. Evolution of the number-average molar mass, M_n with time. Dashed lines are guides for the eye only. (a) Hydrolytic degradation in THF with 5% KOH in methanol of P(MMA-co-MPDL) as a function of the MPDL fraction: ∇ , $F_{\text{MPDL}} = 0$; \blacktriangle , $F_{\text{MPDL}} = 0.03$; \blacksquare , $F_{\text{MPDL}} = 0.06$; \blacklozenge , $F_{\text{MPDL}} = 0.14$; \bullet , $F_{\text{MPDL}} = 0.29$ and (b) Hydrolytic degradation in aqueous 5% KOH of P(OEGMA-co-MPDL) as a function of the content in MPDL: \blacklozenge , $F_{\text{MPDL}} = 0$; \blacktriangle , $F_{\text{MPDL}} = 0.04$; \bullet , $F_{\text{MPDL}} = 0.11$; \blacksquare , $F_{\text{MPDL}} = 0.25$.

Although this type of hydrolytic degradation proved the presence of ester functions in the polymer backbone, the quite harsh conditions do not reflect their normal conditions of use. Thus, degradation experiments were performed under physiologic conditions; that is in PBS, pH 7.4 at 37 °C for 12 months. Importantly, their hydrolysis was benchmarked against

traditional polyesters (PLGA, PLA and PCL) to confront our polymers with FDA-approved polyesters that still represent gold standards in the biomedical field.

Hydrolytic degradation in PBS

However, long-term hydrolysis of the hydrophobic P(MMA-*co*-MPDL) copolymers gave rather disappointing results. Their high hydrophobicity prevented dispersion in water and significant water uptake, leading to very limited hydrolysis. P(MMA-*co*-MPDL) exhibited a slower degradation rates than that of PCL, with a M_n decrease close to 20 % after 12 months, and without noticeable effect of the MPDL content (Figure 9a).

As predicted, the kinetics of hydrolysis of water-soluble P(OEGMA-*co*-MPDL) in PBS was affected by the MPDL content (F_{MPDL}) and gave tunable degradation rates; from -40 % in M_n decrease to -70 % after 12 months (Figure 9b). These promising results suggested that OEGMA-containing copolymers are competitive polyesters regarding their degradation rate that spanned in between those of PLA and PCL.

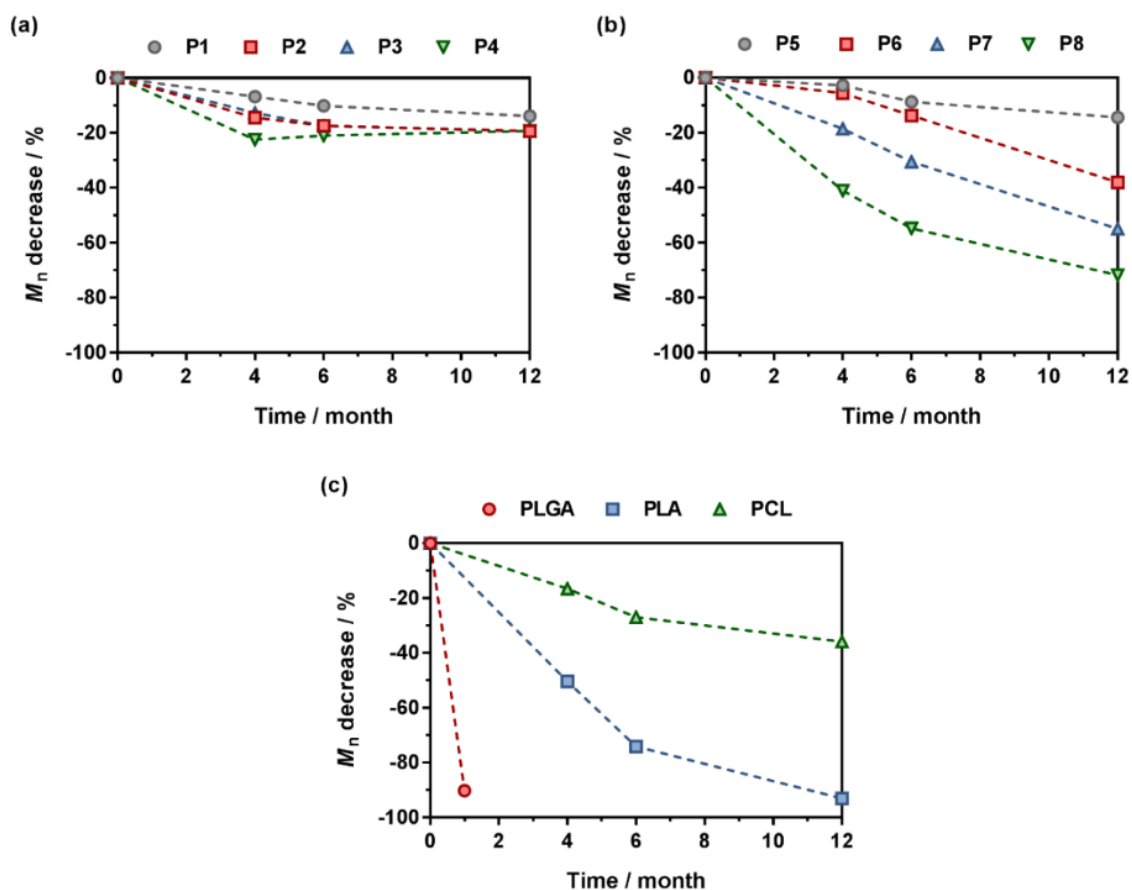


Figure 9. Evolution of the number-average molar mass, M_n , with time of the different copolymers during the hydrolytic degradation in PBS at 37 °C. (a) P(MMA-*co*-MPDL): **P1**

($F_{\text{MPDL}} = 0$); **P2** ($F_{\text{MPDL}} = 0.08$); **P3** ($F_{\text{MPDL}} = 0.12$); **P4** ($F_{\text{MPDL}} = 0.27$). (b) P(OEGMA-*co*-MPDL): **P5** ($F_{\text{MPDL}} = 0$); **P6** ($F_{\text{MPDL}} = 0.09$); **P7** ($F_{\text{MPDL}} = 0.15$); **P8** ($F_{\text{MPDL}} = 0.27$). (c) PLGA; PLA; PCL.

Importantly, pH was monitored over time during hydrolytic degradation of OEGMA-based copolymers and of PLGA, PLA and PCL. Hydrolytic degradation of polyester leads to carboxylic acid chain-end frequently associated with a drop in pH. As previously observed, pH of PLGA and PLA dispersions decreased from 7.4 to 5.5 after 1 and 12 months, respectively.^{19,20} Remarkably, pH of the different P(OEGMA-*co*-MPDL) solutions remained rather constant and > 6.8 . This high pH stability is very relevant and represents a meaningful advantage compared to aliphatic polyesters as their *in vivo* degradation may not lead to local acidification and probably to detrimental local inflammatory response.

Physical erosion of films

Erosion of P(MMA-*co*-MPDL) films in PBS was also investigated. Whatever the MPDL content, both water uptake and mass loss were very low ($< 10\%$). In comparison, the kinetics of hydrolysis of our films were comparable to that of PCL, thus much slower than that of PLGA and PLA, which were completely degraded after respectively 1 or 4 months.

PMMA-based materials are strongly hydrophobic and stiff, consequently the resulting films were highly compact. Water was unable to enter inside the polymer matrix and bulk erosion was not promoted. Only the surface, in contact with water, was likely to be hydrolyzed. Therefore, surface erosion was qualitatively confirmed by SEM and AFM, and films containing the highest MPDL fraction exhibited micrometric cavities on their surface after 6 months.

Microsphere Degradation in PBS

Erosion of microspheres (MS) was also investigated to evaluate their potential as degradable drug-loaded polymer nanocarrier. MS were selected instead of nanoparticles to facilitate microscopic observations.

MS were prepared by the emulsion/solvent evaporation technique and incubated in PBS at 37 °C for one year (Figure S1). PLGA and PLA MS were significantly degraded in one month. In comparison, the degradation rate of PCL MS was much slower: the average diameter of the MS decreased by half in one year, from $\sim 7.4\ \mu\text{m}$ before hydrolysis to ~ 3.7

µm after 12 months (average value over 30 measurements).

As expected, control PMMA-based MS without MPDL (MPDL was replaced by S) were stable, without noticeable change in size or morphology. Unfortunately, no significant modification was observed for the different P(MMA-*co*-MPDL) MS within the 12-month period. Similarly to films, the high stability of the polymer in aqueous media was attributed to a combination of hydrophobicity and rigidity, resulting in highly compact microsphere preventing water uptake and bulk degradation. A very slow surface erosion was likely the sole degradation mechanism, not significant enough though to induce notable changes in MS diameters.

Enzymatic degradation

Degradation of the different copolymers was attempted in the presence of enzymes for one week, in particular lipases from *Candida Antarctica*.

Water-soluble P(OEGMA-*co*-MPDL) displayed moderate M_n decrease (~6-15 %). This incomplete enzymatic hydrolysis could be explained by the steric hindrance around the ester bond, provided by both hydrophobic MPDL units and PEG side chains (known to induce steric repulsion of proteins), leading to a lack of affinity between the enzyme and the ester groups. Surprisingly, the lowest MPDL content gave the highest degradation. This trend could be related to the hydrophobicity of the copolymers which may further limit the interaction between the enzyme and the ester functions to be cleaved. Although modest, enzymatic degradation rate could be enhanced by prolonging the incubation time and by replacing the degradation medium regularly.²¹

Unfortunately for P(MMA-*co*-MPDL), no degradation was observed. We postulated that the too hydrophobic copolymer backbone prevented interaction between the enzyme and the ester groups.

Microsomal Degradation in PBS

Degradation of our copolymers by biological entities was evaluated under oxidative conditions, in the presence of microsomes from human liver. Microsomes are vesicle-like artifacts constituted from the endoplasmic reticulum obtained after differential centrifugation of cells. Microsomes contain cytochrome P450 enzymes, belonging to hemoproteins family, which catalyze oxidation, reduction and oxidative hydrolysis of

various endogenous and exogenous compounds.^{22,23} For instance, Couvreur and coworkers evidenced the oxidative hydrolysis of poly(isobutyl cyanoacrylate) nanoparticles through microsomal action.²⁴

P(MMA-*co*-MPDL) nanoparticle ($D_z \sim 500$ nm) suspensions and solutions of P(OEGMA-*co*-MPDL) were subjected to microsomal environment but the M_n remained constant (Figure S2 and S3). The lack of selectivity of the enzyme for the polymer and the steric hindrance around the ester bond may explain the stability of our copolymers under oxidative conditions.

d. Biocompatibility of PEG-based degradable copolymers

Biomedical applications require non-toxic materials. Therefore, we performed preliminary in vitro and in vivo toxicity study of P(OEGMA-*co*-MPDL) copolymers, given their promising results in terms of degradability. Although PEG-based polymethacrylates are known to be non-toxic,^{8,25} insertion of MPDL units bearing an aromatic group (often said to be detrimental for biomedical applications) may modify the toxicity of the resulting copolymers.

Therefore, non-cytotoxicity of degradable P(OEGMA-*co*-MPDL) was evidenced in vitro on two representative mammalian cell types (Figure 10a). Because of formation of carboxylic acids chain-ends during ester bond hydrolysis, degradation may induce a slight change of the pH and may potentially affect the cells. However, cell viability assays after incubation of cells with the degradation products exhibited high cell viability (> 70 % up to high concentration, 1 mg.mL^{-1}). Therefore, neither the copolymer nor its degradation products were cytotoxic.

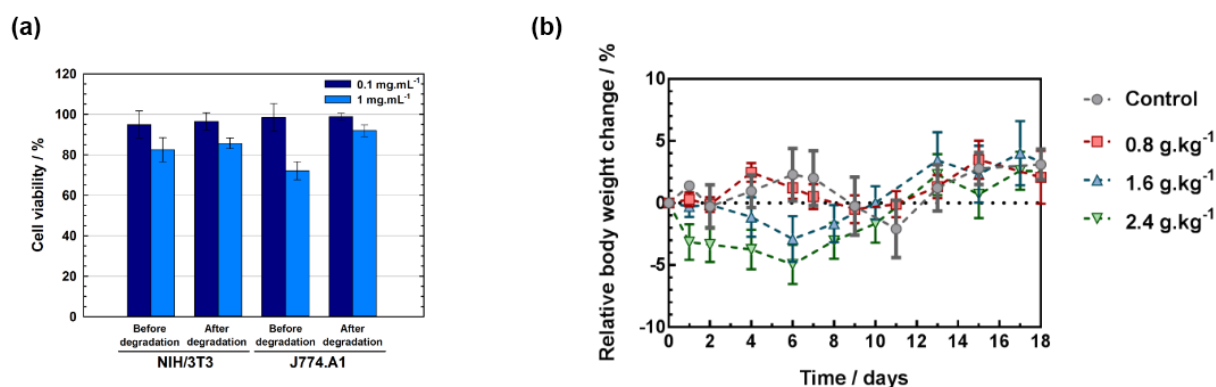


Figure 10. Biological evaluation of P(OEGMA-*co*-MPDL) copolymer ($F_{\text{MPDL}} = 0.113$). (a) Cell viability (MTT assay) after incubation of NIH/3T3 cells and J774.A1 cells with at 0.1 and 1 mg.mL^{-1} . Results were expressed as percentages of absorption of treated cells (\pm SD) in

comparison to that of untreated ones as a control. (b) Relative body weight change of mice, as a function of time after intravenous injections of PBS or P(OEGMA-*co*-MPDL).

P(OEGMA-*co*-MPDL) copolymers containing high MPDL content were then administered to mice. Mice body weight was monitored for 20 days after a single intravenous injection of copolymer solutions with concentrations comprised between 0.8 and 2.4 g.kg⁻¹. Except a slight decrease during the first week at high concentration (< 5 %), their body weight was maintained constant during the experiment duration (Figure 10b). No mortality neither noticeable modification in terms of feeding and behavior were observed, suggesting the safety of the copolymers.

III. Degradable Polymer Prodrugs with Adjustable Activity from Drug-Initiated Radical Ring-Opening Copolymerization

On one hand, the NMrROP of CKA enabled the synthesis of degradable vinyl polymers and on the other hand, the “*drug-initiated*” strategy has only been applied to persistent vinyl polymers. So the idea was to combine those two strategies to report on, for the first time, degradable vinyl polymer prodrugs (Figure 11).

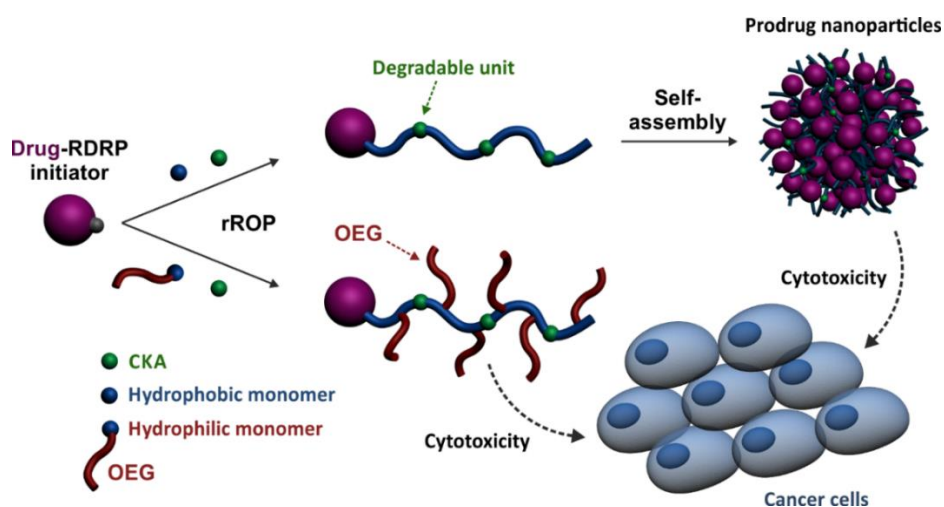


Figure 11. Synthetic strategy for the design of degradable Gemcitabine-based polymer prodrugs by ‘drug-initiated’ nitroxide-mediated radical ring-opening copolymerization (NMrROP).

a. Drug-initiated synthesis of degradable polymer prodrugs

The previously-developed copolymerization systems were employed but this time, the NMrROP was initiated by Gem-functionalized secondary alkoxyamines from Figure 3. To adjust the Gem release kinetics, and consequently the cytotoxicity, we indeed tested two different linkers between Gem and the copolymer, either the amide bond (Gem-AMA-SG1) or the more labile diglycolate linker (Gem-digly-AMA-SG1). Copolymerizations yielded the following degradable polymer prodrugs: Gem-P(MMA-*co*-MPDL), Gem-P(OEGMA-*co*-MPDL), Gem-digly-P(MMA-*co*-MPDL) and Gem-digly-P(OEGMA-*co*-MPDL).

The NMrROP of methacrylates with MPDL from secondary alkoxyamines was no exception regarding the trends highlighted previously (*refer to Chapter 3 & 4*): the higher the initial fraction of MPDL, the better the control of the copolymerization. As predicted from the structure-control relationship (*refer to section I.1*), copolymerizations initiated by the BlocBuilder gave better control than those initiated by Gem-functionalized secondary alkoxyamine. Interestingly, as previously predicted from the alkoxyamine structures (*refer to section I.1*), the control over the copolymerizations was better with Gem-digly-AMA-SG1 rather than Gem-AMA-SG1, which is prone to IHB.

Afterward, a small library of well-defined prodrugs with a final drug-loading ranging from 2 to 2.5 mol.% were prepared for further biological evaluation.

Increasing the drug-loading

One of the features of the “*drug-initiated*” strategy is the possibility to fine-tune the drug loading by varying the M_n of the grown polymer; the lower the M_n , the higher the drug loading. Therefore, one objective was to increase the drug-loading to 5 mol.% by targeting $M_n \sim 5000 \text{ g}\cdot\text{mol}^{-1}$. Regardless of the MPDL initial content ($f_{\text{MPDL},0} = 0.4$ or 0.7) or the methacrylic ester monomer (MMA or OEGMA), the resulting copolymers contained high MPDL content (Table 3): $\sim 30\%$ for $f_{\text{MPDL},0} = 0.4$ and $\sim 70\%$ for $f_{\text{MPDL},0} = 0.7$, significantly above those obtained when lower drug-loadings were targeted.

Table 3. Characterization of Gem-P(OEGMA-*co*-MPDL) polymer prodrugs.

$f_{\text{MPDL},0}$ (mol.%)	conv (%) / temps (h)	M_n (g/mol)	D	F_{MPDL} (mol.%)	% ring-retained MPDL	%Gem (wt.%)
Gem-P(MMA-<i>co</i>-MPDL)						
0.4	40 / 8	3 700	1.44	0.34	62	7.1

0.7	57 / 8	4 200	1.61	0.68	66	6.3
Gem-P(OEGMA-co-MPDL)						
0.4	23 / 8	6 200	1.80	0.28	95	2.9
0.7	20 / 8	7 300	1.55	0.7	100	2.3

CKAs can polymerize either via radical ring-opening polymerization (rROP) or via vinyl propagation.²⁶ When inserted by vinyl polymerization, the ring is retained, thereby the CKA no longer provides degradability to the polymer.²⁶ For both MPDL contents (F_{MPDL}), the amount of ring-retained MPDL were estimated by ¹H NMR (Table 3). Increasing the drug-loading enabled insertion of a larger number of MPDL units in the copolymer but the majority was incorporated by vinyl propagation (~60–100 % of ring-retained MPDL). With such ring-retained proportion, the resulting prodrugs did not meet with the expected criteria in terms of degradability and were not biologically evaluated.

RAFT synthesis of degradable prodrugs

We also applied our system to RAFT polymerization; another RDRP technique. We employed a trithiocarbonate chain transfer agent (CTA) functionalized with Gem (4-cyano-4-[(dodecylsulfanylthiocarbonyl)sulfanyl]pentanoic acid, CDP, Figure S3) already developed in the lab.

RAFT polymerization of OEGMA in the presence of Gem-CDP reached nearly complete conversion and led to well-defined copolymers of approximately 10 000 g.mol⁻¹ (Table 2), without noticeable influence of the MPDL initial content ($f_{\text{MPDL},0} = 0.2\text{--}0.7$). The control provided by RAFT was much better than the one by NMP, with significantly lower dispersities. However, MPDL was inserted into the copolymer to a lesser extent compared to NMP, with final contents comprised between 3 % ($f_{\text{MPDL},0} = 0.2$) and 8 % ($f_{\text{MPDL},0} = 0.7$).

Table 2. Characterization of Gem-P(OEGMA-co-MPDL) polymer prodrugs obtained via RAFT polymerization.

$f_{\text{MPDL},0}$ (mol.%)	conv (%) / temps (h)	M_n (g/mol)	\mathcal{D}	F_{MPDL} (mol.%)	%Gem (wt.%)
0.2	95 / 7	9 100	1.15	0.03	2.9
0.4	98 / 7	11 200	1.13	0.05	2.3
0.7	96 / 7	9 100	1.09	0.08	2.9

In the literature, the RAFT copolymerization of BMDO, a seven-membered CKA, with traditional vinyl monomers (MMA²⁷, NIPAAm²⁸, vinyl acetate^{29,30}, OEGMA³¹ and glycoacrylate³²) was already reported. More particularly, Junkers and coworkers copolymerized BMDO with MMA and determined the reactivity ratios of BMDO and MMA.²⁷ Similarly to NMP, the reactivity ratios obtained for RAFT polymerization were unfavorable for CKA ($r_{\text{BMDO}} = 0.3$ and $r_{\text{MMA}} = 6.0$), which explains the low amount of MPDL inserted during the copolymerization.

Although RAFT polymerization led to a good control of the M_n with low dispersity, too low MPDL insertion did not encourage us to continue with such polymerization technique.

b. Hydrolytic degradation of the prodrugs under accelerated conditions

The hydrolytic degradation was assessed under accelerated conditions (i.e., KOH 5%) to confirm and probe the presence of opened MPDL units. The level of degradation was in direct relationship with the final open MPDL content in the copolymer. M_n decrease ranged from -10 % for the lowest MPDL content to -70% for the highest one.

c. Physico-chemical characterization

Because of their opposite solubility, two class of prodrugs were obtained; either water-soluble Gem-P(OEGMA-*co*-MPDL) prodrugs or Gem-P(MMA-*co*-MPDL) nanoparticles.

The nanoprecipitation of MMA-containing prodrugs gave narrowly dispersed nanoparticles with an average diameter in the 110-200 nm range exhibiting great colloidal stability (for at least one month). Interestingly, prodrugs obtained from Gem-digly-AMA-SG1 were smaller than those obtained from Gem-AMA-SG1 (by ~50-90 nm), perhaps owing to a better stabilization provided by additional hydrophilicity of the diglycolate linker. Further investigations would however be necessary for a better understanding.

For OEGMA-containing prodrugs, hydrophilicity of OEGMA dominated over hydrophobicity of MPDL and the vast majority (> 84%) of Gem-P(OEGMA-*co*-MPDL) gave nanoparticles upon nanoprecipitation.

Effect of concentration on nanoparticle formulation

In vivo intravenous administration to laboratory animals requires careful consideration of several parameters, such as volume of administration, site of delivery, pH of the substance, etc.³³ To minimize blood volume variation and thus potential adverse effects for the animal, the recommended volumes of administration to rodents for intravenous injection in the tail vein is equal to 5 mL.kg^{-1} (which corresponds to $\sim 100 \text{ }\mu\text{L}$ per injection for a mice).³³ Therefore, the maximal injected dose of Gem only depends on the drug loading and on the nanoparticles concentration in solution.

Moreover, size is an essential factor affecting clearance and biodistribution of the nanoparticles.³⁴⁻³⁶ In the bloodstream, nanosystems smaller than 5 nm are rapidly cleared from the organism through filtration by the kidney. Larger particles exhibit prolonged circulation although the reticuloendothelial system (RES) eliminates nanosystems larger than 200 nm. Thus, nanoparticles diameter suitable for in vivo application should lie in the 5-200 nm range.

Nanoparticles were prepared by nanoprecipitation of Gem-P(MMA-*co*-MPDL) in water. The influence of the polymer concentration on the nanoparticle size was investigated, with concentrations ranging from 0.5 to 2.5 mg.mL^{-1} (Figure S4). For a final concentration of 2.5 mg.mL^{-1} , three populations of particles were obtained (microspheres and nanoparticles of $\sim 500 \text{ nm}$ and $\sim 200 \text{ nm}$). Intermediate concentration of 1 mg.mL^{-1} resulted in too large nanoparticles ($\sim 660 \text{ nm}$), out of the range allowed in nanomedicine. It was thus necessary to decrease the polymer concentration down to 0.5 mg.mL^{-1} to obtain narrowly dispersed nanoparticles with an appropriate diameter of 190 nm. And so, for the rest of the work, P(MMA-*co*-MPDL)-based nanoparticles were prepared at a concentration of 0.5 mg.mL^{-1} to target a size adapted to nanomedicine.

d. Biological evaluation

First, the release of Gem was studied in human serum to mimic biological conditions, from which clear trends emerged (Figure 13). Several structural parameters were compared to establish structure-activity relationships such as: (i) the hydrophilicity of the methacrylic ester, (ii) the composition of the copolymer (i.e., MPDL content) and (iii) the nature of the linker between Gem and the polymer.

For P(OEGMA-*co*-MPDL) prodrugs containing a simple amide linker, Gem release gradually increased from 7 to 25 %, when the MPDL content was decreased. This trend could be correlated to the hydrophobicity around the drug-polymer bond, which increased with the MPDL fraction. By changing the nature of the linker and using the more labile diglycolate moiety, the same trends were observed but the release rates were significantly higher and reached ~70 % for the prodrugs containing the lowest amount of MPDL.

Replacing hydrophilic OEGMA by hydrophobic MMA drastically reduced the release of Gem. With the amide bond, Gem was almost not released (< 2 %). These results could be correlated to the degradation experiments of MMA-based materials, which were shown to be very hydrophobic and compact. Therefore, we assumed that only the fraction of Gem located at the surface of the nanoparticle could be potentially cleaved. However, it appeared that the amide bond was too stable in such conditions and Gem was almost not released. With the more labile diglycolate linker, a more pronounced release of Gem was noticed but it did not exceed 15%.

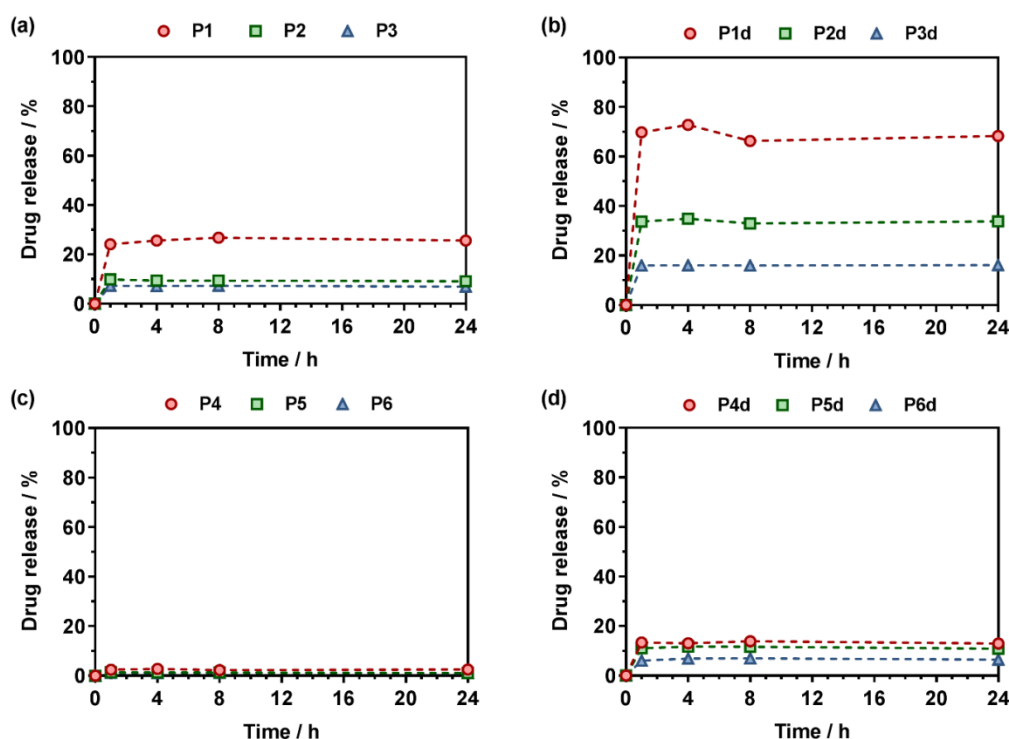


Figure 13. Gem release profiles at 37 °C in human serum from (a) Gem-P(OEGMA-*co*-MPDL) (**P1–P3**), (b) Gem-digly P(OEGMA-*co*-MPDL) (**P1d–P3d**), (c) Gem-P(MMA-*co*-MPDL) (**P4–P6**) and (d) Gem-digly-P(MMA-*co*-MPDL) (**P4d–P6d**).

Then, we verified whether these trends could be directly transposed into anticancer activity. The *in vitro* cytotoxicity was investigated on cell lines corresponding to clinically relevant cancer models for Gem (Figure 14). Similarly to Gem release experiments, cytotoxicity was independently governed by: (i) the MPDL content as lower MPDL contents gave higher cytotoxicity; (ii) the nature of the linker; the presence of the more labile diglycolate facilitated the release of Gem and (iii) the hydrophilicity of the methacrylate; the PEGylated prodrugs exhibit a much greater toxicity than the nanoparticles.

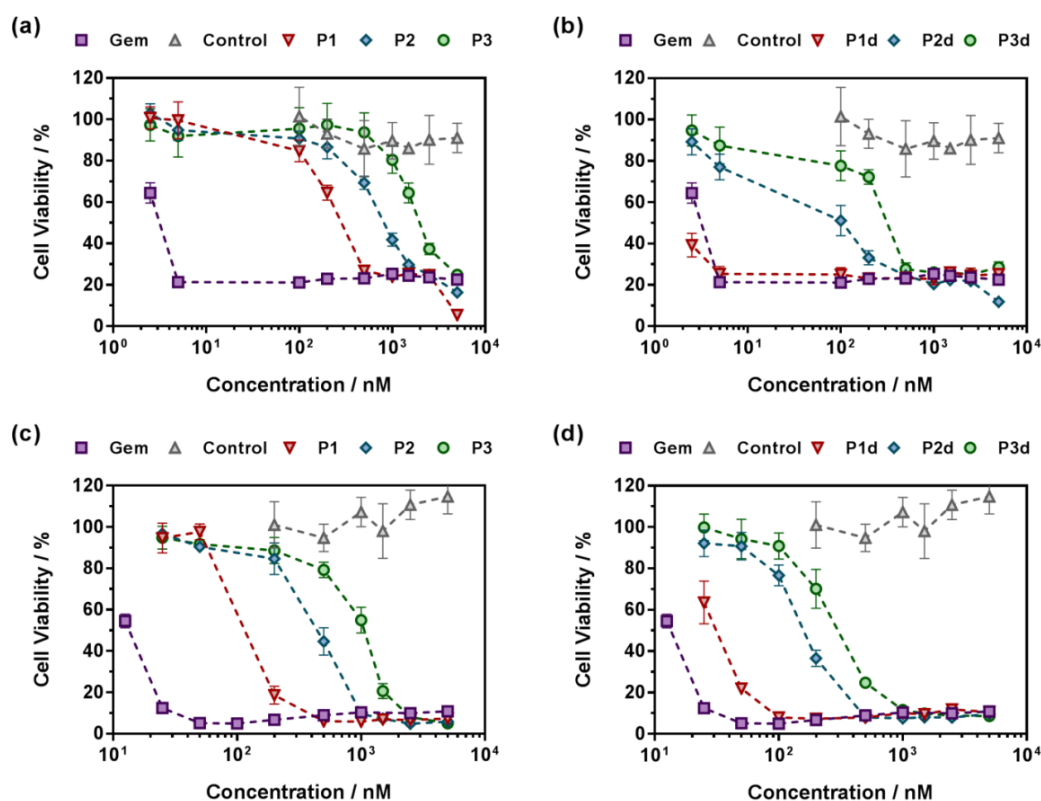


Figure 14. Cell viability (MTT test) with increasing concentrations of (a, c) Gem-P(OEGMA-co-MPDL) (P1–P3) or (b, d) Gem-digly-P(OEGMA-co-MPDL) (P1d–P3d) on (a, b) A549 cells and (c, d) MiaPaCa-2 cells.

IV. Limitations, remaining questions and perspectives

a. Disenchantment of MMA-based prodrug nanoparticles

As gemcitabine was not significantly cleaved from P(MMA-co-MPDL) copolymers and thus could not fully exert its therapeutic effects, the resulting nanoparticles displayed very limited anticancer activity *in vitro*, even though the diglycolate linker had a beneficial effect. In addition, even if hydrolysis of the prodrugs was demonstrated under accelerated conditions,

hydrolysis under physiological conditions (i.e., long-term hydrolysis in PBS and enzymatic hydrolysis) turned to be rather limited.

These disappointing results were related to the high hydrophobicity and rigidity of the PMMA-based prodrugs, resulting in highly compact nanoparticles preventing: (i) water uptake for bulk hydrolysis and (ii) action of enzyme capable to cleave the drug from the polymer (e.g., cathepsin B) during drug release experiments.

Thus, this kind of materials may not be adapted for *short-term* drug delivery purposes, where drug release and degradation of the nanocarrier should be rather quick, but could find applications in other fields of ³⁷ medicine, such as implanted devices (e.g., prosthesis, implants) requiring a longer lifetime in the body and thus longer degradation timescales.³⁸⁻⁴¹

b. Promising OEGMA-based prodrugs

Despite encouraging *in vitro* cytotoxicity, the question of the *in vivo* fate of low molecular weight and water-soluble Gem-digly-P(OEGMA-*co*-MPDL) prodrugs should be raised.

Hydrodynamic diameter of soluble polymers has significant effects on: (i) the transport of polymers throughout the body, (ii) their elimination by the reticuloendothelial system (RES), kidney and liver, and (iii) their internalization into tumor cells.⁴²⁻⁴⁴ Elimination by renal clearance occurs through filtration across glomerulus pore of ~5 nm in size, corresponding approximatively to 30–50 kg.mol⁻¹ (depending on the polymer composition, shape, conformation, etc.) and macromolecules with hydrodynamic radius smaller than glomerular pores are rapidly eliminated in the urine.

Therefore, the hydrodynamic radius of the prodrugs in solution is a crucial parameter to prevent rapid clearance and obtain high circulation time in the body. Parameters affecting the hydrodynamic radius are mainly the molecular weight of the polymer, the macromolecular architecture and the conformation (e.g., linear or branched polymers). Recently, Ozer et al. determined the hydrodynamic diameter of POEGMA polymers of $M_n = 10\,000\text{ g.mol}^{-1}$ in cell culture media supplemented with 10% of serum and obtained an average diameters of ~6-8 nm⁴⁵; that is in the same order of magnitude than glomerulus pores. In our case, because of similar M_n , this would probably only partially prevent *in vivo* elimination by renal filtration of Gem-digly-P(OEGMA-*co*-MPDL) prodrugs, unless: (i) the M_n is increased (at the expense of the drug loading); (ii) the prodrugs are made amphiphilic to self-assemble into nanoparticulate systems via hydrophobization for instance or (iii) targeting ability is implemented on the

polymer to optimize drug accumulation at the tumor site. These copolymers could also be advantageously used for the PEGylation of therapeutic proteins, thus conferring a degradable PEG-based protection.

Some questions can also arise from the drug-release and the *in vitro* toxicity. The fast release of gemcitabine in serum *in vitro* may induce a fast release *in vivo*. If the linker is hydrolyzed before reaching the action site, then we may face the same limitations as those of the parent drug (e.g., early metabolization etc.). This problem could be easily solved by using site-specific sensitive linkers such as the disulfide bridge (reduction by glutathione) or the hydrazine linker (hydrolytic degradation under acidic conditions), that may promote drug release in the tumor environment. Other strategies would consist in designing amphiphilic block conjugates that self-assemble in water and possess stealth properties provided by the P(OEGMA-*co*-CKA) corona.

Interestingly, P(OEGMA-*co*-MPDL) copolymers demonstrated promising degradation rate under hydrolytic conditions and might be envisioned for *short-* or *mid-term* applications such as nanoscale drug-delivery systems and meet a need for hydrophilic degradable materials with tunable degradation kinetics. However, the steric repulsion of protein provided by PEG side chains have a detrimental effect on the enzymatic degradation of the copolymers. Some improvement would consist in replacing OEGMA by other hydrophilic vinyl monomer such as *N,N* dimethylacrylamide (DMAA), for instance.

c. Design of new CKAs

This work shows the great potential of CKAs to confer degradability to vinyl polymers. CKAs were copolymerized with traditional vinyl monomers such as styrene,^{46,47} methacrylic ester,^{27,48-51} acrylic ester,^{32,52,53} maleimide^{54,55} or vinylcyclopropane.⁵⁶ However, the functionalities provided by traditional CKAs (e.g., MDO, BMDO or MPDL) are limited and their architecture/hydrophobicity can lead to poor degradation (hydrolytic and/or enzymatic) as demonstrated with MPDL in this PhD thesis.

Therefore, significant efforts are currently made to synthesize new CKAs. For instance, replacing the aromatic group by hydrophilic or less bulky moieties should improve water uptake and therefore degradation. Another strategy consists in the modification of the side chain to bring new functionalities (e.g., fluorescent probes, drugs) or for subsequent functionalization (e.g., click chemistry).

V. Experimental part (grey boxes)

a. Degradation experiments

Hydrolysis of polymer microspheres (MS). MS were prepared by the emulsion/solvent evaporation technique.⁵⁷ 100 mg of polymer were dissolved in DCM. The polymer solution was then emulsified in 20 mL of sodium cholate aqueous solution (1.5 w.%) using an Ultraturrax T25 (IKA) operating with a SN25-10G dispersing tool at a velocity of 8000 rpm. Emulsification was performed in a 50 mL beaker placed over ice for 2 min. DCM was evaporated by magnetic stirring for 4 h at 300 rpm at RT. Residual surfactant was removed by centrifugation (1 min, 13 400 rpm) and water was replaced by PBS. MS were mechanically stirred in an orbital shaker thermostated at 37 °C. Aliquots of 1 mL were taken out after selected degradation time (1, 6 and 12 months) and washed by centrifugation to remove the salts.

Microsomal degradation. Copolymers (polymer concentration in PBS of 0.5 mg.mL⁻¹) were poured in PBS by the solvent assisted method. 50 mg of copolymers were solubilized in 2.5 mL of THF and added dropwise to 10 mL of PBS. THF was evaporated and microsome from human liver (microsomal concentration of 5 mg.mL⁻¹) were added. After one week stirred at 40 °C, the mixture was lyophilized and 2 mL of chloroform were added for filtration. Then, the degradation products were analyzed by SEC.

b. Polymer synthesis

Synthesis of Gem-poly(oligo(ethylene glycol) methyl ether methacrylate)-co-(2-methylene-4-phenyl-1,3-dioxolane), with 90 % initial MPDL (Gem-P(OEGMA-co-MPDL)) by NMP. Copolymers with M_n around 10 000 g.mol⁻¹ were prepared, following the procedure described in the Chap. 4. For 10 % initial SG1, [OEGMA (1.1298 g, 4.33 mmol), MPDL (0.5887 g, 36.3 mmol), Gem-AMA-SG1 alkoxyamine initiator (2.7 mg, 4.41 × 10⁻³ mmol), free SG1 (0.2 mg, 4.48 × 10⁻⁴ mmol) and anhydrous toluene (0.71 g, 0.82 mL)]. The amount of ring-retained MPDL was calculated by ¹H NMR spectroscopy by comparing the methine proton attached to both oxygen and phenyl protons of ring-retrained MPDL (5.0 ppm) with the aromatic protons of MPDL (7.3 ppm).

Synthesis of short Gem-poly(oligo(ethylene glycol) methyl ether methacrylate)-co-(2-methylene-4-phenyl-1,3-dioxolane) (Gem-P(OEGMA-co-MPDL)) by NMP. Shorter

copolymers with M_n around $5\,000\text{ g}\cdot\text{mol}^{-1}$ were prepared, following the procedure described in the Chap. 4. For $f_{\text{MPDL},0} = 20\%$ [OEGMA (1.7618 g, 5.87 mmol), MPDL (0.2382 g, 1.47 mmol), Gem-AMA-SG1 alkoxyamine initiator (100.0 mg, 1.64×10^{-1} mmol), free SG1 (6 mg, 1.76×10^{-2} mmol) and anhydrous toluene (2.0 g, 2.31 mL)], for $f_{\text{MPDL},0} = 40\%$ [OEGMA (1.4704 g, 4.90 mmol), MPDL (0.5296 g, 3.27 mmol), Gem-AMA-SG1 alkoxyamine initiator (102.0 mg, 1.68×10^{-1} mmol), free SG1 (6 mg, 1.76×10^{-2} mmol) and anhydrous toluene (2.0 g, 2.31 mL)] and for $f_{\text{MPDL},0} = 70\%$ [OEGMA (0.8862 g, 2.95 mmol), MPDL (1.1138 g, 6.88 mmol), Gem-AMA-SG1 alkoxyamine initiator (33.0 mg, 0.53×10^{-1} mmol), free SG1 (1.8 mg, 0.525×10^{-2} mmol) and anhydrous toluene (2.0 g, 2.31 mL)]. ^1H NMR spectroscopy by comparing the methine proton attached to both oxygen and phenyl protons of ring-retrained MPDL (5.0 ppm) with the aromatic protons of MPDL (7.3 ppm).

Synthesis of Gem-poly(oligo(ethylene glycol) methyl ether methacrylate)-*co*-(2-methylene-4-phenyl-1,3-dioxolane) (Gem-P(OEGMA-*co*-MPDL)) by RAFT. A typical solution copolymerization procedure ($f_{\text{MPDL},0} = 20\%$) is as follows. A mixture of OEGMA (1.3214 g, 4.40 mmol), MPDL (0.1786 g, 1.10 mmol), Gem-RAFT agent⁵⁸ (281.6 mg, 3.21×10^{-1} mmol), ACPA (5.9 mg, 2.11×10^{-2} mmol) and anhydrous dioxane (1.5 g, 1.46 mL) was degassed by 3 freeze–pump–thaw cycles and stirred at 80 °C for 7 h. The same procedure was followed by adapting the amount of the reactants for $f_{\text{MPDL},0} = 40\%$ [OEGMA (1.1028 g, 3.68 mmol), MPDL (0.3972 g, 2.45 mmol), Gem-RAFT Agent (131.3 mg, 1.50×10^{-1} mmol), ACPA (2.9 mg, 1.05×10^{-2} mmol) and anhydrous dioxane (1.5 g, 1.46 mL)] and $f_{\text{MPDL},0} = 70\%$ [OEGMA (0.6633 g, 2.21 mmol), MPDL (0.8367 g, 5.17 mmol), Gem-RAFT Agent (114.4 mg, 1.30×10^{-1} mmol), ACPA (2.6 mg, 9.25×10^{-3} mmol) and anhydrous dioxane (1.5 g, 1.46 mL)].

c. Nanoparticle preparation

Nanoparticle preparation from Gem-P(MMA-*co*-MPDL). Nanoparticles were prepared by the nanoprecipitation technique. Briefly, 2 mg, 4 mg or 10 mg (for final concentrations of respectively 0.5, 1 and 2.5 mg·mL⁻¹) of copolymer prodrug were dissolved in 2 mL of THF, and added dropwise to 4 mL of MilliQ water under stirring. THF was evaporated at ambient temperature using a Rotavapor. Average diameter (D_z) measurements were carried out in triplicate.

References

- (1) Harrisson, S.; Nicolas, J.; Maksimenko, A.; Bui, D. T.; Mougin, J.; Couvreur, P. *Angew. Chem., Int. Ed.* **2013**, *52*, 1678.
- (2) Bao, Y.; Boissenot, T.; Guégain, E.; Desmaële, D.; Mura, S.; Couvreur, P.; Nicolas, J. *Chem. Mater.* **2016**, *28*, 6266.
- (3) Bao, Y.; Nicolas, J. *Polym. Chem.* **2017**.
- (4) Bao, Y.; Guégain, E.; Nicolas, V.; Nicolas, J. *Chem. Commun.* **2017**.
- (5) Perrier, S.; Takolpuckdee, P. *Journal of Polymer Science, Part A: Polymer Chemistry* **2005**, *43*, 5347.
- (6) Bertin, D.; Gimes, D.; Marque, S. R.; Tordo, P. *Macromolecules* **2005**, *38*, 2638.
- (7) Moad, G.; Rizzardo, E. *Macromolecules* **1995**, *28*, 8722.
- (8) Chenal, M.; Boursier, C.; Guillaneuf, Y.; Taverna, M.; Couvreur, P.; Nicolas, J. *Polym. Chem.* **2011**, *2*, 1523.
- (9) Toschi, L.; Finocchiaro, G.; Bartolini, S.; Gioia, V.; Cappuzzo, F. **2005**.
- (10) Kopčanský, P.; Tomašovičová, N.; Koneracka, M.; Timko, M.; Závašová, V.; Tomčo, L. *Acta Electrotechnica et Informatica* **2010**, *10*, 10.
- (11) Liu, J.; Liu, W.; Weitzhandler, I.; Bhattacharyya, J.; Li, X.; Wang, J.; Qi, Y.; Bhattacharjee, S.; Chilkoti, A. *Angewandte Chemie International Edition* **2015**, *54*, 1002.
- (12) Delplace, V., Université Paris Sud-Paris XI, 2014.
- (13) Delplace, V.; Tardy, A.; Harrisson, S.; Mura, S.; Gimes, D.; Guillaneuf, Y.; Nicolas, J. *Biomacromolecules* **2013**, *14*, 3769.
- (14) Delplace, V.; Harrisson, S.; Tardy, A.; Gimes, D.; Guillaneuf, Y.; Nicolas, J. *Macromol. Rapid Commun.* **2014**, *35*, 484.
- (15) McElvain, S.; Curry, M. J. *J. Am. Chem. Soc.* **1948**, *70*, 3781.
- (16) Bailey, W. J.; Wu, S. R.; Ni, Z. *Macromol. Chem. Phys.* **1982**, *183*, 1913.
- (17) Nicolas, J.; Dire, C.; Mueller, L.; Bellene, J.; Charleux, B.; Marque, S. R.; Bertin, D.; Magnet, S.; Couvreur, L. *Macromolecules* **2006**, *39*, 8274.
- (18) Nicolas, J.; Mueller, L.; Dire, C.; Matyjaszewski, K.; Charleux, B. *Macromolecules* **2009**, *42*, 4470.
- (19) Taylor, M.; Daniels, A.; Andriano, K.; Heller, J. *J Appl Biomater* **1994**, *5*, 151.
- (20) Ignatius, A.; Claes, L. E. *Biomaterials* **1996**, *17*, 831.
- (21) Zhang, Y.; Zheng, M.; Kissel, T.; Agarwal, S. *Biomacromolecules* **2012**, *13*, 313.
- (22) Meyer, R. P.; Hagemeyer, C. E.; Knoth, R.; Kurz, G.; Volk, B. *Biochem. Biophys. Res. Commun.* **2001**, *285*, 32.
- (23) Peng, H.-M.; Raner, G. M.; Vaz, A. D.; Coon, M. J. *Arch. Biochem. Biophys.* **1995**, *318*, 333.
- (24) Lenaerts, V.; Couvreur, P.; Christiaens-Leyh, D.; Joiris, E.; Roland, M.; Rollman, B.; Speiser, P. *Biomaterials* **1984**, *5*, 65.
- (25) Chenal, M.; Mura, S.; Marchal, C.; Gimes, D.; Charleux, B.; Fattal, E.; Couvreur, P.; Nicolas, J. *Macromolecules* **2010**, *43*, 9291.
- (26) Pan, C. Y.; Lou, X. D. *Macromolecular Chemistry and Physics* **2000**, *201*, 1115.
- (27) Kobben, S.; Ethirajan, A.; Junkers, T. *Journal of Polymer Science Part A: Polymer Chemistry* **2014**, *52*, 1633.
- (28) Siegwart, D. J.; Bencherif, S. A.; Srinivasan, A.; Hollinger, J. O.; Matyjaszewski, K. *Journal of Biomedical Materials Research Part A* **2008**, *87*, 345.
- (29) d'Ayala, G. G.; Malinconico, M.; Laurienzo, P.; Tardy, A.; Guillaneuf, Y.; Lansalot, M.; D'Agosto, F.; Charleux, B. *Journal of Polymer Science Part A: Polymer Chemistry* **2014**, *52*, 104.

- (30) Hedir, G. G.; Bell, C. A.; O'Reilly, R. K.; Dove, A. P. *Biomacromolecules* **2015**, *16*, 2049.
- (31) Decker, C. G.; Maynard, H. D. *European polymer journal* **2015**, *65*, 305.
- (32) Ganda, S.; Jiang, Y.; Thomas, D. S.; Eliezar, J.; Stenzel, M. H. *Macromolecules* **2016**, *49*, 4136.
- (33) Turner, P. V.; Brabb, T.; Pekow, C.; Vasbinder, M. A. *Journal of the American Association for Laboratory Animal Science* **2011**, *50*, 600.
- (34) Owens, D. E.; Peppas, N. A. *International journal of pharmaceutics* **2006**, *307*, 93.
- (35) Vonarbourg, A.; Passirani, C.; Saulnier, P.; Benoit, J.-P. *Biomaterials* **2006**, *27*, 4356.
- (36) Alexis, F.; Pridgen, E.; Molnar, L. K.; Farokhzad, O. C. *Molecular pharmaceutics* **2008**, *5*, 505.
- (37) Benoit, D.; Grimaldi, S.; Robin, S.; Finet, J.-P.; Tordo, P.; Gnanou, Y. *Journal of the American Chemical Society* **2000**, *122*, 5929.
- (38) Ulery, B. D.; Nair, L. S.; Laurencin, C. T. *J. Polym. Sci. Pol. Phys.* **2011**, *49*, 832.
- (39) Middleton, J. C.; Tipton, A. J. *Biomaterials* **2000**, *21*, 2335.
- (40) Sabir, M. I.; Xu, X.; Li, L. *J. Mater. Sci.* **2009**, *44*, 5713.
- (41) Yao, D.; Smith, A.; Nagarajan, P.; Vasquez, A.; Dang, L.; Chaudhry, G. R. *Journal of Biomedical Materials Research Part B: Applied Biomaterials* **2006**, *77*, 287.
- (42) Pasut, G.; Veronese, F. *Prog. Polym. Sci.* **2007**, *32*, 933.
- (43) Petrak, K.; Goddard, P. *Adv. Drug Delivery Rev.* **1989**, *3*, 191.
- (44) Rypáček, F.; Drobnik, J.; Chmelař, V.; Kalal, J. *Pflugers Arch.* **1982**, *392*, 211.
- (45) Ozer, I.; Tomak, A.; Zareie, H. M.; Baran, Y.; Bulmus, V. *Biomacromolecules* **2017**, *18*, 2699.
- (46) Bailey, W. J.; Kuruganti, V. K.; Angle, J. S.; ACS Publications: 1990.
- (47) Wickel, H.; Agarwal, S. *Macromolecules* **2003**, *36*, 6152.
- (48) Chung, I. S.; Matyjaszewski, K. *Macromolecules* **2003**, *36*, 2995.
- (49) Lutz, J.-F.; Andrieu, J.; Üzgün, S.; Rudolph, C.; Agarwal, S. *Macromolecules* **2007**, *40*, 8540.
- (50) Agarwal, S.; Ren, L. *Macromolecules* **2009**, *42*, 1574.
- (51) Paulusse, J. M.; Amir, R. J.; Evans, R. A.; Hawker, C. J. *J. Am. Chem. Soc.* **2009**, *131*, 9805.
- (52) Huang, J.; Gil, R.; Matyjaszewski, K. *Polymer* **2005**, *46*, 11698.
- (53) Hedir, G. G.; Bell, C. A.; Jeong, N. S.; Chapman, E.; Collins, I. R.; O'Reilly, R. K.; Dove, A. P. *Macromolecules* **2014**, *47*, 2847.
- (54) Shi, Y.; Agarwal, S. *e-Polymers* **2015**, *15*, 217.
- (55) Hill, M. R.; Guégain, E.; Tran, J.; Figg, C. A.; Turner, A. C.; Nicolas, J.; Sumerlin, B. S. *ACS Macro Letters* **2017**, *6*, 1071.
- (56) Shi, Y.; Schmalz, H.; Agarwal, S. *Polym. Chem.* **2015**, *6*, 6409.
- (57) O'Donnell, P. B.; McGinity, J. W. *Adv. Drug Delivery Rev.* **1997**, *28*, 25.
- (58) Trung Bui, D.; Maksimenko, A.; Desmaële, D.; Harrisson, S.; Vauthier, C.; Couvreur, P.; Nicolas, J. *Biomacromolecules* **2013**, *14*, 2837.

Supporting Information

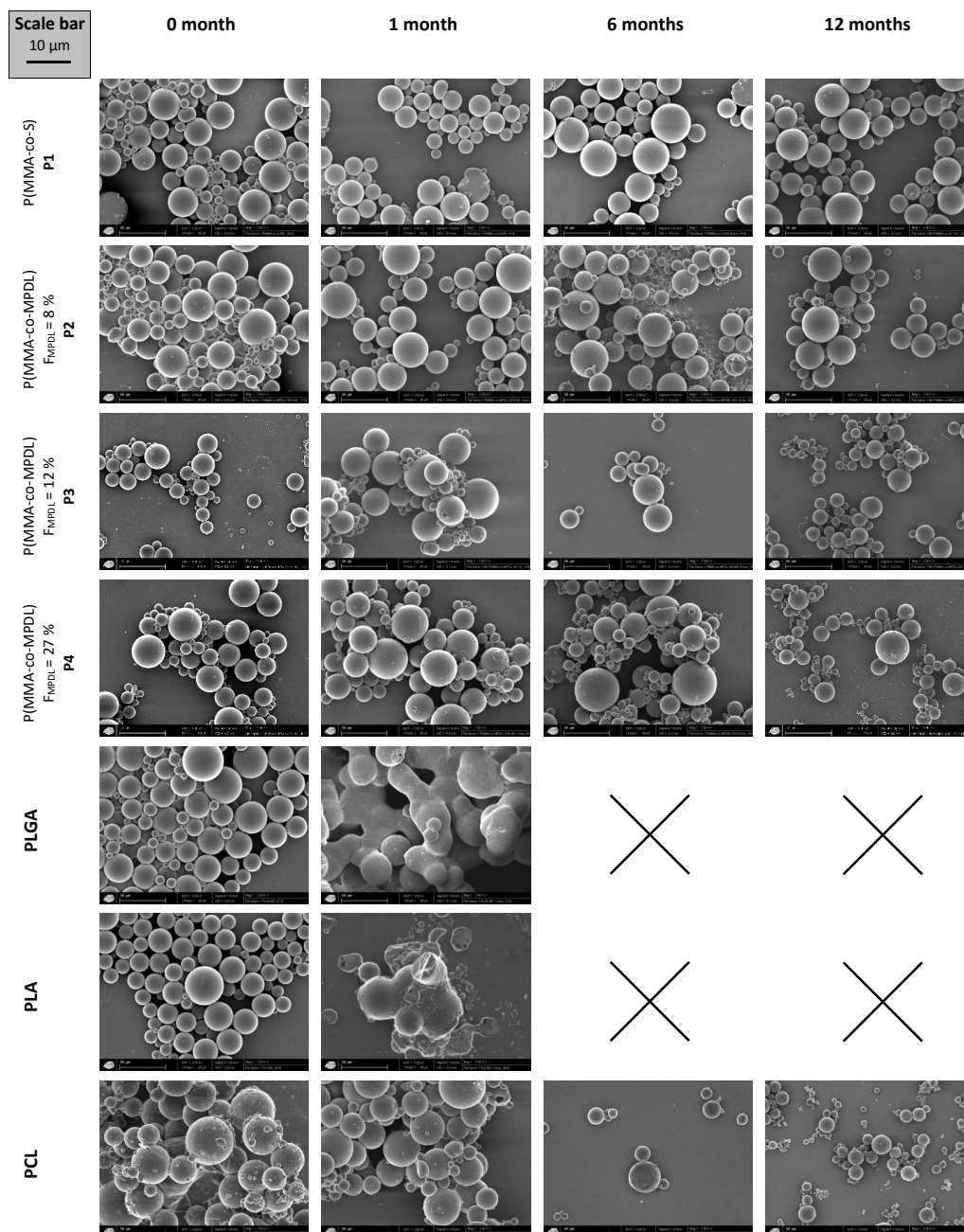


Figure S1. Evolution of the SEM images obtained during microsphere hydrolysis (Mag = 2.5 KX). The scale is indicated at the top left of the table (black bar).

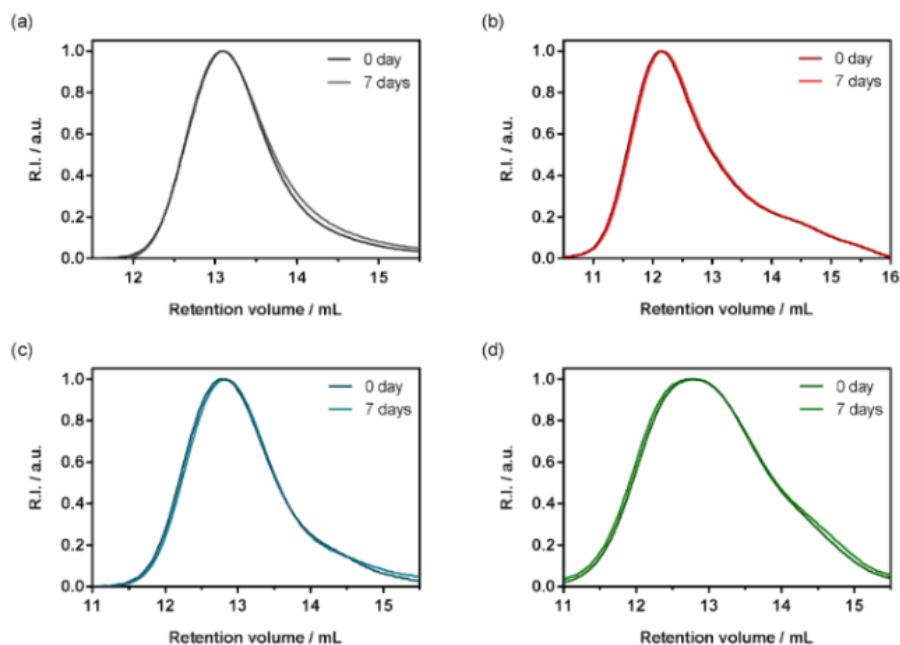


Figure S2. Oxidative degradation of P(MMA-*co*-MPDL) as a function of the MPDL fraction. Evolution of the SEC chromatograms before and after incubation with microsomes of: (a) P1 ($F_{\text{MPDL}} = 0\%$); (b) P2 ($F_{\text{MPDL}} = 8\%$); (c) P3 ($F_{\text{MPDL}} = 12\%$); (d) P4 ($F_{\text{MPDL}} = 27\%$).

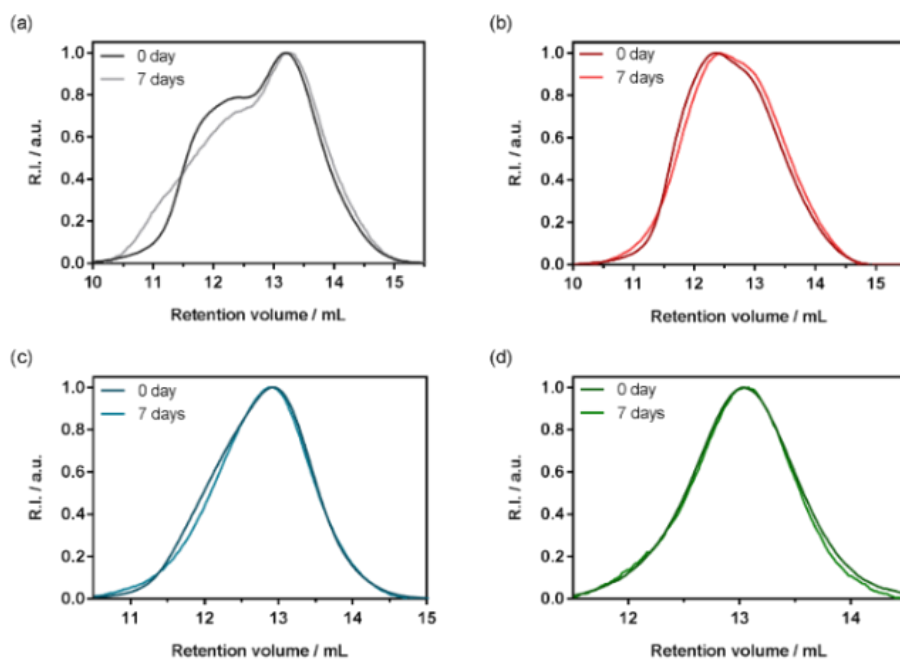


Figure S3. Oxidative degradation of P(OEGMA-*co*-MPDL) as a function of the MPDL fraction. Evolution of the SEC chromatograms before and after incubation with lipases of: (a) P5 ($F_{\text{MPDL}} = 0\%$); (b) P6 ($F_{\text{MPDL}} = 9\%$); (c) P7 ($F_{\text{MPDL}} = 15\%$); (d) P8 ($F_{\text{MPDL}} = 27\%$).

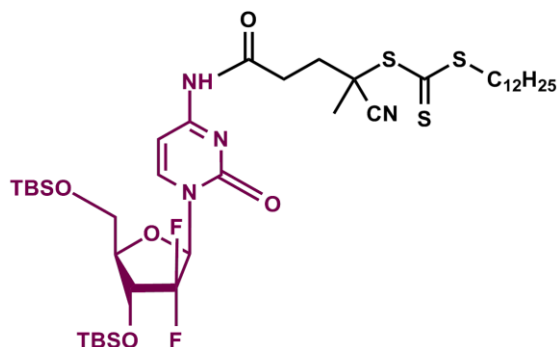


Figure S3. Chemical structure of the Gem-CTA employed for RAFT copolymerization of OEGMA and MPDL.

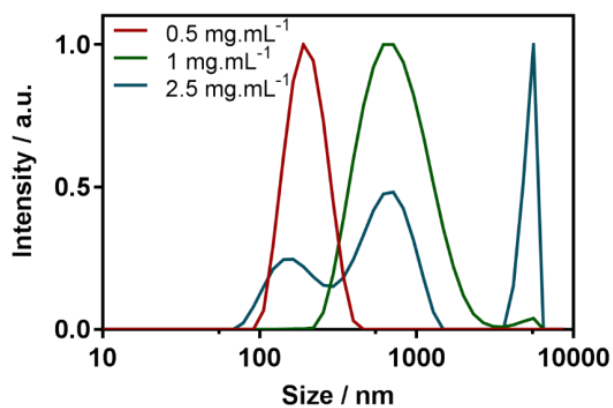


Figure S4. Size distribution obtained by dynamic light scattering (DLS) of Gem-P(MMA-co-MPDL) with $F_{\text{MPDL}} = 10\%$ (P4) at different final concentrations, from 0.5 to 2.5 mg.mL⁻¹.

Conclusion Générale

Ce projet de thèse a porté sur le développement de nouveaux polymères dégradables par polymérisation radicalaire par ouverture de cycle contrôlée par les nitroxydes (NMRROP), offrant une grande flexibilité en termes de synthèse ainsi que des possibilités de fonctionnalisation et des caractéristiques physicochimiques variées. Globalement, les objectifs étaient : (i) de préparer des copolymères vinyliques à base d'esters méthacryliques et d'acétals de cétène cyclique, capables de se dégrader à des vitesses comparables à celles de polyesters traditionnels, toujours considérés comme une référence dans le domaine biomédical et (ii) de démontrer leur potentiel pour la délivrance de principes actifs pour la thérapie du cancer en développant et en évaluant biologiquement des prodrogues polymères basés sur ces copolymères. Ce projet a permis l'obtention des résultats suivants :

- Des relations entre la **structure de diverses alcoxyamines fonctionnelles** basées sur le nitroxyde SG1 et leur capacité à **contrôler la NMP** de monomères vinyliques traditionnels ont été établies.
- Une **nouvelle voie de synthèse** du **MPDL** (le CKA utilisé pendant cette thèse), qui est plus efficace et reproductible que les méthodes précédentes, a été mise au point.
- Deux **nouvelles familles de copolymères vinyliques dégradables** basées sur la copolymérisation du MMA (hydrophobe) ou de l'OEGMA (hydrophile) avec le **MPDL**, donnant des copolymères de solubilité opposées, ont été synthétisées. Il a en particulier été montré que le MPDL se comportait comme un **comonomère de contrôle** de la NMP des méthacrylates et qu'il pouvait s'insérer de manière satisfaisante et contrôlable au sein des squelettes polyméthacrylates, en induisant une forte dégradabilité.
- La relation entre la **structure/solubilité** des copolymères et leur **vitesse de dégradation** en conditions **physiologiques** (PBS, pH 7.4, 37 °C) a été établie. Nous avons notamment démontré que nos **copolymères PEGylés** pouvaient avoir des cinétiques de dégradation **compétitives** avec celles de polyesters aliphatiques traditionnels comme le PLA ou le PCL (et facilement ajustable en fonction du taux de MPDL inséré dans le copolymère), sans présenter de diminution de pH, comme pour le PLA. En revanche, les copolymères totalement hydrophobes ont présenté une hydrolyse modérée, plus lente que celle du PCL.
- Enfin, l'évaluation biologique d'une bibliothèque de **prodrogues polymères dégradables** préparées par la méthode du '*principe actif amorceur*', en utilisant la Gemcitabine comme principe actif anticancéreux, a permis de démontrer que **relargage**

du principe actif ainsi que la **cytotoxicité** étaient indépendamment gouvernées par : (i) la nature de la liaison entre le copolymère et le principe actif ; (ii) l'hydrophilie de l'ester méthacrylique utilisé et (iii) le taux de MPDL incorporé dans le copolymère. Dans les meilleures conditions, nous avons retrouvé la cytotoxicité du principe actif libre.

L'ensemble de ces résultats démontre que l'insertion de fonction esters dégradables dans une chaîne polymère vinylique à l'aide d'acétals de cétènes cycliques représente une méthode efficace pour la préparation de matériaux vinyliques dégradables et facilement fonctionnalisables, possédant un champ applicatif large ; allant de la délivrance de principes actifs à la médecine régénérative.

Pendant ces trois ans de thèse, de nombreuses opportunités m'ont également permis de participer à plusieurs collaborations, notamment avec le **Dr Yinyin Bao** pour la mise au point de prodrogues vinyliques variées par la méthode du '*principe actif amorceur*' à partir soit d'agent anticancéreux comme la Cladribine (*Chem. Mater.* **2016**) soit d'une sonde fluorescente pour l'imagerie, le Naphtalimide (*Chem. Commun.* **2017**) et avec **Megan Hill** pour la synthèse de copolymères alternés dégradables en copolymérisant le MPDL avec des maléimides (*ACS Macro Lett.* **2017**).

Titre : Prodrogues Polymères Dégradables par Polymérisation Radicalaire par Ouverture de Cycle Contrôlée par les Nitroxydes

Mots clés : Polymérisation radicalaire contrôlée par les nitroxides, Polymérisation radicalaire par ouverture de cycle, Acétals de cétène cyclique, Dégradabilité, Prodrogue, Méthode du principe actif amorceur, Nanoparticules.

Résumé : La copolymérisation radicalaire par ouverture de cycle contrôlée par les nitroxydes entre les esters méthacryliques et les acétals de cétène cycliques a permis de synthétiser des copolymères vinyliques bien contrôlés et dégradables contenant des fonctions esters le long de la chaîne polymère. Plus précisément, des copolymérisations entre le 2-méthylène-4-phenyl-1,3-dioxolane (MPDL) et l'oligo(éthylène glycol) méthyl éther méthacrylate (OEGMA) ou le méthacrylate de méthyle (MMA) ont été amorcées par une alkoxyamine basée sur le nitroxyde SG1. Des copolymères de type P(OEGMA-co-MPDL) et P(MMA-co-MPDL) ont été obtenus et dégradés hydrolytiquement en conditions accélérées ou physiologiques. Leurs cinétiques de dégradation furent également comparées à celles de polyesters traditionnels (*e.g.*, PLGA, PLA and PCL) où il a été montré que la dégradation des copolymères de P(OEGMA-co-MPDL) pouvait être ajustée par la stœchiométrie initiale en monomères et qu'elle se situait entre celles du PLA et du PCL. En revanche, les copolymères de P(MMA-co-MPDL), plus hydrophobes, ont présenté une hydrolyse très lente, bien inférieure à celle du PCL. Dans un deuxième temps, une nouvelle famille de prodrogues polymères dégradables a été synthétisée par copolymérisation radicalaire par ouverture de cycle contrôlée par les nitroxydes entre le MPDL et l'OEGMA ou le MMA, à partir d'un amorceur couplé à un principe actif (méthode du principe actif amorceur). Pour ce faire, la Gemcitabine, un principe actif anticancéreux, a été couplé à une alkoxyamine à base SG1 qui fut ensuite utilisée pour amorcer la réaction de copolymérisation. Les copolymères ainsi obtenus ont montré des propriétés de libération de la Gem et des activités cytotoxiques sur différentes lignées cellulaires en relation avec la nature de l'ester méthacrylique utilisé, la nature de la liaison entre la Gem et le copolymère ainsi que le taux de MPDL dans le copolymère. Cette étude nous a permis d'extraire des relations de type structure-activité importantes pour des développements futurs.

Title: Degradable Polymer Prodrugs by Nitroxide-Mediated Radical Ring-Opening Polymerization

Keywords: Nitroxide-mediated polymerization, Radical ring-opening polymerization, Cyclic ketene acetals, Degradability, Prodrug, Drug-initiated method, Nanoparticles.

Abstract: Nitroxide-mediated radical ring-opening copolymerization of methacrylic esters and cyclic ketene acetals was investigated and enabled the synthesis of well-defined degradable vinyl copolymers containing ester groups along the main chain, whose amount was readily adjusted by changing the initial comonomer feed. More specifically, the copolymerizations of 2-methylene-4-phenyl-1,3-dioxolane (MPDL) and either oligo(ethylene glycol) methyl ether methacrylate (OEGMA) or methyl methacrylate (MMA) were initiated by an alkoxyamine initiator based on the SG1 nitroxide. It led to a library of P(OEGMA-co-MPDL) and P(MMA-co-MPDL) materials that were hydrolytically degraded under both accelerated and physiological conditions. Their hydrolytic degradation kinetics were also benchmarked against traditional polyesters (*e.g.*, PLGA, PLA and PCL) where P(OEGMA-co-MPDL) copolymers showed tunable degradation rates as function of the MPDL content, being in between those of PLA and PCL. Conversely, the more hydrophobic P(MMA-co-MPDL) copolymers exhibited much slower hydrolysis than that of PCL. In a second step, a new class of degradable polymer prodrugs was developed by nitroxide-mediated radical ring-opening copolymerization of MPDL with OEGMA or MMA, from a drug-bearing initiator ('drug-initiated' method). To do so, Gemcitabine, an anticancer drug, was derivatized with a SG1-based alkoxyamine to initiate the copolymerization reaction. The resulting degradable polymer prodrugs exhibited interesting characteristics in terms of drug release and *in vitro* cytotoxicity, depending on the nature of the methacrylic ester used, the nature of the linker between the drug and the polymer and the MPDL content. This study enabled us to extract important structure-activity relationships of great importance for further development.

